ISSN 0202—3822

НАЦИОНАЛЬНЫЙ ИССЛЕДОВАТЕЛЬСКИЙ ЦЕНТР
«КУРЧАТОВСКИЙ ИНСТИТУТ»

ВОПРОСЫ АТОМНОЙ НАУКИ И ТЕХНИКИ

СЕРИЯ
ТЕРМОЯДЕРНЫЙ СИНТЕЗ

2021

Том 44
Выпуск 2

Этот выпуск журнала содержит 20 докладов и восемь кратких сообщений о докладах, представленных на 4-й Международной конференции по подкритическим гибридным системам ядерного синтеза-деления, которая проходила в Москве с 25 по 27 ноября 2020 г.

Интерес к гибридным системам синтеза-деления среди специалистов по ядерным реакторам деления и термоядерным реакторам ярко проявился ещё в конце 70-х годов прошлого столетия [1—3]. Тогда, изучая вопрос, в какой области энергетики термоядерные установки могут быть наиболее востребованными, ведущие специалисты СССР и США отметили, что с помощью гибридных реакторов синтеза-деления можно более эффективно, чем, применяя другие технологии, обеспечить делящимся топливом ядерную энергетику в условиях надвигающегося дефицита источников энергии.

При этом отмечалось, что сооружение первых гибридных реакторов должно встретить меньшие технологические трудности, чем сооружение первых «чистых» термоядерных реакторов, так как в гибридных реакторах заметно смягчается требование обеспечить большую плотность потока нейтронов на первую стенку. Задача наработки делящегося топлива вместо непрерывной выработки электроэнергии снимает требование стационарной работы термоядерного компонента установки. При наработке делящегося топлива в гибридной системе удельный выход радиоактивности, согласно оценкам, существенно меньше, чем при других способах трансмутации чётных тяжёлых изотопов в нечётные. Гибридные системы синтеза-деления, ориентированные одновременно на воспроизводство делящихся изотопов и производство электроэнергии, выгодно отличаются от обычных энергетических ядерных реакторов деления уровнем ядерной безопасности благодаря своей подкритичности.

Международные конференции по гибридным системам синтеза-деления проводятся под эгидой МАГАТЭ. Постепенно в разработки гибридных реакторов включаются новые коллективы. Китайские коллеги активно изучают эти реакторы с самого начала работ в этой стране по термоядерной тематике. Евратом длительное время игнорировал гибридные реакторы. Тем более приятно было видеть на прошедшей конференции итальянские доклады с большим числом авторов из разных городов страны.

Министерство науки и высшего образования Российской Федерации поручило организовать подготовку и проведение конференции заведующему кафедрой физики плазмы МИФИ В.А. Курнаеву. К великому сожалению, он скончался за два дня до начала конференции, и организационные функции взяли на себя Ю.М. Гаспарян (МИФИ) и Б.В. Кутеев (НИЦ «Курчатовский институт»). Они обратились к редколлегии нашего журнала с просьбой напечатать труды конференции. Редколлегия согласилась на этот эксперимент, хотя у неё отсутствовал опыт такого рода. Эксперимент был нелёгкий. Все доклады, а их число было вдвое больше обычного числа статей в журнальном выпуске, представлялись на английском языке. Опыта же редактирования англоязычных рукописей у нас практически нет. Пришлось обратиться к специалисту по английскому языку. Результаты этого эксперимента представляются вашему вниманию.

Список литературы

1. **Головин И.Н., Шаталов Г.Е., Колбасов Б.Н.** Некоторые вопросы гибридных термоядерных реакторов. — В сб.: АН СССР. Энергетика и транспорт, 1975, № 6, с. 28—34.
2. **Головин И.Н., Колбасов Б.Н., Орлов В.В., Пистунович В.И., Шаталов Г.Е.** Проблема ядерного топлива и гибридные реакторы. — В сб.: Труды 2-го советско-американского семинара. Москва, 14.03—01.04.1977. — М.: Атомиздат, 1978, с. 5—14.
3. **Velikhov E.P., Glukhikh V.A., Gur'ev V.V., Kadomtsev B.B. et al.** Tokamak-type thermonuclear hybrid reactor for the production of fission fuel and electric energy. — Soviet Atomic Energy, 1978, vol. 45(1), p. 653—660.

Редколлегия журнала «ВАНТ. Сер. Термоядерный синтез».

НАЦИОНАЛЬНЫЙ ИССЛЕДОВАТЕЛЬСКИЙ ЦЕНТР «КУРЧАТОВСКИЙ ИНСТИТУТ»

ВОПРОСЫ АТОМНОЙ НАУКИ И ТЕХНИКИ

научно-технический сборник

СЕРИЯ

ТЕРМОЯДЕРНЫЙ СИНТЕЗ

ИЗДАЁТСЯ С 1978 г.

Том 44

Выпуск 2

МОСКВА — 2021

Редактор Карпова Татьяна Юрьевна
karpova.tat@fc.iterru.ru, тел.: 7-499-196-98-31

Журнал (основан в 1978 г.) зарегистрирован в реестре Федеральной службы по надзору в сфере связи, информационных технологий и массовых коммуникаций ПИ № ФС77-73164 от 02 июля 2018 г.; электронное периодическое издание Эл. № ФС77-73162 от 22 июня 2018 г.

Подписной индекс в Каталоге периодики агентства «Урал-Пресс» № 70541

Соучредители: Автономная некоммерческая организация Координационный центр «Управляемый термоядерный синтез — международные проекты» (УТС-Центр), федеральное государственное бюджетное учреждение «Национальный исследовательский центр «Курчатовский институт»

Журнал включён в Перечень журналов ВАК, индексируется в базах данных Scopus, Ulrich's Periodicals Directory и РИНЦ на платформе Web of Science, имеет цифровой идентификатор статей (digital object identifier — DOI), реферируется в РЖ ВИНИТИ РАН, имеет в открытом доступе полнотекстовую электронную версию на сайте http://vant.iterru.ru и на платформе Российской научной электронной библиотеки http://www.elibrary.ru
Импакт-фактор журнала в РИНЦ: 0,407

NATIONAL RESEARCH CENTRE «KURCHATOV INSTITUTE»

PROBLEMS OF ATOMIC SCIENCE AND TECHNOLOGY

Collected scientific and technical papers

Series
THERMONUCLEAR FUSION

PUBLISHED since 1978

Volume 44

Issue 2

[Voprosy Atomnoi Nauki i Tekhniki. Seriya: Termoyadernyi Sintez]

MOSCOW — 2021

The journal (established in 1978) is filed in the registry of the Federal Service for Supervision of Communications, Information Technology and Mass Media PI № FS77-73164 of 02 June 2018; electronic periodical is filed in the registry El. № FS77-73162 of 22 June 2018
Subscription index in the catalogue of periodicals of the «Ural-Press» agency № 70541

Co-founders: Autonomous non-profit organization Coordinating center «Controlled Thermonuclear Fusion — International Projects» (CTF-Center);
Federal state budgetary National Research Centre «Kurchatov Institute»

The journal is included into the list of the Supreme Certification Commission key journals. Its indexes are available in the databases Scopus, the Ulrich's Periodicals Directory and the Russian Science Citation Index (RSCI) on the Web of Science platform. The papers published in it have digital object identification (DOI). The abstracts of the papers published in it are available in the abstract journal of the VINITI RAS. All the free access full-text electronic versions of the papers are available on the site http://iterru.ru and on the platform of the Russian Scientific Electronic Library http://www.elibrary.ru
The impact factor of the journal in RSCI: 0,407

УДК 061.3

4-Я МЕЖДУНАРОДНАЯ КОНФЕРЕНЦИЯ ПО ПОДКРИТИЧЕСКИМ ГИБРИДНЫМ СИСТЕМАМ СИНТЕЗА-ДЕЛЕНИЯ

Б.В. Кутеев

НИЦ «Курчатовский институт», Москва, Россия

В МИФИ с 25 по 27 ноября 2020 г. прошла 4-я Международная конференция по подкритическим гибридным системам синтеза-деления (FUNFI-4).

В рамках конференции были обсуждены вопросы применения гибридных технологий для управления потоками радиоактивных отходов атомной энергетики и производства топлива для ядерных реакторов, а также проблемы безопасности инновационных нейтронных технологий. В заседаниях конференции участвовали более 50 учёных из России, Италии, Китая, Великобритании, Украины, Швеции, Индии, Турции, а также сотрудники МАГАТЭ (Австрия). Участники конференции представляли как государственные научные организации и университеты, так и частные компании («Tokamak Energy», Великобритания).

Борис Васильевич Кутеев, заместитель руководителя Отделения токамаков по гибридным системам, д.ф.-м.н.; НИЦ «Курчатовский институт», 123182 Москва, пл. Академика Курчатова 1, Россия; профессор; НИЯУ МИФИ, 115409 Москва, Каширское ш. 31, Россия
Kuteev_BV@nrcki.ru

На заседаниях было представлено 26 устных и пять стендовых докладов, посвящённых:

— различным типам термоядерных источников нейтронов, таким как компактные и классические токамаки, стеллараторы, пинчи с обращённым полем и открытые газодинамические ловушки;

— источникам нейтронов на основе ускорителей с реакциями DD- и DT-синтеза, имеющим широкий круг приложений не только в энергетике, но и в других областях, включая материаловедение и медицину;

— проблемам конструкционных и функциональных материалов для термоядерных источников нейтронов и гибридных систем синтеза-деления;

— системным исследованиям включения гибридных систем в топливные циклы действующей и будущей атомной энергетики, в том числе в производство топливных нуклидов и переработку долгоживущих радиоактивных отходов.

Доцент кафедры Физика плазмы Ю.М. Гаспарян представил обзорный доклад о деятельности НИЯУ МИФИ в направлении развития термоядерных установок и гибридных систем синтеза-деления.

В заключительный день Б.В. Кутеев (НИЦ «Курчатовский институт», профессор НИЯУ МИФИ), Ю. Ву (директор Института безопасного применения ядерных технологий, Китай) и Ф. Орситто (Итальянское национальное агентство по новым технологиям, энергетике и устойчивому экономическому развитию, Италия) в своих заключительных докладах подвели итоги конференции. Суммировав прогресс в развитии компактных токамаков и открытых ловушек, они сформулировали научные и технологические задачи, которые необходимо будет решить в ближайшей перспективе для создания демонстрационных гибридных систем синтеза-деления.

В рамках завершающей дискуссии совместно с представителем МАГАТЭ М. Барбарино были намечены шаги к трансформации конференции FUNFI в техническое совещание МАГАТЭ. Участники конференции были приглашены принять участие в совещании МАГАТЭ в рамках действующего координационного проекта МАГАТЭ по компактным источникам термоядерных нейтронов в октябре 2021 г.

В связи со сложной эпидемиологической ситуацией конференция прошла в дистанционном режиме. Участники совещания отметили высокий уровень организации конференции со стороны НИЯУ МИФИ и НИЦ «Курчатовский институт».

4TH INTERNATIONAL CONFERENCE ON FUSION-FISSION SUBCRITICAL HYBRID SYSTEMS

B.V. Kuteev

NRC «Kurchatov Institute», Moscow, Russia

The 4th International Conference on Fusion-Fission Subcritical Hybrid Systems (FUNFI-4) was held at MEPhI from November 25 to 27, 2020.

The conference discussed the use of hybrid technologies for managing the flow of radioactive waste from nuclear power engineering and the production of fuel for nuclear reactors, as well as the safety of innovative neutron technologies. The conference was attended by more than 50 scientists from Russia, Italy, China, Great Britain, Ukraine, Sweden, India, Turkey, as well as employees of the IAEA (Austria). The conference participants represented both state scientific organizations and universities, as well as private companies («Tokamak Energy», UK).

At the meetings, 26 oral and 5 poster presentations were presented on the following topics:

— various types of fusion neutron sources, such as compact and classical tokamaks, stellarators, reverse-field pinches, and open gas-dynamic traps;

— neutron sources based on accelerators with DD- and DT-fusion reactions, which have a wide range of applications not only in energy, but also in other fields, including materials science and medicine;

— problems of structural and functional materials for fusion neutron sources and hybrid fusion-fission systems;

— systematic studies of the inclusion of hybrid systems in the fuel cycles of current and future nuclear power, including the production of fuel nuclides and the processing of long-lived radioactive waste.

Associate Professor of the Department of Plasma Physics Yu. M. Gasparyan presented an overview report on the activities of the MEPhI Research University in the direction of the development of thermonuclear installations and hybrid fusion-fission systems.

On the final day, B.V. Kuteev (NRC «Kurchatov Institute», Professor of the MEPhI Research University), Yu. Wu (Director of the Institute for the Safe Application of Nuclear Technologies, China), and F. Orsitto (Italian National Agency for New Technologies, Energy and Sustainable Economic Development, Italy), in their final reports, summed up the results of the conference. Summing up the progress in the development of compact tokamaks and open traps, they formulated the scientific and technological tasks that will need to be solved in the near future to create demonstration hybrid fusion-fission systems.

As part of the final discussion, together with the representative of the IAEA, M. Barbarino, steps were outlined to transform the FUNFI conference into an IAEA technical meeting. The conference participants were invited to participate in the IAEA meeting within the framework of the current IAEA coordination project on compact sources of thermonuclear neutrons in October 2021.

Due to the difficult epidemiological situation, the conference was held remotely. The participants of the meeting noted the high level of organization of the conference by the MEPhI Research University and the NRC «Kurchatov Institute».

DOI: 10.21517/0202-3822-2021-44-2-5-6

UDC 544.022.341, 544.022.382

FUSION-FISSION HYBRID SYSTEM DEVELOPMENT AND INTEGRATION INTO RUSSIA'S NUCLEAR POWER ENGINEERING

B.V. Kuteev[1], Yu.S. Shpanskiy[1, 2] and DEMO-FNS Team[3]

[1]*NRC «Kurchatov Institute», Moscow, Russia*
[2]*National Research University, Moscow Power Engineering Institute, Moscow, Russia*

Combining nuclear fusion and fission reactions in a single design offers the possibility of implementing nuclear energy systems with qualitatively new characteristics and properties. Development of the fusion-fission hybrid facility based on the superconducting tokamak DEMO-FNS is underway in Russia to allow steady-state fusion and nuclear technologies to be operated simultaneously and produce vel up to 40 MW of fusion power and about 400 MW of fission power. Such a facility could provide burning the minor actinides accumulated by the Russian nuclear fuel cycle during the operation of nuclear power plants earlier and in the future. This paper presents an overview of the latest achievements in the area of the DEMO-FNS design and describes different operation scenarios for this facility. Related research activities are part of ongoing Russia's Nuclear Energy Research Program

Key words: fusion and fission reactions, hybrid facility, superconducting tokamak, minor actinides, vacuum vessel, hybrid fuel cycle.

DOI: 10.21517/0202-3822-2021-44-2-7-14

РАЗВИТИЕ ГИБРИДНЫХ СИСТЕМ «СИНТЕЗ-ДЕЛЕНИЕ» И ИХ ИНТЕГРАЦИЯ В ЯДЕРНУЮ ЭНЕРГЕТИКУ РОССИИ

Б.В. Кутеев[1], Ю.С. Шпанский[1, 2] и команда DEMO-FNS

[1]*НИЦ «Курчатовский институт», Москва, Россия*
[2]*Национальный исследовательский университет «Московский энергетический институт», Москва, Россия*

Наличие реакций ядерного синтеза и деления в одной установке позволит достичь принципиально новых характеристик и свойств ядерной энергетической системы. В России продолжается разработка гибридной установки термоядерного синтеза на основе сверхпроводящего токамака для комплексного использования стационарных и ядерных технологий мощностью до 40 МВт для термоядерного синтеза и 400 МВт для реакций деления. В дальнейшем эта гибридная система может быть интегрирована в ядерную систему России для пережигания (трансмутации) минорных актинидов в отработавшем ядерном топливе ядерных энергетических реакторов. Такая установка могла бы обеспечить сжигание минорных актинидов, накопленных российским ядерным топливным циклом в процессе эксплуатации атомных электростанций в настоящем и будущем. В данной статье представлен обзор последних достижений в области проектирования демонстрационного ТИН и описаны различные сценарии эксплуатации этой установки. Научно-исследовательская работа, проводимая в рамках этой проблемы, является частью Российской программы исследований в области ядерной энергетики.

Ключевые слова: реакции синтеза и деления, гибридная установка «синтез-деление», сверхпроводящий токамак, минорные актиниды, вакуумная камера, гибридный топливный цикл.

INTRODUCTION

At present, Russia's nuclear industry is shifting to the closed fuel cycle with an emphasis on thermal and fast power reactors. This calls for new spent fuel and radioactive waste management/incineration technologies, as well as the development of «fusion-fission» hybrid systems. Combining fusion and fission processes in one design offers the possibility of implementing nuclear energy systems with qualitatively new characteristics and properties A project is underway in Russia to develop a fusion-fission hybrid facility based on the DEMO-FNS superconducting tokamak to allow steady-state fusion and nuclear technologies to be operated simultaneously

[3]S.S. Ananiev, A.A. Glebova, A.V. Golubeva, E.D. Dlougach, D.N. Demidov, A.Yu. Dnestrovskij, B.V. Ivanov, A.V. Klischenko, B.N. Kolbasov, A.S. Kukushkin, V.E. Lukash, V.V. Lukianov, S.Yu. Medvedev, A.A. Morozov, A.Yu. Pashkov, V.S. Petrov, A.B. Sivak, A.V. Spitsyn, R.R. Khairutdinov, V.I. Khripunov, M.N. Shlenskiy, A.V. Zhirkin (NRC «Kurchatov Institute», Moscow, Russia); E.N. Bondarchuk, A.A. Voronova, E.R. Zapretilina, A.A. Kavin, S.V. Krasnov, A.N. Labusov, A.B. Mineev, V.P. Muratov, I.Yu. Rodin, V.A. Trofimov, M.V. Khohlov (Efremov Institute, St. Petersburg, Russia); I.V. Danilov, A.V. Lopatkin, I.B. Lukasevitch, V.E. Popov, Yu.S. Strebkov, A.G. Sysoev (NIKIET, Moscow, Russia); V.Yu. Sergeev, P.R. Goncharov, A.V. Skokov (St. Petersburg University (SPbPU), St. Petersburg, Russia).

and produce up to 40 MW (more than 10^{19} neutrons per second) of fusion power and 400 MW of fission power This research is part of Russia's Nuclear Energy Research Program.

The project aims at achieving a steady-state operation with a 14 MeV-neutron wall loading of ~0.2 MW/m^2, and a life-cycle neutron fluence of ~2 MW·year/m^2. In addition, the blanket's plasma-facing surface should be ~100 m^2, i.e. large enough to enable the testing of materials and components in the energy spectrum of DT-thermonuclear neutrons, to conduct transmutation studies, generate energy and produce fission fuel nuclides and tritium.

The analysis of the interaction of the DEMO-FNS facility and further industrial options with the nuclear fuel cycle is carried out. Going forward, the discussed hybrid system could be integrated with Russian nuclear power plants to allow the burnup of minor actinides accumulated by the country's nuclear fuel cycle facilities. Under a closed fuel cycle, spent fuel, enriched in an industrial hybrid facility, goes back to the cycle, reducing the need for storage facilities and bringing down overall radiotoxicity. This paper presents the latest achievements in the area of the DEMO-FNS design (2019—2020) and describes different operation scenarios for this facility. The DEMO-FNS tokamak has the following key characteristics:

plasma current I_P, MA . . .	5
major radius R_0, m . . .	3.2
minor radius a, m . . .	1.0
aspect ratio R/a . . .	3.2
plasma elongation k_x/k_{95} . . .	2.0/1.9
triangularity, x . . .	0.2—0.5
Power parameters:	
D—T-fusion power, MW . . .	40
fission power, MW . . .	400
electric power, MW . . .	200
total power, MW . . .	700

Auxiliary heating power P_{aux} = 36 MW, including 30 MW of neutral beam power and 6 MW of ECR heating power (at 170 GHz). The DEMO plant is expected to help accomplish the following tasks:

— comprehensive testing of systems and technologies enabling the FNS steady-state operation, including hybrid blankets, electric power generation system and radiochemical equipment;

— testing of the prototypes of FNS hybrid breeder blankets (based on steady-state and molten salt technologies);

— scientific and technical support of pilot and industrial hybrid plants.

DEMO-FNS DESIGN

DEMO-FNS general layout is presented in Fig. 1.

DEMO-FNS is a complex facility that includes a superconducting magnetic system, a vacuum chamber, a hybrid blanket located in it (consists of six modules), and two (upper and lower) divertor units. The blanket module includes: the module body, an active core with a transmutation capability, a blanket breeder zone, and coolant collectors.

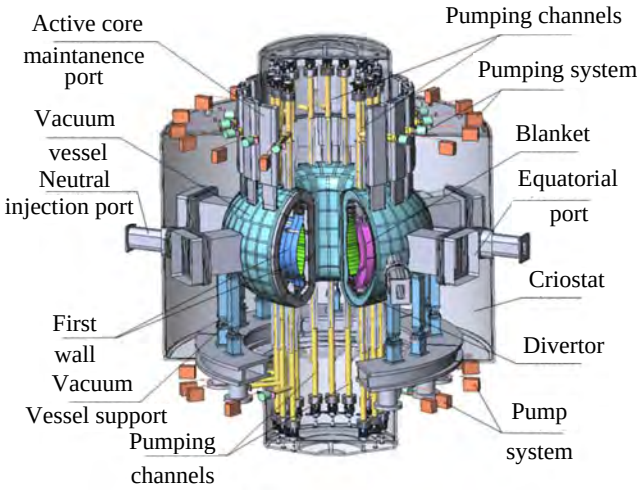

Fig. 1. DEMO-FNS device key design features (magnetic system not shown)

Magnetic system. In accordance with the design principles, the magnetic system (MC) for the DEMO-FNS must ensure a reliable operation of the system with a hybrid blanket and the corresponding hybrid nuclear fuel cycle. The DEMO-FNS's superconducting magnetic system includes: 18 toroidal field coils (TFCs); 6 sectioned central solenoid units); 4 pairs of poloidal field coils (PFCs); 18 correction coils arranged in 3 groups; 2 vertical control coils; current leads fabricated of high temperature superconductors. Materials used in toroidal and poloidal coils include: Nb_3Sn, NbTi; SS, Cu-alloys; polyimide insulator; He-coolant. The MS and vacuum vessel configuration accommodates up to 18 vertically loaded hybrid blanket

active cores and allows them to be retrieved for remote maintenance, which takes place in a designated area. Analyses of the electromagnetic forces and the stress analyses of DEMO-FNS MS were carried out. TFCs were found to be experiencing the heaviest stresses. After considering different options, an ITER-like design was chosen as optimal for the TFCs. View of the toroidal coil and its finite elements mesh is shown in Fig. 2.

A stress-strain analysis of the coils revealed that the proposed coil design meets the static strength criteria (Fig. 3)

Vacuum vessel. The vacuum vessel (VV) is an all-welded two-layer toroidal shell (Fig. 4) inside the magnetic system. The space between the inner and outer shells is filled with water and steel plates (an iron-water shielding) to provide adequate neutron protection. The VV has the following main components (see Fig. 1):

— body;

— equatorial ports, which provide access inside the vessel for remote handling and maintenance operations and plasma diagnostics;

— injection ports for introducing neutral particles into plasma;

— pipes for vacuum pumping;

— support structure that bears the VV's weight and protects it from electromagnetic loads;

— support system for steadying the divertor, blanket, turns of passive and active plasma stabilization, first wall elements and other in-vessel components;

— collectors of water cooling the VV and its internal components.

The VV wall inner shell is 0.72 m thick (this helps reduce volumetric heat deposition in the TFC superconductor materials), and the outer shell has a thickness of 0.60 m. At this stage of the design development, the VV was considered, adapted for a hybrid blanket with a steady-state breeding zone and a reloadable active core containing fuel assemblies with minor actinides.

Vertical ports for reloading the blanket active core are in the VV upper part. Each sector has three rectan-

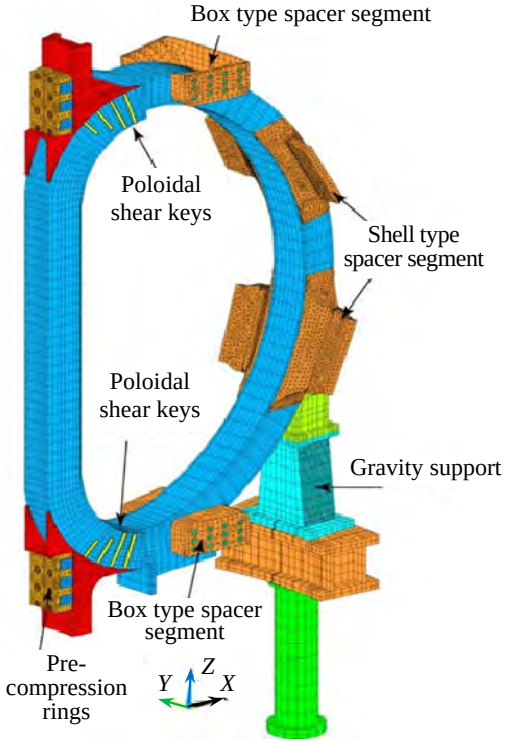

Fig. 2. View of a toroidal coil modeled with a finite element mesh

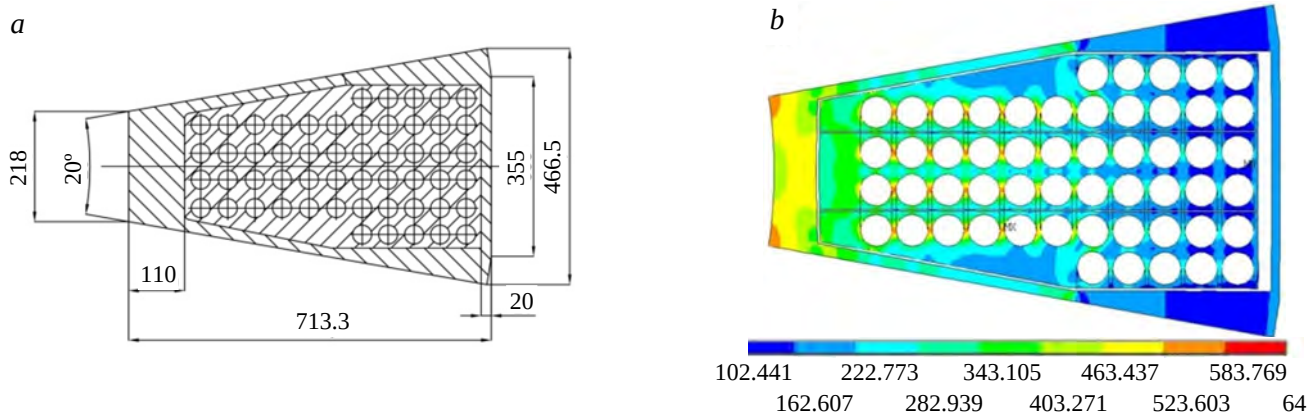

Fig. 3. Cross-section dimensions (*a*) and equivalent stresses (MPa) of the toroidal coil (*b*)

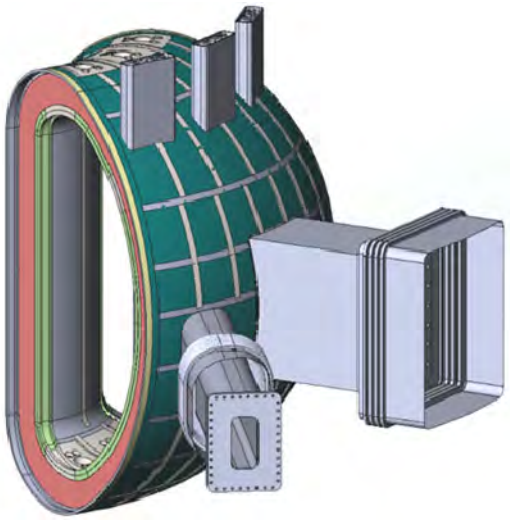

Fig. 4. VV general layout

gular branch pipes making the total number of branch pipes in the FNS facility 18. With the existing arrangement of the blanket core reloading ports, exhaust tubes, cooling water outlet channels, the installation of mounting welded joints of the vacuum vessel sectors is possible only under the toroidal field coils. Two supports are provided for the VV installation on each sector. One is located beneath the equatorial port at the junction with the outer shell of the vacuum vessel, the other is beneath the pipe used for injecting neutral particles. At the top and at the bottom, the supports are equipped with articulated joints that allow the vessel to move freely in the radial direction, compensating for the change in its dimensions at various operating temperatures. The supports in the lower part rest on supports, which are installed on a base common with the magnetic system. Dielectric inserts are provided between the supports and fittings that electrically insulate the VV supports from the common base. For convenience and in order to speed up on-site assembly operations, the vacuum vessel will be assembled of six 60-degree sectors.

Blanket. The DEMO-FNS's hybrid blanket consists of two parts, the active core (AC) and the breeding zone (BZ):

— the AC includes 12 full-size and 6 shortened units;

— the BZ, intended for reproduction of tritium, is placed on the outer bypass of the FNS VV for the entire operation life and is to be dismounted only in case of failure or emergency;

— reloading of the AC of the hybrid blanket of the FNS, the general view of which is shown in Fig. 1, is carried out through the vertical service channels at the stopped facility;

— BZ modules mounting/dismantling is carried out through six equatorial (horizontal) service ports of in-vessel components.

The AC structure, whose general arrangement is shown in Fig. 5, includes: body; cover of the AC case; eight fuel assemblies containing fuel elements with a mixture of minor actinides (MA); two flexible mechanical supports.

The AC of the hybrid blanket consists of *8* fuel assemblies assembled with fuel elements containing a mixture of MA in a metallic form. Each fuel assembly consists of 56 fuel rods. BZ cases, are mounted on the external bypass of the VV. Mounting / dismantling of the BZ cases is carried out through the equatorial port of the in-vessel components of the FNS facility. Structurally, BZ is a canister structures that occupy all the available space located between the rear surface of the AC case and the surface of the VV. The breeding zone includes modules of varous sizes. General view and volumes of BZ modules are shown in Fig. 6.

BZ modules are filled with lithium-containing ceramics — lithium orthosilicate Li_4SiO_4 in the spherical form with a volumetric filling of at least 60% and a granule diameter of 1—1.5 mm. To accelerate the release of tritium and its subsequent removal of the BZ, a purge gas is pumped through the ceramics under a pressure of

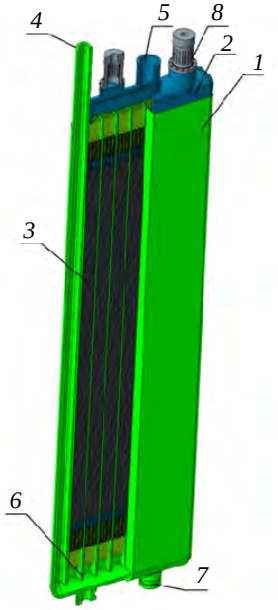

Fig. 5. General view of AC of DEMO-FNS hybrid blanket: *1* — AC case; *2* — cover of the AC case; *3* — fuel assembly with fuel rods from MA; *4* — inlet coolant pipe; *5* — outlet coolant branch pipe; *6* — inter-channel partition; *7* — the counterpart of the collet fastening of the AC to the VV; *8* — flexible mechanical supports

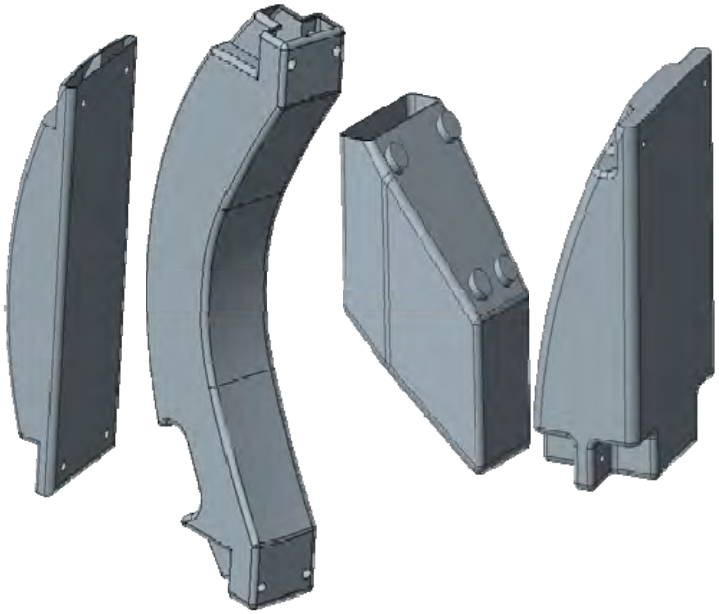

Fig. 6. General view of BZ blanket modules

0.15—0.2 MPa. Purge gas for tritium is helium with the addition of 1% hydrogen. Many coolants were consid cred during design development — liquid metal, water, water-steam mixture and supercritical CO_2 (SCO_2). Two last ones seem to be preferable due to hydrodynamics and neutron physics advantages.

Thermal scheme of energy conversion. It is assumed that DEMO-FNS facility will generate 200 MW of electric power for its own needs. Electricity production is expected with efficiency of 40%. Fig. 7 shows the thermal diagram of a two-circuit power conversion of DEMO-FNS facility with SCO_2 cooling of active core (high temperature heating).

The first circuit includes a gas loop that cools AC *3*, a heat accumulator *5*, a steam generator *6*, a primary circuit coolant blower *17*, a bypass valve *18*. The second circuit includes steam generator *6*, turbo generator *7*, condenser *8*, condensate pump *9*, low pressure regenerative heaters *10*, deaerator *12*, feed pump *13*, high pressure regenerative heaters *14*. Low-grade heat generated by the first wall *1* and the lithium-containing breeding zone *2* is transferred to the regenerative heating system through the water-to-water *11* and gas-to-water *15* heat exchangers, respectively by the pump *19* and the blower *16*. Low-temperature heat can be partially used for heating needs. In the AC, heat is generated at a coolant temperature of up to 500 ºC. The high-temperature heat of the gaseous coolant is effectively converted into electricity according to the conventional scheme of a two-circuit nuclear power plant using a steam generator and a turbine. In order to prevent the equipment from being subjected to 100% load surges, a heat accumulator is included in the thermal circuit of the facility. It is charged with excess heat during the working part of the cycle and transfers the accumulated heat to the coolant during a pause, compensating for the power failure. One of the types of heat storage devices are phase change batteries. They are based on the phenomenon of melting and crystallization of an accumulating substance, accompanied by absorption or release of latent heat of the phase transition.

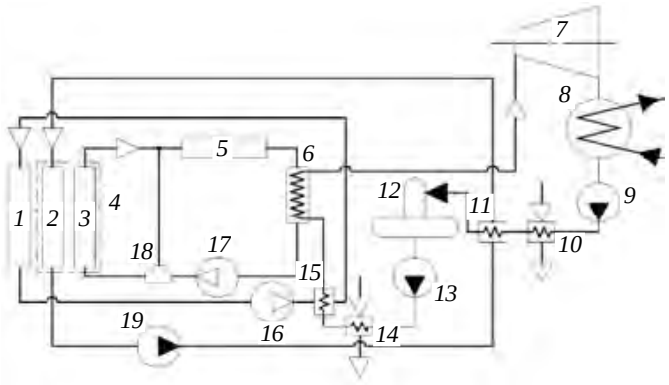

Fig. 7. Thermal diagram of a two-circuit hybrid facility: *1* — first wall; *2* — breeding zone; *3* — active core; *4* — blanket; *5* — heat accumulator; *6* — steam generator; *7* — steam turbine; *8* — condenser; *9* — condensate pump; *10* — regenerative low pressure heaters; *11* — water-to-water heat exchanger; *12* — deaerator; *13* — feed pump; *14* — high pressure regenerative heaters; *15* — gas-water heat exchanger; *16* — first wall coolant blower; *17* — active core coolant blower; *18* — bypass valve; *19* — circulation pump of the lithium-containing zone cooling

MA composition. It is assumed that in the implementation of FNS with a hybrid blanket, the materials loaded by MA will have an exposure time of 10 to 50 years. The starting fuel composition corresponds to the MA composition obtained by 2050 after reprocessing spent nuclear fuel from thermal reactors within the framework of calculating the scenario of the development of nuclear power in the Russian Federation in a system of thermal reactors with a maximum achievable power of 28.5 GW. The composition of MA considered in the calculation is presented in Table.

Composition of MA mixture, from accumulated SNF by 2050

Nuclide	Mass fraction, %
^{237}Np	30.0
^{241}Am	65.0
^{242m}Am	0.06
^{243}Am	4.5
^{243}Cm	0.02
^{244}Cm	0.42

INTEGRATION OF FFHS IN RUSSIAN NUCLEAR POWER ENGINEERING

The universal system model of nuclear power in Russia was chosen as an analysis tool. This tool was developed at JSC NIKIET under the leadership of E.V. Muraviev. The model is embedded in the USM-1 software product («Universal System Model-1» [4]) and contains the history of nuclear power in Russia and forecasts for

the future period to 2130. This program allows working with a large number of information collected on all operating, as well as commissioned, power plants and provides the ability to extrapolate data up to 2130.

In this work assessment was carried out of the impact the fusion neutron sources operation on the amount of MA in the nuclear power system, taking into account the capabilities of the fuel cycle enterprises for spent nuclear fuel (SNF) reprocessing and fuel fabrication. The following assumptions were taken into account:

— an optimistic and moderate scenario for the development of nuclear power was considered;

— modeling takes into account export of nuclear power plants and reprocessing of the SNF returned;

— SNF reprocessing - centralized and on-site;

— modeling is carried out assuming the two-component nuclear energy in Russian Federation;

— the roadmap of the project at the moment provides for the creation of three facilities in the interval from 2033 to 2055:

— DEMO-FNS (year 2033) — loading 100 t U, 20 t MA. Duty factor (DF) = 0.3; thermal power 500 MW;

— pilot FNS (year 2045) — loading: 100 t U, 20 t MA. DF = 0.8, thermal power 500 MW;

— industrial FNS (year 2055) — loading 150 t U, 40 t MA. DF = 0.95, thermal power 1365 MW.

The optimistic scenario for the development of nuclear power assumes the achievement of 115 GW of the installed capacity of nuclear power plants in Russia and 177 GW taking into account the installed capacity of exported NPPs by 2130. The moderate scenario of the development of nuclear power assumes the achievement of 67 GW of the installed capacity of nuclear power plants in Russia and 123 GW taking into account the installed capacity of exported NPPs by 2130. The results of the analyses are shown in Figs 8—11.

Optimistic scenario of nuclear power development assumes SNF reprocessing enterprises will produce 472 t of MA by 2130, of which 374 t of MA will remain, taking into account the operation of the FNSs (Fig. 10), provided that blanket is fully loaded. Moderate scenario of nuclear power development, SNF reprocessing enterprises will produce 170 t of MA by 2130, of which 72 t of MA will remain, taking into account the operation of the FNSs, provided that blanket is fully loaded.

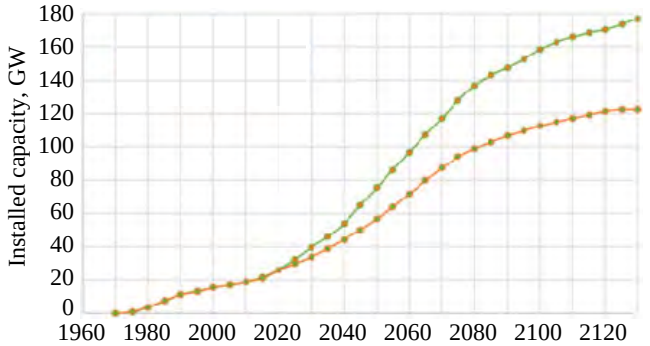

Fig. 8. Installed Power of nuclear power plants in Russia and export nuclear power: —○— — optimistic scenario; —○— — moderate scenario

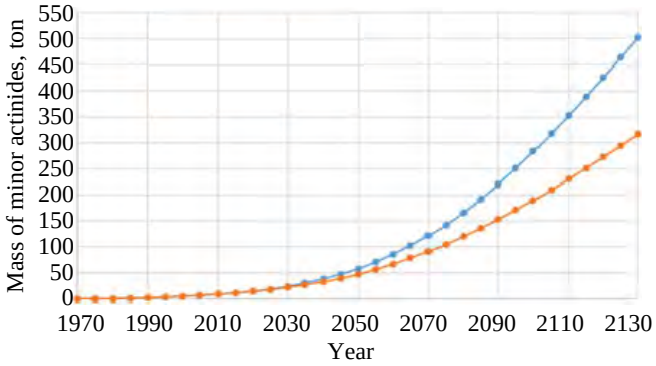

Fig. 9. Amount of accumulated MA in the nuclear energy system: —•— — optimistic scenario; —•— — moderate scenario

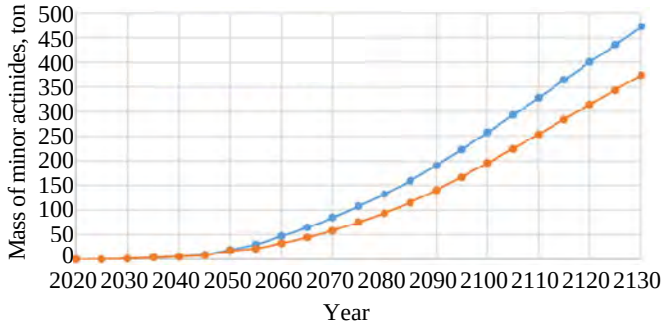

Fig. 10. Mass of allocated MA in the nuclear energy system of Russia (+export). Optimistic scenario: —•— — extracted MA; —•— — left after all FNS work

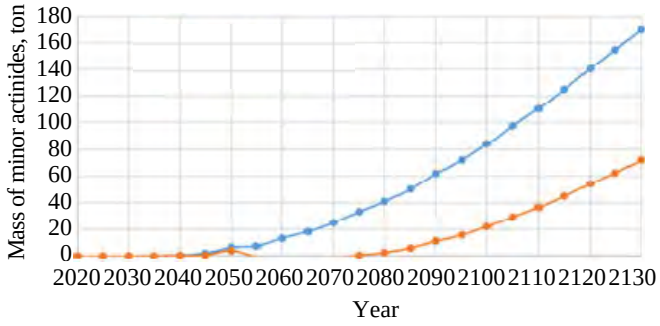

Fig. 11. Mass of allocated MA in the nuclear energy system of Russia (+export). Moderate scenario: —•— — extracted MA; —•— — left after all FNS work

From the results obtained, it can be assumed that 3—4 hybrid systems are able to ensure the balance of the produced and transmuted MA in the power system, provided that the necessary capacities for SNF reprocessing and fuel fabrication are provided. Evolution of specific activity for MA, fission products and decay products during and after single irradiation in DEMO-FNS (per 1 t of initial fuel) was analyzed (Fig. 12).

The MA activity after irradiation remains slightly higher than that initial. MA total amount decreases. 906 kgs from 26 t of very active materials are transmuted into decay the activity of which decreases much faster. The rest of MA ceases to belong to the waste class and is included in the nuclear fuel cycle, where it is gradually converted into fission products.

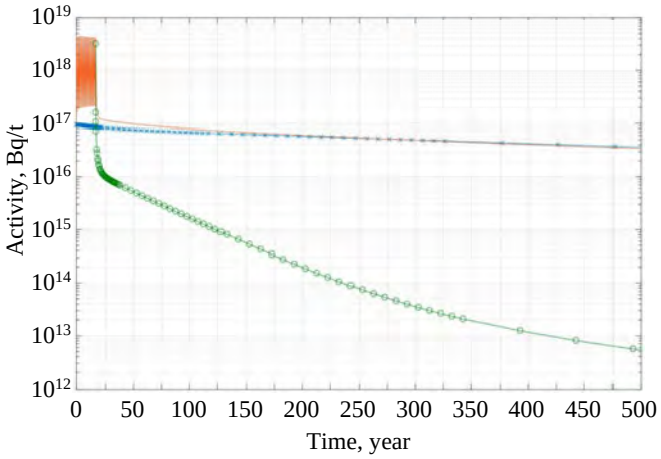

Fig. 12. Evolution of specific activity for MA, fission products and decay products during and after single irradiation in DEMO-FNS: –×– — MA without irradiation; — — irradiated w/o processing; –o– — fission and decay products after MA irradiation

Organization of DEMO-FNS project development. At the beginning of 2021, the Russian government adopted a program for the development of fusion-fission hybrid systems. Scientific management was entrusted to NRC «Kurchatov Institute». The proposal of project management structure is the following.

Project management structure (proposal):

Project office — State corporation Rosatom;

Scientific management — NRC «Kurchatov Institute»;

General designer of tokamak — D.V. Efremov Institute of Electrophysical Apparatus;

General designer of blanket and fuel cycle — Dollezhal Institute of Power Engineering;

General Designer of Materials — Bochvar High-Technology Institute for Inorganic Materials;

General project designer — JSC Eleron;

Development of the divertor — Peter the Great St. Petersburg Polytechnic University;

Heat engineering and energy conversion — Joint Institute for High Temperature RAS + Moscow Power Engineering Institute + Budker Institute of Nuclear Physics, Siberian Branch of RAS;;

Staffing — Ministry of Education + State corporation Rosatom (1200 people);

Regulator — Rostechnadzor.

CONCLUSIONS

Enabling systems of DEMO-FNS were upgraded including: vacuum vessel, radiation shield, divertor, blanket, fueling cycle, design activity was supported by R&D in neutronics, optimization of the device layout, subsystems including MS, VV, divertor, blanket and T-fuel cycle. 3 to 4 Industrial FNS systems are capable of ensuring the equilibrium of the produced and transmuted MA in the RF nuclear power system, provided that the necessary capacities for SNF reprocessing and fuel fabrication are implemented.

REFERENCES

1. **Kuteev B.V., Azizov E.A., Alexeev P.N., Ignatiev V.V., Subbotin S.A., Tsibulskiy V.F.** Development of DEMO-FNS tokamak for fusion and hybrid technologies. — Nucl. Fusion, 2015, vol. 55, p, 073035 (8 p.).
2. **Kuteev B.V., Shpanskiy Yu.S. and DEMO-FNS Team**. Status of DEMO-FNS development. — Nucl. Fusion, 2017, vol. 57, p. 076039.
3. **Shpanskiy Yu.S. and DEMO-FNS Team.** Progress in the design of the DEMO-FNS hybrid facility. — Nucl. Fusion, 2019, vol. 59, p. 076014.

4. **Muraviev E.** Generator of system models USM-1. — M.: FGUP Dollezhal RDIPE, 2008. 115 p.
5. **Kuteev B.V., Goncharov P.R.** Fusion-fission hybrid systems: yesterday, today, and tomorrow. — Fusion Science and Technology, 2020, vol. 76, p. 836—847; DOI: https://doi.org/10.1080/15361055.2020.1817701.

AUTHORS

Boris V. Kuteev, Professor, Deputy Head Tokamak Department Fusion Research Centre; NRC «Kurchatov Institute», 1, Academika Kurchatova sq., Moscow, 123182, Russia, Kuteev_BV@nrcki.ru

Yury Sergeevich Shpanskiy, Head of division, PhD Sci; NRC «Kurchatov Institute», 1, Academika Kurchatova sq., Moscow, 123182, Russia, Shpanskiy_YS@nrcki.ru

Статья поступила в редакцию 15 января 2021 г.
После доработки 16 марта 2021 г.
Принята к публикации 25 марта 2021 г.
Вопросы атомной науки и техники.
Сер. Термоядерный синтез, 2021, т. 44, вып. 2, с. 7—14.

UDC 621.039.623

TOKAMAKS WITH EXTERNAL X-POINTS: STABILITY LIMITS AND NEW PROSPECTS

S.Yu. Medvedev[1, 2], A.A. Martynov[1, 2], B.V. Kuteev[1], A.Yu. Dnestrovskiy[1], V.V. Drozdov[3]

[1]*NRC «Kurchatov Institute», Moscow, Russia*
[2]*Keldysh Institute of Applied Mathematics RAS, Moscow, Russia*
[3]*Tokamak Energy Ltd, United Kingdom*

This paper considers the prospects of outer X-point tokamak configurations that exhibit MHD stability properties similar to those of negative triangularity tokamaks. The most recent numerical studies of ideal MHD stability for outer X-point configurations provide evidence of beta limits, $\beta_N \geq 3$, and the passive stabilization of axisymmetric modes in plasmas with an elongation close to unity. Formation of an outer X-point with the help of a simple magnetic system is examined. A more general outlook on the external X-point tokamaks is offered including power exhaust, edge stability and divertor geometry.

Key words: tokamak, divertor, X-points, MHD stability.

DOI: 10.21517/0202-3822-2021-44-2-15-20

ТОКАМАКИ С ВНЕШНИМИ Х-ТОЧКАМИ: ПРЕДЕЛЫ УСТОЙЧИВОСТИ И НОВЫЕ ВОЗМОЖНОСТИ

С.Ю. Медведев[1, 2] А.А. Мартынов[1, 2], Б.В. Кутеев[1], А.Ю. Днестровский[1], В.В. Дроздов[3]

[1]*НИЦ «Курчатовский институт», Москва, Россия*
[2]*Институт прикладной математики им. М.В. Келдыша РАН, Москва, Россия*
[3]*Tokamak Energy Ltd, Великобритания*

Рассмотрены перспективы конфигураций токамаков с внешней Х-точкой, обладающих свойствами МГД-устойчивости, аналогичными конфигурациям с отрицательной треугольностью. Новые расчёты идеальной МГД-устойчивости показывают пределы по $\beta_N \geq 3$ и пассивную устойчивость осесимметричных мод для плазмы с вытянутостью, близкой к единице. Изучается формирование внешней Х-точки с помощью упрощённой магнитной системы. Обсуждаются более общие перспективы токамаков с внешней Х-точкой, включая отвод мощности, устойчивость краевой плазмы и геометрию дивертора.

Ключевые слова: токамак, дивертор, Х-точки, МГД-устойчивость.

INTRODUCTION

Power handling in magnetic plasma confinement systems is a major challenge for fusion programs around the world. The tolerance limits of steady-state and transient thermal stresses in tokamaks are constrained by different materials-engineering issues. In addition, a stationary confinement regime is required for tokamak-based reactors as well as tokamak-based fusion neutron sources. No matter how good an energy confinement is, a poorly performing power exhaust system makes a stationary machine design dysfunctional. That is why the «power exhaust first» paradigm comes up with a particular stress on the negative triangularity plasmas. Tokamak plasma with negative triangularity has been actively investigated both experimentally [1, 2] and theoretically, as part of plasma confinement [3] and demonstration reactor power exhaust studies [4]. Numerical studies of the ideal MHD stability for negative triangularity plasmas with X-points shifted to the outer side of the torus [5] confirmed that even in the absence of a magnetic well with elongated cross-section, stability limits imposed by external kink modes meet the reactor requirements for normalized beta $\beta_N \geq 3$. At the same time, plasma pressure in the pedestal near the plasma edge is about 4 times lower compared to that in conventional tokamaks with a D-shaped cross section and positive triangularity [6]. Therefore, strong ELMs (edge localized modes), unacceptable in large tokamaks, are expected to be robustly avoided.

However, some core confinement advantages observed in negative triangularity experiments, providing insight into the prospects of negative triangularity tokamaks as fusion systems, are not explained by plasma theory yet and all projections for reactor scales are very preliminary. The high energy confinement mode (H-mode) in negative triangularity diverted plasmas is still to be demonstrated. Vertical axisymmetric instabilities also pose a problem for negative triangularity plasmas with elongated cross-sections [5]. There are other new engineering challenges to overcome, including the rejection of low-stressed D-shaped toroidal field coils substituted by the coils compatible to the outer divertor with a wider separatrix wetted area at larger major radius. A more general

question arises concerning configurations that would allow a greater plasma volume to be pushed into a domain with a lower toroidal field without changing the aspect ratio (especially relevant for spherical tokamaks): is it a necessary handicap for a stationary outboard power exhaust?

Are there other tokamak plasma configurations, which are ELM-proof and power exhaust oriented and still simple and versatile? This question opens up the pathway to consider external X-points (primarily single-outer X-point) tokamak configurations that exhibit MHD stability properties similar to those of negative triangularity tokamaks. An outer X-point divertor configuration was tested as part of the JT-60 tokamak original version (1985 — November 1989, upgraded to JT-60U (1991—2010), see [7]) with limited success: the H-mode was not properly attained with a hydrogen plasma. However, even back in the 1980's it was clear that the presence of an X-point at the torus outside did not preclude high beta values [8]. The configurations with outer X-points and oblate cross-sections are also relevant to constant mean curvature surfaces providing maximal volume among all toroidal surfaces of a given area [9].

This paper presents new calculations of the free boundary equilibrium and ideal MHD stability for external X-point tokamaks. External kink-imposed limits for equilibria with prescribed boundary shapes are treated in the next section together with stability calculations for axisymmetric $n = 0$ modes. Examples of magnetic system layouts and free boundary equilibria are given. The prospects of eXternal X-point (XX) configurations are discussed.

OUTER X-POINT: MHD-STABILITY

The KINX stability code [10] was used to calculate ideal MHD-limits for a series of equilibria with a fixed boundary parameterized as follows:

$$R = R_{0X} + a_X f(\theta)\cos\theta - \delta_X \sin^2\theta,\ \ Z = Z_0 + a_X k_X \sin\theta,\ -\pi < \theta < \pi,$$
$$f(\theta) = 1 + X(1 - |\sin\theta|)^{p_X},\ \ X = k_X/p_X,\ \ k_X = k/(1 - 0.5k/p_X), \qquad (1)$$
$$a_X = a/(1 + X/2),\ R_{0X} = R_0 - a_X X/2,\ \delta_X = \delta(1 + X/2) - X/2.$$

This plasma shape features outer X-point at $R = R_0 + a$ (the 90-degree angle between separatrix branches is provided by $X = k_X/p_X$) and prescribed major and minor radii, R_0 and a, as well as elongation k and triangularity δ (Fig. 1, *a*).

Given the plasma shape and initial parallel current density and pressure profiles (Fig. 1, *b*), the limiting pressure profile was computed against the ballooning mode stability with the current density profile kept fixed, and the pressure gradient iteratively adjusted. The resulting plasma profiles are shown in Fig. 2, *a*. The norma-

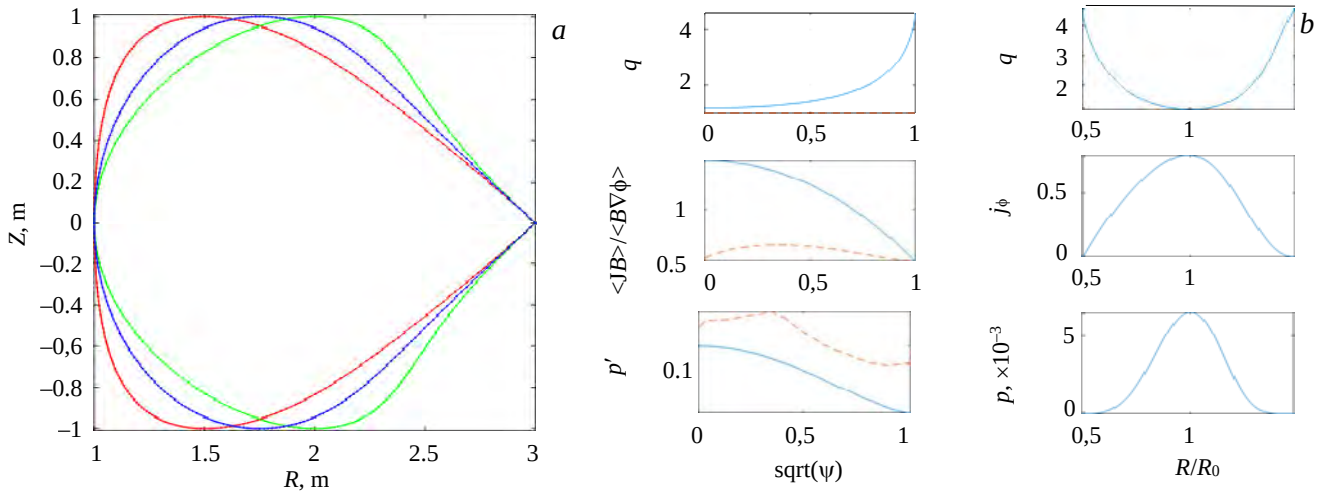

Fig. 1. Plasma shapes with outer X-point: $R_0 = 2$ m, $a = 1$ m, $k = 1$, $p_X = 2$, —— $\delta = 0$, —— $\delta = 0.25$; —— $\delta = 0.5$ (*a*); plasma profiles for the initial equilibrium with prescribed parallel current density and pressure gradient profiles: $\delta = 0$, internal inductance $l_i = 0.89$, $I_N = 0.79$, $\beta_N = 0.84$ (*b*); dashed lines show the bootstrap current in collision-less limit, the ballooning mode limiting pressure gradient and $q = 1$ in the corresponding plots

lized current $I_N = I(\text{MA})/a(\text{m})/B(\text{T}) = 0.79$ where I, a and B are plasma current, minor radius and vacuum magnetic field at the plasma center respectively, corresponds to the safety factor $q_{95} = 4.0$. The normalized beta is defined as $\beta_N = (2\mu_0 \langle p \rangle / B^2)/I_N$. One can also note a quite high bootstrap current fraction $f_b = 0.64$ (bootstrap current density in the collision-less limit is indicated by dashed line in the parallel current plot in Fig. 2, *a*) and

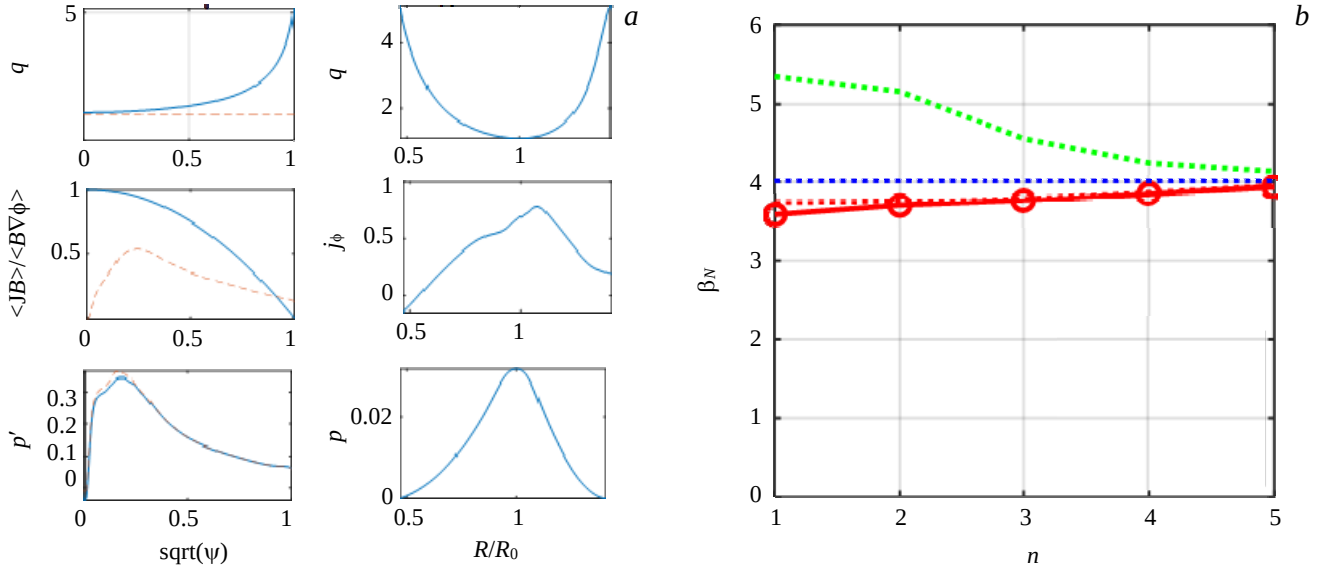

Fig. 2. Plasma profiles for the ballooning mode optimized equilibrium with prescribed parallel current: $l_i = 0.88$, $I_N = 0.79$, $\beta_N = 4.02$ (*a*); limiting values of normalized β_N for different toroidal mode numbers; no wall, conformal wall at the 1.3 *a* radius from plasma and wall at plasma boundary cases are compared: —o— no wall, ····· — wall 1.3, ····· — internal, ····· — ballooning, (*b*)

the evidence of access to the second stability region in the core (local marginally stable pressure gradient, shown in the dashed line in the corresponding plot is higher than the pressure gradient in the core). The ballooning mode optimized pressure profile was then rescaled and the marginally stable β_N was determined for external kink modes with toroidal mode numbers n from 1 to 5 (Fig. 2, *b*). The $n = 1$ mode sets the overall limit $\beta_N = 3.6$ for such an equilibrium series without wall stabilization. Only a slight increase in β_N due to the presence of ideally conducting wall indicates the strong coupling between external and internal modes (for internal modes alone, i.e. with ideally conducting wall at plasma boundary, $\beta_N > 5$ for $n = 1$).

For edge stability calculations the core pressure gradient was multiplied by 0.6 to step back from the global mode stability boundary. Hyperbolic tangent pedestal profiles were introduced (Fig. 3, *a*) and then rescaled as in

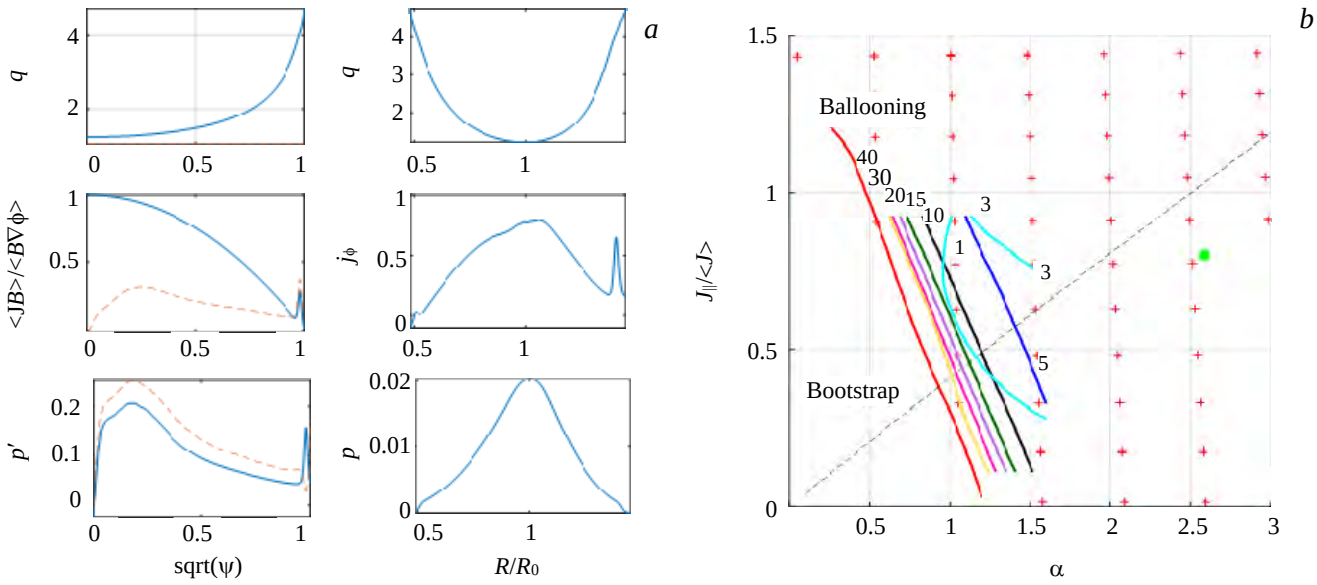

Fig. 3. Plasma profiles for the equilibrium with pedestal $\beta = 0.02$, $I_N = 0.79$, $\beta_N = 2.56$ (*a*); edge stability diagram with margins for different toroidal mode numbers and ballooning modes, red crosses correspond to ballooning unstable region, green circle — parameters of initial equilibrium with pedestal, maximal pressure gradient at $\text{sqrt}(\psi_0) = 0.98$, $J_{\text{edge}}/J = 0.071$, $p'_{\text{edge}}/p' = 0.284$ (*b*)

[11]. The calculated edge stability diagram for the rescaled pedestal profiles is presented in Fig. 3, *b*. Here α is the normalized pressure gradient and $J_\parallel/\langle J\rangle$ is the normalized parallel current density, where $\langle J\rangle = I_p/S_p$ is the average current density over plasma cross-section, they are estimated at the position of maximum pressure gradient p′ in the pedestal region. The pedestal limit is very low — a factor of 2.5 lower than in the initial equilibrium with pedestal (pedestal parameters are represented as the green circle). The scaling for pedestal height in ITER-like D-shape plasmas [11] $\beta_{p,\mathrm{ped}} \approx 3D^{3/4}/I_N^{1/3}$ gives the poloidal beta limit $\beta_{\mathrm{p,\,ped}}$ of 0.44 which is more than 5 times as large as that for the outer X-point case (0.08) for the chosen pedestal depth parameter $D = 0.07$ (in normalized poloidal flux units). The remarkable thing is that internal $n = \infty$ ballooning modes go unstable first with increasing pedestal height (approximately along the bootstrap dashed line).

Axisymmetric modes $n = 0$ are expected to be passively stable (without wall stabilization) for the XX-equilibria with an elongation of 1. This is indeed the case of the equilibrium with plasma profiles shown in Fig. 1, *b* with the pressure gradient going to zero at the plasma boundary. However, the horizontal mode is destabilized for the equilibrium with rescaled ballooning mode optimized pressure gradient (see Fig. 2, *a*), which is finite at the boundary. The corresponding mode is localized in the X-point vicinity and there is a kind of a beta limit for such a mode close to $\beta_N = 4.1$ for passive stability.

OUTER X-POINT: MAGNETIC SYSTEM AND SCENARIOS

In this section some examples of magnetic systems capable of sustaining the XX free boundary equilibria are demonstrated. The poloidal field (PF) coils and vacuum chamber layout for the DEMO-FNS [11] are used for reference. An additional divertor coil lying in the equatorial plane is needed to generate the outer X-point. The numeric studies of the free boundary equilibrium using the SPIDER code have shown that such a coil, accompanied by two closely adjacent pushing coils, provides a very economical PF layout in terms of the sum of the PF coils' absolute currents to plasma current ratio $\sum_i |I_{\mathrm{PF},i}|/I_p$, which is just above 1 in the case of the X-point lying close to the divertor coil (Fig. 4, *a*).

The farther the X-point is from the divertor coil, the larger is the $\sum_i |I_{PF,i}|/I_p$ current ratio (Fig. 4. *b*). Of course, a solenoid is needed to support the plasma current drive in addition to a group of the divertor coils. In preliminary scenarios a gradual increase of the divertor coil current produces the outer X-point starting from a limiter plasma inboard the vacuum vessel. Such a magnetic system looks quite simplistic and potentially provides a large volume available above and below the plasma equator, but does not seem

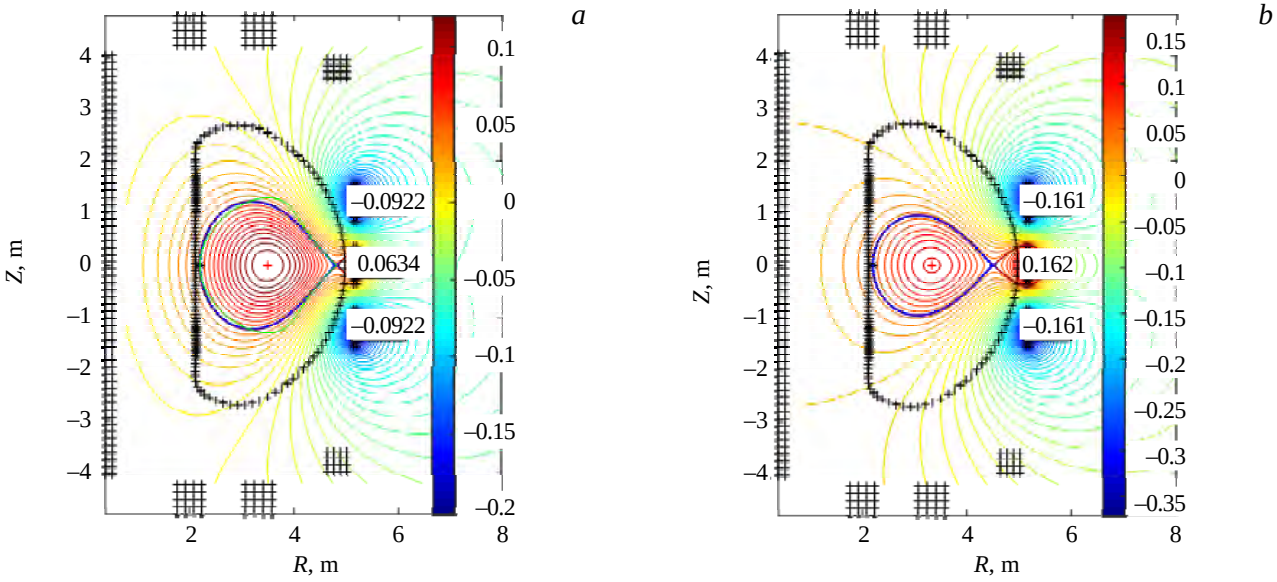

Fig. 4. Poloidal flux contours for free boundary equilibria sustained by the currents in three outboard PF coils: *a* — plasma boundary fitted to the XX shape (green contour, δ = 0) with X-point radius 4.8 m, current ratio 1.55; *b* — X-point radius 4.5 m, current ratio 3.0. Plasma current 0.16 MA, PF coil currents in MA are shown, color bar for poloidal flux in Wb/(2π)

compatible with neural beam injectors (NBI). More flexibility and volume would also be desirable for the divektor control. That is why an array of horizontal coils was tried out as an alternative option (Fig. 5). While being quite flexible (and also allowing snowflake divertor, Fig. 5, *c*) and seemingly better NBI compatible, this configuration requires much larger PF current due to divertor coils distanced farther away from the plasma. Moreover, the plasma scenario and control look more complicated. Let us note that for the case with the X-point displaced from the equatorial plane (see Fig. 5, *b*) not only the PF coils but also divertor structures can be removed from the beam path. More realistic scenario calculations are planned using the ASTRA/SPIDER plasma evolution code [13].

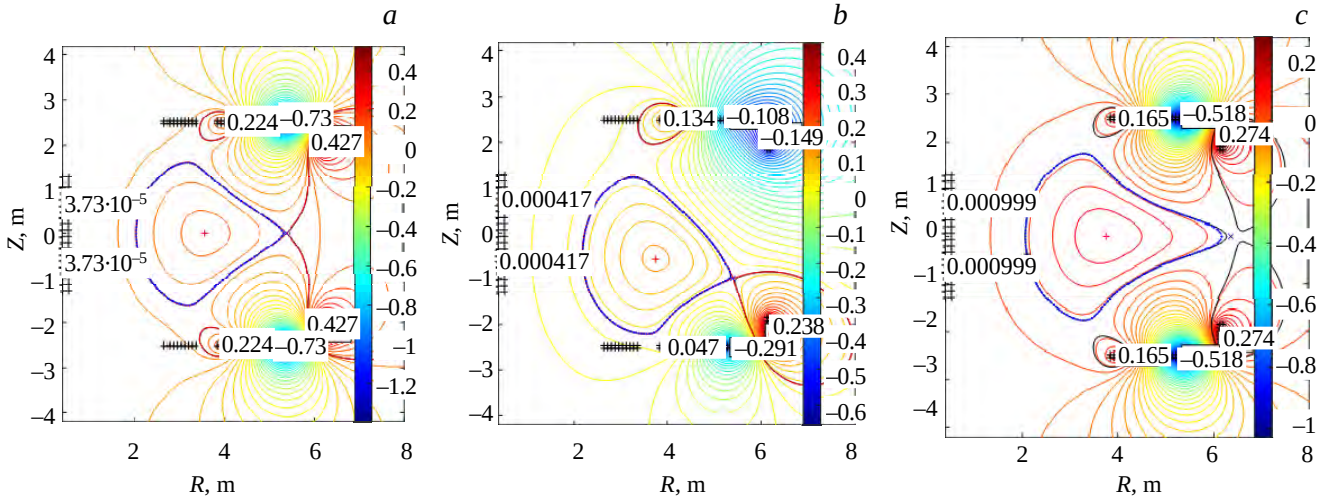

Fig. 5. Poloidal flux contours for free boundary equilibria sustained by horizontal arrays of PF coils: *a* — X-point radius 5.4 m, current ratio 17; *b* — X-point coordinates (5.4 m, –1 m), current ratio 6; *c* — X-point radius 6.4 m, current ratio 12. Plasma current 0.16 MA, PF coil currents in MA are shown, colorbar for poloidal flux in Wb/(2π)

DISCUSSION

In terms of MHD-stability, the main advantage of the XX configurations is a robust low pedestal limit set by internal localized modes and the lack of access to the second stability region. This can give rise to soft edge plasma limits, imposed by an electro-magnetic turbulence or, at least, by much milder ELM crashes. However the second stability access is still possible in the core of an elongated positive triangularity plasma and the pressure-driven external kink limit β_N exceeds 3. Axisymmetric $n = 0$ modes can manifest themselves as coupled vertical/horizontal modes featuring a destabilizing pressure gradient near the edge.

Considering XX configurations as an alternative divertor solution, one can notice a simple magnetic system and possible NBI compatible flexible configurations with easier outer divertor access and better pumping conductance if the X-point is displaced from the equatorial plane. Anyway, larger outer X-point major radius for separatrix wetted area favors the power exhaust capability combined with a stationary — no ELMs — confinement. At the same time the main plasma bulk can reside in a higher B domain leaving the shaping coils in lower magnetic field region, e.g. making NbTi superconductor applicable for the shaping coils. Key remaining questions relate to energy confinement properties of the discussed configurations. As there are favorable indications for negative triangularity in terms of core confinement, the «JT-60 curse» for the confinement in XX configurations could be overcome: it might be time for the XX-experiment second try.

REFERENCES

1. **Camenen Y. et al.** — Nucl. Fusion, 2007, vol. 47, p. 510.
2. **Austin M.E. et al.** — Phys. Rev. Lett., 2019. vol. 122, p. 115001.
3. **Fontana M. et al.** — Nucl. Fusion, 2018, vol. 58, p. 024002.
4. **Kikuchi M. et al.** — Nucl. Fusion, 2019, vol. 59, p. 056017.
5. **Medvedev S.Yu. et al.** — Nucl. Fusion, 2015, vol. 55, p. 063013.

6. **Merle A. et al.** — Plasma Phys. Control. Fusion, 2017, vol. 59, p. 104001.
7. **Kikuchi M. et al.** — Eur. Phys. J. H, 2018, https://doi.org/10.1140/epjh/e2018-90054-2.
8. **Ozeki T. et al.** — Nucl. Fusion, 1988, vol. 28, p. 1861.
9. **Ilgisonis V.I., Skovoroda A.A., Sorokina E.A.** — Physics of Atomic Nuclei, 2017, vol. 80, № 7, p. 1307—1312. (Original Russian Text 2016, published in Voprosy Atomnoi Nauki i Tekhniki, Seriya: Termoyadernyi Sintez, 2016, vol. 39, № 1, p. 22—29).
10. **Degtyarev L., Martynov A., Medvedev S., Troyon F., Villard L., Gruber R.** — Comput. Phys. Comm., 1997, vol. 103, p. 10—27.
11. **Medvedev S.Yu. et al.** — Plasma Phys. Rep., 2016, vol. 42, p. 472—485.
12. **Shpanskiy Yu.S. and the DEMO-FNS Project Team.** — Nucl. Fusion, 2019, vol. 59, p**.** 076014.
13. **Dnestrovskiy A.Yu. et al.** — In: Proc. 45th EPS Conf. Plasma Phys., 2018, vol. 42A, P4.1080.

AUTHORS

Sergey Yurievich Medvedev, PhD in physics and mathematics, Leading Researcher, Keldysh Institute of Applied Mathematics RAS, 125047 Moscow, Miusskaya sq. 4, Russia; Leading Engineer, NRC «Kurchatov Institute», 123182 Moscow, pl. Academician Kurchatova 1, Russia, Medvedevsyu@keldysh.ru

Alexander Alexandrovich Martynov, PhD in physics and mathematics, Senior Researcher, Keldysh Institute of Applied Mathematics RAS, 125047 Moscow, Miusskaya sq. 4, Russia; Leading Engineer, NRC «Kurchatov Institute», 123182 Moscow, pl. Academician Kurchatova 1, Russia, Martynov22@gmail.com

Boris Vasilievich Kuteev, deputy head of the Department for Hybrid Systems, Doctor of Physics and Mathematics; NRC «Kurchatov Institute», 123182 Moscow, pl. Academician Kurchatov 1, Russia, Kuteev_BV@nrcki.r

Alexey Yurievich Dnestrovskiy, Leading Engineer, PhD in physics and mathematics; NRC «Kurchatov Institute», 123182 Moscow, pl. Academician Kurchatova 1, Russia, Dnestrov0@gmail.com

Vladimir Victorovich Drozdov, PhD in physics and mathematics, Scientific Consultant, Tokamak Energy Ltd, 173 Brook Drive Milton Park, Oxfordshire OX14 4SD, United Kingdom, VVDrozdov0712@gmail.com

Статья поступила в редакцию 15 января 2021 г.
После доработки 16 марта 2021 г.
Принята к публикации 25 марта 2021 г.
Вопросы атомной науки и техники.
Сер. Термоядерный синтез, 2021, т. 44, вып. 2, с. 15—20.

UDC 621.039.54; 621.039.6

POTENTIAL ROLE OF FUSION NEUTRON SOURCE IN NUCLEAR POWER SYSTEMS

G.G. Kulikov, A.N. Shmelev, V.A. Apse, E.G. Kulikov

National Research Nuclear University MEPhI, Moscow, Russia

The paper analyzes the possibility of integrating hybrid thermonuclear reactors (HTRs) into existing nuclear power systems. This is supposed to involve the production of non-traditional nuclear fuel in a D—T-plasma operated HTR with a thorium blanket. Non-traditional fuel to be produced is peculiar in that it contains in significant amounts of rare isotopes, such as ^{231}Pa and ^{232}U, alongside the traditional ^{233}U. High-energy (14.1 MeV) thermonuclear neutrons have a unique ability to promote the accumulation of significant amounts of ^{231}Pa and ^{232}U via threshold (*n*, 2*n*)- and (*n*, 3*n*)-reactions. Non-traditional fuel compositions for nuclear power thermal reactors (the most common nuclear reactor class in the world), hold promise due to the following factors. As is known, the neutron balances for reactors fueled with ^{235}U are better (in terms of the breeding ratio enhancement) than for reactors fueled with ^{233}U or reactor-grade plutonium. A better neutron balance is likely to translate into higher fuel breeding ratios and help ease the thermal reactors' fuel self-sustainability problem. Because ^{231}Pa and ^{232}U are fertile and moderately fissionable nuclides, they can stabilize the time-dependent behavior of the thermal reactor power and prolonging a thermal reactor's lifetime through higher fuel burnup. Being a strong α-emitter, ^{232}U can be used to control unauthorized use of ^{233}U-based nuclear explosives and thereby contribute to nuclear non-proliferation. All this suggests that D—T-plasma operated HTRs with a thorium blanket can be integrated into nuclear power systems to generate very promising non-traditional fuel compositions for conventional nuclear power reactors.

Key words: hybrid thermonuclear reactor, fusion neutron source, thorium blanket, ^{231}Pa and ^{232}U.

DOI: 10.21517/0202-3822-2021-44-2-21-26

ПОТЕНЦИАЛЬНАЯ РОЛЬ ТЕРМОЯДЕРНОГО НЕЙТРОННОГО ИСТОЧНИКА В ЯДЕРНЫХ ЭНЕРГЕТИЧЕСКИХ СИСТЕМАХ

Г.Г. Куликов, А.Н. Шмелев, В.А. Апсэ, Е.Г. Куликов

Национальный исследовательский ядерный университет «МИФИ», Москва, Россия

Анализируется возможность включения гибридных термоядерных реакторов (ГТР) в существующие ядерные энергетические системы. Предлагается наработка нетрадиционного ядерного топлива в ториевом бланкете ГТР на (D—T)-плазме. Особенность нарабатываемого нетрадиционного топлива заключается в значительном количестве таких редких изотопов, как ^{231}Pa и ^{232}U. Только термоядерные нейтроны высоких энергий (14,1 МэВ) могут обеспечить накопление значительных количеств ^{231}Pa и ^{232}U через пороговые (*n*, 2*n*)- и (*n*, 3*n*)-реакции. Изотопы ^{231}Pa и ^{232}U, являясь сырьевыми и умеренно делящимися нуклидами, способны стабилизировать размножающие свойства ядерного топлива и обеспечить достижение сверхглубокого выгорания. Изотоп ^{232}U, являясь интенсивным источником α-частиц, способен предотвратить любые попытки несанкционированного использования ^{233}U в оружейных целях, т.е. ^{232}U может усилить режим ядерного нераспространения. Таким образом, ГТР на (D—T)-плазме с ториевым бланкетом можно использовать для наработки перспективных топливных композиций для традиционных ядерных энергетических реакторов.

Ключевые слова: гибридный термоядерный реактор, источник термоядерных нейтронов, ториевый бланкет, ^{231}Pa, ^{232}U.

INTRODUCTION

Thermonuclear reactors (TRs) have gone through several development stages. Initially, they were looked upon as just sources of energy, to be generated solely by fusion reactions between light isotopes. Such TRs are dubbed «pure TRs». Their attractiveness is based on the following:

— safety, as there is no way for uncontrolled power excursion (possible in fission reactors) to occur;

— unlimited fuel supply, especially when using heavy hydrogen isotopes;

— no high activity, long-lived nuclear waste (the only issue is neutron-induced radioactivity in fusion structural materials).

However, there are many physical and engineering challenges in implementing stand-alone TRs. This gave rise to the idea of combining fusion and fission into a nuclear facility with a fusion plasma core surrounded by a blanket of heavy fissile materials (the so-called «hybrid thermonuclear reactor», HTR). In a HTR, thermonuclear plasma acts mainly as a source of neutrons for the blanket, where most of is generated. The blanket operates as a subcritical system, which allows the pure TR's first fundamental strength, safety, to be preserved. Unfortu-

nately, the TR's two other strengths, the unlimited fuel supply and absence of radioactive wastes, are lost in the HTR. However, as in the case of a pure TR, the development of a HTR is confronted with many physical and engineering obstacles. They are related to the HTR concept, according to which most of energy is generated by fission reactions in the HTR blanket, while thermonuclear fusion reactions play the role of an energy release control tool, needed to provide safe HTR operation and enable a practically instant shutdown whenever need arises.

The same function in nuclear fission reactors is performed by numerous control and safety systems. To sum it up, combining fusion and fission in one power facility is a daunting task. Indeed, current HTR projects are lagging behind nuclear power reactors in terms of economic competitiveness.

In the past few years, HTR projects have been developed, in which hybrids are used for breeding fissile materials for nuclear power reactors [1, 2] rather than energy generation. In such projects, a HTR is used as a fusion neutron source (FNS), and its blanket has to be filled with fertile materials, such as natural uranium, depleted uranium and natural thorium.

Historically, the world nuclear power industry has been using natural uranium as a primary source of fuel. Therefore, blankets of natural or depleted uranium have been traditionally used to breed plutonium. From the viewpoint of neutron physics, plutonium the best choice as material for fast breeder reactors (FBRs), which, according to Russia's 2018 Strategy for Nuclear Power Development throughout this century are one of the pillars of the nuclear power industry in this country [3]. However, it should be kept in mind that thermal reactors, primarily light-water reactors (LWRs), are today the most common nuclear power generating units in the world, including Russia [4]. Although intensely developing and advancing, FBRs are less effective economically than thermal reactors. Strategy-2018 includes the scenarios of a two-component nuclear power system consisting mainly of thermal reactors, supplemented by FBRs. Unfortunately, present-day thermal reactors have fuel breeding ratios (BRs) of about 0.5, which prevents them from being self-contained and generating their own fuel. Two advanced thermal reactors have been implemented, namely, an LWR with a controlled neutron spectrum and the SLWR with supercritical-pressure light water-cooled reactors (SCLWR). Their BRs are 0.6—0.7 and 0.8—0.9 respectively. As one can see, thermal reactors need to add just a little to their BRs to catch up with FBRs (whose typical BRs are ≥ 1). It is this small deficiency that can be accommodated by using the FNS blanket.

As is known, isotope ^{233}U is more effective than ^{235}U and plutonium in terms of maintaining the thermal reactor neutron balance. ^{233}U can accumulate in the FNS thorium blanket. Unfortunately, natural thorium, like rare-earth elements, is strongly dispersed in the natural environment, and there are no Th-rich ores or deposits. So far, natural thorium is recovered at a low cost as a by-product (even waste) of rare-earth mining. Russia's natural thorium inventory is estimated at 6,000 metric tons (MT) [5], roughly equivalent to Russia's 2-year production of natural uranium. Natural thorium can be used as a fertile material and converted to fissile isotope ^{233}U in the FNS thorium blanket.

Let us consider a scenario where thorium is no longer mined, and only a limited thorium inventory of 6,000 MT is available. In these circumstances, only a small part (say, one-tenth, or around 600 MT) of this inventory can be converted into ^{233}U, as the rest would be required to fill the FNS blanket.

As is known, the electrical power of Russian nuclear power plants (NPPs) totalled around 30 GW(e) installed capacity in 2020. A 1 GW(e) thermal reactor burns 1 MT of fissile isotopes annually and accumulates 1 MT of fission products. Consequently, Russian NPPs' total demand for ^{233}U can be ~30 MT a year. Conclusion: Russia's current natural thorium inventory is sufficient to supply all the country's NPPs with ^{233}U for 20 years — even if the «open» or «once-through» nuclear fuel cycle is used. If a system consisting of thermal reactors with a BR of about 0.5 and using a closed fuel cycle is employed, the available inventory is enough to meet an up to 40-years' demand. If, in accordance with Strategy-2018, Russia switches over to the closed nuclear fuel cycle with SCLWRs (BR ~ 0.8—0.9) introduced in a span of 25—35 years, then this inventory will last for 100—200 years. One SCLWR will consume ~100—200 kg Th per GW(e) year**.** This means that only 3—6 MT of natural thorium will have to be mined annually to supply Russian NPPs with their total installed capacity of ~30 GW(e). This seems practicable, considering that Russia' thorium mining capacities will only account for 0.1—0.2% of its current uranium mining capacities. With Russian NPPs' total installed capacity tripling to 90—100 GW(e) in accordance with Strategy-2018, the total demands for mined thorium will increase to

9—18 MT a year by the end of the century. In that case, thorium production will be 0.3—0.6% of the current uranium production, which, again, seems accomplishable.

In regard to the potential use of thorium-based fuel cycles to support future requirements of nuclear power systems, it is appropriate to highlight the following two specific aspects.

The first has to do with the required scale of deploying thorium mining capacities and infrastructure. The example of the small thorium inventory in Krasnoufimsk, Russia, demonstrates, how salient the impact of tapping this source could be, even at an early stage, and how the first steps in harnessing the thorium potential can be made. It is noteworthy that Russia's available thorium inventory is insufficient for loading thermal and fast nuclear power reactor cores, but adequate for filling thermonuclear reactor blankets.

The second important aspect is related to international affairs. BRICS, the association of five major emerging economies (Brazil, Russia, India, China and South Africa) was founded in 2006 at Russia's initiative to coordinate economic activities of the member nations. Brazil, India and South Africa have large geological reserves of natural thorium [6, 7]. Brazil and India use their well-explored reserves of natural thorium and rare-earth elements mainly to recover rare-earth elements, while thorium is produced as a by-product and put in storage for future use. In this context, Russia benefits from its membership in the BRICS, as this opens up the opportunity for it to incorporate imported thorium into its nuclear fuel cycle without conducting exploration and establishing costly mining and processing facilities. Such cooperation can be used as a way to save efforts needed to incorporate natural thorium resources into nuclear power systems of Russia and other BRICS countries within the framework of international collaboration.

SELECTION OF PLASMA COMPOSITION FOR FUSION NEUTRON SOURCE

The following nuclear reactions can take place in thermonuclear D—D-plasma:

$$D + T \rightarrow {}^4He + n\ (14.1\ MeV);$$

$$D + {}^3He \rightarrow {}^4He + p;$$

$$D + D \rightarrow 50\%: {}^3He + n\ (2.5\ MeV);$$

$$D + D \rightarrow 50\%: T + p.$$

Fusion of two deuterium nuclei can produce, with a 50% probability, either one neutron with a relatively high energy (2.5 MeV), plus one ^{3}He nucleus, or one tritium nucleus plus one proton. The produced nuclei (^{3}He and tritium) are highly likely to enter into concomitant thermonuclear reactions with deuterium nuclei. This is due to the fact that the probability of the D—^{3}He- and the D—T-reactions is one and two orders of magnitude, respectively, higher than for the original D—D-reaction. The micro cross-sections of these three thermonuclear reactions are shown in Fig. 1 as functions of the energy of D, ^{3}He and T relative motions. The micro cross-sections of the ^{235}U fission reaction as a function of neutron energy are presented in the same figure for comparison.

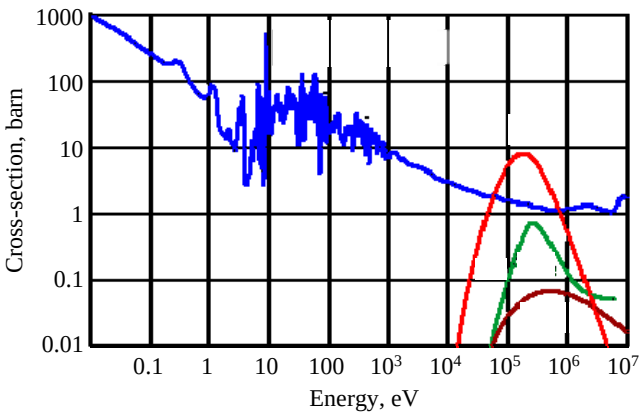

Fig. 1. Micro cross-sections of the ^{235}U fission reaction as a function of neutron energy and micro cross-sections of three thermonuclear reactions of light nuclei as functions of the energy of D, ^{3}He and T relative motions: — — — ^{235}U fussion, — — — D—T, — — — D—^{3}H, — — — D—D

One basic D—D-reaction and two concomitant reactions can produce 0.5 neutron (of 2.5 MeV) and 0.5 neutron (of 14.1 MeV) on average. The density of plasma is seven orders of magnitude lower than typically for solid materials. The magnetic field used for plasma confinement is unable to retain uncharged neutrons. That is why thermonuclear neutrons are highly likely to escape from both plasma and the FNS. In the case of D—T-plasma, a single D—T-reaction produces one high-energy (14.1 MeV) neutron.

Using D—T-plasma instead of D—D-plasma seems appropriate for the following two reasons. Firstly, the micro cross-sections of the D—T-reaction are two orders of magnitude larger than for the D—D-reactions. This

suggests that the construction and starting up of a thermonuclear reactor operated with D—T-plasma would be much easier. Secondly, the D—T-reactions can emit twice as many high-energy (14.1 MeV) neutrons than D—D-reactions. These high-energy neutrons are able to produce, by neutron irradiation of natural thorium in the HTR blanket, one 'traditional' fissile isotope ^{233}U and two 'non-traditional' but very promising isotopes ^{231}Pa and ^{232}U. As shown in [8—10], ^{231}Pa can stabilize nuclear fuel's neutron-multiplying properties (the result being a deeper fuel burnup and a longer fuel lifetime), while ^{232}U can provide proliferation protection of ^{233}U-based fuel compositions.

When using D—T-plasma, HTR operators have to handle radioactive tritium (whose half-life is 12.3 years). So, tritium remote handling technologies must be worked out and implemented. Tritium does not exist in the nature because of its relatively short half-life. Significant tritium quantities can be produced by neutron irradiation of Li-containing materials in HTR via the ^{6}Li(n, α)T-reaction.

Because one tritium nucleus is consumed in the ^{6}Li(n, α)T-reaction to breed one high-energy neutron, and because another neutron is needed to produce a new tritium nucleus via the same reaction, one may get a wrong impression that all thermonuclear neutrons need to be used to replenishing the burnt tritium, and that there are no neutrons left to produce new fissile materials. In reality, high-energy thermonuclear neutrons can be intensely multiplied by threshold (n, 2n)- and (n, 3n)-reactions with a multiplication factor of about 1.5. Reproduction of one tritium nucleus requires slightly above one neutron (roughly, 1.06 neutrons with account taken of reprocessing losses and tritium's short half-life). According to approximate evaluations, about 0.15 neutrons will be absorbed by HTR coolant, neutron moderator, structural materials, and lost as a neutron leakage. So, only 0.3 neutrons from one D—T-reaction may be used to produce new fissile materials.

The FBRs' breeding ratio reaches unity, i.e. excessive neutron amount in the FBR is three-fold larger than in a HTR operated with D—T-plasma. However, one excessive neutron in the FBR is produced by fission reaction with an energy release of 200 MeV. One D—T-reaction in HTR can only produce 0.3 excessive neutrons. One D—T-reaction releases some 21 MeV of energy (roughly, ten times lower), with account taken of γ-rays and the capture of radiative neutrons in the Th-blanket. If the FBR and HTR thermal powers are the same, then a D—T-plasma-operated HTR can produce more (3x) fissile than FBR.

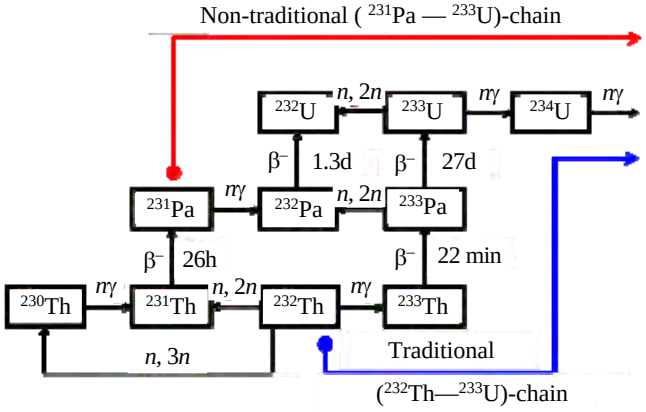

Fig. 2. Chains of isotopic transformations in the fuel (Th—U)-cycle

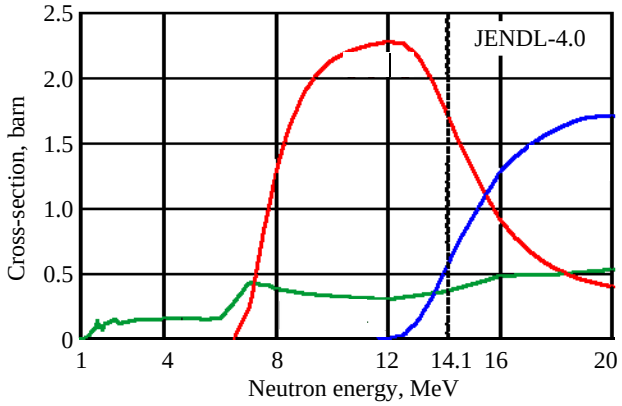

Fig. 3. Micro-cross-sections of fission, (n, 2n)- and (n, 3n)-reactions involving ^{232}Th: – – — (n, 3n), – – — (n, 2n), – – — fission

The following facts are worthy of note. Mean neutron energy in the FBR is around 0.1 MeV. Mean neutron energy in the spectrum of fission neutrons is about 2 MeV. Mean energy of spallation neutrons in accelerator-driven facilities varies from 1 to 10 MeV. Therefore, thermonuclear neutrons emitted by D—T-plasma in HTR have the highest energy (14.1 MeV). This huge energy potential can be employed to produce «non-traditional» isotope compositions containing ^{233}U, ^{231}Pa and ^{232}U, intended for introduction into fresh fuel, to be used in traditional thermal reactors. Shown in Fig. 2 are the key, most effective, chains of isotopic transformations associated with neutron irradiation of the thorium blanket.

As is seen, isotopes ^{231}Pa and ^{232}U are produced by threshold (n, 2n)- and (n, 3n)-reactions, which can only be initiated by high-energy neutrons. Micro cross-sections of ^{232}Th(n, f), ^{232}Th(n, 2n)- and ^{232}Th(n, 3n)-reactions are shown in Fig. 3.

As indicated in the figure, the probability of necessary threshold (n, 2n)- and (n, 3n)-reactions in the high-energy neutron region (above 7 MeV) is larger than for fission reactions. Then it is possible to produce non-traditional isotopes with little heat genera-

tion in the thorium blanket, which is important from the blanket engineering prospective (this may substantially facilitate the development and implementation of HTR projects). Thus, high-energy (14.1 MeV) thermonuclear neutrons emitted by D—T-plasma make it possible in principle to produce non-traditional isotopes. As is known, ^{232}Th is a threshold fissile isotope (Fig. 4). That is why slow neutrons will be mainly absorbed by ^{232}Th to produce ^{233}U after two relatively short β-decays (see Fig. 2).

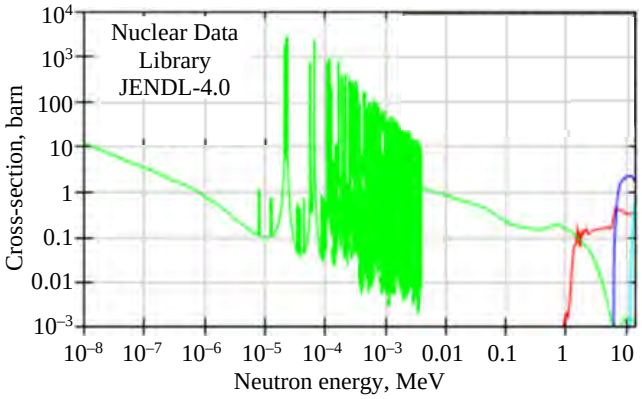

Fig. 4. Micro cross-sections of ^{232}Th: — — — (n, 3n)-reaction, — — — (n, 2n)-reaction, — — — radiative capture, — — — fission

The micro cross-sections of neutron ^{232}Th reactions within the energy range from 0.01 eV to 14.1 MeV are shown in Fig. 4 [11, 12]. As is seen, threshold (n, 2n)- and (n, 3n)-reactions dominate in the high-energy (above 7 MeV) neutron region, and fission reactions come to prominence in the 2—7 MeV energy range, while the radiative neutron capture comes to the fore in the lower energy region. To sum it up, firstly, non-traditional isotopes ^{231}Pa and ^{232}U can only be produced by high-energy (7—14 MeV) neutrons. Secondly, fission reaction only plays a significant role in a rather narrow energy range (2—7 MeV). Fission reactions can occur with a relatively low probability because fission cross-sections are at the level of decimal barn fractions, which are lower than cross-sections of threshold (n, 2n)-, (n, 3n)-reactions and those of radiative neutron capture reactions by an order of magnitude. As a result, heat generation rate in the Th-blanket will be very small. Low-intensity heat generation can simplify the requirements for the thermal-technical equipment needed for heat utilization or removal. Thirdly, slow neutrons (with energies below 2 MeV) can be used to produce fissile isotope ^{233}U, a nuclide better suited for thermal reactors than ^{235}U (from the ‘neutron budget’ viewpoint).

CONCLUSION

If a thorium blanket is used in HTRs to produce fissile materials for nuclear power reactors, then Russia’s available inventories of natural thorium are sufficient to supply national NPPs, even operated under the open fuel cycle conditions, for a long period of time (up to 20 years).

If SCLWRs with a breeding ratio of 0.8—0.9 come into play by the end of the century and operate under the closed fuel cycle conditions, then the demands for mined thorium from Russian NPPs (whose total installed electrical capacity is expected to increase three-fold) will be 0.3—0.6% of the current uranium production.

It seems reasonable to use D—T-plasma in HTRs because, firstly, it may be relatively easily ignited, and, secondly, it can act as a very productive source of high-energy neutrons, which are able to produce non-traditional isotope compositions through threshold (n, 2n)- and (n, 3n)-reactions.

An HTR operated with D—T-plasma is able to produce larger (3x) amounts of fissile materials than the FBR of a similar thermal power.

The reported study was funded by RFBR, project number 19-29-02006.

REFERENCES

1. **Велихов Е.П., Давиденко В.Д., Цибульский В.Ф.** Заметки о будущем ядерной энергетики. — ВАНТ. Сер. Термоядерный синтез, 2019, т. 42, вып. 1, с. 5.
2. **Blandinsky V.Yu., Davidenko V.D., Zinchenko A.S., Moryakov A.V., Rodionova E.V., Chukbar B.K., Tsibulsky V.F.** Power perspectives of thermonuclear fusion. — Atomic Energy, 2020, vol. 128(1), p. 37—40.
3. **Strategy** for Development of Russian Nuclear Power System up to 2050 and, in Perspective, up to 2100—2018. Moscow: the State Corporation Rosatom.
4. **Andrianov A.A., Kuptsov I.S., Osipova T.A., Andrianova O.N., Utyanskaya T.V.** Optimization models of a two-component nuclear energy system with thermal and fast reactors in a closed nuclear fuel cycle. — Nuclear Energy and Technology, 2019, vol. 5(1), p. 39—45.
5. **https:**//smart-lab.ru/blog/241711.php.
6. **Katz G., Seaborg G., Morss L.** Chemistry of Actinides. Moscow, 1991, Mir.
7. **World** Thorium Occurrences, Deposits and Resources, 2019, IAEA-TECDOC-1877.

8. **Kulikov G.G., Shmelev A.N., Geraskin N.I., Kulikov E.G., Apse V.A.** Advanced nuclear fuel cycle for the rf using actinides breeding in thorium blankets of fusion neutron source. — Nuclear Energy and Technology, 2016, vol. 2, p. 147—150.
9. **Shmelev A.N., Kulikov G.G.** On the role of fusion neutron source with thorium blanket in forming the nuclide composition of the nuclear fuel cycle of the Russian Federation. — Physics of Atomic Nuclei, 2016, vol. 79, p. 1508—1512.
10. **Kulikov G.G., Shmelev A.N., Kulikov E.G., Apse V.A.** Proliferation-protected, ultra-high burn-up reactor fuel produced in the thorium blanket of a fusion neutron source. — In: GLOBAL 2019 — International Nuclear Fuel Cycle Conference and TOP FUEL 2019 — Light Water Reactor Fuel Performance Conference, p. 1088—1092.
11. **Soppera N., Bossant M., Dupont E.** JANIS 4: an improved version of the NEA java-based nuclear data information system. — Nuclear Data Sheets, 2014, vol. 120, p. 294—296.
12. **Shibata K. et al.** 2011 JENDL-4.0: a new library for nuclear science and engineering. — J. of Nuclear Science and Technology, 2020, vol. 48, p. 1—30.

AUTHORS

Gennadij Genrichovich Kulikov, leading engineer, PhD in Physics & Mathematics; National Research Nuclear Univ. MEPhI, 115409 Moscow, Kashirskoe sh. 31, Russia, ggkulikov@mephi.ru

Anatolij Nikolaevich Shmelev, professor, Dr. of Science Degree in Engineering; National Research Nuclear Univ. MEPhI, 115409 Moscow, Kashirskoe sh. 31, Russia, shmelan@mail.ru

Vladimir Aleksandrovich Apse, engineer, PhD in Engineering; National Research Nuclear Univ. MEPhI, 115409 Moscow, Kashirskoe sh. 31, Russia, apseva@mail.ru

Evgenij Genrichovich Kulikov, Associate Professor, PhD in Engineering; National Research Nuclear Univ. MEPhI, 115409 Moscow, Kashirskoe sh. 31, Russia, egkulikov@mephi.ru

Статья поступила в редакцию 15 января 2021 г.
После доработки 16 марта 2021 г.
Принята к публикации 25 марта 2021 г.
Вопросы атомной науки и техники.
Сер. Термоядерный синтез, 2021, т. 44, вып. 2, с. 21—26.

UDC 621.039.674.3

SUBCRITICALITY MONITORING IN FUSION-FISSION HYBRID REACTORS

N. Burgio[1, 2], M. Carta[1], V. Fabrizio[1], L. Falconi[1], A. Gandini[2], R. Gatto[2, 3], V. Peluso[4], E. Santoro[1], M.B. Sciarretta[2]

[1]*ENEA CRE Casaccia, Santa Maria di Galeria, Italy*
[2]*Sapienza University of Rome, DIAEE, Corso Vittorio Emanuele, Roma, Italy*
[3]*CR Enrico Fermi, Roma, Italy*
[4]*ENEA CR Bologna, Bologna, Italy*

Based on the heuristically generalized perturbation theory (HGPT) adapted to subcritical systems [1], a procedure for online operational monitoring of the subcriticality level of a hybrid fusion-fission system in which an "external" neutron source is generated in a magnetically confined tokamak-type plasma is described. This procedure [2], commonly referred to as power control-based subcriticality monitoring (PCSM), consists of compensating of slow and small movements of a specialized control rod in the nuclear fission zone, previously calibrated using a standard procedure, with equally slow and small alterations of the fusion neutron source. PCSM is verified by solving the multigroup transport equation for the direct flux, as well as for the importance function, associated with normalized fission power [3], and a technique is proposed for modifying the fusion neutron source strength based on plasma compression/expansion. Plasma and confining magnetic field adjustments, needed to implement the PCSM, are estimated with due account of the 0-D-plasma power balance.

Key words: fusion-fission hybrid reactor, subcritical fission core, subcritical multiplication factor, reactivity monitoring.

DOI: 10.21517/0202-3822-2021-44-2-27-41

КОНТРОЛЬ ПОДКРИТИЧНОСТИ В ГИБРИДНЫХ РЕАКТОРАХ СИНТЕЗА-ДЕЛЕНИЯ

Н. Бурджио[1, 2], М. Карта[1], В. Фабрицио[1], Л. Фалькони[1], А. Гандини[2], Р. Гатто[2, 3], В. Пелузо[4], Е. Санторо[1], М.Б. Шьяретта[2]

[1]*Национальное агентство по новым технологиям, энергии и устойчивому экономическому развитию (ENEA), Исследовательский центр (ИЦ) Касаччиа, ул. Ангильярезе 301, 00123 Санта-Мария-ди-Галерия, Италия*
[2]*Сапиенца — Римский университет, Отделение космической электротехники и энергетики, проспект Виктора-Эммануила II 244, 00186 Рим, Италия*
[3]*ИЦ им. Энрико Ферми, ул. Паниперна 89а, 00184 Рим, Италия*
[4]*ENEA, Болонский ИЦ, ул. Мартири Монте Соле 4, 40129 Болонья, Италия*

На основе распространения методологии HGPT (Эвристически обобщённой теории возмущений) на подкритические системы [1] описана процедура оперативного мониторинга уровня подкритичности гибридной системы синтеза-деления, в которой внешний источник нейтронов генерируется в магнитно-замкнутой плазме типа токамак. Процедура [2], обычно называемая методом PCSM (Power Control-Based Subcritality Monitoring), заключается в компенсации медленных малых перемещений специализированного регулирующего стержня в зоне деления ядер, предварительно откалиброванного с использованием стандартной процедуры, такими же медленными малыми изменениями источника термоядерных нейтронов. Метод верифицируется путём решения многогруппового уравнения переноса как для прямого потока, так и для функции важности. Последняя связана с нормированной мощностью деления [3]. Предлагается процедура изменения силы источника термоядерных нейтронов на основе сжатия/расширения плазмы. С учётом 0-D-баланса мощности плазмы дана оценка изменения параметров плазмы и ограничивающего магнитного поля, необходимого для реализации метода PCSM.

Ключевые слова: гибридный реактор синтеза-деления, подкритическая зона деления ядер, подкритический коэффициент размножения, измерение реактивности.

INTRODUCTION

A fusion-fission hybrid system consists in a fusion part, where fusion nuclear reactions taking place in a high-temperature plasma generate neutrons, and a surrounding subcritical fission core. When fusion power is based on D—T-reactions, as assumed in the present work, an additional tritium production zone is required. The fission core, where neutrons can induce fission events or undergo radiative capture reactions, offers two main potential applications and benefits that could be pursued: radioactive waste management, and nuclear fuel breeding. Thanks to their high energy, fusion-generated neutrons are particularly suitable for coupling with a fast-spectrum fission core to create an optimal environment for fertilization and nuclear waste burning. Fission nuclear energy is also produced, even though this is not nowadays regarded as the hybrid system's priority. As for waste management aspect, the most interesting thing is the possibility to achieve the so-called «deep-burn» mode of operation. The «external» fusion neutron source, independent with respect to the fission core, can be used to substantially increase

the fuel burnup compared to a critical reactor, by maintaining the neutron chain reaction longer, for comparable enrichment. In principle, with an extremely deep burnup it may be possible to employ a once-through «burn and bury» fuel cycle that would eliminate, or drastically reduce, the need for reprocessing and enrichment [4].

Due to its potential promise in addressing the issue of the long-term sustainability of nuclear energy, the fission-fision combination, initially conceptualized in the 1950's [5—7], has been periodically revisited, and today keeps being the subject of theoretical studies and experimental exploration. Several fusion-fission hybrid concepts have been proposed, differing in the plasma confinement scheme and the fission core material [8]. In this work, we focus on magnetically confined plasmas, particularly the high-temperature deuterium-tritium (D—T)-plasma confined in a tokamak device by a combination of a toroidal and a poloidal magnetic field (with the latter self-generated by plasma current). An externally generated vertical magnetic field is required to keep the plasma in equilibrium and to conveniently shape it for improved performance. While the prospect of implementing a pure fusion power plant based on the tokamak concept remains distant, a hybrid system, for which the physical and engineering requirements are much less stringent, can be seen as an intermediate step in the quest for fusion energy, plus a way to drive fission energy toward a more sustainable future.

Any subcritical system requires a dedicated control system, capable of a real-time monitoring of the fission core subcriticality. This study is concerned with the feasibility of applying the so-called «power control-based sub-criticality monitoring (PCSM)», already discussed in the context of ADS systems [2, 3], to fusion-fission hybrids based on the tokamak concept. Formally, the theoretical arguments undrelying the proposed monitoring procedure apply equally to ADS and fusion driven systems. The hybrid's novelty is in the interplay between fission and fusion powers. We propose a method for adjusting fusion power to values consistent with the PCSM procedure using plasma compression/expansion through small alterations of the confining magnetic field.

This paper is formatted into two main parts. In the first part, we carry out a numerical verification of the PCSM method by neutronic calculations done with the ERANOS code [9]. For a credible evaluation of the PCSM effectiveness in monitoring a nuclear system subcriticality, we used a fairly accurate model of the core of a real-life research reactor, *viz*., TRIGA-RC1, run at the ENEA-Casaccia Research Center [10]. The JEFF-3.1 nuclear data library, adopted in the lattice cell calculations for collapsing the fine energy group cross-section structure into one of 33 groups, was used for Sn neutron transport calculations (BISTRO code [11]) of the direct flux and the importance function. This was the operating environment for the PCSM execution and subcritical reactivity measurement. In the second part of this work, we describe the method for modulating the strength of the fusion neutron source, required to implement the PCSM procedure. To this end, we set up a simple model of a fusion-fission hybrid, based on a 1D cylindrical geometry representation. The internal cavity filled with plasma is overlaid with five zones. They are, starting from the one closest to the plasma, the first wall, the fission core, the fusion blanket, the reflector and the shield. The neutronic calculations are repeated in this simpler setting, and the method to vary the fusion neutron source is implemented. The latter consists in compressing/expanding the plasma by changing the strength of the confining magnetic field.

Following this Introduction, the paper presents a brief overview of the PCSM method and the expression for the subcritical multiplication factor. The next section is concerned with neutronic calculations based on the TRIGA-RC1 reactor modelization. The reactor's layout and main characteristics are provided, the reference and perturbed fission core configurations are defined, and the multiplication factor is calculated according to the PCSM formula. In the section that follows we describe two plasma compression methods for modulating the fusion neutron source, as required by the PCSM procedure. After describing a simplified hybrid system, we define the plasma operating regime with due account of the plasma power balance, and determine plasma's key characteristics, including the strength of the fusion neutron source. Two plasma compression methods are proposed: number one, described in detail in the respective subsection of the «Fusion Neutron Source Modulation» section, relies on the plasma inward displacement. Number two, described only succinctly in the same section, consists in the direct reduction of the plasma minor radius, with the center point kept fixed. The last section is titled «Summary and Conclusions».

SUBCRITICAL SYSTEMS AND THE PCSM METHOD

The PCSM is rooted in the point kinetics equation related to subcritical systems [1, 2].

Point kinetics equation for a subcritical system. The point kinetics equations related to a subcritical system are derived from equations governing neutron flux vector $\mathbf{\Phi}$ and precursor densities m_i (i = 1, 2, …, M), with M representing the number of delayed neutron groups, each characterized by decay constant λ_i under transient conditions in a multi-group neutron energy setting (the bold-face characters are for vectors and matrices):

$$\mathbf{V}^{-1}\frac{\partial \mathbf{\Phi}}{\partial t} = \mathbf{A}\ \mathbf{\Phi} + (1-\beta)\boldsymbol{\chi}^{\mathrm{P}}\ \mathbf{S}_{\mathrm{fis}}\ \mathbf{\Phi} + \boldsymbol{\chi}^{\mathrm{D}}\ \mathbf{U}\sum_{i=1}^{M}\lambda_i m_i + \mathbf{S}; \tag{1}$$

$$\frac{\partial m_i}{\partial t} = \beta_i (\nu\mathbf{\Sigma}_f)^{\mathrm{T}}\ \mathbf{\Phi} - \lambda_i m_i . \tag{2}$$

Here **A** is the transport (diffusion), capture and scattering matrix operator (of a $G\times G$ dimension, where G denotes the number of energy groups), **V** is the diagonal neutron velocity matrix ($G\times G$), and **U** is the unit (G component) vector: $\mathbf{S}_{\mathrm{fis}} = \begin{bmatrix} (\nu\Sigma_f)_1 & \cdots & (\nu\Sigma_f)_G \\ \cdots & \cdots & \cdots \\ (\nu\Sigma_f)_1 & \cdots & (\nu\Sigma_f)_G \end{bmatrix}_{G\ \mathrm{rows}}$ is the fission matrix, $(\nu\mathbf{\Sigma}_f)^T = \nu\left[\Sigma_{f,1} \quad \cdots \quad \Sigma_{f,G}\right]$, and the prompt ($P$) and delayed ($D$) spectra are $\boldsymbol{\chi}^X = \mathrm{diag}\left[\chi_1^X \quad \cdots \quad \chi_G^X\right]$ with $\chi = P$ or D.

We assume that the transient is initiated at a given time by a perturbation that generally changes unperturbed operators $\mathbf{A}_0$, $\mathbf{S}_{\mathrm{fis},0}$, and neutron source $\mathbf{S}_0$ into **A** (= $\mathbf{A}_0$ + $\delta\mathbf{A}$), $\mathbf{S}_{\mathrm{fis}}$ (= $\mathbf{S}_{\mathrm{fis},0}$ + $\delta\mathbf{S}_{\mathrm{fis}}$), **S** (= $\mathbf{S}_0$ + $\delta\mathbf{S}$), respectively, and transforms unperturbed neutron flux $\mathbf{\Phi}_0$ into $\mathbf{\Phi}$ (= $\mathbf{\Phi}_0$ + $\delta\mathbf{\Phi}$).

To arrive at an expression accommodating the generalized reactivity derived in the context of the HGPT methodology, we introduce importance function $\mathbf{\Psi}^*$, associated with normalized fission power, which is governed by equation $\mathbf{A}_0^*\ \mathbf{\Psi}^* + \mathbf{S}_{\mathrm{fis},0}^{\mathrm{T}}\left[(1-\beta)\boldsymbol{\chi}^{\mathrm{P}} + \beta\boldsymbol{\chi}^{\mathrm{D}}\right]\mathbf{\Psi}^* + \frac{\gamma}{W_0}\mathbf{\Sigma}_{f,0} = 0$. The importance relative to the precursor densities is conveniently defined as $m^* = \mathbf{U}^{\mathrm{T}}\boldsymbol{\chi}^{\mathrm{D}}\mathbf{\Psi}^*$.

After multiplying Eqs. (1) and (2) on the left by $\mathbf{\Psi}^{*\mathrm{T}}$ and m^*, respectively, space-integrating on the fission core volume, dropping second order terms, and doing some algebra, we obtain (assuming that the neutron flux showing up in the ratios (numerator and denominator) is unperturbed, and accounting for the general dependence of the delayed neutron distribution on nuclide species and energy [1])

$$\ell_{\mathrm{eff}}\frac{dP}{dt} = (\rho_{\mathrm{gen}} - \alpha\beta_{\mathrm{eff}})P + \sum_{i=1}^{M}\lambda_i\xi_i + \zeta(1-P) + \rho_{\mathrm{source}}; \tag{3}$$

$$\frac{d\xi_i}{dt} = \alpha\beta_{\mathrm{eff},i}P - \lambda_i\xi_i , \tag{4}$$

where the coefficients represent physically significant quantities given by expressions: $P(t) = \frac{W(t)}{W_0(1+q)}$, with $q = \frac{\left\langle \delta\mathbf{\Sigma}_f^{\mathrm{T}}, \mathbf{\Phi}_0 \right\rangle}{\left\langle \mathbf{\Sigma}_{f,0}^{\mathrm{T}}, \mathbf{\Phi}_0 \right\rangle}$ (normalized power); $\xi_i = \frac{\left\langle m^*,\ m_i \right\rangle}{\left\langle \mathbf{\Psi}^*, \hat{\boldsymbol{\chi}}\mathbf{S}_{\mathrm{fis},0}\mathbf{\Phi}_0 \right\rangle}$ (i-th effective precursor density); $\ell_{\mathrm{eff}} = \frac{\left\langle \mathbf{\Psi}^*,\ \mathbf{V}^{-1}\mathbf{\Phi}_0 \right\rangle}{\left\langle \mathbf{\Psi}^*,\ \hat{\boldsymbol{\chi}}\mathbf{S}_{\mathrm{fis},0}\mathbf{\Phi}_0 \right\rangle}$ (effective prompt neutron lifetime), where $\hat{\boldsymbol{\chi}}\mathbf{S}_{\mathrm{fis},0}\ \mathbf{\Phi}_0$ is the unperturbed fission source:

$$\rho_{\mathrm{gen}} = \frac{\left\langle \mathbf{\Psi}^*, (\delta\mathbf{A} + \hat{\boldsymbol{\chi}}\delta\mathbf{S}_{\mathrm{fis}})\mathbf{\Phi}_0 \right\rangle}{\left\langle \mathbf{\Psi}^*, \hat{\boldsymbol{\chi}}\mathbf{S}_{\mathrm{fis},0}\mathbf{\Phi}_0 \right\rangle} \quad \text{(generalized reactivity)}, \tag{5}$$

$\rho_{\mathrm{source}} = \frac{\left\langle \mathbf{\Psi}^*,\ \delta\mathbf{S}_n \right\rangle}{\left\langle \mathbf{\Psi}^*,\ \hat{\boldsymbol{\chi}}\mathbf{S}_{\mathrm{fis},0}\mathbf{\Phi}_0 \right\rangle}$ (source reactivity), $\alpha = \frac{\langle \mathbf{\Psi}^*, \boldsymbol{\chi}^{\mathrm{D}}\ \mathbf{S}_{\mathrm{fis},0}\ \mathbf{\Phi}_0 \rangle}{\langle \mathbf{\Psi}^*, \hat{\boldsymbol{\chi}}\ \mathbf{S}_{fis,0}\ \mathbf{\Phi}_0 \rangle}$, $\zeta = \frac{1}{\left\langle \mathbf{\Psi}^*, \hat{\boldsymbol{\chi}}\mathbf{S}_{\mathrm{fis},0}\mathbf{\Phi}_0 \right\rangle} \equiv \frac{1-k_{\mathrm{sub}}}{k_{\mathrm{sub}}}$, and $\beta_{i,\mathrm{eff}} = \frac{\sum_{j=1}^{\mathrm{J}}\beta_i^j\langle \mathbf{\Psi}^*, \boldsymbol{\chi}_i^{\mathrm{D},j}\ \mathbf{S}_{\mathrm{fis},0}\ \mathbf{\Phi}_0 \rangle}{\langle \mathbf{\Psi}^*, \hat{\boldsymbol{\chi}}\ \mathbf{S}_{\mathrm{fis},0}\ \mathbf{\Phi}_0 \rangle}$, $\beta_{\mathrm{eff}} = \sum_{i=1}^{\mathrm{M}}\beta_{i,\mathrm{eff}}$ for J fissile isotopes. The subcritical multiplication factor $k_{\mathrm{sub}} = \frac{\langle \mathbf{\Psi}^*, \hat{\boldsymbol{\chi}}\ \mathbf{S}_{\mathrm{fis},0}\ \mathbf{\Phi}_0 \rangle}{1+\langle \mathbf{\Psi}^*, \hat{\boldsymbol{\chi}}\ \mathbf{S}_{\mathrm{fis},0}\ \mathbf{\Phi}_0 \rangle}$.

In the above expressions, γ is energy released in one fission event, and $\hat{\chi} = \chi^{P}(1-\beta) + \chi^{D}\beta$ is the neutron fission spectrum consisting of the prompt and the delayed components (β is the delayed neutron fraction). It can be shown that k_{sub} merges into k_{eff} (the multiplication factor related to the fundamental eigenfunction) as the system approaches criticality [1].

Eqs. (3) and (4) can be considered as a generalization of the point kinetics system equation derived by Usachev for critical systems [12], that converge with the Usachev's equation when the system approaches criticality.

The PCSM method. Assume that a dedicated control rod has been calibrated so that its displacement Δz may be associated with (experimental) reactivity values $(\Delta k_{eff}/k_{eff})^{exp}$. The associated ρ_{gen}^{exp} of the (experimental) generalized reactivity can be assumed to be given as follows:

$$\rho_{gen}^{exp} = \rho_{gen}^{calc} f_b, \tag{6}$$

with ρ_{gen}^{calc} given by Eq. (5), and the bias factor, $f_b = \dfrac{(\Delta k_{eff}/k_{eff})_B^{exp}}{(\Delta k_{eff}/k_{eff})_B^{calc}}$, the bias being between the control rod calibration value $(\Delta k_{eff}/k_{eff})_B^{exp}$ and the calculated standard perturbation expression

$$(\Delta k_{eff}/k_{eff})_B^{calc} : \left(\frac{\Delta k_{eff}}{k_{eff}}\right)_B^{calc} = \frac{\left\langle \mathbf{\Phi}_0^*, \delta\mathbf{M}_B \mathbf{\Phi}_0 \right\rangle}{\left\langle \mathbf{\Phi}_0^*, k_{eff}^{-1}\hat{\chi}\mathbf{S}_{fis,0}\mathbf{\Phi}_0 \right\rangle}).$$

Here $\mathbf{\Phi}_0^*$ is an unperturbed standard adjoint flux, and $\delta\mathbf{M}_B = \delta\mathbf{A}_B + \hat{\chi}\delta\mathbf{S}_{fis,B}$ is the perturbation of the diffusion (transport) operator related to the control rod insertion (quantity ρ_{gen}^{exp} given by Eq. (6) could be obtained, and even more accurately, experimentally via the control rod calibration under subcritical conditions by measuring the k_{sub} multiplication factor vs. control rod insertion via pulsed source or source jerk techniques [13]).

Likewise, source reactivity ρ_{source}^{exp} associated with a given measured external neutron source change $\delta\mathbf{S}_n^{exp}$ may be written as $\rho_{source}^{exp} = \dfrac{\langle \mathbf{\Psi}^*, \delta\mathbf{S}_n^{exp} \rangle}{\langle \mathbf{\Psi}^*, \hat{\chi}\, \mathbf{S}_{fis,0}\, \mathbf{\Phi}_0 \rangle}$.

Recalling the definition of importance and assuming that a source perturbation corresponds to a (measured) fractional change of its strength, written as $\delta S_n^{exp}/S_{n,0}$, we can express ρ_{source}^{exp} in terms of the subcritical multiplication factor:

$$\rho_{source}^{exp} = \frac{\delta S_n^{exp}}{S_{n,0}} \frac{1}{\langle \mathbf{\Psi}^*, \hat{\chi}\, \mathbf{S}_{fis}\, \mathbf{\Phi}_0 \rangle} \equiv \frac{\delta S_n^{exp}}{S_{n,0}} \frac{1-k_{sub}}{k_{sub}}. \tag{7}$$

If changes in the dedicated control rod and the fusion neutron source do not affect the fission power level, the following relation holds, considering Eqs. (3) and (4):

$$\rho_{gen}^{exp} + \rho_{source}^{exp} = 0, \tag{8}$$

and indicates the compensation of the experimental source reactivity and experimental generalized reactivity. Substituting expression (7), we finally obtain a «working» expression for the subcritical multiplication factor:

$$k_{sub} = \frac{\delta S_n^{exp}/S_{n,0}}{\delta S_n^{exp}/S_{n,0} - \rho_{gen}^{exp}}. \tag{9}$$

Note that $\delta S_n^{exp}/S_{n,0}$ and ρ_{gen}^{exp} have opposite signs.

Following the PCSM method, Eq. (9) can be evaluated by adjusting the neutron source intensity to compensate the control rod insertion. If the online monitoring of this subcriticality index is done with small and slow variations of the source strength, the fission power level will remain practically unaffected.

NUMERICAL VERIFICATION OF THE PCSM METHOD

A numerical calculation is carried out to verify the PCSM accuracy, assuming that the external neutron source can be modulated to reset the fission power, as required by the procedure [see Eq. (8)]. The calculation is

performed using the ERANOS code [9] and modeling the fission core in such a way as to make it representative of the TRIGA-RC1 research reactor [10] run at the ENEA-Casaccia Research Center.

The TRIGA-RC1 reactor. The TRIGA-RC1 reactor is a thermal pool research reactor, based on the General Atomic TRIGA Mark II reactor design, operating at a thermal power of 1 MW [10]. The core, in the actual configuration, is a cylindrical system including 111 fuel elements, control rods and an Am—Be-source. Water inside the vessel occupies about 1/3 of the core volume and acts as the first biological shield, neutron moderator and coolant. The RC1-core, surrounded by a graphite reflector, consists of a lattice of TRIGA stainless steel standard fuel elements, graphite dummy elements, as well as control and regulating rods. There are 127 channels on the upper grid plate available for those core components, while the grid itself is divided into seven concentric rings. One channel houses a start-up source (Am—Be), and two fixed channels (the central one and a rabbit) are available for irradiation. A TRIGA fuel element is made of a HZr—U ternary alloy, containing H and Zr atoms in a ratio of 1.7 to 1. Due to this ratio, the alloy's crystal lattice has a high level of stability from the metallurgical and nuclear points of view [13]. The fuel is uranium, of which 20 w/o is ^{235}U. Neutron moderation is therefore provided not only by the water coolant, but also by zirconium hydride contained in the alloy, the result being a high-temperature-ready negative coefficient (Doppler effect); and a reactor, which is intrinsically safe. The fuel element is clad in a 0.5 mm thick stainless steel (AISI 304) tube with graphite cylinders (axial reflectors) at the ends. The fuel element is provided extraneously with two fittings to allow for remotely controlled movements and correct placement into the grid plates.

The reactor power is controlled by a fine regulation rod and three fuel follower rods, two shim rods and a safety rod. The control rods are made from boron carbide, a strong neutron absorber, and have a stainless steel coating.

A cylindrical graphite structure around the core acts as the reactor's lateral reflector. Surrounding this external reflector is a lead thermal shield for gamma rays from the core, and a concrete wall of an average thickness of 2.2 m serves as a biological shielding.

Thermal power is removed from the core by natural convection and released to the environment through two thermo-hydraulic loops, coupled by two heat exchangers and two cooling towers.

The horizontal section of the core surrounded by the graphite reflector, and the components of the core system, including the fuel elements, control rods and graphite dummy elements. are shown in Fig. 1.

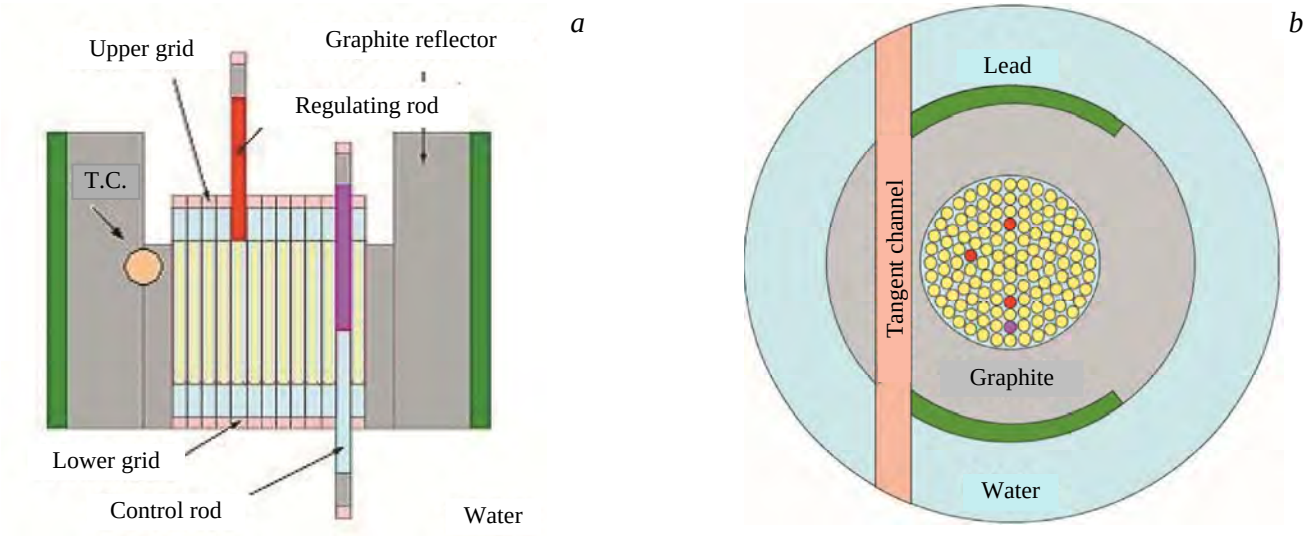

Fig. 1. The core of the TRIGA reactor, vertical section (*a*), standard configuration (*b*)

Calculation model. For the TRIGA-RC1 model, neutronic calculations were done with the ERANOS-2.2 deterministic code [9]. The JEFF-3.1 nuclear data library [14] has been adopted in the lattice cell calculations for collapsing the fine energy group cross-section structure into one of 33 groups, to be used for the Sn transport calculations of the direct flux and the importance functions. A bi-dimensional *RZ*-geometry was selected.

Prior to setting up the TRIGA-RC1 model, a study was conducted to investigate the influence of the reactor heterogeneity on its fundamental parameters. The model of choice was a simplified cylindrical model composed of eight zones. They are, starting from the core center, the central channel (labelled as SA), six shells with different fuel compositions (labelled as SB, SC, SD, SE, SF, SG) and the external graphite reflector (labelled as

SH). The axial and radial sections of the model are shown in Fig. 2, where the central channel is represented in white, the fuel in red and the graphite reflectors in gray.

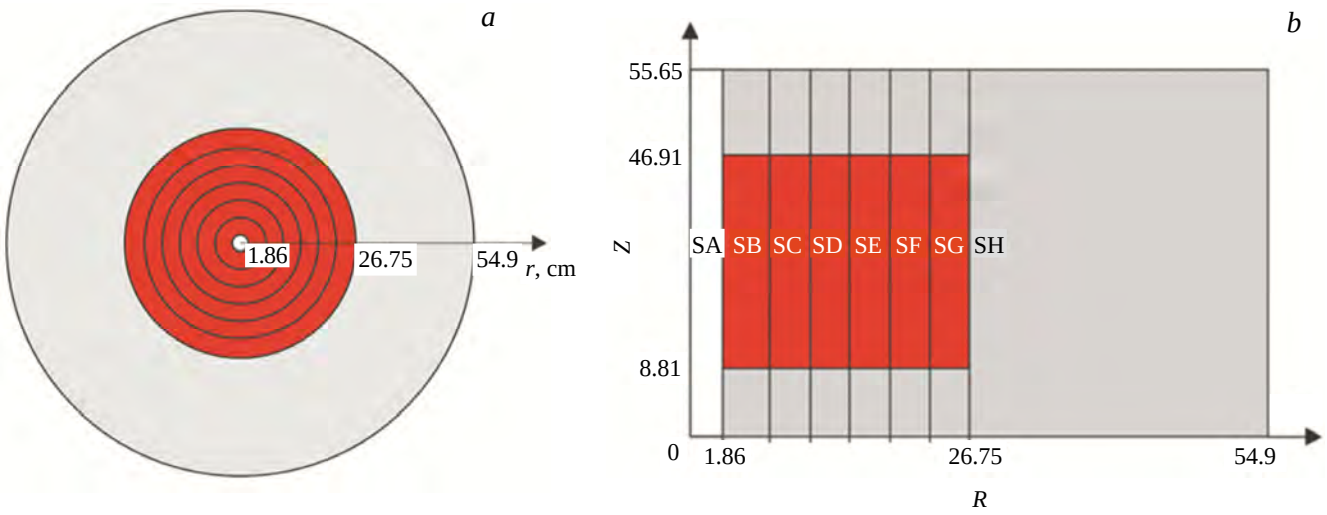

Fig. 2. Sections of the TRIGA reactor core. where the central channel is marked in white, the fuel in red and the graphite reflectors, in gray, radial section (*a*), axial section (*b*)

Reference and perturbed configurations. Once the TRIGA critical model is created, it is necessary, for the PCSM applicability purposes, to define two different subcritical configurations. a reference one and a perturbed one.

The subcritical reference configuration used for a PCSM-based analysis is derived from the critical one by moving the control rods and involves a core of k_{eff} = 0.97083.

The reference configuration is perturbed by introducing a reactivity variation, $\Delta\rho$ = –0.00866, by properly moving the control rods to arrive at k_{eff} = 0.96272. Although the relative control rods height between the discussed two subcritical configurations is small, the absorber's effect on the neutron flux is pronounced due to approximations introduced in the control rod model. In fact, the control rods were modeled as a homogenized region in the SC zone, and thus affected a large part of the core, a configuration that differst from the original one, in which the rods are at specific positions relative to the core.

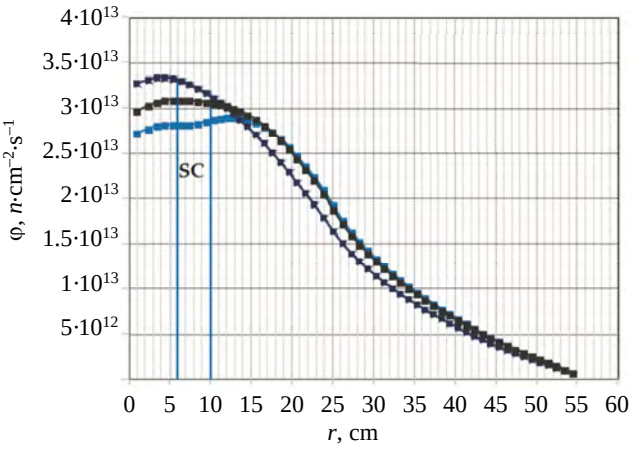

Fig. 3. Critical vs reference vs perturbed configuration, total flux radial traverse at core mid-plane, *k*: ■ — 0.96, ■ — 1, ■ — 0.97

In Fig. 3, we present a homogeneous flux relevant to the three configuration cases described above (critical, reference subcritical and perturbed subcritical). The alteration of the flux shape due to the neutron absorber is evident when passing from the critical configuration to the reference and the perturbed ones.

The adjoint flux and the importance function. The PCSM verification calls for evaluating both the adjoint flux and the importance function the latter being associated with normalized fission power (the «adjoint source»). From the neutronics point of view, the importance function satisfies the inhomogeneous equation derived from the adjoint flux homogeneous equation by adding the adjoint source.

A test subcritical configuration was considered as a starting point for comparing the trends of the importance and the standard adjoint flux functions. They are almost equal when the system is close to criticality and become more and more different as the system deviates from criticality. To investigate this behavior, we

insert the control rods at an axial height corresponding to k_{eff} = 0.99048 (a quasi-critical level). The calculation results are shown in Fig. 4.

The geometry was then modified by displacing the control rods to obtain k_{eff} = 0.96. The calculation results are shown Fig. 5.

External neutron source. If the average power of the TRIGA-RC1 reactor in the critical state is about 1 MW, the external source is expected to produce the same power in the subcritical state (in accordance with a multiplication factor of 0.97063, obtained by positioning the control rods at the central channel in an axial position, z = 34.29 cm). The source intensity is determined by calculating fission rates corresponding to a given power. The fission rate corresponding to a power of 1 MW, $S_0 = 1.091\times10^{14}$ n/s. The source intensity is given in a 33-energy-group structure.

The reference case has then been perturbed by moving the control rods in the axial position, z = 32.28 cm, to decrease reactivity by about 0.00866 (k_{eff} = 0.96272). In this case, the external source intensity, modified in order to re-establish the initial fission rate, has integral value, $S_1 = 1.508\times10^{14}$ n/s, reflecting a 38% increase.

The subcritical multiplication factor. The neutronic calculation described above provides all the information required for the verification of the PCSM method: the direct flux, the adjoint flux and the importance function for the reference configuration; the perturbation of the Boltzmann operator that leads to the perturbed subcritical configuration; the external source in the reference configuration, and its modified strength in the perturbed configuration, needed to keep the fission power unaltered.

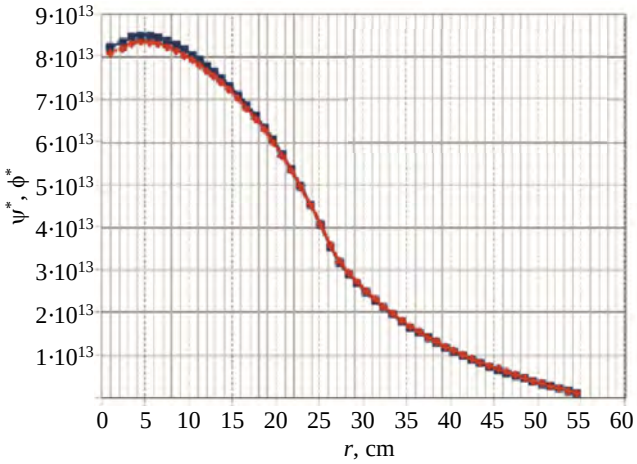

Fig. 4. Adjoint flux and importance radial traverse at core mid-plane: test case with k_{eff} = 0.99: —▪— — adjoint flux, —●— — adjoint importance

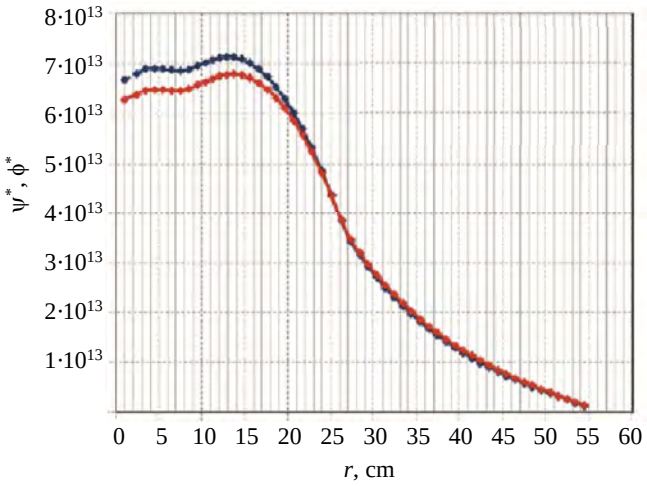

Figure 5. Adjoint flux and importance radial traverse at core mid-plane: modified case with k_{eff} = 0.96: —•— — adjoint flux, —●— — adjoint importance

The generalized reactivity Eq. (5) was calculated using the HGPT methodology, and the system's subcritical reactivity Eq. (9) was obtained. The results are summarized below. Multiplication coefficient k_{sub}:

Method . . .	k_{sub}
PCSM . . .	0.97188
Reference . . .	0.97083
Difference, % . . .	0.108

As one can see, the uncertainty in measuring the discrepancy between the multiplication factors resulting from the PCSM numerical implementation of the PCSM procedure and corresponding to reference conditions is within 0.1%.

This shows how the proposed methodology can be effectively used to determine the subcriticality level of a subcritical reactor without significantly interfering with its normal operation. In summary, steps involved in the PCSM procedure are as follows: (1) preliminary calibration of the dedicated control rod, where a relationship between the rod position change and the corresponding reactivity alteration is established; (2) during operation, a small, slow insertion of the control rod, parallel with the adjustment of the «external» source intensity to ensure that the ex-core and in-core neutron detector readings (proportional to the fission power level) are kept constant; (3) the determination of generalized reactivity, Eq. (5), and k_{sub} in accordance with Eq. (9).

FUSION NEUTRON SOURCE MODULATION

For a fusion-fission hybrid system, the «external» neutron source is generated in a confined plasma, and the PCSM applicability depends on the modulation of the fusion neutron source intensity, intended to reset the fission power.

Several options for modulating the power of a tokamak-confined plasma (and hence changing the fusion neutron source) can be considered. Here, we focus on a method based on plasma compression/expansion. A calculation is therefore carried out to determine the level of plasma compression required to reset the fission power, and in particular the altered values of plasma density and temperature. Depending on adopted compression scheme, a compressed plasma may get out of the toroidal force equilibrium. In that case, an additional calculation is required to determine how the confining magnetic fields should be modified to restore the balance.

Hybrid system specification. The modeling of the hybrid neutronic system is based on a large tokamak, a device with an intermediate toroidal magnetic field operated with D—T-fuel and including a fission core zone in a region between the first wall and the tritium generating blanket. To simplify the neutronic calculations, we have modeled a system with an infinite cylinder (a 1D approximation) with a vacuum cavity at the center and seven homogeneous shells, as shown in Fig. 6.

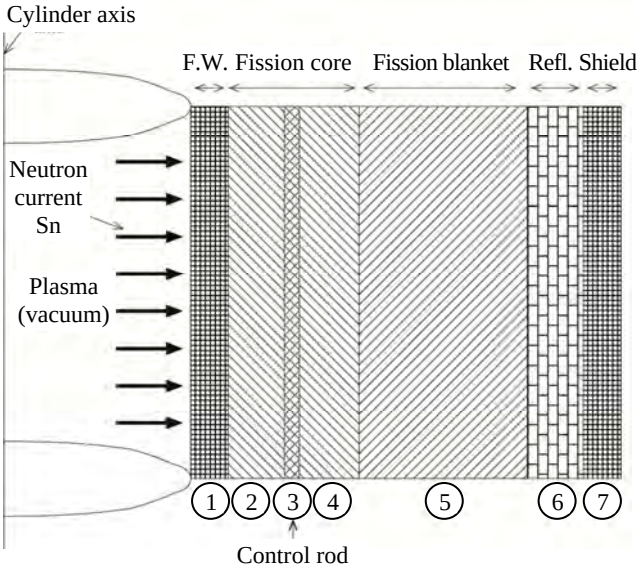

Fig. 6. 1D-modeling of the hybrid system

The central cavity corresponds to the plasma region, where D—T-fusion reactions generate neutrons (the «external» source). The first zone is the tokamak's first wall and vacuum chamber. Zones 2, 3 and 4 constitute the fission core, with zone 3 representing the dedicated control rod. Zone 5 is the fusion (or tritium producing) blanket, followed by the reflector and the shield. The radial distance of the leftmost boundary of zones 1, 2, 5, 6 and 7 are located, respectively, at R = 485, 498, 535, 609 and 622 cm. The cylinder terminates at R = 633 cm.

Since the objective of this study is to verify the applicability of the PCSM method to a hybrid system, the details of the material composition of the various zones are not particularly relevant, as long as they are representative of a hybrid system. We therefore omit them and only specify the type of materials selected for each different zone. Zone 1 (the first wall) contains iron as a structural material and water as a coolant. Zones 2 and 4 comprising the fission core contain a homogeneous mixture of materials typical of a fast reactor core with the MOX fuel: UO_2, PuO_2, AmO_2, plus iron as a structural material and lead as a coolant. The volume fractions for these materials are (the reference configuration): $V_{f,\,Pb} = 0.15$, $V_{f,\,Fe} = 0.05$, $V_{f,\,UO_2} = 0.3509$, $V_{f,\,PaO_2} = V_{f,\,AmO_2} = 0.2245$. Zone 3 has the same composition as zones 2 and 4 when the control rod is extracted (the reference configuration), and a modified composition, in which boron-10 replaces part of the fuel, when the control rod is partially inserted (the perturbed configuration). Zone 5 (the fusion blanket) contains lithium and lead, the latter acting both as a multiplier and a coolant medium. Zone 6 (the reflector) is made of carbon and water, while the last zone is a shield with the same material composition as zone 1.

Fusion plasma's sub-ignited reference state. The reference configuration of the hybrid system consists of a plasma operating in a sub-ignited steady state during some form of auxiliary heating, and a subcritical fission core ($k_{eff} \sim 0.97$). To specify the plasma state, and in particular its working temperature, we consider its energy balance. After that, we can determine the fusion neutron source which maintains the fission core subcriticality.

Plasma operating regime. In the reference configuration, we assume that a D—T-plasma (50/50 deuterium/tritium) of a 1.1×10^{20} 1/m^3 density is used. The tokamak major radius, $R_{ax} = R_0 = 350$ cm, the horizontal minor radius, a = 120 cm, the elongation of the plasma cross-section, $\kappa = b/a = 1.74$. As a result, plasma volume,

$V_{pl} = 2\pi a^2\kappa = 1.74$ m^3. The on-axis toroidal magnetic field, $B_t = 5.5$ T, the safety factor on the plasma edge, $q^* = 3.5$, and the total plasma current at flat-top is set equal to $I_{pl} = 11$ MA.

For simplicity, we consider the 0-D-equation for the time evolution of plasma thermal energy [15]:

$$\frac{dW(t)}{dt} = \langle S_\alpha \rangle + \langle S_\Omega \rangle + S_{aux} - \langle S_B \rangle - \langle S_{tr} \rangle \quad \left[\text{W/m}^3\right], \tag{10}$$

where plasma internal energy, $W = \langle 3nT \rangle$, fission power carried by alpha particles, $S_\alpha = \langle E_\alpha n^2 \langle \sigma v \rangle / 4 \rangle$, ohmic heating power, $S_\Omega = \langle \eta J^2 \rangle$, and auxiliary heating power, S_{aux}, the Bremsstrahlung and transport power losses, $S_B = \langle C_B n^2 T^{1/2} \rangle$ and $S_{tr} = \langle 3nT/\tau_E \rangle$, are given in MKSA units by: $W(t) = 5.34\times10^4 \bar{n}_{20} \bar{T}_k(t)$, $\langle S_\alpha \rangle = 2.31\times10^5 \bar{n}_{20}^2 \langle \sigma v \rangle_n$, $\langle S_\Omega \rangle = \frac{1}{V_{pl}} \frac{5.6\times10^4}{1 - 1.31\varepsilon^{1/2} + 0.46\varepsilon} \frac{I_{pl,M}^2 R_0}{a^2 \kappa \bar{T}_k^{3/2}(t)}$, S_{aux} = given function of $\bar{T}_k(t)$, $\langle S_B \rangle = 6.14\times10^3 \bar{n}_{20}^2 \bar{T}_k^{1/2}(t)$, $\langle S_{tr} \rangle = 5.34\times10^4 \frac{\bar{n}_{20} \bar{T}_k(t)}{\tau_E}$.

In the above equations, $\langle \cdots \rangle$ denotes averaging over the plasma volume, the over-bar indicates averaging over the plasma cross-section, $\bar{n}_{20} = \bar{n} / 10^{20}$ is the particle density in $1/m^3$ divided by 10^{20}, $\varepsilon = a/R_0$ is the inverse aspect ratio, $I_{pl,M}$ is the total plasma current in MA, and $\langle \sigma v \rangle_n = \langle \sigma v \rangle / 10^{-22}$, where the reactivity $\langle \sigma v \rangle = 10^{-6} \exp\left[-21.38 / T_k^{0.2935} - 25.20 - 7.101\times10^{-2} T_k + 1.938\times10^{-4} T_k^2 + 4.925\times10^{-6} T_k^3 - 3.984\times10^{-8} T_k^4\right]$ is expressed in m^3/s, when temperature is in keV.

For simplicity, we assume plasma confinement time, $\tau_E = 1.2$ s, to be constant. This is a rather crude approximation, as the plasma regime is sustained by auxiliary heating. However we use this assumption, considering the demonstration nature of our study. The various powers in the plasma temperature function are shown in Fig. 7.

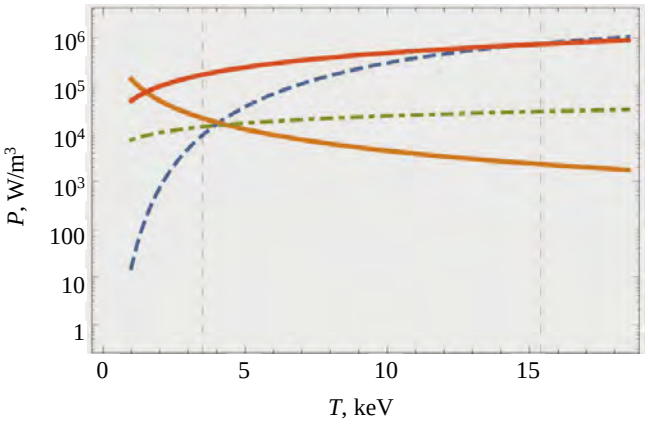

Fig. 7. Power components contributing to the plasma energy balance. Vertical lines indicate Bremmstrahlung and ignition temperatures. Bremmstrahlung and transport powers are multiplied by –1 for ease of comparison: – – – — +FUS, ——— — +CHM, -·-·- — –BR, ——— — –TR

The vertical lines indicate two important temperatures characterizing a magnetized fusion plasma: the Bremsstrahlung temperature, defined by balance $\langle S_\alpha \rangle + \langle S_\Omega \rangle = \langle S_B \rangle$, and the ignition temperature, defined by $\langle S_\alpha \rangle + \langle S_\Omega \rangle = \langle S_B \rangle + \langle S_t \rangle$. We find $T_B = 3.512$ keV and $T_1 = 15.400$ keV, respectively.

We solved Eq. (10) modeling the auxiliary heating function to obtain a steady-state sub-ignited regime with working temperature, $T_{sub} = 9$ keV. In our simulation, temperature 0.95 T_{sub} is reached in about 16.2 s, and the steady-state is sustained by auxiliary heating, $S_{aus} = 0.228\times10^6$ W/m^3.

Plasma neutron source. The fusion neutron source depends on the rate of the fusion reaction in plasma, which in turn depends on plasma temperature and density. Plasma eccentricity, $e \equiv \sqrt{1 - 1/\kappa^2} = 0.821$. The fusion reaction rate, $R_{fus} = n^2 \langle \sigma v \rangle / 4$ in $1/(m^3 \cdot s)$, and is also equal to the number of fusion neutrons produced per unit plasma volume per second, n_f. In the reference sub-ignited plasma configuration with $T_k = 9$ keV, we find $n_f = 2.483\times10^{11}$ $1/(cm^3 \cdot s)$. Introducing factor f_b denoting the fraction of the plasma which is burning, that is, actually undergoing an appreciable number of fusion reactions, we obtain the total number (rate) of fusion neutrons produced in the plasma per second, $N_f = n_f V_{pl} f_b = 8.647\times10^{18}$ 1/s.

We then evaluate the density of the current of fusion neutrons impinging on the first wall. The latter, with its horizontal and vertical minor radii denoted by a_w and b_w, respectively, is assumed to be 15 cm away from the

plasma boundary. Its total surface, $S_w = 8\pi b_w R_0 E(e_w) = 2.419\times10^6$ cm^2, where E denotes the complete elliptic integral, and $e_w = \sqrt{1-1/\kappa_w^2}$, with $\kappa_w = b_w/a_w$. The fusion neutron current hitting the outer part of the first wall is

$$J_{pl,0} = \frac{N_f}{S_w} = \frac{\pi}{16}\frac{n^2\langle\sigma v\rangle(T)a^2 f_b}{a_w E(e_w)} = 3.574\times10^{12}\ 1/(\text{cm}^2\cdot\text{s}). \quad (11)$$

Fission core reference subcritical state. Neutronic calculations for the reference and perturbed configurations of the hybrid system were carried out using a 1D-code based on a finite-difference numerical technique, writen specifically for this study. It allows solving multi-group diffusion equation with and without an external source. It calculates both the direct and adjoint fluxes, as well as relevant importance functions. The code has been benchmarked against analytical solutions of the 2-group, 2-zone problem, while a more throughout validation work using the ERANOS code is underway.

We have discretized the radial dimension in 45 grid points, and chosen a 6-group scheme. The group upper energies are 20×10^6, 4.5×10^6, 0.82×10^6, 0.14×10^6, 3.71×10^3, 3.06 eV, with the fission spectrum given by χ = (0.18, 0.655, 0.215, 0.012, 0, 0). Where needed, the high-energy neutron source is introduced, but only in the high-energy group (g = 1) equation. The neutronic group constants were prepared by processing ENDF/B data with the NJOY code, using a fusion-dedicated weighting spectrum. The solution procedure is the conventional power iteration method. In all computations, we used convergence tolerances for the multiplication factor and the flux ($\in_k = 10^{-5}$ and $\in_\varphi = 10^{-4}$, respectively).

The neutronic calculation performed for this model of a hybrid system are identical to those outlined in the «Numerical verification of the PCSM method» section in respect of the TRIGA reactor model, and are only summarized here in the form of key verification results. The subcritical reference configuration has k_{eff} = 0.97001, and is maintained in steady state by the fusion neutron current density given in Eq. (11), while generating a fission power of $W_0 = 2.307\times10^5$ W. The perturbed configuration, on the other hand, has k_{eff} = 0.96, and generates a fission power of 1.814×10^5 W with the same fusion neutron source as the one used in the reference configuration. To reset the reference fission power W_0, the fusion plasma current $J_{pl,1}$ needs to be increased to 5.128×10^{12} 1/(cm^2·s).

To produce a higher fusion neutron current, plasma density n and temperature T must be changed accordingly. Using Eq. (11), the condition to be satisfied by the new plasma parameters is (the subscript «1» stands for final state)

$$\frac{n_1^2\langle\sigma v\rangle(T_1)a_1^2 f_b}{a_w E(e_w)} = \frac{16}{\pi}J_{pl,1} = 2.612\times10^{13}, \quad (12)$$

with density indicated in 1/cm^3, temperature in keV, and $\langle\sigma v\rangle(T_1)$ in cm^3/s, and where a_1 and a_w denote the minor radius of the compressed plasma and of the first wall.

Fusion neutron source modulation by plasma compression/expansion. Finally, it is necessary to consider a method for increasing the fusion neutron source strength, as required by the PCSM procedure. We expect the required fusion power modulation to be achieved through a continuous series of plasma quasi-static compressions/expansions, induced by appropriate changes of the confining toroidal and/or vertical magnetic field. Ultimately, this is accomplished by simply varying the currents flowing in the toroidal field coils (say, I_{TFC}) and/or poloidal field coils (I_{PFC}). In general, an I_{TFC} increase amplifies the toroidal magnetic field and reduces the plasma minor radius (invariance of the toroidal magnetic flux). A I_{PFC} increase on the contrary, raises the inward force acting on the plasma, which, in accordance with the toroidal force balance, counteracts the outward-directed forces associated with the pressure and the magnetic field (the toroidal effects) [15]. If the plasma is in toroidal equilibrium, an increase in I_{PFC} displaces the plasma inward toward a new equilibrium position. If it is out of equilibrium, an appropriate change in I_{PFC} can restore the equilibrium without the need for any displacement. Note that a plasma displaced inward encounters a stronger toroidal field ($B_{tor} \propto 1/R$), and becomes compressed [16]. Adiabatic plasma compression experiments that have been carried out since the 1970s have proved the effectiveness of this heating technique [17, 18].

The scaling laws for the magnetic compression were discussed in [19] with the assumption that plasma is perfectly conductive (the «frozen-in» plasma compression). These scaling laws are derived from three basic lowest order constraints, which apply when a plasma is compressed slowly in relation to particle collision time τ_p («collisional» compression: time $\tau_c < \tau_p$), but rapidly in relation to energy confinement time τ_E («adiabatic» compression time $\tau_c > \tau_E$). These are the total number of particles inside a magnetic surface, the toroidal magnetic flux inside a magnetic surface, and the rotational transform (equivalently, the poloidal flux). In a zero-dimensional approximation, these constraints, augmented by the adiabatic energy law, read $r^2 R_{ax} n = \text{const}$, $r^2 B_t = \text{const}$, $q = \dfrac{rB_t}{R_{ax} B_p} = \text{const}$, $\dfrac{T}{n^{2/3}} = \text{const}$, where n, B_t, B_p, q indicate the density, the toroidal and poloidal magnetic fields, and the safety factor (inverse of the rotational transform), respectively, r localizes the magnetic surface, and R_{ax} denotes the major radius. Assuming that $r = a$, we obtain the following general compression scaling laws [19]:

$$n = \frac{\text{const}}{a^2 R_{ax}}; \quad T = \frac{\text{const}}{a^{4/3} R_{ax}^{2/3}}; \quad I_{pl} = \frac{\text{const}}{R_{ax}}; \tag{13}$$

$$B_t\left(R_{ax}\right) = \frac{\text{const}}{a^2}; \quad B_p = \frac{\text{const}}{a R_{ax}}. \tag{14}$$

A scaling law will also be needed for the plasma inductance. Neglecting plasma resistivity, we assume [20]:

$$L_{pl} I_{pl} \simeq \text{const} \Rightarrow L_{pl} = \text{const}\, R_a. \tag{15}$$

Here L_{pl} is the total inductance of the plasma, which comprises both the internal and the external contributions: $L_{pl} = L_{in} + L_{ext}$.

Whareas in [19] three different compression types are described, here we consider only two of them, namely, those denoted in [19] as «*R*-and-*a*-compression, type B» and «Constant-*R* *a*-compression».

Compression based on inward plasma displacement. In this compression mode (the «*R*-and-*a*-compression, type B» sketched in Fig. 8), the external vertical field increases (due to the I_{PFC} increase) displacing plasma radially inward and thereby inducing a compression in the minor radius due to increased toroidal field. No change in I_{TFC} is required. The application of the toroidal flux conservation $a_1^2 B_{t,1}(R_{ax,1}) = a_0^2 B_{t,0}(R_{ax,0})$, augmented by the $1/R$ law $B_{t,1}(R_{ax,1}) = B_{t,0}(R_{ax,0}) R_{ax,0}/R_{ax,1}$, leads to $(a_1/a_0)^2 = R_{ax,1}/R_{ax,0}$ and to the compression scaling $a = \text{const}\, R_{ax}^{1/2}$ (as shown in Fig. 8). In [19] this compression method is proposed as an auxiliary heating mechanism to be used during the discharge startup to heat up the plasma to required temperatures. Large plasma displacements were therefore envisaged, with the consequent need for a greater plasma chamber. In the context of this study, compression is performed with the only goal of inducing relatively small temperature changes, as required by the PCSM, and this practical disadvantage is minimized.

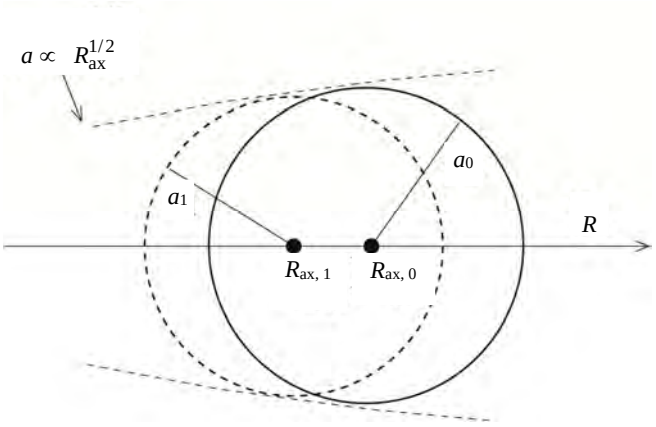

Fig. 8. Sketch of the compression scheme based on inward plasma displacement [19]

Defining the compression factor, $C_R \equiv R_{ax\,0}/R_{ax\,1} = (a_0/a_1)^2$, we obtain $B_{t,1}(R_{ax,1}) = B_{t,0}(R_{ax,0})\, C_R$ and, for the aspect ratio, $A_1 = A_0 / C_R^{1/2}$. The (13)—(15) scalings describing this compression approach are $n_1 = n_0 C_R^2$, $T_1 = T_0 C_R^{4/3}$, $p_1 = p_0 C_R^{10/3}$, $B_{t,1}(R_{ax,1}) = B_{t,0}(R_{ax,0}) C_R$, $I_{pl,1} = I_{pl,0} C_R$, $q_1(a_1) = q_0(a_0)$, $B_{p,1}(a_1) = B_{p,0}(a_0) C_R^{3/2}$ and $L_{pl,1} = L_{pl,0}/C_R$. Introducing these scalings in Eq. (12) we obtain the following relation for the required compression parameter C_R:

$$\frac{C_R n_0^2 \langle \sigma v \rangle (T_0 C_R^{4/3}) a_0^2 f_b}{a_w E(e_w)} = 2.612 \times 10^{13},$$

where, as assumed, elongation κ is invariant under compression. A numerical solution leads to C_R = 1.084, and consequently $a_1 = a_0/\sqrt{C_\mathrm{R}} = 1.153$ m, $R_{\mathrm{ax},1}$ = 3.230 m, n_1 = 1.292×10^{20} 1/m^3 and T_1 = 10.020 keV. The increment in the number of fusion neutrons produced in the compressed plasma, $N_{\mathrm{f},1}/N_{\mathrm{f},0} = C_\mathrm{R}^2 \langle\sigma v\rangle(T_0 C_\mathrm{R}^{4/3}) / \langle\sigma v\rangle(T_0) = 1.555.$

We now calculate the change in the vertical magnetic field required to implement the compression described above. The vertical field is necessary in a toroidal configuration to enforce the toroidal force balance, which requires that forces tending to drive the plasma outward are counteracted by an inward Lorentz force induced by a vertical magnetic field F_v. There are three plasma-expanding forces, namely, the F_p «tire-tube» force, the $F_{1/R}$ «1/R» force, and the F_hoop «hoop» force: $F_\mathrm{p} + F_{1/R} + F_\mathrm{hoop} = F_v$. An explicit expression for these four forces in the limit of a circular plasma cross section can be found in [15]. Here we only report the expression for a (externally imposed) vertical magnetic field needed to establish the toroidal equilibrium:

$$\frac{B_\mathrm{v}}{B_\mathrm{p}(a)} = \frac{1}{4}\frac{a}{R_\mathrm{ax}}\left[\frac{2\mu_0\overline{p(r)}}{B_\mathrm{p}(a)^2} + \frac{B_\mathrm{t}(a)^2 - \overline{B_\mathrm{t}(r)^2}}{B_\mathrm{p}(a)^2} + \ell + 2\right], \tag{16}$$

where $\ell = \ell_\mathrm{int} + \ell_\mathrm{ext}$ is the total normalized plasma inductance comprising the internal and the external contributions. In these expressions, $p(r) = n(r)T(r)$ is the plasma pressure, while B_t, B_p, B_v are the toroidal, poloidal (induced by the plasma current), and external vertical magnetic fields. The $B_{\mathrm{t,ex}}$ field is the vacuum (externally imposed) magnetic field, calculated at $R = R_\mathrm{ax}$.

To obtain a numerical value for B_v before and after the compression, we need to specify the corresponding radial dependence of plasma profiles $p(r) = n(r)T(r)$, $B_\mathrm{t}(r)$, $B_\mathrm{p}(r)$. A good model for the minor radius dependence of the plasma profiles in the reference configuration (i.e., before compression) is provided by the screw-pinch approximation to the tokamak case, which is formally obtained by the torus straightening out into a cylinder. The radial pressure balance for the screw-pinch reads

$$\frac{d}{dr}\left(p(r) + \frac{B_\theta^2(r)}{2\mu_0} + \frac{B_\varphi^2(r)}{2\mu_0}\right) + \frac{B_\theta^2(r)}{\mu_0 r} = 0. \tag{17}$$

Based on experimental results on pinch devices, as well as simplicity considerations, we adopt the following magnetic field components [21]:

$$B_\theta(r,\theta) = B_\theta(r)\frac{R_\mathrm{ax}}{R(r,\theta)}, \quad \text{where } B_\theta(r) = \frac{\mu_0 I_\mathrm{pl}}{\pi}\frac{r}{r^2+a^2};$$

$$B_\varphi(r,\theta,\lambda) = B_\varphi(r)\frac{R_\mathrm{ax}}{R(r,\theta)}, \quad \text{where } B_\varphi^2(r) = B_{\varphi,\mathrm{ex}}^2 - 2\mu_0\lambda p(r;a), \tag{18}$$

where $B_{\varphi,\mathrm{ex}}$ is the externally applied toroidal field (which is a constant, as it does not include the 1/R dependence), and where $0 < \lambda < 1$ is a parameter quantifying the degree of diamagnetism (reduction of the externally imposed toroidal magnetic field due to the presence of the plasma) — we will take $\lambda = 0.50$. In particular, the toroidal field on axis is given by $B_\varphi(0,0)^2 = B_{\varphi,\mathrm{ex}}^2 - 2\mu_0\lambda p(0;a)$. Once the magnetic field is defined, Eq. (17) gives the pressure profile: $p(r,a) = \hat{p}(a)\left[4(3a^4 - 2a^2r^2 - r^4)\right] / \left[3(a^2+r^2)^2\right]$, where $\hat{p}(a) = (3\mu_0 I_\mathrm{pl}^2) / \left[32\pi^2 a^2 (1-\lambda)\right]$ is the value on axis, and $p(\pm a, a) = 0$.

With this information at hand, we can find an expression for the vertical magnetic field needed to establish the toroidal equilibrium in the initial (pre-compression) configuration. We obtain

$$B_{\mathrm{v},0} = \frac{\mu_0 I_{\mathrm{pl},0}}{8\pi R_{\mathrm{ax},0}}\left[\frac{1+\lambda}{1-\lambda} + 2\ln\left(\frac{8R_{\mathrm{ax},0}}{a_0}\right) - \frac{3}{2}\right],$$

where the first term inside the square brackets includes the tire-tube force and the 1/R force, and the last two terms come from the hoop force.

The compression scaling for the pressure is derived from density and temperature scalings. From the generic expressions for the latter two profiles, $n(r) = \hat{n} f_n(r; a)$ and $T(r) = \hat{T} f_T(r; a)$ respectively [with the f functions becoming 1 at $r = 0$], we obtain $p_0(r) = \hat{n}_0 f_n(r; a_0) \hat{T}_0 f_T(r; a_0) \equiv \hat{p}(a_0) f_p(r; a_0)$ and $p_1(r) = C_R^{10/3} \hat{p}(a_0) f_p(r; a_1)$, where $f_p(r; a) = 4(3a^4 - 2a^2 r^2 - r^4) / \left[3(a^2 + r^2)^2\right]$. From Eq. (18), we finally obtain the scaling for the toroidal magnetic field: $B_{t,1} = \left\{C_R^2 B_{t,ex,0}^2 - 2\mu_0 \lambda C_R^{10/3} \hat{p}(a_0) \left[4(3a_1^4 - 2a_1^2 r^2 - r^4) / 3(a_1^2 + r^2)^2\right]\right\}^{1/2}$.

Introducing the scaling properties of various quantities in Eq. (16), we obtain the following expression for the required magnetic field after compression: $B_{v,1} = \frac{\mu_0 I_{pl,0}}{8\pi R_{ax,0}} \left\{C_R^{7/3} \frac{1+\lambda}{1-\lambda} + C_R^2 \left[2\ln\left(\frac{8R_{ax,0}}{a_0}\right) - \frac{3}{2}\right]\right\}$.

Numerically, we find that the vertical field should be changed from 1.786 T before the compression, to 2.121 T after the compression, a ~18.7% increase.

Compression based on plasma minor radius reduction. We also considered a second compression scheme, the one identified as «Constant-R a-compression» in [19]. In this approach, the toroidal field is increased to a point allowing plasma compression while the vertical field is increased to maintain the toroidal force balance. The plasma major radius remains unchanged during the compression, $R_{ax,1} = R_{ax,0}$ (no plasma displacement). A convenient parameter to describe this type of compression is the ratio of the plasma radius before and after the compression: $C_a \equiv a_0/a_1 > 1$. The aspect ratio scaling, $A_1 = A_0 C_a$.

A procedure similar to the one presented above yields the following results: C_a = 1.0678; plasma radius compression from a_0 = 120 to a_1 = 112.38 cm; new plasma density and temperature $n_0 = 1.100 \times 10^{20} \rightarrow n_1 = 1.254 \times 10^{20}$ 1/m^3 and $T_0 = 9 \rightarrow T_1$ = 9,823 keV; increment in the total number of fusion neutrons produced in compressed plasma, $N_{f,1}/N_{f,0}$ = 1.435. To maintain the toroidal plasma balance, the vertical magnetic field must be strengthened from $B_{v,0}$ = 1.786 to $B_{v,1}$ = 1.859, a ~ 3.6% increase.

SUMMARY AND CONCLUSIONS

We investigate the possibility of applying the PCSM (power control-based subcriticality monitoring) to safely determine a fusion-fission hybrid subcriticality without significantly interfering with the normal operation of the fission core, where nuclear waste can be transmuted and/or fissile fuel can be bred. The method consists in: (i) a standard calibration of a dedicated control rod in the fission core — a relationship between a control rod position change and the corresponding reactivity alteration may then be established; (ii) during operation, a small, slow insertion of the control rod and associated adjustment of the fusion neutron source (i.e., fusion power generated in the plasma) to ensure that the ex-core and in-core neutron detector readings are kept constant and the fission power level is unchanged; (iii) an evaluation of the subcritical multiplication factor using Eq. (9).

Neutronic calculations based on the multi-group transport equation and the PCSM procedure allowed the subcritcality evaluation with an accuracy of the order of 0.1%, suggesting that the proposed methodology can be effectively used to determine a hybrid system's subcriticality. The enhancement of the fusion neutron source strength required to reset the fission power following the control rod insertion was accomplished using plasma compression. The application of a simple 0-D-plasma power balance equation alongside a screw-pinch modelization of plasma profiles showed that the compression scheme based on inward displacement of the major radius requires minor radius and vertical magnetic field changes of –3.9% and +18.7%, respectively, while the plasma compression scheme based on a reduced minor radius and a fixed major radius requires minor radius and vertical magnetic field changes of –6.3% and +3.6%, respectively. The size of these changes seems to be acceptable from an operational point of view.

Due to a number of simplifications used in our calculation, especially those regarding the plasma compression modeling, this study is far from providing a convincing evidence that the PCSM coupled with a plasma compression/expansion technique can be implemented in an hybrid system based on the tokamak concept. In particular, the fusion power modulation by compression, required by the PCSM, is a delicate

endeavor, because the parameters of a magnetically confined plasma, such as density, temperature and pressure must meet strict constraints to avoid instabilities. The latter can cause irregularities in the operation, from anomalously large transport rates, to major disruptions (a sudden loss of confinement). Our simplified approach to fusion power modulation via plasma compression/expansion did not consider the issue of plasma stability.

In addition to plasma stability, several other points remain to be addressed in order to be confident about the suitability of the PCSM method coupled with the plasma compression/expansion technique, adopted to hybrids. The time scales associated with the control rod movement and plasma compression must be quantified, and a clear and practicable action plan should be envisaged. Some of these points can be addressed once a more definitive hybrid system design is conceived.

REFERENCES

1. **Gandini A.** HGPT based sensitivity methods for the analysis of subcritical systems. — Ann. Nucl. Energy, 2001, vol. 28, p. 1193.
2. **Gandini A.** ADS subcriticality evaluation based on the generalized reactivity concept. — Ann. Nucl. Energy, 2004, vol. 31/7, p. 813.
3. **Carta M., Fabrizio V., Falconi L., Gandini A., Iorio M.G., Peluso V., Santoro E., Burgio N.** The Power Control Based Subcriticality Monitoring (PCSM) method for ADS reactors. — In: RRFM/IGORR 2016, Berlin, Germany, 13—17 March 2016. ISBN: 978-92-95064-25-6.
4. **Snead L.L., Besmann T.M., Collins E.D., Bell G.** Deep Burn Development of Transuranic Fuel for High-Temperature Helium-Cooled Reactors. July 2010; DOI 10.2172/1023825.
5. **Sakharov A.** Memoirs. — 1978, translated by R. Lourie (Knopf, 1990).
6. **Bethe H.** — Physics Today, 1979, vol. 32, p. 44—51.
7. **Bethe H.** The Fusion Hybrid Reactor. Report SAND 81-1265, August 1981 (Colloquium at Sandia National Laboratories, United States Department of Energy, September 19, 1980).
8. **Proceedings** of FUNFI3 — 3rd International Conference on Fusion-Fission Subcritical Systems for Waste Management and Safety. Hefei, Anhui, China, 19—21 November 2018, Edited by A. Pizzuto and F.P. Orsitto, ENEA, ISBN: 978-88-8286-384-5 (2019).
9. **Rimpault G., Plisson D., Tommasi J., Jacqmin R., Rieunier J.-M., Verrier D., Biron D.** The ERANOS code and data system for fast reactor neutronic analyses. — In: International Conference PHYSOR 2002. Seoul, Korea.
10. **Di Palo L.** RC-1 Reattore 1 MW — progetto definitivo e rapporto di sicurezza. CNEN Centro Studi Nucleari Casaccia, 1966 (in Italian).
11. **Gho C.J., Palmiotti G.** BISTRO: Bidimensionnel SN transport optimisé. Un programme bidimensionnel de transport SN aux différences finies, Note No 1: Définition des algorithmes pour la géométrie X-Y, Note Technique, CEA, SPRC/LEPh 84-270, 1984 (in French).
12. **Usachev L.N.** Equations for the neutron value, reactor kinetics and perturbation theory. — In: Proceedings of International Conference on Peaceful Uses of Atomic Energy, UNO, Geneva, Switzerland, 8—20 August 1955, vol. 5, p. 503. (Доклады советской делегации на Международной конференции по мироному использованию атомной энергии. — М.: Изд-во АН СССР, 1955. 308 с.).
13. **Carta M., D'Angelo A.** — Nucl. Sci. Eng., 1999, vol. 133, p. 3.
14. **Koning A., Forrest R., Kellett M., Mills R., Henriksson H., Rugama Y.** The JEFF-3.1 Nuclear Data Library. — OECD/NEA, 2006, № 6190.
15. **Freidberg J.P.** Plasma Physics and Fusion Energy. — Cambridge University Press, 2007.
16. **Greene J.M., Johnson J.L., Weimer K.E.** Tokamak equilibrium. — Phys. Fluids, 1971, vol. 14, № 3, p. 671—683.
17. **Tait G., Bell M.G., Bell J.** Adiabatic Toroidal Compression and Free-Expansion Experiments in TFTR. — International Atomic Energy Agency, 1985.
18. **Golant V.E.** The investigation of adiabatic compression in tokamaks. — Plasma Phys. Control. Fusion, 1984, vol. 26, p. 77—86.
19. **Furth H.P., Yoshikawa S.** Adiabatic compression of tokamak discharges. — Phys. Fluids, 1970, vol. 13, № 10, p. 2593—2596.
20. **Li Ge.**The inductance of compressed plasma. — Nucl. Fusion, 2015, vol. 55, p. 033009.
21. **Freidberg J.P**. Ideal Magnetohydrodynamics. — Plenum, 1987.

AUTHORS

N. Burgio, First Researcher, Master of Art Degree (Chemistry) and PhD student (Energy and Environment), ENEA — Italian National Agency for New Technologies, Energy and Sustainable Economic Development — C.R. Casaccia, via Anguillarese 301, 00123 S. Maria di Galeria, Rome, Italy, and Sapienza University of Rome, Department of Astronautical, Electrical and Energy Engineering, Corso Vittorio Emanuele II 244, Rome, Italy, nunzio.burgio@enea.it

Mario Carta, Research Manager, PhD (Physics), ENEA — Italian National Agency for New Technologies, Energy and Sustainable Economic Development — C.R. Casaccia, via Anguillarese 301, 00123 S. Maria di Galeria, Rome, Italy, mario.carta@enea.it

Valentina Fabrizio, Researcher, PhD (Energy and Environment), ENEA — Italian National Agency for New Technologies, Energy and Sustainable Economic Development — C.R. Casaccia, via Anguillarese 301, 00123 S. Maria di Galeria, Rome, Italy, valentina.fabrizi@enea.it

Luca Falconi, Researcher, Master of Art (Physics), ENEA — Italian National Agency for New Technologies, Energy and Sustainable Economic Development — C.R. Casaccia, via Anguillarese 301, 00123 S. Maria di Galeria, Rome, Italy, luca.falconi.1@enea.it

Augusto Gandini, Honorary Fellow, PhD (Physics), Sapienza University of Rome, Department of Astronautical, Electrical and Energy Engineering, Corso Vittorio Emanuele II 244, Rome, Italy, augusto.gandini@uniroma1.it

Renato Gatto, Associate Professor, Master of Art (Physics) and PhD (Nuclear Engineering), Sapienza University of Rome, Department of Astronautical, Electrical and Energy Engineering, Corso Vittorio Emanuele II 244, Rome, Italy, renato.gatto@uniroma1.it

Vincenzo Peluso, Researcher, PhD (Energy and Environment), ENEA — Italian National Agency for New Technologies, Energy and Sustainable Economic Development — C.R. Bologna, Via dei Martiri di Monte Sole, 4 – 40129, Bologna, Italy, vincenzogiuseppe.peluso@enea.it

Emilio Santoro, Consultant, Master (Nuclear Physics), ENEA — Italian National Agency for New Technologies, Energy and Sustainable Economic Development — C.R. Bologna, Via dei Martiri di Monte Sole, 4 – 40129, Bologna, Italy, emilio.santoro1618@gmail.com

Maria Beatrice Sciarretta, Business developer, Master of Art (Energy Engineering), ENEL, Viale Regina Margherita 125, Rome, Italy, mbsciarretta@gmail.com

Статья поступила в редакцию 15 января 2021 г.
После доработки 16 марта 2021 г.
Принята к публикации 25 марта 2021 г.
Вопросы атомной науки и техники.
Сер. Термоядерный синтез, 2021, т. 44, вып. 2, с. 27—41.

УДК 621.039.51.15

SET UP OF A DETERMINISTIC CALCULATION MODEL FOR THE ANALYSIS OF FUSION-FISSION HYBRID SYSTEMS

F. Panza[1, 2], M. Carta[1], A. Cemmi[1, 3], N. Cherubini[1], V. Fabrizio[1], L. Falconi[1], F. Filippi[1,4], G. Grasso[5], F.P. Orsitto[1], V. Peluso[5]

[1]ENEA — Dipartimento Fusione e Tecnologie per la Sicurezza Nucleare — Divisione Tecnologie, Impianti e Materiali Per la Fissione Nucleare, Roma, Italy
[2]Istituto Nazionale di Fisica Nucleare — Sezione di Genova, Genova, Italy
[3]Istituto Nazionale di Fisica Nucleare — Sezione di Roma Tre, Roma, Italy
[4]Istituto Nazionale di Fisica Nucleare —Laboratori Nazionali di Frascati, Frascati, Italy
[5]ENEA — Dipartimento Fusione e Tecnologie per la Sicurezza Nucleare — Divisione Sicurezza e Sostenibilità del Nucleare, Bologna, Italy

A simplified Fusion-Fission Hybrid System (FFHS) deterministic calculation model has been developed in order to study the coupling between a fusion machine and a subcritical fission system. Monte-Carlo (MC) codes are very flexible and they have to be considered as reference calculation tools for complex systems like FFHS. On the other hand, deterministic codes can provide, in shorter calculation time respect to MC codes, parametric and sensitivity analysis, also by exploiting General Perturbation Theory (GPT) methodologies, which can usefully support the global FFHS theoretical analysis. This work describes the comparison between the results obtained for a simplified FFHS model by using a MC code (MCNP6.1, MC N-Particle) and a deterministic code (ERANOS). In particular, in this preliminary study, integral parameters like k_{eff}, thermal power, neutron fluxes and some key reaction rate profiles, will be compared. If the comparison between the two mentioned codes will give encouraging results further, more refined, studies will be performed in order to consider deterministic codes as a powerful workhorse for the FFHS analysis, including time dependent analysis devoted to transient and reactivity monitoring issues.

Key words: FFHS, Monte-Carlo codes, deterministic codes.

DOI: 10.21517/0202-3822-2021-44-2-42-46

РАЗРАБОТКА ДЕТЕРМИНИРОВАННОЙ РАСЧЁТНОЙ МОДЕЛИ ДЛЯ АНАЛИЗА ГИБРИДНЫХ СИСТЕМ СИНТЕЗА-ДЕЛЕНИЯ

Ф. Панза[1, 2], М. Карта[1], А. Чемми[1, 3], Н. Черубини[1], В. Фабрицио[1], Л. Фалькони[1], Ф. Филиппи[1], Г. Грассо[4], Ф.П. Орситто[5], В. Пелузо[4]

[1]Национальное агентство по новым технологиям, энергии и устойчивому развитию (ENEA), Отделение термоядерного синтеза и технологий ядерной безопасности, Отдел технологий, установок и материалов для ядерного деления, Рим, Италия
[2]Национальный институт ядерной физики, Генуэзское отделение, Генуя, Италия
[3]Национальный институт ядерной физики, Третье римское отделение, Рим, Италия
[4]ENEA, Отделение термоядерного синтеза и технологий ядерной безопасности, Отдел ядерной безопасности и устойчивого развития, Болонья, Италия
[5]Консорциум CREATE, Университет Неаполя им. Федерико II, Неаполь, Италия

Для изучения связи между термоядерной установкой и докритической зоной деления была разработана упрощённая детерминированная расчётная модель гибридной системы синтеза-деления (ГССД). Вычислительные программы Монте-Карло (МК) очень гибки и могут рассматриваться как эталонные инструменты расчёта для сложных систем, таких как ГССД. Детерминированные коды могут за более короткое расчётное время, чем программы МК, выполнить параметрический анализ и анализ чувствительности, также используя методы общей теории возмущений (ОТВ), ускорив этим глобальный теоретический анализ ГССД. В данной работе сравниваются результаты, полученные для упрощённой модели ГССД с использованием кода МК (MCNP6.1, Monte-Carlo N-Particle) и детерминированного кода (ERANOS). В частности, в этом предварительном исследовании сравниваются интегральные параметры: $k_{\text{эф}}$, тепловая мощность, потоки нейтронов и некоторые ключевые профили скорости ядерных реакций. Если сравнение результатов, полученных двумя упомянутыми кодами, будет признано обнадёживающим, в дальнейшем будут проведены уточнённые исследования с целью обосновать использование детерминированных кодов в качестве эффективного средства для анализа ГССД, включая зависящий от времени анализ мониторинга переходных процессов и реактивности.

Ключевые слова: гибридная программа синтеза-деления, вычислительные программы Монте-Карло, детерминированные коды.

INTRODUCTION

A Fusion-Fission Hybrid System (FFHS) [1], obtained by coupling a fusion machine and a sub-critical fission system, could, in principle, have some potential applications, including fission nuclear waste management.

This system can be seen as an Accelerator Driven System (ADS), where a subcritical fission blanket is driven by neutrons emerging from the fusion plasma instead of coming from an accelerator.

With a view to the component-by-component evaluation strategy extensively used in the ADS studies [2], one can separately analyze the FFHS's two main characteristics: the intensive neutron source and the subcritical fission blanket.

MC codes are very flexible and can be considered as reference calculation tools to deal with complex systems, such as FFHSs. On the other hand, deterministic codes can be a quicker alternative to MC codes when it comes to doing a parametric and sensitivity analysis, especially using the GPT-based methodologies [3], which are useful in supporting the global FFHS theoretical analysis.

In this work we compare, in a preliminary way, results obtained for a simplified FFHS model using a MC code (MCNP6.1) [4] and a deterministic code (ERANOS). [5]. In particular, we compare integral parameters like k_{eff}, neutron fluxes and some key reaction rate profiles.

CALCULATION MODEL SET-UP

A simplified cylindrical 2D-RZ model, with different homogenized coaxial zones, has been defined to study the subcritical fission blanket behavior with two different codes.

The model is composed by four different regions (Fig. 1). They are, starting from the center:

— plasma chamber;

— sub-critical fission blanket;

— tritium breeding blanket;

— lead-steel shielding.

In this preliminary study, neutrons were assumed to be produced from a DT-plasma, therefore the calculation model considered a monoenergetic isotropic neutron source with an emission rate of ~10^{19} n/s, placed in the center (the plasma chamber). The plasma chamber's volume is 27.5 m^3.

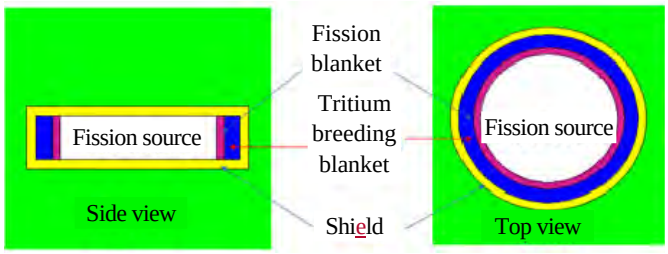

Fig. 1. RZ geometry model

A subcritical fission blanket was defined starting from an elementary fuel cell where fuel pin and lattice cell are set to allow affordable power densities and coolant flow rates. Homogeneous materials compatible with the LFR technology were chosen for the fission blanket, and their homogenization followed the design summarized in Table 1.

T a b l e 1. **Volume fractions of the fission blanket composition material**

Material	Volume fraction, %
Fuel (MA-doped MOX)	27.5
Steel (AIM1)	8.5
Void (He)	4.3
Coolant (Pb)	59.7

In the LFR concept, lead-lithium is used in the blanket as the breeder material, with a composition detailed in Table 2.

T a b l e 2. **Volume fraction of the breeding blanket component materials**

Material	Volume fraction, %
Breeder (PbLi)	40.0
Steel (AISI 316L)	60.0

The shielding zone is composed by a mixture of lead and stainless steel (AISI 316L) as shown in Table 3.

T a b l e 3. **Volume fraction of the shielding component materials**

Material	Volume fraction, %
Lead	35.0
Steel (AISI 316L)	65.0

Then a reactor with a subcritical k_{eff}, of about 0.97 was modelled with the ERANOS deterministic code and then loaded in the MCNP code.

Homogenized cross sections for different zones were evaluated with the help of the ERANOS ECCO cell code using the JEFF-3.1.1 [6] nuclear data library with a standard 172 energy group structure, scattering approximation in P3 and S4 for angular distribution.

The BISTRO 2D-RZ flux module has been used for both «homogenized» and source calculations.

The neutron source considered was a DT generator that emitted 14 MeV neutrons isotropically and uniformly in the central volume of the geometry.

The same geometry and material composition were used in the MCNP6.1 based simulation. Starting from an isotropic neutron source homogeneously generated inside the « plasma chamber» region, neutrons propagated in other regions. The KCODE card was used to determine the k_{eff}, and the SDEF card was considered as a way to calculate fluxes and reaction rates.

RESULTS

The results of the effective neutron multiplication factor, k_{eff}, calculation with different reference codes are presented in Table 4.

T a b l e 4. **ERANOS vs. MCNP calculation of the effective multiplication factor**

Reference case	k_{eff}	ρ
ERANOS	0.97054	–3035
MCNP	0.98893	–1119

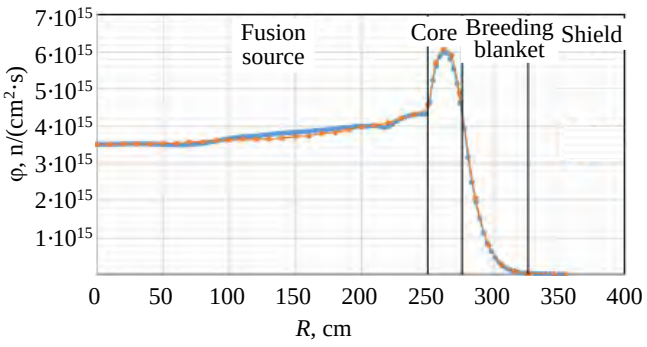

Fig. 2. Comparison of the radial flux distribution as a function of the radial distance from the cylindrical system's center, calculated with the ERANOS (•) and MCNP (•) codes

Evaluating the source neutrons' importance relative to fission neutrons from the subcritical core is of relevance for an understanding of the subcritical core behavior. The source relative importance, φ^* [7], is defined as:

$$\varphi^* = \frac{\left(\frac{1}{k_{eff}} - 1\right)}{\left(\frac{1}{k_s} - 1\right)}.$$

The ERANOS deterministic code assesses the source's importance as: $R = \varphi^* = \frac{\frac{\Phi^*,\ S}{S}}{\frac{\Phi^*,\ F\Phi}{F\Phi}}$, where Φ^* — adjoint flux of the homogeneous case; Φ — direct flux of the inhomogeneous case; S — the external source.

The results are listed below: k_{eff} = 0.97054; k_s = 0.97403; φ^* = 1.121.

The ERANOS vs. MCNP comparison also covered the neutron flux and some reaction rates along the radial distribution at the middle height of the system. It was chosen to normalize all the results obtained to the ERANOS value in the center of the geometry. Comparison of the radial flux distributions, calculated with the ERANOS and MCNP codes (Fig. 2) shows a good agreement for the whole system.

Several reaction rates derived by the two codes were compared. Fission rates were calculated using ^{235}U, ^{238}U and ^{241}Am, with the results shown in Figs. 3—5.

The behavior of the ^{235}U fission reaction rate in the fission blanket zone shows some discrepancies between the two codes, this could reflect the difference for k_{eff} value presented in Table 3.

Comparison of the ^{238}U fission reaction rate radial distributions (see Fig. 4), calculated with the two codes, suggests a good agreement for the whole fission zone.

In the case of ^{241}Am, fission rate radial distributions have a traverse similar to ^{238}U's (see Fig. 5), and one can see a good agreement between results obtained with the two codes.

Then, the rates of capture reactions involving ^{237}Np and ^{238}U, as well as ^{6}Li(n, α) were analyzed and compared (Figs. 6—8).

There are notable discrepancies in the behavior of the ^{237}Np capture rate radial sampling (see Fig. 6) in the fission blanket zone, simulated with the two codes, which call for an explanation.

Discrepancies similar to those found for ^{237}Np are revealed for the ^{238}U capture rate in Fig. 7, although in the latter case the study is in progress.

The comparison between the two codes for the ^{6}Li(n, α) rate radial distributions, in the breeding blanket zone, shows a very good agreement along all the radial direction (see Fig. 8).

CONCLUSIONS

The coupling of a subcritical blanket with a fusion source, like in FFHS, may allow the fundamental problem of disposing of long-lived radioactive waste from the back end of the fuel cycle to be approached.

A simplified Fusion-Fission Hybrid System (FFHS) model could allow to study and evaluate some important parameters using different calculation methodologies.

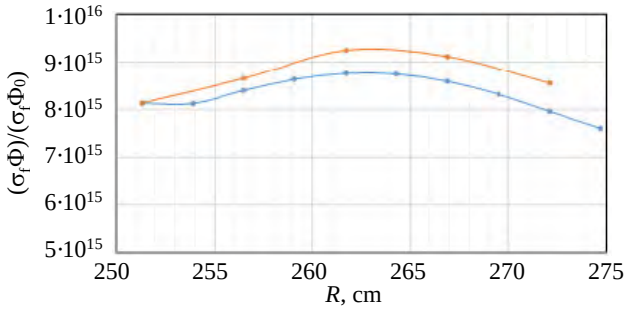

Fig. 3. Comparison of the ^{235}U fission reaction rate as a function of the radial distance from the cylindrical system's center, calculated with the ERANOS (•) and MCNP (•) codes

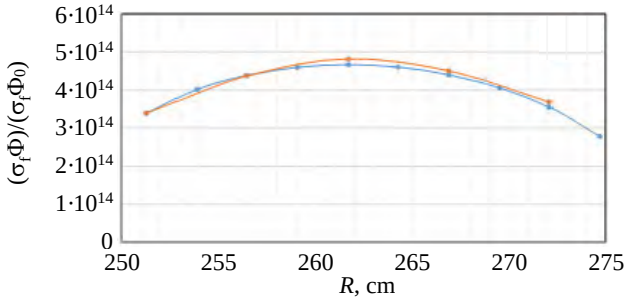

Fig. 4. Comparison of the ^{238}U fission rate radial distribution as a function of the radial distance from the cylindrical system's center, calculated with the ERANOS (•) and MCNP (•) codes

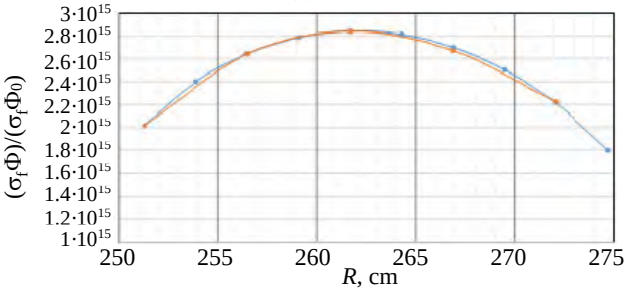

Fig. 5. Comparison of the ^{241}Am fission reaction rate as a function of the radial distance from the cylindrical system's center, calculated with the ERANOS (•) and MCNP (•) codes

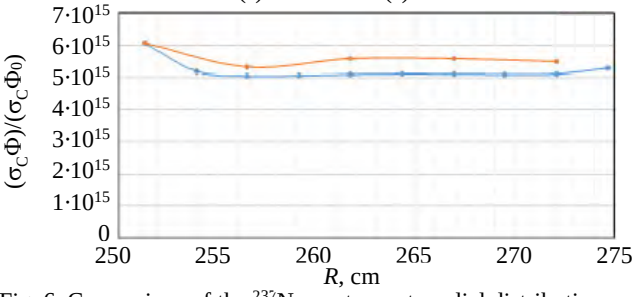

Fig. 6. Comparison of the ^{237}Np capture rate radial distribution as a function of the radial distance from the cylindrical system's center, calculated with the ERANOS (•) and MCNP (•) codes

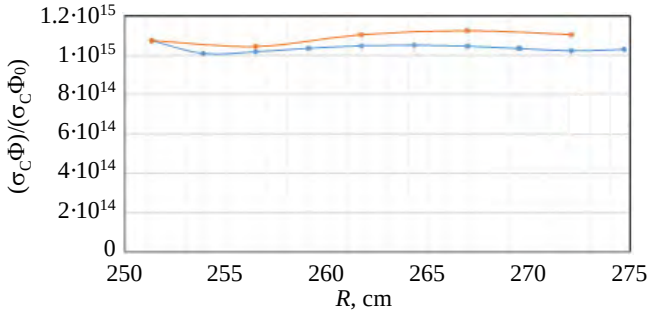

Fig. 7. Comparison of the ^{238}U capture rate radial distribution as a function of the radial distance from the cylindrical system's center, calculated with the ERANOS (•) and MCNP (•) codes

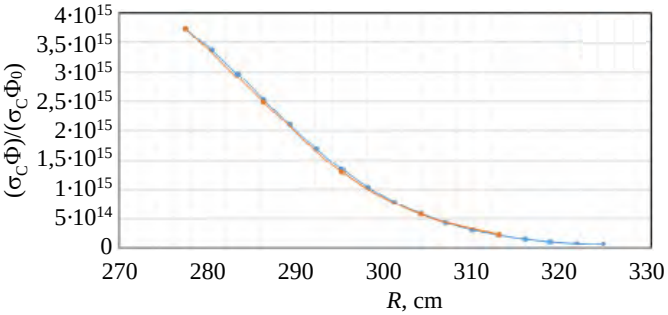

Fig. 8. Comparison of the ^{6}Li capture rate radial distribution as a function of the radial distance from the cylindrical system's center, calculated with the ERANOS (•) and MCNP (•) codes

The simplified RZ model developed in this work was analyzed by both deterministic and Monte Carlo calculations, the analysis was focused on some preliminary parameters, such as the neutron multiplication factor and fluxes and the radial distribution of some reaction rates. This preliminary comparison yields some evidence of a fairly good agreement between the Monte-Carlo and deterministic codes.

There are some differences between the k_{eff} results and consequently for flux absolute values, which fact calls for further and more in-depth research and subsequent verification.

A full agreement between these results will allow the deterministic code to be useful in performing some important evaluations concerning the FFHSs.

REFERENCES

1. **Bethe H.A.** The fusion hybrid. — Phys. Today, 1979, vol. 32 (5), p. 44—51.
2. **Salvatores M.** Physics features comparison of TRU burners: fusion/fission hybrids, accelerator-driven systems and low conversion ratio critical fast reactors. — Annals Nucl. Energy, 2009, vol. 36, p. 1653—1662.
3. **Gandini A.** Generalized Perturbation Theory (GPT) Methods. A Heuristic Approach. — In: Advances in Nuclear Science and Technology, vol. 19, J. Lewins and M. Becker Eds., Plenum Publishing Corporation, New York, 1987.
4. **Goorley T. et al.** Initial MCNP6 release overview. — Nuclear Technology, 2012, vol. 180, p. 298—315.
5. **Rimpault G., Plisson D., Tommasi J., Jacqmin R., Rieunier J.-M., Verrier D., Biron D.** The ERANOS code and data system for fast reactor neutronic analyses. — In: Intern. Conf. PHYSOR, Seoul, Korea, 2002.
6. **The JEFF-3.1.1** Nuclear Data Library, JEFF Report 22, Validation Results from JEF-2.2 to JEFF-3.1.1- OECD NEA 2009, ISBN 978-92-64-99074-6.
7. **Gandini A., Salvatores M.** The physics of subcritical multiplying systems. — J. of Nuclear Science and Technology, 2002, vol. 39:6, p. 673—686; DOI: 10.1080/18811248.2002.9715249.

AUTHORS

Fabio Panza, Researcher, PhD; ENEA Dipartimento Fusione e Tecnologie per la Sicurezza Nucleare — Divisione Tecnologie, Impianti e Materiali per la Fissione Nucleare, Roma, Italy; Istituto Nazionale di Fisica Nucleare, Sezione di Genova, Genova, Italy fabio.panza@enea.it

M. Carta; Dipartimento Fusione e Tecnologie per la Sicurezza Nucleare — Divisione Tecnologie, Impianti e Materiali Per la Fissione Nucleare, Roma, Italy;

A. Cemmi; ENEA Dipartimento Fusione e Tecnologie per la Sicurezza Nucleare — Divisione Tecnologie, Impianti e Materiali Per la Fissione Nucleare, Roma, Italy; Istituto Nazionale di Fisica Nucleare — Sezione di Roma Tre, Roma, Italy

N. Cherubini; ENEA Dipartimento Fusione e Tecnologie per la Sicurezza Nucleare — Divisione Tecnologie, Impianti e Materiali Per la Fissione Nucleare, Roma, Italy

V. Fabrizio; ENEA Dipartimento Fusione e Tecnologie per la Sicurezza Nucleare — Divisione Tecnologie, Impianti e Materiali Per la Fissione Nucleare, Roma, Italy

L. Falconi; ENEA Dipartimento Fusione e Tecnologie per la Sicurezza Nucleare — Divisione Tecnologie, Impianti e Materiali Per la Fissione Nucleare, Roma, Italy

F. Filippi; ENEA Dipartimento Fusione e Tecnologie per la Sicurezza Nucleare — Divisione Tecnologie, Impianti e Materiali Per la Fissione Nucleare, Roma, Italy ; Istituto Nazionale di Fisica Nucleare — Laboratori Nazionali di Frascati, Frascati, Italy

G. Grasso; ENEA Dipartimento Fusione e Tecnologie per la Sicurezza Nucleare — Divisione Sicurezza e Sostenibilità del Nucleare, Bologna, Italy

F.P. Orsitto; Consorzio CREATE Università di Napoli Federico II, Napoli, Italy

V. Peluso; ENEA Dipartimento Fusione e Tecnologie per la Sicurezza Nucleare — Divisione Sicurezza e Sostenibilità del Nucleare, Bologna, Italy

Статья поступила в редакцию 15 января 2021 г.
После доработки 16 марта 2021 г.
Принята к публикации 25 марта 2021 г.
Вопросы атомной науки и техники.
Сер. Термоядерный синтез, 2021, т. 44, вып. 2, с. 42—46.

UDC 621.039.673

HIGH FIELD TOKAMAKS AS COMPACT NEUTRON SOURCES

F.P. Orsitto[1], M. Romanelli[2], M. Vinay[3]

[1]*ENEA, Department Fusion and Nuclear Safety, Frascati, Italy*
[2]*Tokamak Energy Ltd., 173 Brook Drive, Milton Park, Oxon, OX14 4SD, United Kingdom*
[3]*Institute of Plasma Research, Gandinaghar, Gujarat, India*

Fusion reactor scaling laws can be used to define plasma parameters of high field compact tokamak for low fusion gain applications as it is the case of compact neutron sources. The attractive physics of the high field tokamaks explored on Alcator devices and FTU has demonstrated that tokamaks (at magnetic field $B \geq 7$ T) can be operated in L-mode with substantial increase of confinement. In particular the operation with pellets is attractive in this respect because it opens up the possibility of operating the machine in ohmic plasmas at very high density (plasma density $n_e \geq 1 \cdot 10^{20}$ m^{-3}) with improved confinement properties. The compact high field tokamaks are characterized by a fundamental ohmic confinement with possibly a low RF heating power because of the limited space available. This paper is dedicated to i) a summary of the physics of high field tokamaks as derived from the database of FT, FTU and Alcator devices (including Alcator-C-MOD); ii) a discussion of their confinement properties in scenarios operated with pellets; iii) the scaling laws for fusion reactors, which allow for the evaluation of the geometry and plasma parameters of compact high field ($B \geq 7$ T) tokamaks at aspect ratio $A \geq 2.5$ and at low aspect ratio ($A < 2$); iv) the technical feasibility of these neutron sources and their technology readiness level.

Key words: high field tokamaks, compact fusion neutron sources.

DOI: 10.21517/0202-3822-2021-44-2-47-56

ТОКАМАКИ С СИЛЬНЫМ ПОЛЕМ КАК КОМПАКТНЫЕ ИСТОЧНИКИ НЕЙТРОНОВ

Ф.П. Орситто[1], М. Романелли[2], М. Винай[3]

[1]*ENEA (Национальное агентство по новым технологиям, энергетике и устойчивому развитию экономики), Отделение безопасности термоядерной и ядерной энергетики, Фраскати, Италия*
[2]*ООО «Токамак Энерджи», 173 Brook Drive, Milton Park, Oxon, OX14 4SD, Великобритания*
[3]*Институт исследований плазмы, Гандинагар, Гуджарат, Индия*

Законы масштабирования термоядерного реактора могут быть использованы для определения параметров плазмы компактного токамака с сильным полем (ТСП), с низким отношением термоядерной мощности к затрачиваемой, как в случае компактных источников нейтронов. Привлекательная физика ТСП, исследованных на токамаках Alcator и FTU, показала, что токамаки (при магнитном поле $B \geq 7$ Тл) могут работать в L-режиме с значительным увеличением удержания. В частности, привлекательна инжекция пеллет, поскольку она открывает возможность работы токамака с омической плазмой, имеющей очень высокую плотность ($n_e \geq 1 \cdot 10^{20}$ м$^{-3}$) и обеспечивающей лучшее удержание. Компактные ТСП характеризуются тем, что в них в основном используется омическое удержание с небольшой добавкой радиочастотного нагрева из-за ограниченного пространства. В статье даётся обзор физики ТСП на основе данных, полученных на токамаках FT, FTU и ALCATOR (включая Alcator-C-MOD), обсуждается удержание плазмы в таких токамаках при инжекции пеллет, рассматриваются скейлинги для термоядерных реакторов, позволяющие оценить геометрические характеристики и параметры плазмы компактных ТСП ($B \geq 7$ Тл) при аспектных соотношениях $A \geq 2{,}5$ и при $A < 2$, обсуждается техническая осуществимость этих источников нейтронов и уровень их технологической готовности.

Ключевые слова: токамаки с сильным полем, компактные термоядерные источники нейтронов.

INTRODUCTION

Recently, advances in the area of superconducting magnet technologies have opened up the prospekt of operating tokamak-type fusion reactors at higher magnetic fields [1, 2]. However, experimental data available for tokamak plasmas at high fields (>6 T) are scarce. Advantages of high field operation for fusion based tokamaks are well known. At fusion relevant temperatures in the range of 10—20 keV, the fusion power scales as $P_{\text{fus}} = \beta^2 B^4 R^3 / A^2$, where B is the toroidal magnetic field on axis, R the major radius of the tokamak, the aspect ratio A — major radius/minor radius, β = kinetic pressure/magnetic pressure. Various high field based tokamak fusion reactors are proposed for this purpose, such as Ignitor [3], SPARC [1] and ARC [4]. Current experiments however operate at relatively lower magnetic fields (<5 T). Extensive data for studying the physics at high fields $B > 6$ T is only limited to a handful of tokamaks that are currently not in operation. There is also a need to create a dedicated database for high field tokamaks that will serve as a basis for the design of tokamaks operating at

high fields in the near future due to the advancement of magnetic technologies capable of operating at higher fields. Only five tokamaks have operated till date with fields higher that 6 T. These are the Alcator family — Alcator-A, Alcator-C, and Alcator-C-MOD [5—9], the Frascati Tokamak (FT) [10—12] and Frascati Tokamak Upgrade (FTU) [13, 14]. This paper will mainly focus on the experimental results from these high field tokamaks in the ohmic regime which will serve as the possible baseline operational scenario for the compact neutron source. Operation in the ohmic regime has the advantage over the standard ELMy H-mode due to the absence of ELMs (edge localized modes). Moreover the power threshold for entering into the H-mode (high confinement mode) P_{LH} scales with the toroidal magnetic field [15]: i.e. $P_{LH} \approx B^{4/5}$, and this means that higher power would be needed to get into H-mode. Experiments on Alcator-C-MOD showed that the scaling of the power threshold for entering the H-mode is approximately P_{LH}, MW = 0.044nBS where n is the line average electron density, S is the last close magnetic surface area [20]. More detailed investigations in Alcator-C-MOD (for magnetic fields $B \leq 5.4$ T) showed that there is a minimum power $P_{LH} \approx 1.5$ MW at a density close to $n = 1.5\ 10^{20}$ m^{-3} [21]. H-mode obtained at $B = 7.9$ T with lithium pellet injection is reported using ICRF H and He^3 minority heating. High field operation for spherical tokamaks (ST) is also considered in the present study [16—19]. The extrapolation of low field ST data to high fields is used for determining the scaling at higher fields. The paper is divided into five sections. i) will summarise briefly the experimental evidences from high field tokamaks having a large aspect ratio supporting the operation in the ohmic regime; ii) is dedicated to design criteria for a MCF (magnetic confinement fusion) neutron source to define the scaling laws for tokamak fusion reactor plasmas. The determination of the parameters of a high field tokamak as a fusion neutron source is carried out. The method used was presented at FUNFI3 conference [22]; iii) includes the determination of the parameters of an ST as a neutron source based on the confinement scaling laws of NSTX, START and MAST [19]; iv) is dedicated to the technology readiness level (TRLs) of tokamak sub-systems. Conclusion and perspectives for the future work are outlined in v). The results reported are based only on theoretical physics analysis, the engineering constraints (such as the shieldings which must be included in the design of tokamak devices) are not considered in the present analysis.

SUMMARY OF RELEVANT EXPERIMENTAL RESULTS FROM HIGH FIELD TOKAMAKS: ALCATOR-A, ALCATOR-C, C-MOD, FT AND FTU

A summary of ohmic based discharges from high field machines Alcator A-C, Alcator-C-MOD, FT, and FTU is reviewed here. Table 1 below shows the main physics parameters of the machines. While FT, FTU and Alcator-C are all circular limiter plasma machines, Alcator-C-MOD is the only divertor machine to operate at a field of more than 5 T. Operation at higher field allows operation at higher densities thus allowing operation at a higher Lawson confinement parameter.

T a b l e 1. **High field machine parameters**

Parameter	Alcator-A	Alcator-C	Alcator-C-MOD	FT	FTU
Major radius, m	0.54	0.58—0.71	0.68	0.83	0.935
Minor radius, m	0.10	0.10—0.17	0.21	0.20	0.305
Plasma current, MA	0.3	0.8	3.0	0.6	1.6
Magnetic field, T	9	13	9	10	8
Divertor/Limiter	Circular plasmas	Circular limiter plasmas	Divertor plasma	Circular plasmas	Circular limiter plasms
Heating					
ECRH					140 GHz, 0.5 MW
LHCD	2.45 GHz 100 kW	2.45 GHz, 70 kW and 4.6 GHz, 1.5 MW	4.6 GHz, 3 MW	2.45 GHz	8 GHz, 1 MW
ICRH		180 MHz, 500 kW	40—80 MHz, 8 MHz		433 MHz, 0.5 MW

Ohmic confinement and density limit in high field tokamaks. *Alcator-C tokamak.* Experiments performed on Alcator-C at densities $\leq 8\times10^{20}$ m^{-3}, plasma current $\leq$0.75 MA and magnetic fields $\leq$13 T [28] showed that the turbulent trapped electron modes (TEM) regime dominates at lower densities, in the linear ohmic confiment, where the Alcator scaling is valid, and ion temperature gradient (ITG) turbulence dominate at higher densities, leading to a saturation of the energy confinement time at high densities. Subsequent experiments with frozen deuterium pellets [30] showed that pellet fuelled plasmas do not show a saturation of the confinement time as seen in conventional gas puffing due to supression of the ITG regime, leading to an

increase in confinement time. Fig. 1 below has been adopted directly [30], shows the increase in the confinement time with pellets.

FTU Tokamak. High density experiments on FTU have been extensively performed using pellets with the repeatative pellet enhanced plasma (PEP) modes leading to improved confiment [29]. This is again due to the reduced ion transport accompanied with supression of sawtooth activity. Experiments were carried out at a magnetic field of 7.1 T and a plasma current of 0.8 MA, where the density was increased from 1.5×10^{20} to 7.0×10^{20} m^{-3} with a drastic increase in the neutron rate of 4×10^{12} n/s. Further optimization extended this regime to 8 T and 1.25 MA plasma current with multiple pellets. Record neutron rates were achieved for FTU up to 1.5×10^{13} n/s, High confinement factor $H_{97} \geq 1.1$ with respect to the ITER-97L scaling law was achieved with these parameters. The figures reported in this section are extracted from [13, 14]. The ohmic operation at high field in FT, FTU, Alcator-C and Alcator-C-MOD was characterized by the Alcator scaling (the FTU ohmic scaling law is presented here):

$$\tau_E, \text{ ms} = Kn_e(10^{20}\ \text{m}^{-3})q^{1.42\pm0.07},\ K = 7.1\pm0.6, \qquad (1)$$

where K is a dimensional numerical constant, q the cylindrical safety factor and τ_E is the confinement time, ms.

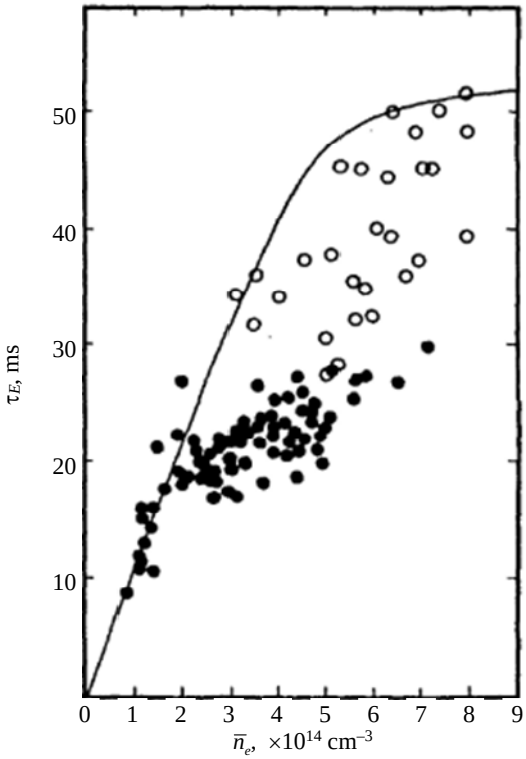

Fig. 1. Effect of pellets on the confinement time (adopted from [30]): • — gas-fueled; ○ — pellet-fueled

Fig. 2 shows a database of FTU where the confinement time vs the electron density is reported at various currents [1]. In Fig. 2, it is seen that the linear (vs density) ohmic confinement (LOC) regime holds up to a critical density, beyond which the SOC (saturated ohmic confinement) holds. The LOC regime is however seen to extend beyong the critical density with pellet operation, thus allowing for higher confinement times. Fig. 3 shows a comparision of the confinement time in FTU before and after pellet injection. There is good consistency of the confinement time with the L-mode scaling. There is almost a doubling of the confiment time as shown for the FTU pulse № 12 744 with the L-mode ITER-89P scaling law of confinement, in presence of pellets $\frac{\tau_{E_{\text{Pellet}}}}{\tau_{E_{\text{ITER-89P}}}} \sim 2$.

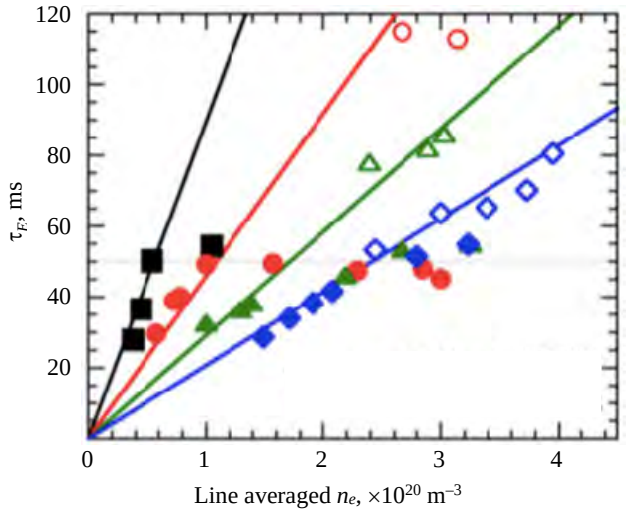

Fig. 2. FTU confinement time vs electron density at various plasma currents: ■ — 0.5; • — 0.8; ▲ — 1.1; ◆ — 1.4 MA. Open symbols correspond to pellet operations. The horizontal line is the value of the saturated ohmic confinement time on FTU. The plot shows that pellet operation recovers the linear scaling at high density [13, 14]. $\tau_{E\text{-linear}} = Kn_e(10^{20}\ \text{m}^{-3})q^{1.42\pm0.07}$, $K = 7.1\pm0.6$

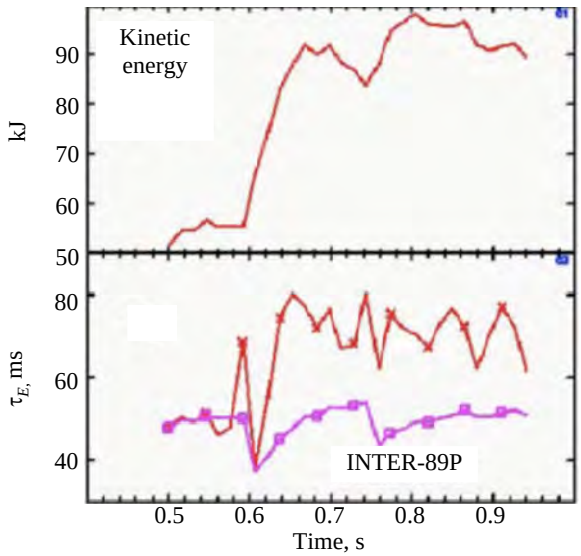

Fig. 3. Comparison between the ITER-89P L-mode confinement scaling law and confinement time measured with pellets, together with the increase of the plasma kinetic energy evolution are shown. Plasma parameters of FTU pulse № 12 744 are: B_T = 6.88 T, n_e (line average) = $2\cdot10^{20}$ m^{-3}

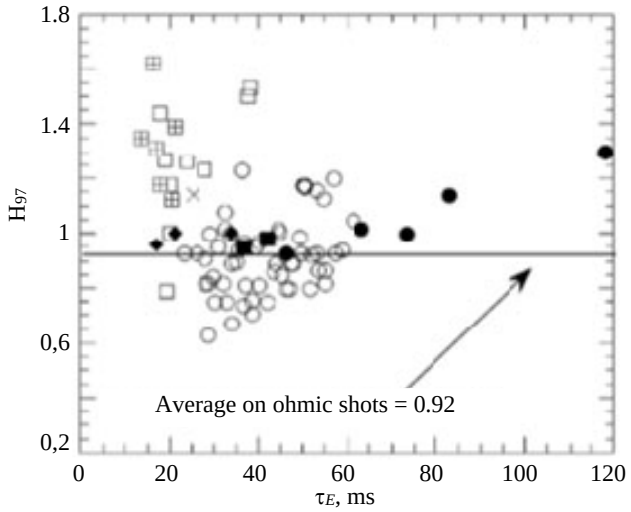

Fig. 4. FTU Database showing the H_{97} confinement improvement factor with respect to the L-mode confinement scaling law ITER-97P. $H_{97} \leq 1.3$ with pellet operation: ○ — OH; □ — LH —; ⊞ — LH + ECRH; × — ECRH; ◆ — IBW; ■ — RI; ● — pellet

Fig. 4 shows a plot of the confinement factor H_{97} of the FTU database with the ITER-97 L-mode scaling where $H_{97} = \tau_E$ measured/τ_E ITER-97 is the ratio of measured confinement time and that evaluated using the ITER L-mode scaling. The results indicate that a confinement factor of $H_{97} \approx 1.3$ can be obtained with pellet fuelled discharges.

Fig. 4 also includes data from discharges with ohmic heating and ohmic pellet operation, as well auxiliary radiofrequency (RF) heated discharges using Lower Hybrid (LH), electron cyclotron (ECRH), IBW (Ion Bernstein wave), and RI (improved highly radiating mode). In this context it can be noted that ohmic pellet operation reaches H_{97} values close to that obtained in ITB discharges where LH was combined with ECRH.

The Table 2 shows the detailed consistency of the parameters of the FTU pellet injected pulse № 12 744 (see also Fig. 2) with those obtained by the system code SPECTRE [26] using L-mode ITER-97P confinement scaling law: $H_{97} = 1.27$ is found by the system code to reproduce the FTU discharge parameters.

T a b l e 2. **Plasma parameters of the FTU pellet pulse № 12 744 with SPECTRE system code calculations using ITER-97P L-mode confinement scaling law**

Parameters	FTU 12 747	SPECTRE system code
H_{97}	1.23	1.25
R_0, m	0.9414	0.9407
A	3.35	3.35
I_p, MA	0.7931	0.7904
B_T, T	6.88	6.88
n_{line}, 10^{20} m^{-3}	2.71	2.64
n_{avg}, 10^{20} m^{-3}	—	1.32
$<T_e>$, keV	—	1.1
T_{e0}, keV	1.47	1.77
τ_E, ms	88.1	87.1
P_{OH}, MW	1.18	1.06
q_{95}	4.869	4.27
Z_{eff}	1.0	1.27
β_P	0.393	0.372
W_{therm}, kJ	107.3	103
V_{loop}, V	1.489	1.47
Neutron yield, s^{-1}	5.4×10^{12}	—

The parameters of the FTU pulse are included in the database international multi-tokamak confinement profile database http://tokamak-profiledb.ukaea.org.uk.

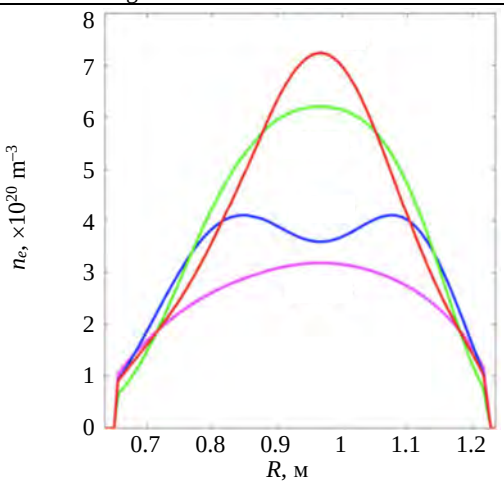

Fig. 5. Time evolution of the Abel-inverted interferometer density profile after pellet injection In ohmic discharge. FTU pulse № 25 255 (reprinted from [13]): — 67; — 8; — 0.4 ms; — pre pellet

One of the most important characteristics of the ohmic regime with pellets is the density peaking as is shown in Fig. 5. The density peaking improves by a substantial factor after the pellet injection.

A feature of high field machines is the dependence of the density limit on the magnetic field. The Fig. 6 reports a comparison of the FTU data ordered vs the value of $I_p/(\pi a^2)$ (Greenwald density) and vs the toroidal magnetic field on axis B_T: showing that it's the latter the order parameter for the central density limit. The central density limit is therefore given by the following scaling law [23] $n_{e\ new} = CB^{1.5}$, where C is a function of the safety factor.

Summary of the experimental evidences from high field tokamaks ALCATOR-C-MOD. Experiments on

Alcator-C-MOD confirmed that there is a critical density after which the LOC (Linear ohmic confinement) switches to saturated ohmic confiment (SOC) and the confinement time is seen to follow the τ_E ITER-89P scaling law [5]. Fig. 7 shows the SOC density (i.e. the critical transition density above which the ohmic confinement saturates) vs the major radius for various devices as reported in [5]: the density at the confinement saturation is decresing as 1/*R*.

It has been demonstrated on Alcator-C-MOD that the transition to SOC happens at a fixed collisionality where $\nu^* = \frac{\text{collision frequency}}{\text{bounce frequency}} \approx \frac{qRZ_{\text{eff}} n_e A^{3/2}}{T^2}$ [5], validating the scaling $n_{e\,\text{SOC}} \approx \frac{1}{qR}$. These data are taken on Alcator-C-MOD at a toroidal magnetic field B_T = 5.2 T. In Fig. 8 the transition from LOC to SOC is reported in a density scan, together with the curves representing the neo-Alcator scaling (eq. 1) and the ITER-89P L-mode scaling.

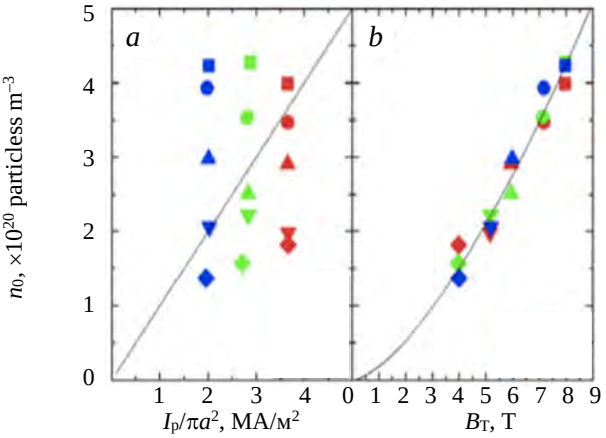

Fig. 6. Central line-averaged density at the disruption for the density limit versus the plasma current density for different BT (*a*) and versus BT for different Ip values (*b*). See boxes in the figure for the meaning of symbols and colours. The solid lines correspond to the Greenwald density limit n_G: ■ — 8; ● — 7.2; ▲ — 6; ▼ — 5.2; ◆ — 4 T (*a*) and to the new scaling law $n_{e\,\text{new}}$ (reprinted from [23]): ● — 900; — 700; — 500 kA (*b*)

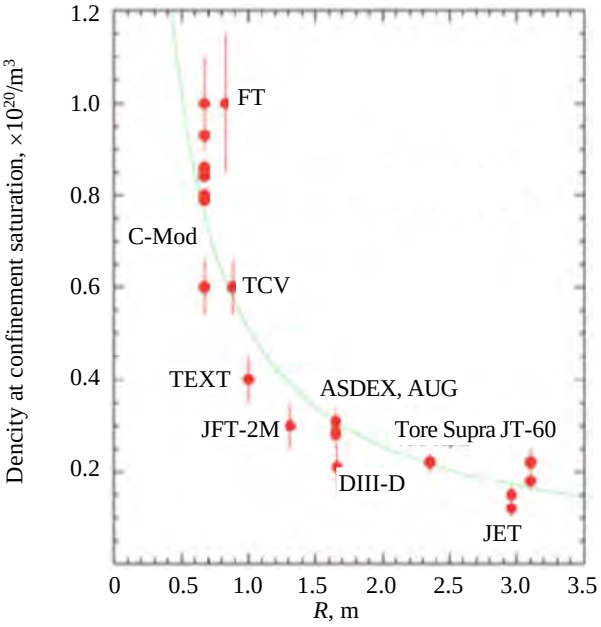

Fig. 7. The transition density from LOC to SOC as a function of major radius for different devices at fixed values of *q* (safety factor) in the interval *q* = 2.8—3.8. The solid curve represents 1/*R* dependence (reprinted from [5])

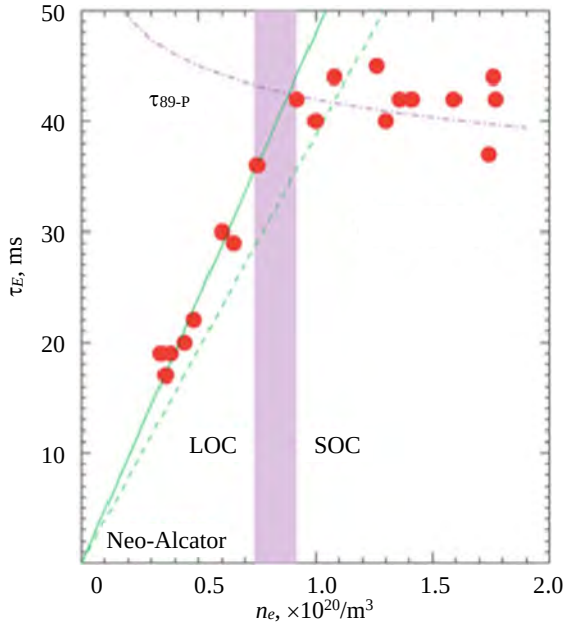

Fig. 8. The energy confinement time (from kinetic profiles) as a function of average electron density for a series of 5.2 T, 0.81 MA ohmic discharges. The shaded vertical bar indicates the boundary between the LOC and SOC regimes. The dashed line is the neo-Alcator scaling, the solid line is the best fit to the low density points, and the dash-dot line is the ITER-89P L-mode scaling. (reprinted from [5])

DESIGN CRITERIA FOR A MCF (MAGNETIC CONFINEMENT FUSION) NEUTRON SOURCE: SCALING LAWS FOR TOKAMAK FUSION REACTOR PLASMAS

The criteria determining the parameters for a fusion neutron source can be set by conditions useful to derive scaling laws specific for fusion reactors, where the alpha particle power is an important quantity entering the physics of the system. We can define a set of conditions useful for determining the working parameters of a fusion reactor (FR) [22, 24]:

— FR1. $Q = Q_0$ fixed: the fusion gain factor Q is taken fixed to a defined value $Q = Q_0$;

— FR2. $\tau_{SD} = \Lambda_{SD}\tau_E(\Lambda_{SD} << 1)$, i.e. τ_{SD} slowing down time of alpha particles $<<\tau_E$ energy confinement time, Λ_{SD} is a numerical constant);

— FR3. $P_0 = \Lambda_{LH} P_{LH}$ (P_α is the alpha power; P_{LH} here is the power threshold for entering the H-mode (High Confinement mode) and the formula used is the Martin scaling [15]; Λ_{LH} is a numerical constant). Here two possibilities are considered in relation to the value of the numerical constant Λ_{LH};

— FR3.1. $\Lambda_{LH} < 1$, the alpha heating can be relatively low and not sufficient to keep the plasma in H-mode;

— FR3.2. $\Lambda_{LH} > 1.5$, the alpha heating can be sufficient to keep the plasma in H-mode.

If we use the L-mode confinement time scaling [25] for defining the functional dependences on the plasma parameters in the previous condition FR2, We find that the scaling parameter linking equivalent fusion plasmas is:

$$S_{FR}\left[\text{L-mode}\right] = f(\Lambda_{SD}, \Lambda_{LH}, f_\alpha, M_{eff}) R B^{5/2} A^{-3/4} Q_0^{-0.7}, \tag{2}$$

where R is the tokamak major radius; B the toroidal magnetic field on axis; the aspect ratio of the tokamak ($A = R/a$); Q_0 is the fusion gain factor, which here is supposed not high. The function $f(\Lambda_{SD}, \Lambda_{LH}, f_\alpha, M_{eff})$ depends on the numerical constants Λ_{SD}, Λ_{LH}, M_{eff} (plasma effective ion mass) and f_α (the plasma diluition).

The possibility of having enough alpha particles power to keep the plasma in H-mode can be also considered: therefore in condition FR2 the ITER H-mode IPB-98 (y, 2) scaling law of confinement time [25] must be used and $\Lambda_{LH} > 1$ is implicit in condition FR3. The scaling parameter for these fusion plasmas is:

$$S_{FR}\left[\text{H-mode}\right] = f(\Lambda_{SD}, \Lambda_{LH}, f_\alpha, M_{eff}) R B^{4/3} A^{-1} Q_0^{1/3}. \tag{3}$$

The scaling law was used in [22] for the analysis of medium size tokamaks parameters.

In this paper Spherical Tokamaks (ST) are considered as well, as candidate neutron sources: in this case, in the condition FR2, the confinement time scaling typical of the ST [19] will be used together with the condition $\Lambda_{LH} > 1.5$ and the same scaling law for the H-mode power threshold. The same calculations (as in the previous cases) can be done and the result is the scaling parameter S_{ST} (NSTX scaling) or ST:

$$S_{ST}[\text{NSTX scaling}] = C_{ST} R_{ST}^{-1} Q_0^{0.61} B^{-1.13} A^{1.59} M_{eff}^{0.22} q^{0.4};$$

$$C_{ST} = \left(\frac{\Lambda_{SD}}{A_{SD}}\right)^{-0.036} \left(\frac{\Lambda_{LH} A_{lh}}{f_\alpha}\right)^{0.24}, \tag{4}$$

where A_{SD}, A_{lh} are numerical constants related to the slowing down time, and to the L—H-transition scaling law. The following meaning can be associated to the eqs. 2, 3 and 4: the value of S_{FR} and S_{ST} define families of equivalent fusion plasmas in terms of confinement and fusion gain. In equations 2, 3 and 4, a DT-plasma is considered. Strictly speaking the formula (4) is derived using the NSTX confinement scaling law, which is valid only for $A = 1.4$ and the safety factor $q = q$ NSTX, then we can use the final form of the ST scaling parameter:

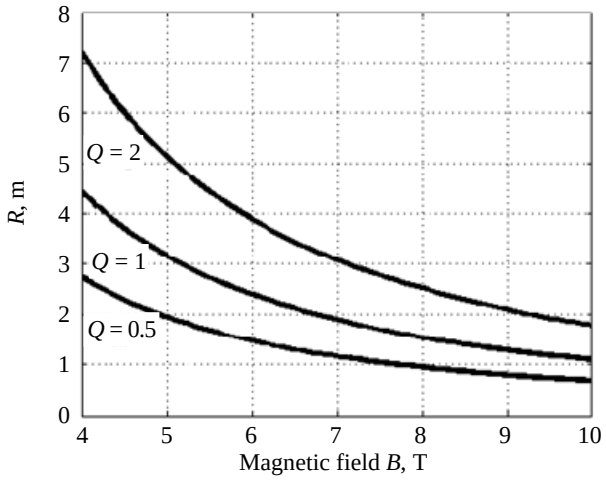

Fig. 9. Major radius vs magnetic field on axis at gain factors $Q_0 = 0.5$, 1, 2, for devices with aspect ratio $A = 2.5$, $q_{cyl} = 3.47$

$$S_{ST}[\text{NSTX scaling}] = C'_{ST} R_{ST}^{-1} Q_0^{0.61} B^{-1.13};$$

$$C'_{ST} = \left(\frac{\Lambda_{SD}}{A_{SD}}\right)^{-0.036} \left(\frac{\Lambda_{th} A_{lh}}{f_a}\right)^{0.24} \left[A^{1.59} M^{0.22} q^{0.4}\right]_{NSTX}. \tag{5}$$

Determination of the parameters of a high field tokamak as a fusion neutron source. Using the above scaling relations, we can evaluate the design characteristics of a high field tokamak as a neutron source. Two design scenarios are considered — a medium aspect ratio machine with $A = 2.5$ and a low aspect ratio machine with $A < 1.8$.

The Fig. 9 shows a plot of the major radius versus the magnetic field on axis at gain factors $Q_0 = 0.5$, 1,2, for aspect ratio $A = 2.5$ and $q_{cyl} = 3.47$, corresponding to the family of tokamaks having the scaling factor of eq. 2. and following the L-mode ITER-97P confinement scaling.

From Fig. 9 the following parameters of devices can be deduced: Q = 1, B = 8 T, R = 1.5 m, A = 2.5, q_{cyl} = 3.47; Q = 2, B = 8 T, R = 2.5 m, A = 2.5, q_{cyl} = 3.47.

To check the validity of the scalings, the SPECTRE [26] code was used to generate a self consistent design for the Q = 1 device, working at B = 8 T, consistent with P_{fus} = 8 MW. The plasma parameters of such a device where a neutron yield of the order of 10^{18} n/s is reported:

Parameters	Value
H_{97} . . .	1.2
A_{SP} . . .	2.5
Q . . .	1
R_0, m . . .	1.66
a, m . . .	0.66
Kappa . . .	1.8
I_p, MA . . .	7.26
B_T, T	8.0
P_{fus}, MW . . .	8.0
n_{avg}, 10^{20} m^{-3} . . .	1.43
$<T_e>$, keV . . .	3.9
τ_E, s . . .	0.56
P_{OH}, MW . . .	3.95
q_{95} . . .	4.45
Z_{eff} . . .	1.7
β_P . . .	0.22
W_{therm}, MJ . . .	6.64
Neutron yield, s^{-1} . . .	2.84×10^{18}

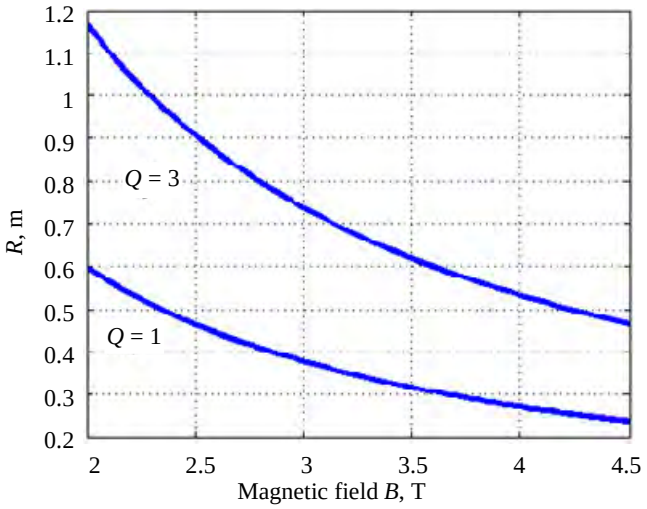

Fig. 10. Major radius vs magnetic field B on axis for spherical tokamaks with aspect ratio A = 1.8

Plasma parameters evaluated by SPECTRE system code for a Q = 1 device, B = 8 T and consistent with the calculations reported in Fig. 9.

Fig.10 reports the major radius vs magnetic field, using the scaling (5) for ST. Two sets of parameters can be deduced from Fig. 10: A = 1.8, B = 3 T, Q = 1, R = 0.4 m; A = 1.8, B = 3 T, Q = 3, R = 0.75 m.

The analysis made using the SPECTRE system code has been extended also to the ST, whose parameters can be deduced from Fig. 10. SPECTRE system code evaluation of a Q = 1.6, A = 1.6 and Q = 3, A = 1.8 ST device:

H_{98} . . .	3.3	2.9
A_{SP} . . .	1.6	1.8
Q . . .	1.6	3.0
R_0, m . . .	0.4	0.75
a, m . . .	0.25	0.416
Kappa . . .	2.8	2.8
I_p, MA . . .	2.94	4.5
B_T, T . . .	3.0	3.0
P_{fus}, MW . . .	16.25	30.1
n_{avg}, 10^{20} m^{-3}, . . .	4.18	2.15
$<T_e>$, keV . . .	7.8	9.9
τ_E, s . . .	0.17	0.47
q_{95} . . .	8.8	7.0
Z_{eff} . . .	1.73	1.73
β_{th}, % . . .	29	19.2
β_N . . .	7.45	5.33
W_{therm}, MJ . . .	2.04	6.96
Neutron yield, s^{-1} . . .	5.78×10^{18}	1.1×10^{19}

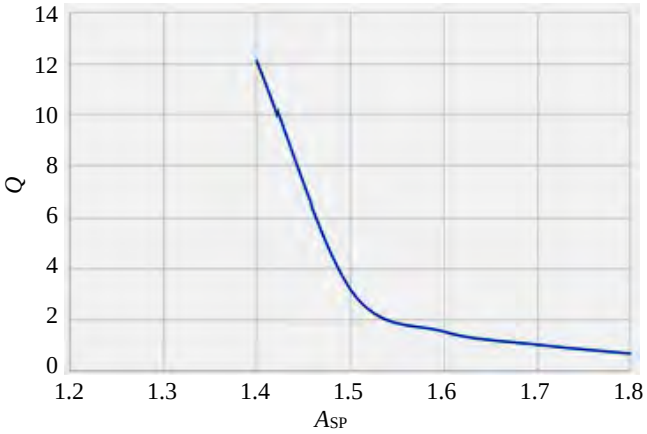

Fig. 11. System code results of the gain factor Q vs aspect ratio A_{SP} for a ST with R = 0.4 m, heating power P_{heat} = 10 MW, HH = 3.3 (the confinement factor with respect to the ITER IPB-98 (y 2) confinement scaling law), and magnetic field on axis B = 3 T

The parameters of a Q = 3 ST device working at aspect ratio A = 1.8 evaluated by the SPECTRE system code, and consistent with the results shown in Fig. 10.

A study has been carried out using the SPECTRE system code [26] related to the maximun gain factor achievable by a ST with R = 0.4 m, heating power P_{heat} = 10 MW, HH = 3.3 (the confinement factor with respect to the ITER IPB-98 (y 2) confinement scaling law), and magnetic field on axis B = 3 T, varying the aspect ratio. The results are shown in Fig. 11: the gain factor is a critical function of the aspect ratio: in the region of A_{SP} = 1.4—1.5 the gain factor can change by a substantial factor (5X).

TRL (TECHNOLOGY READINESS LEVEL) ASSESSMENTS FOR FUSION FISSION HYBRID REACTOR APPLICATION

In the context of FFH reactors, the following type of machine is in consideration:

— fusion gain $Q \sim 2$—3 machine with long pulses (say >3 hrs)/steady state, DT-plasma $P_{DT} \sim 20$—100 MW, $P_{in} \geq 10$—30 MW;

— low level of probability of disruptions: plasma parameters chosen to be away from strong MHD and density limits (for example with $\beta_N < 2.5$ for $A \geq 2.5$, $n/n_{Gr} < 0.8$);

— power on the divertor definitely lower than 5 MW/m^2: in this case the problem of the divertor is easier;

— a blanket for tritium breeding with power gain and neutron multiplication from fission;

— a machine with high reliability, working continuously;

— all maintenance by remote handling;

— modularity (facilitating rapid interventions on the divertor);

— few and simple diagnostics (the acceptable level of complexity of the diagnostics and controls depends on the plasma scenario and on the physics model).

The meanings of the different technology readiness levels are as described in [27].

The Table 3 (for devices with pulse length of 100 s) and Table 4 for devices with pulse length of 1000 s show TRL for the main subsystems of a tokamak neutron source for FFH: it seems that only ECRH (electron cyclotron resonant heating) systems are at a level of engineering maturity for the insertion in a FFH, while the other main systems need to be demonstrated in a neutron flux environment Although the most important developments differ slightly, the steps in TRL are not fine enough to distinguish the 100 and 1000 s FFH concepts.

T a b l e 3. **Technology Readiness Level for prototype with 100-second pulses**

Subsystem	TRL 100 s	Comments
Superconducting magnets	4	Not demonstrated in a neutron flux environment.
NBI (100 keV)	4	Need to demonstrate immunity to gamma and neutron effects (e.g. grid flash-over due to the ionising radiation or grid insulation degeneration).
ECRH (1 MW gyrotron)	6	The gyrotrons are not in any radiation field and steady state operation has been demonstrated at the developer's works, for hours if not months, but only on test-beds.
ICRH (1 MW)	4	As NBI but for antenna operation; also parasitic currents may inject antenna material into the plasma.

T a b l e 4. **Technology Readiness Level for prototype with 1000-second pulses**

Subsystem	TRL 1000 s	Comments
Superconducting magnets	4	Not demonstrated in accumulated neutron fluence.
NBI (100 keV)	4	Need to show long-term reliability and immunity to large neutron fluence (e.g. grid distortion).
ECRH (1 MW gyrotron)	6	As NBI but for antenna damage.
ICRH (1 MW)	4	As NBI but for antenna damage.

Table 5 shows the TRL for the plasma scenarios: here only the H-mode demonstrated on JET DTE1 at $Q < 1$ can be considered for FFH reactor designs. The other scenarios need a demonstration at least at low power.

T a b l e 5. **Technology Readiness Level for possible operational scenarios**

Scenario	TRL	Comments
L-mode and H-mode	6	OK in JET at $Q \sim 0.6$, needs demonstration at $Q \sim 2$
Hybrid mode	4	Needs demonstration in relevant $Q \approx 1$ environment – possibly JET DTE2
Advanced mode	3	To be demonstrated in a near steady-state machine

CONCLUSIONS

The recent advances of the superconductor technology has brought the attention to the possible feasibility of very compact fusion reactors at high field. Along this line of research in this paper , tokamak neutron sources working with a magnetic field $B \approx 8$ T, and aspect ratio $A = R/a = 2.5$ are considered. The paper summarizes the main experimental evidences deduced from the operation of the high field tokamaks of the Alcator family (Alcator-A, Alcator-C and Alcator-C-MOD) and the Frascati tokamaks (FT) and FTU (Frascati tokamak upgrade): ohmic operation or operation in L-mode (see ITER Phys Basis [25]) is considered. A scaling law for fusion reactors working with D:T mixture in L-mode is derived following the analysis of [22, 24] and a $Q \approx 1$

fusion neutron source with major radius $R \approx 1.5$ m at $B = 8$ T is determined. The ST are also considered in the analysis of fusion neutron sources. The scaling law of confinement derived from the operations of NSTX, START and MAST [16—19] spherical tokamaks is used in the scheme for the derivation of scaling law for ST reactors. In this case the parameters for a $Q = 1$, aspect ratio $A = 1.8$, neutron source are $B = 2$ T and $R = 0.8$ m. The TRL of tokamak subsystems is analyzed, where the TRL classification reported in [27] is adopted. A TRL ≈ 4 can be associated (in average) to the subsystems of a tokamak neutron source: this means that the basic validation in laboratory has been carried out for the main subsystems. The TRL ≈ 6 can be associated to the plasma scenarios L-mode and H-mode: this means that the scenarios must still be validated in $Q > 1$ plasma environment. The results reported are based only on theoretical physics analysis, the engineering constraints (such as the shieldings which must be included in the design of tokamak devices) are not considered in the present analysis.

REFERENCES

1. **Creely A.J. et al.** Overview of the SPARC tokamak. — J. Plasma Phys., 2020, vol. 86, p. 865860502.
2. **Whyte D.** Small, modular and economically attractive fusion enabled by high temperature superconductors. — Phil. Trans. R. Soc. A377, p. 20180354.
3. **Coppi B. et al.** Optimal regimes for ignition and the Ignitor project. — Nucl. Fusion, 2001, vol. 41, p. 1253.
4. **Sorbom B.N. et al.** ARC: a compact high field fusion nuclear science facility and demonstration power plant with demountable magnets. — Fus. Eng. Des., 2015, vol. 100, p. 378.
5. **Rice J.E. et al.** Ohmic energy confinement saturation and core toroidal rotation reversal in Alcator-C-MOD plasmas. — Phys. Plasmas, 2012, vol. 19, p. 056106.
6. **Rice J.E. et al.** Understanding LOC/SOC phenomenology in tokamaks. — Nucl. Fusion, 2020, vol. 60, p. 105001.
7. **Greenwald M. et al.** Energy confinement of high-density pellet-fuelled plasmas in the Alcator C Tokamak. — Phys. Rev. Lett., 1984, vol. 53, p. 352.
8. **Parker R.R. et al.** Progress in tokamak research at MIT. — Nucl. Fusion, 1985, vol. 25, p. 1127.
9. **Wolfe S.M. et al.** Effect of pellet fuelling on energy transport in ohmically heated Alcator C plasmas. — Nucl. Fusion, 1986, vol. 26, p. 329.
10. **De Marco et al.** High magnetic field tokamaks. — Nucl. Fusion, 1986, vol. 26, p. 1193.
11. **Alladio F. et al.** Energy confinement at high density in FT tokamak. — Nucl. Fusion, 1982, vol. 22, p. 479.
12. **Bracco G., Buratti P., Orsitto F., Santi D.** Energy confinement scaling laws for FT ohmic plasmas. — In: 17th EPS Conference on Controlled Fusion and Plasma Heating. Amsterdam, 25—29 June 1990, vol. 14B, p. 118; and ENEA Report RT/NUCL/90/04.
13. **Fusion** Science and Technology Special Issue on Frascati Tokamak Upgrade (FTU) 2004, vol. 45, № 3: Chapter 2. **Gormezano C. et al.** Highlight of the physics studies in the FTU, p. 203; Chapter 4. **Frigione D. et al.** High Density regimes, p. 339; Chapter 6. **Esposito B. et al.** Transport studies, p. 370.
14. **Esposito B. et al.** Transport analysis of ohmic, L-mode and improved confinement discharges in FTU. — Plasma Phys. Controlled Fusion, 2004, vol. 46, p. 1793.
15. **Martin Y.R. et al.** Power requirements for accessing the H-mode in ITER. — J. of Physics Conf. Series, 2008, vol. 123, p. 01233.
16. **Menard J.E. et al.** Overview of the physics and engineering design of NSTX. — Nucl. Fusion, 2012, vol. 52, p. 083015, and **Menard J.E. et al.** Overview of NSTX upgrade initial results and modelling highlights. — Nucl. Fusion, 2017, vol. 57, p. 102006.
17. **Gryaznevich M. et al.** Overview and status of construction of ST40. — Fus. Eng. Des., 2017, vol. 123, p. 177.
18. **Chuyanov V.A., Gryaznevich, M.P.** Modular fusion power plant. — Fus. Eng. Des., 2017, vol. 122, p. 238.
19. **Buxton P.F. et al.** On the energy confinement time in spherical tokamaks: implications for the design of pilot plants and fusion reactors. — Plasma Phys. Contr. Fusion, 2019, vol. 61, p. 035008.
20. **Snipes J. et al.** Characteristics of high-confinement modes in Alcator-C-MOD. — Phys. Plasmas, 1996, vol. 3, p. 1992.
21. **Ma. Y. et al.** Scaling of H-mode threshold power and L—H edge conditions with favourable ion grad-B frift in Alcator-C-MOD tokamak. — Nucl. Fusion, 2012, vol. 52, p. 023010.
22. **Orsitto F.P., Todd T.N.** Tokamaks as neutron sources for Fusion-Fission hybrid reactors: analysis of design parameters and technology readiness levels. — In: Proceedings FUNFI3 Conference 2019; https://www.enea.it/en/publications/abstract/funfi3-international-conference-on-fussion-fission.
23. **Pucella G. et al.** Dependence of the density limit on the toroidal magnetic field on FTU. — Nucl. Fusion, 2013, vol. 53, p. 023007.
24. **Romanelli M. et al.** On the optimal choice of the dimensionless paramenters of burning plasma physics experiments. — In: 28th EPS Conference on Contr. Fusion and Plasma Phys., Funchal 18—22 june 2001, ECA vol. 25 p. 697.
25. **ITER** Physics basis. Chapter 2. Plasma confinement and transport. — Nucl. Fusion, 1999, vol. 39, p. 2204 (formula (21) for H-mode energy confinement time), and p. 2205 (formula (25) for L-mode).
26. **Menon V.** Physics Design and Analysis code SPECTRE for Tokamak based fusion reactors. — 25th IAEA FEC 2014.
27. **Orsitto F.P. et al.** Diagnostics and controls for steady state and pulsed tokamak DEMO. — Nucl. Fusion, 2016, vol. 56, p. 026009.
28. **Blackwell B. et.al.** Energy and Impurity Transport in the Alcator C Tokamak. IAEA-CN-41/I-3. Plasma Physics and Controlled Nuclear Fusion Research. IAEA FEC Conference Baltimora, 1982; see also **C. Gao et al.** Non-local heat transport in Alcator-C-MOD ohmic L-mode plasmas. — Nucl. Fusion, 2014, vol. 54, p. 083025.

29. **Gormezano C.** Highlights of the physics studies in the FTU. — Fusion Science and Technology, 2004, vol. 45.
30. **Greenwald M. et al.** Energy confinement of high-density pellet-fueled plasmas in the Alcator C Tokamak. — Physical Review letters, 1984, vol. 53, № 4.

AUTHORS

Francesco Paolo Orsitto; ENEA Department for Fusion and Nuclear safety, C.R. Frascati, E. Fermi 45, 00044 Frascati, Italy, francesco.orsitto@enea.it

M. Romanelli; Tokamak Energy Ltd., 173 Brook Drive, Milton Park, Oxfordshire, OX14 4SD, United Kingdom

M. Vinay; Institute of Plasma Research, Gandinaghar, Gujarat, India

Статья поступила в редакцию 15 января 2021 г.
После доработки 16 марта 2021 г.
Принята к публикации 25 марта 2021 г.
Вопросы атомной науки и техники.
Сер. Термоядерный синтез, 2021, т. 44, вып. 2, с. 47—56.

UDC 621.039.674.3: 621.039.623

NOVEL HYBRID PILOT EXPERIMENT PROPOSAL FOR A FUSION-FISSION SUBCRITICAL COUPLED SYSTEM

M. Ciotti[1], F. Panza[2, 3], A. Cardinali[1], R. Gatto[4, 5], G. Ramogida[1], G. Lomonaco[3, 6], G. Ricco[3, 5], M. Ripani[3, 5], M. Osipenko[3]

[1]ENEA Dipartimento Fusione e Tecnologie per la Sicurezza Nucleare, Divisione Fisica della Fusione, Frascati, Italy
[2]ENEA Dipartimento Fusione e Tecnologie per la Sicurezza Nucleare, Divisione Tecnologie, Impianti e Materiali per la Fissione Nucleare, Roma, Italy
[3]Istituto Nazionale di Fisica Nucleare, Sezione di Genova, Genova, Italy
[4]Sapienza Univ. Roma Dipartimento di Ingegneria Astronautica, Elettrica ed Energetica, Roma, Italy
[5]Centro Fermi, Museo storico della fisica e centro studi e ricerche Enrico Fermi, Roma, Italy
[6]GeNERG/DIMETEC Università degli studi di Genova, Genova, Italy

Fusion-fission hybrid systems (FFH) represent a coupling between a fusion device and a subcritical fission reactor driven by neutrons produced by fusion reactions. This kind of systems, in principle, can be useful for different purposes, for example, as energy amplifier or as nuclear waste burner. In this work, the preliminary characteristics and potentialities of a FFH based on a tokamak device characterized by high magnetic field ($B > 9$ T) and high-density plasma ($n > 10^{14}$ cm^{-3}) have been evaluated. During the years high magnetic field compact tokamaks have been designed, built and operated. Thanks to their characteristics, such as compactness, high field and high density plasma, these devices can produce intense neutron fluxes, and therefore are good candidates to be incorporated in FFH while operating in a sub-ignited regime. An additional advantage is that their design is based on relatively simple existing technology. In this work, a coupling between a tokamak (operating in DD-mode) and a subcritical molten salt fission blanket has been proposed. Molten salt reactor could be adapted for this purpose and could help the hybrid system to increase its energy balance. A model with a molten salt fission blanket ($k_{\text{eff}} = 0.92$, $P = 95$ MW) instead of the lithium one, has been considered and studied in terms of neutronic evaluations. Presented preliminary numerical calculations based on a neutron Monte-Carlo code confirm the potentialities of the system.

Key words: Fusion-fission hybrid system, subcritical molten salt fission blanket, nuclear waste burner, compact tokamak with high magnetic field and high density plasma, neutron Monte-Carlo code.

DOI: 10.21517/0202-3822-2021-44-2-57-64

НОВОЕ ПРЕДЛОЖЕНИЕ О РАЗРАБОТКЕ ЭКСПЕРИМЕНТАЛЬНОЙ ПОДКРИТИЧЕСКОЙ ГИБРИДНОЙ УСТАНОВКИ СИНТЕЗА-ДЕЛЕНИЯ

М. Чиотти[1], Ф. Панза[2, 3], А. Кардинали[1], Р. Гатто[4, 5], Д. Рамогида[1], Д. Ломонако[3, 6], Д. Рикко[3, 5], М. Рипани[3, 5], М. Осипенко[3]

[1]Национальное агентство по новым технологиям, энергии и устойчивому экономическому развитию (ENEA), Отделение термоядерного синтеза и технологий ядерной безопасности, Отдел физики термоядерного синтеза, Фраскати, Италия
[2]Национальное агентство по новым технологиям, энергии и устойчивому экономическому развитию (ENEA), Отделение термоядерного синтеза и технологий ядерной безопасности, Отдел технологий, установок и материалов для ядерного деления, Рим, Италия
[3]Национальный институт ядерной физики, Генуэзское отделение, Генуя, Италия
[4]Сапиенца — Римский университет, Отдел технологических проблем астронавтики, электротехники и энергетики, Рим, Италия
[5]Центр им. Ферми, Музей истории физики и Центр исследований им. Энрико Ферми, Рим, Италия
[6]GeNERG / DIMETEC — Университет Генуи, Генуя, Италия

Гибридные системы синтеза-деления (ГССД) представляют собой объединение в одной установке термоядерного компонента и подкритического реактора деления, в котором реакция инициируется нейтронами, образующимися в результате реакций термоядерного синтеза. Такие системы, в принципе, могут быть полезны для различных целей, например, для увеличения производства энергии или сжигания ядерных отходов. В данной работе оценены характеристики и возможности ГССД на основе токамака с сильным магнитным полем ($B > 9$ Тл) и большой плотностью плазмы ($n > 10^{14}$ см$^{-3}$). В течение многих лет разрабатывались, строились и эксплуатировались компактные токамаки с сильным магнитным полем. Благодаря компактности, сильному магнитному полю и большой плотности плазмы такие токамаки могут генерировать интенсивные потоки нейтронов и, следовательно, являются хорошими кандидатами для включения в ГССД при их работе в подкритическом режиме. Их дополнительным преимуществом является то, что их конструкция основана на относительно простой существующей технологии. В этой работе был рассмотрен токамак, работающий на DD-реакции, с подкритическим бланкетом деления на основе расплавленной соли. Такой бланкет может увеличить выработку энергии в гибридной системе. Были изучены нейтронно-физические характеристики ГССД при замене литиевого бланкета бланкетом деления с расплавленной солью ($k_{\text{эф}} = 0{,}92$, $P = 95$ МВт). Предварительные численные расчёты на основе нейтронного кода Монте-Карло подтверждают потенциальные возможности системы.

Ключевые слова: гибридная система синтеза-деления, подкритический бланкет деления на основе расплавленной соли, ядерное уничтожение радиоактивных отходов, компактный токамак с сильным магнитным полем и большой плотностью плазмы, нейтронная вычислительная программа Монте-Карло.

INTRODUCTION

Fusion-fission hybrid systems (FFH) [1] represent a coupling between a fusion device and a subcritical fission reactor driven by neutrons produced by fusion reactions. This kind of systems, in principle, can be useful for different purposes, for example, as energy amplifier or as nuclear waste burner. In this work, we studied the characteristics and potentialities of a FFH based on tokamak device characterized by high magnetic field ($B > 9$ T) and high-density plasma ($n > 10^{14}$ cm^{-3}). During the years high magnetic field compact tokamaks have been built and operated (see for example FTU in Frascati (Italy) and C-MOD (MIT, Boston USA) and some like Ignitor [2—4] and Columbus projects [5, 6] have been designed. The latter two systems were originally conceived to explore the physics of burning plasmas with «Columbus» being a slightly enlarged version of Ignitor.

Thanks to their characteristics, such as compactness, high field and high density plasma, these devices can produce intense neutron fluxes [7], and therefore are good candidates to be incorporated in FFH [8] while operating in a sub-ignited regime. An additional advantage is that their design is based on relatively simple existing technology. Preliminary numerical calculations based on a neutron Monte-Carlo code are presented, confirming the potentialities of a FFH based on the coupling of a compact, high field tokamak with a fission region based on the molten salt concept as a preliminary device to start to gain experience in operating fusion fission subcritical coupled systems.

IDEA AND BACKGROUND

Several hybrid reactor configurations have been evaluated in the past years in order to verify conceptual ideas and machine potentialities.

The aim of this proposal is to evaluate the main characteristics for a new FFH device having as main goal, if realized, to short-cut the demonstration of the first energy producing system based on a fusion device. The achievement of this goal is currently foreseen in the fusion roadmap with the DEMO demonstrator, where a thermal power production of several hundred MW should be achieved for a relatively long time, but still in pulsed mode. On the other hand, DEMO overall energy balance [9], due to the large amount of needed power for re-circulation, for cryogenic cooling under intense high energy radiation flow, to additional power systems and, in general to its high technological complexity level, may not be necessarily positive. In addition, the roadmap for such a pure fusion demonstrator is still affected by several physical and technological challenging problems [10] some of them far to be solved, with at least 10 years of ITER operating time and IFMIF/DONES material testing, i.e. probably far away in this century.

In this paper, an experimental machine configuration, ready to be designed for a relevant net thermal power production demonstration is presented, with as much as simple and cheap solutions as possible. This device could be the first hybrid experimental system to be realized with the possibility to produce a relevant quantity of power (comparable to DEMO) starting from a fusion system. With this option the cost, realization time, overall system complexity, and consequently affordability, will be extremely reduced. This machine, in principle, could ensure a positive power net balance due to the lack of strong power needs. Additional heating, in fact, is not essential to the ignition (or at least a remarkable neutron rate production), that could be reached by Ohmic heating alone. The presence of a few MW (3—5 MW) of ICRH system will expand the capabilities of the device.

This new proposed configuration has few open points from both the physical and technological point of view, and its detailed planning and construction could be started in a relatively short time.

According to these guidelines a fusion compact, high density, high magnetic field non superconducting machine has been considered. The main consequences of this choice are the following: i) cheapness: machine compactness together with the use of normal copper magnets reduce the cost and the complexity of the machine; ii) possibility to operate even in DD-mode with acceptable neutron production [11]. High density compact machine can achieve a neutron production useful for a first experimental power generation test, if coupled with a fission system as shown hereafter. The DD-regime reduces the system complexity caused by the management of large

quantities of tritium and overcome the possible uncertainty on the lack of tritium for the starting of the operations (one of the DEMO challenges); in addition, due to DD operations, it would be possible to replace the original lithium blanket for tritium production with a blanket filled with circulating liquid molten salts mixed with fission elements placed partly inside the vacuum vessel, for higher neutron flow.

On the other hand, the non-superconducting choice limits the discharge time in a way non-compatible with a real reactor needs, limiting this system to the exclusive purpose of a demonstrator able to start the exploration of the hybrid experimental configuration. In addition, the generation of DD 2.45 MeV neutrons, instead of the DT 14 MeV, reduces the fission rate of 45% due to a reduced *n*-U235/238 cross-section. Even with these limits the configuration is able to produce in principle a relevant amount of power.

In Table I it is reported a parameter comparison between compact high-magnetic field tokamaks, which may be expected to be well-suited as neutron sources for hybrid systems (FIRE, Ignitor, Columbus), and the ITER tokamak presently under construction.

T a b l e 1. **Comparison between ITER, FIRE, Ignitor and Columbus main parameters**

Relevant parameters	ITER	FIRE	Ignitor	Columbus
Pulse flat top t_{pulse}, s	400	20	6	11.4
Minor radius a, m	2	0.595	0.47	0.535
Peak el. temperature T_{e0}, keV	19	11	10.5	11.5
Peak ion temperature T_{i0}, keV	19	11	10.5	10.5
Peak density n, m^{-3}	10^{20}	5×10^{20}	9×10^{20}	9.5×10^{20}
Profile parameter α_T, parab	1	1	2	2
Purity parameter Z_{eff}	1.7	1.4	1.2	1.2
DD-neutron yield Y_{DD}, n/s	10^{18}	10^{17}	10^{17}	10^{18}
DT-neutron yield Y_{DT}, n/s	10^{20}	10^{19}	10^{20}	10^{20}

COMPACT DEVICE IN DD OPERATION MODE

Due to its physics characteristics, high magnetic field compact tokamaks can generally operate both in DT- and in DD-mode. Here we focus on the latter mode of operation, which has the advantage of not needing a tritium breeding region in addition to the fission blanket, to have an idea of the potential performances of DD-operational mode.

A simple evaluation of the neutron emission yield has been performed. Considering, for example, the following plasma parameters: i) density $n_e = 10^{15}$ cm^{-3} with parabolic profile; ii) $\langle\sigma v\rangle = 9\times10^{-20}$ cm^3/s (Fig. 1); iii) $V_{plasma} = 2.5\times10^7$ cm^3; iv) $T_{peak} \approx 10$ keV with parabolic squared profile (note that ion and electron temperature at that plasma density are equivalent); v) no additional heating; the reaction rate can be calculated as: $R = n^2/2 \langle\sigma v\rangle V_{plasma} = 2\times10^{18}$ DD/s. Since two equi-probable production channels are possible for the DD-reaction: i) D + D → ^{3}He + n; ii) D + D → ^{3}H + p; the neutron yield is about $Y = 10^{18}$ n/s.

Considering $E = 3.27$ MeV (^{3}He + n) and 4.03 MeV (^{3}H + p) as emitted energies for both production channels, fusion power can be estimated as 1.16 MW.

The design of a device like high magnetic field compact tokamak must be adapted to the requirements and goals of a FFH. In this contest, flat-top and cooling time duration represent crucial parameters for this configuration and have to be optimized in order to avoid molten salts freezing or complex heat exchanger addition to evacuate the excess heating.

New materials for the magnets might also be considered in order to increase magnetic flux availability and flat top duration, and the mode of operation (plasma temperature and density) should be adjusted to fit the requirements of a FFH.

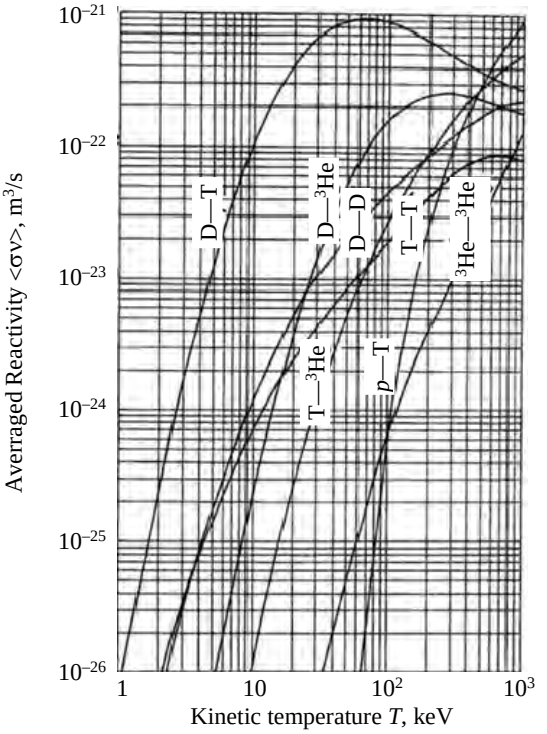

Fig. 1. $\langle\sigma v\rangle$ reaction rate as a function of plasma temperature for several fusion reactions

FUSION-FISSION HYBRID COUPLING

On the basis of the considerations presented in the previous paragraphs, high field tokamak characteristics fit in a very good way with hybrid device requirements.

For the fusion plasma, an adaptation of the parameters to the requirements of an FFH is necessary, and this task will not be pursued here. For the fission zone, the following two main solutions could be considered:

— traditional reactor (with fuel rods) inside an external blanket, cooled by water;

— molten salt reactors (MSR) [12, 13] with fissile/fertile elements dissolved in the molten salt fluid.

Traditional reactors have the advantage in terms of technological knowledge and feasibility coming from decades of operation, but, in this kind of nuclear system, material stresses could represent a weak point especially for fuel rods cladding and structure. In particular, the pulsed behavior of the fusion machine could induce failures in the rod cladding. On the other side MSR solution could be better coupled to the tokamak geometry with the positioning of the blanket entirely, or partially, inside the machine. This has the advantage to intercept all the plasma produced neutrons and to shield the external structure from them.

There are many studies concerning MSR with different characteristics and designs, traditional or breeders, using many kinds of salt mixtures depending from the neutron spectrum inside the core (fast or moderated) [14—18].

The schematic view of MSR is reported in Fig. 2, in which it is possible to observe the molten salt circuit passing through the fission core and then in the heat exchanger loop.

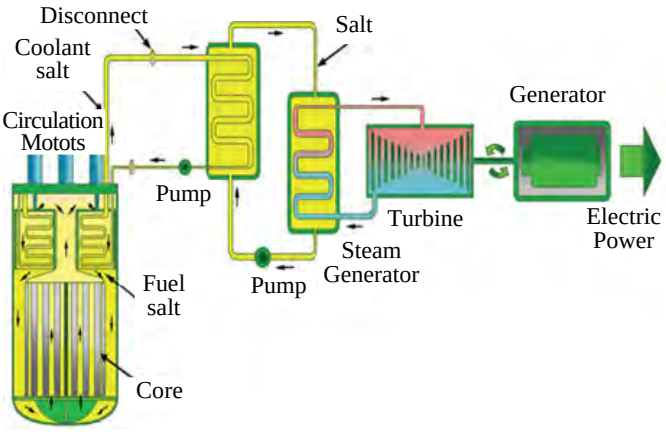

Fig. 2. MSR schematic view in which it is possible to observe the primary fuel loop passing through the reactor core, the secondary and the tertiary loops

A summary of the main features of MSRs which well fit the requirements of a FFH is the following:

— fissile isotopes contained in the salt mixture;

— possibility to use salt mixture containing different kind of isotopes (U/Pu/minor actinides);

— salt mixture chosen considering the fission blanket region temperature; MSR avoid the material stress on the traditional nuclear fuel rods, that could be very high due to the pulsed operational mode of the fusion system;

— salt online reprocessing keeping $k_{\text{eff}} < 1$.

Molten salt fission reactor with dissolved fuel has some limits in terms of system safety. The dissolved fuel may have density fluctuations that may lead the reactor in supercritical state. This is a well-known problem for fission reactor with sudden increase in power production. This difficulty is completely solved in a subcritical system, as the fuel density fluctuations will not be able to reach supercriticality.

SIMPLE HYBRID SYSTEM PRELIMINARY SIMULATIONS

In order to gain a preliminary understanding on the performances of the proposed hybrid system, a simplified simulation model has been considered. The model, as shown in Fig. 3, is based on a high magnetic field compact tokamak device with the following geometric characteristics: major radius R = 200 cm, minor radii a = 54 cm and b = 100 cm (vertical size of the plasma taking into account the elongation ε = 1.85). The first wall is composed by 1 cm thick tungsten, 3 cm thick AISI-316 followed by 29 cm thick molten salt fission blanket. This is supposed to be placed inside the machine vacuum vessel made with 2 cm steel. Just outside the vacuum vessel a 35 cm lead neutron reflector is positioned, to

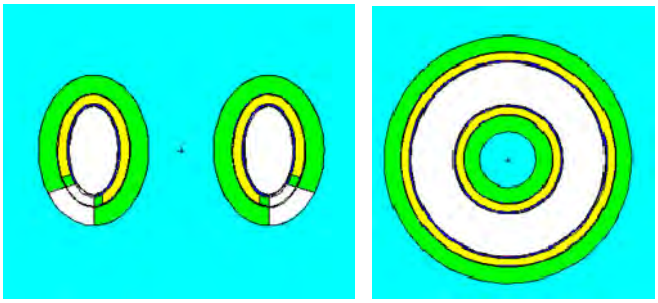

Fig. 3. FFH poloidal and toroidal sections sketches. Molten salt blanket ( ), steel vessel ( ), lead reflector ( )

recover part of the out-flowing source or fission neutrons. In the following sketches a poloidal section (see Fig. 3) is shown with a void sector representing the space for divertor (not designed in this model and not necessarily required) positioning (in white).

The simulations have been performed by using the Monte-Carlo code MCNP6.1 with ENDF/BVII.0 libraries. For effective multiplication factor (k_{eff}) evaluation KCODE mode has been used, while, for neutron and fluxes calculations SDEF mode have been considered.

The isotropic neutron source (from DD-fusion reactions) emitting $Y = 10^{18}$ n/s over 4π solid angle has been implemented uniformly on a circumference passing from the center of the torus as shown in Fig. 4.

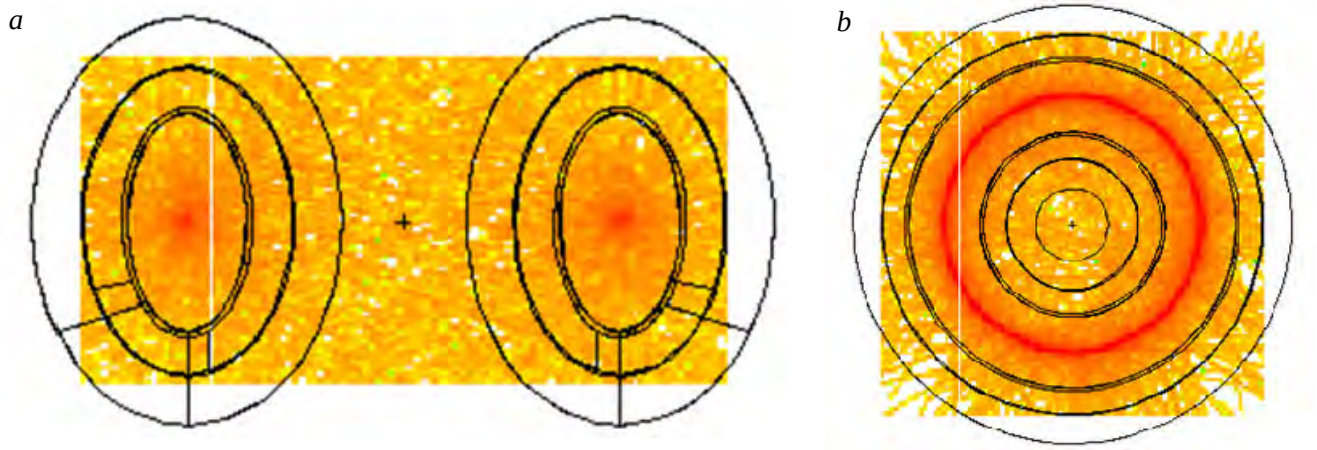

Fig. 4. Poloidal (*a*) and toroidal (*b*) views of the neutron emission from the circumference passing from the center of the torus

For this model, it has been considered a 34.5 cm thick fission blanket filled with molten salt mixture LiF—NaF—UF_4 (44.48%, 24.12%, 31.40%) molten % with 3.4 g/cm^3 density and the following mass composition [19]: 13.5% ^{235}U; 48.5% ^{238}U; 2% ^{7}Li; 31% ^{19}F; 6% ^{23}Na.

The effective multiplication factor for this fission system results to be about 0.92 (in order to guarantee a high safety level) , the integral neutron flux averaged on the whole molten salt volume is about $5{,}85\times10^{13}$ n/(cm^2·s) and the thermal power level is about 95 MW_{th} (assuming a neutron yield of 10^{18} n/s).

In this scenario, the energy distribution for the neutron flux averaged on the whole molten salt volume is shown in Fig. 5.

A map of the integral flux intensities in the hybrid system is shown in Fig. 6.

In Table 2, the integral flux and the integral flux evaluated for three energy bins with their relative percentages in terms of absolute flux are reported to have a quantitative idea of the neutron energy distribution inside the fission blanket.

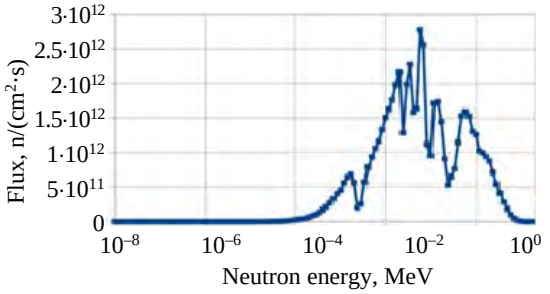

Fig. 5. Neutron energy distribution averaged over the whole molten salt volume

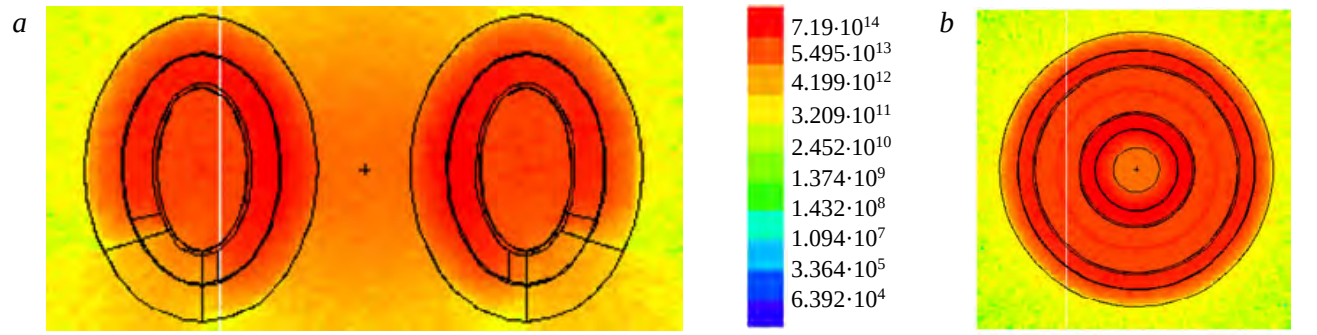

Fig. 6. Poloidal (*a*) and toroidal (*b*) integral flux intensities in the hybrid system in the legend the flux intensities are reported in n/(cm^2·s)

T a b l e 2. **Flux values for different energy bins with their relative percentage with respect to the integral one**

Parameter	Integral	<1 eV	1 eV — 100 keV	>100 keV
Flux, n/(cm^2·s)	5.85×10^{13}	7.36×10^{7}	2.54×10^{13}	2.31×10^{13}
Percentage, %	100.0000	0.0001	60.4550	39.5448

Such a fission blanket can provide a relatively high intensity flux with a good component in the range of fast reactors.

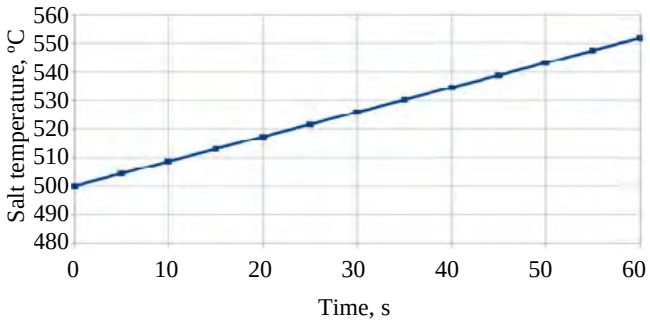

Fig. 7. Salt temperature increase as a function of shot duration

To have a more detailed and quantitative evaluation, starting from a temperature of about 500 °C (higher than fusion temperature) and considering the thermal power generated inside the salt mixture (95 MW_{th}) in stationary situation, the temperature increase as a function of pulse duration is shown in Fig 7.

An optimization regarding the pulse and the cooling time durations can be fundamental for the definition of the hybrid device operation mode in a more detailed model. In this framework, the magnets have to be actively cooled by liquid nitrogen flow during and in between the pulses as already done in the FTU machine [20]. Thermal insulators are still not considered in this preliminary version, but in a more detailed work, could be considered as a fundamental component of the system.

This simple analysis has to be better detailed but could highlight the possible compatibility between a high magnetic field tokamak and a molten salt fission blanket in order to start to gain experimental confidence with a simple fusion fission coupled system with increasing level of criticality.

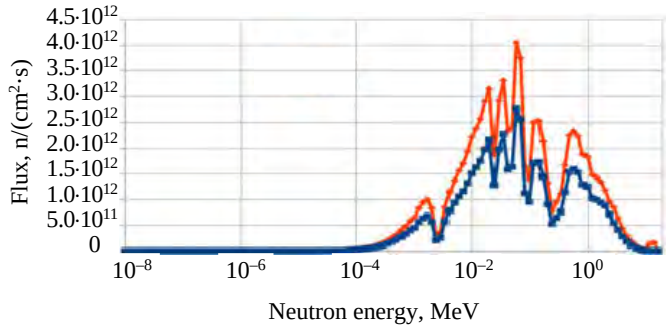

Fig. 8. Neutron energy distributions averaged over the whole molten salt volume for DD source (——) and for DT source (——)

To have an idea of the differences due to the use of 14.1 MeV neutrons instead of considering 2.45 MeV, (as briefly recalled above), the comparison of the neutron spectra sampled inside the fission blanket obtained starting from DD- and DT-fusion reactions is reported in Fig. 8.

Neutron integral flux and thermal fission power in the case of DT-fusion source are 45% higher than in the case of DD-source (maintaining the same neutron intensity of 10^{18} n/s for both cases).

From this comparison, performed by maintaining the same neutron intensity, the better behavior of DT-source is clear, 14.1 MeV neutrons are more efficient for inducing fission reactions inside the fuel. Another important factor is that the neutron intensity is much higher for DT-fusion with respect to DD. In any case, for a first experimental demonstration DD fuel appears to be suitable to drive the fission system.

CONCLUSIONS

In this paper the idea of considering a tokamak neutron source operating with DD fuel coupled with a molten salts fission blanket for a fusion-fission hybrid system preliminary experimental activity has been described. This solution could represent a short-cut towards a first experimental system based on a fusion machine generating an appreciable value of power with a positive overall energy balance. In this way it could be possible to reach the fusion power experimental generation conceptual demonstration several decades ahead of schedule as foreseen in the mainstream fusion roadmap.

High field non-superconducting tokamaks, for their peculiar properties, can act as neutron sources for FFH due to their compactness, their relative technological simplicity and their high neutron emission. An optimization in parameter space is however required in order to adapt the original already existing (i.e. Columbus) high field tokamak design to the hybrid purposes. The simple and feasible technology represents a crucial point with regard the realization of a FFH pilot experiment. Configuration optimization could be performed by modifying the magnetic field intensity and by considering new solutions and materials for the molten salt reactor technolo-

gies, but the proposed technologies are well tested and available and allow to start with a simple and cheap system the coupling studies between fusion sources and fission energy generation module.

A simplified model simulation has been performed by using the MCNP6.1 code concerning a $k_{eff} = 0.92$. The results of these simulations provide some preliminary insights on the main neutron parameters concerning the fission blanket in terms of geometric characteristics, thermal power and fluxes. A power production of about 95 MW_{th} has been calculated along the plasma shot duration, sufficient for the first relevant power production demonstration with a fusion based system. The simulations have given inputs on the required characteristics concerning the fusion device, the geometrical disposition and the neutron emission intensity, providing a starting point for the definition of a pilot FFH experiment, its main characteristics and its operation mode. An important point is represented by molten salt thermal cycle: from a preliminary evaluation seems that the high magnetic field tokamak operation characteristics can match in a good way with the thermal properties of the salt in stationary conditions also allowing to increase, step by step the k_{eff} of the system. A fusion shot of about few tens of seconds in case of an increased k_{eff} could theoretically reach a significantly higher power production. A proper design of the copper magnets cooling system can help to increase the flat-top duration and to reduce the cooling time, in order to improve the FFH operation mode.

Of course, additional studies for a further detailed planning are needed.

REFERENCES

1. **Bethe H.A.** The fusion hybrid. — Phys. Today, 1979, vol. 32 (5), p. 44—51.
2. **Coppi B., Nassi M. and the Ignitor Project Group.** Physics Criteria and Design Solutions for an Advanced Ignition Experiment, MIT Report PTP-92/16 R. L. E., Cambridge, MA, 1992.
3. **Coppi B. et al.** New developments, plasma physics regimes and issues for the Ignitor experiment. — Nucl. Fusion, 2013, vol. 53, p. 104013.
4. **Coppi B. et al.** Perspectives for the high field approach in fusion research and advances within the Ignitor program. — Nucl. Fusion, 2015, vol. 55, p. 053011.
5. **Salvetti M., Coppi B.** The Ignitor-Columbus Path in Fusion Research. — In: 51st Annual Meeting of the APS Division of Plasma Physics. Vol. 54, Atlanta, Georgia, November 2—6, 2009.
6. **Coppi B., Salvetti M.** Highlights of the Columbus Concept. Massachusetts Institute of Technology, Cambridge, MA 02139, MIT (R.L.E.) Report PTP 02/06, December 2002.
7. **Bombarda F., Coppi B., Hartwig Z.S., Sassi M., Zucchetti M.** Compact tokamaks as convenient neutron sources for fusion reactors materials testing. — Fusion Engineering and Design, 2011, vol. 86, p. 2632.
8. **Velikhov E.P., Kovalchuk M.V., Ilgisonis V.I. et al.** Nuclear power system based on fission and fusion reactors is the strategic line of nuclear power industry development. — Phys. Atom. Nuclei, 2018, vol. 81, p. 981—987.
9. **Ciattaglia S., Federici G., Barucca L., Stieglitz R., Taylor N.** EU DEMO safety and balance of plant design and operating requirements. Issues and possible solutions. — Fusion Engineering and Design, September 2019, vol. 146, Part B, p. 2184—2188.
10. **Donné A.J.H.** The European roadmap towards fusion electricity. — Phil. Trans. R. Soc. A 377: 20170432, 2019.
11. **Coppi B.** Private Communication, 2020.
12. **MacPherson H.G.** The molten salt reactor adventure. — Nuclear Science and Engineering, 1985, vol. 90, p. 374—380.
13. **Briggs R.B.** MSR Program Semiannual Progress Report for the Period Ending, July 31, 1964. (ORNL-3708) (66.3 MB PDF), Oak Ridge National Laboratory, U.S. AEC (published November 1964). Retrieved 2008-05-21.
14. **Yamamoto T. et al.** Steady State analysis of molten salt reactor in consideration of the effect of fuel salt flow. — In: 12th International Conference on Nuclear Engineering. Arlington, Virginia, USA, April 25—29, 2004.
15. **Nagy K. et al.** Parametric studies on the fuel salt composition in thermal molten salt breeder reactors. — In: International Conference on the Physics of Reactors Nuclear Power: A Sustainable Resource Casino-Kursaal Conference Center, Interlaken, Switzerland, September 14—19, 2008.
16. **Křepel J. et al.** Molten salt fast reactor blanket design and proliferation resistance assessment. — In: 2014 22nd International Conference on Nuclear Engineering ICONE22 Prague, Czech Republic, July 7—11, 2014.
17. **Nuttin A., Heuer D., Billebaud A., Brissot R., Giorni A. et al.** Thorium fuel cycles: a graphite-moderated molten salt reactor versus a fast spectrum solid fuel system. — In: International Conference on Back-End of the Fuel Cycle. From Research to Solutions (GLOBAL 2001). Paris, France. Sep. 2001, 086 (8 p.).
18. **Siemer D.** Why the molten salt fast reactor (MSFR) is the «best» Gen IV reactor. — Energy Sci. Eng., 2015, vol. 3, p. 83—97.
19. **Woolley R.D.** System Studies of Fission-Fusion Hybrid Molten Salt Reactors. PhD diss., University of Tennessee, 2013; https://trace.tennessee.edu/utk_graddiss/2628.

20. **Migliori S., Bettinali L., Gasparotto M., Pizzuto A.** Liquid nitrogen cooling system for FTU tokamak machine. — In: Proc. of the Twelfth International Cryogenic Engineering Conference. Southampton, UK, 12—15 July 1988, Butterworth—Heinemann, 1988, p. 93—97, ISBN 9780408012591.

AUTHORS

Marco Ciotti; responsible for the physics division, Fusion department. Member of the DTT project board; ENEA Dipartimento Fusione e Tecnologie per la Sicurezza Nucleare, Divisione Fisica della Fusione, Frascati, Italy, marco.ciotti@enea.it

Fabio Panza, Researcher, PhD; ENEA Dipartimento Fusione e Tecnologie per la Sicurezza Nucleare, Divisione Tecnologie, Impianti e Materiali per la Fissione Nucleare, Roma, Italy; Istituto Nazionale di Fisica Nucleare, Sezione di Genova, Genova, Italy fabio.panza@enea.it

Alessandro Cardinali, researcher, PhD; ENEA Dipartimento Fusione e Tecnologie per la Sicurezza Nucleare, Divisione Fisica della Fusione, Frascati, Italy, alessandro.cardinali@enea.it

Renato Gatto, Associate Professor; Sapienza Univ. Roma Dipartimento di Ingegneria Astronautica, Elettrica ed Energetica, Roma, Italy; Centro Fermi Museo storico della fisica e centro studi e ricerche Enrico Fermi, Roma, Italy, renato.gatto@uniroma1.it

Giuseppe Ramogida, researcher, PhD; ENEA Dipartimento Fusione e Tecnologie per la Sicurezza Nucleare, Divisione Fisica della Fusione, Frascati, Italy, giuseppe.ramogida@enea.it

Guglielmo Lomonaco, Associate Professor; Istituto Nazionale di Fisica Nucleare, Sezione di Genova, Genova, Italy; GeNERG/DIMETEC Università degli studi di Genova, Genova, Italy, guglielmo.lomonaco@unige.it

Giovanni Ricco, senior associate, MSc in Physics; Istituto Nazionale di Fisica Nucleare, Sezione di Genova, Genova, Italy; Centro Fermi Museo storico della fisica e centro studi e ricerche Enrico Fermi, Roma, Italy, ricco@ge.infn.it

Marco Ripani, Director of Research, MSc in Physics; Istituto Nazionale di Fisica Nucleare, Sezione di Genova, Genova, Italy; Centro Fermi Museo storico della fisica e centro studi e ricerche Enrico Fermi, Roma, Italy, marco.ripani@infn.it

Mikhail Osipenko, staff scientist, PhD; Istituto Nazionale di Fisica Nucleare, Sezione di Genova, Genova, Italy, osipenko@ge.infn.it

Статья поступила в редакцию 15 января 2021 г.
После доработки 16 марта 2021 г.
Принята к публикации 25 марта 2021 г.
Вопросы атомной науки и техники.
Сер. Термоядерный синтез, 2021, т. 44, вып. 2, с. 57—64.

UDC 621.039.633

INTEGRATED MODELING OF FUEL FLOWS IN THE PLASMA AND THE INJECTION AND PUMPING SYSTEMS FOR THE DEMO-FNS FUSION NEUTRON SOURCE

S.S. Ananyev[1], A.Yu. Dnestrovskij[1], A.S. Kukushkin[1, 2]

[1]NRC «Kurchatov Institute», Moscow, Russia
[2]National Research Nuclear University MEPhI, Moscow, Russia

The paper describes an FC-FNS system code modification that makes it possible to include fuel flows in the core and divertor plasma into the model. A new approach to the description of the density of hydrogen isotopes in the plasma core is proposed, based on the different confinement times for ions from different sources. The model is supplemented by a new scenario of gas supply to the neutral beam injection system, which provides the injection of a $D^0 + T^0$ beam with a closed gas cycle. The flows in the fuel cycle (FC) of the DEMO-FNS fusion neutron source are estimated and the fuel injection parameters are selected that ensure the specified conditions in the core and divertor plasma with varying the isotopic gas composition in the heating injectors. The working range of the hydrogen isotope composition in the divertor plasma is determined, at which the required tritium fraction in the plasma core is provided. An estimate of the total tritium amount in the operating FC system is obtained in the range from 850 to 1150 g.

Keywords: fusion-fission hybrid facility, fusion neutron source, fusion fuel cycle, core and divertor plasma modeling, DT fuel balance code, hydrogen isotopes, FC-FNS.

DOI: 10.21517/0202-3822-2021-44-2-65-77

КОМПЛЕКСНОЕ МОДЕЛИРОВАНИЕ ПОТОКОВ ТОПЛИВА В ПЛАЗМЕ И СИСТЕМАХ ИНЖЕКЦИИ И ОТКАЧКИ ДЛЯ ДЕМОНСТРАЦИОННОГО ТЕРМОЯДЕРНОГО ИСТОЧНИКА НЕЙТРОНОВ ДЕМО-ТИН

С.С. Ананьев[1], А.Ю. Днестровский[1], А.С. Кукушкин[1, 2]

[1]НИЦ «Курчатовский институт», Москва, Россия
[2]Национальный исследовательский университет «МИФИ», Москва, Россия

В работе описана модификация системного кода FC-FNS, позволяющая включить в модель топливные потоки в основной и диверторной плазме. Предложен новый подход к описанию плотности изотопов водорода в основной плазме, основанный на использовании различного времени удержания ионов из различных источников. Модель дополнена новым сценарием газоснабжения системы нагревных инжекторов, предусматривающим инжекцию пучка $D^0 + T^0$ с замкнутым газовым циклом. Оценены потоки в топливном цикле (ТЦ) установки ДЕМО-ТИН и подобраны параметры топливной инжекции, обеспечивающие заданные условия в основной и диверторной плазме при варьировании изотопного состава газа в нагревных инжекторах. Определён рабочий диапазон состава изотопов водорода в диверторной плазме, при котором обеспечивается требуемая доля трития в основной плазме. Получена оценка полного содержания трития в ТЦ действующей установки от 850 до 1150 г.

Ключевые слова: гибридная установка синтеза-деления, источник термоядерных нейтронов, термоядерный топливный цикл, моделирование основной и диверторной плазмы, программа для вычисления баланса D- и T-потоков, изотопы водорода, топливный цикл термоядерного источника нейтронов.

INTRODUCTION

The fuel cycle systems must provide the required conditions in the core and divertor plasma by puffing and coordinated pumping, controlling the plasma core parameters by fuelling, as well as efficient fuel mixture processing to reduce the inventory of radioactive elements. Calculation of fuel isotope fluxes in the systems that circulate the fuel and auxiliary gases in a tokamak-reactor or fusion neutron source (FNS) [1] requires simultaneous consideration of processes in the core and divertor plasma [2, 3]. For industrial facilities of controlled fusion (CF) or fusion-fission hybrid systems (FFHS), it is advisable to use cryogenic pellet injection as the fuel feed [4, 5]. The auxiliary plasma heating system by neutral beam injection (NBI) also supplies the core plasma with particles corresponding to the beam composition. At the same time, it is necessary to calculate the divertor plasma parameters, since the fueling from the divertor plasma by neutrals is also essential [3,

6]. To maintain the operating parameters of the core plasma and the divertor region, it is necessary to use the gas puffing into the vacuum chamber with a flow rate three orders of magnitude higher than the fusion fuel burnup in the core plasma [4—6]. It is this flow that controls the composition and density of neutrals and plasma in the divertor.

During fuel injection (into the vacuum chamber), not all the particles reach the core plasma — some of them immediately enter the divertor layer. Thus, the tritium fraction in the divertor plasma $f_{\mathrm{div}}^{\mathrm{T}}$ will be influenced by pellet injection and NBI.

The core plasma receives particles from three sources (the NBI systems S_{NB}, the cryogenic fuel pellets feed systems S_{pel}, and the neutral flux from the divertor region S_{sep}), comparable in contribution to the core density [3, 6]. A change in the isotopic composition of the core plasma affects the systems for pumping and processing gases (since the magnitude and composition of the gas flows depend on the tritium fraction in the core $f_{\mathrm{core}}^{\mathrm{T}}$ and divertor $f_{\mathrm{div}}^{\mathrm{T}}$ plasma), as well as the fuelling systems, which must provide the specified values of $f_{\mathrm{core}}^{\mathrm{T}}$.

The computer model FC-FNS (Fuel Cycle for Fusion Neutron Source) [6, 7] was used as a tool for modeling processes in the DEMO-FNS facility fuel cycle systems (FC). The updated code version takes into account the self-consistent core and divertor plasma parameters obtained from joint simulation with the SOLPS4.3 [8] and ASTRA [3, 9] codes. The main goal is to develop an approach that provides DEMO-FNS FC simulation in the presence of feedback between the pumping and injection systems, considering the change in the isotopic composition of the edge and core plasma.

In this report, we will call the entire plasma outside the separatrix a «divertor», making no distinction between the divertor itself and the scrape-off layer (SOL). These plasma parameters are calculated in the SOLPS4.3 code and are represented here by the average values of, for example, the plasma density at the separatrix, or the tritium concentration in the edge plasma.

FUEL CYCLE ARCHITECTURE

The fuel cycle (FC) means a complex of systems (often placed in a separate room, for which the term «tritium plant» is used), which serves to circulate the DT fuel through the vacuum chamber of the fusion reactor, maintaining the necessary D- and T-densities in the core plasma. During the conceptual development stage, the operation scenarios for DEMO-FNS were selected, the gas flows in the systems were estimated, and the architecture of the FC systems was chosen [10]. Progress in the project development and the FC simulation allowed moving from the conceptual to the engineering design stage for some systems [5, 7]. At the same time, together with the FC systems elaboration, modeling of the operating scenarios by FC-FNS code made it possible to optimize the system functions [5]. At the moment, the FC systems are grouped according to their functions:

— pumping of gases from the tokamak vacuum chamber;

— hydrogen isotope extraction from the pumped gases;

— additional purification of chemically bound hydrogen isotopes;

— processing of the tritium-containing radioactive waste (including tritium removal from the gases and water);

— hydrogen isotope separation to the required purity level;

— control of the hydrogen isotope sources in the plasma, heating, and fueling systems;

— tritium production and extraction from the propellant gas;

— storing the fuel isotopes;

— ensuring the circulation of the seed impurity gases (Ne).

In the course of the FC optimization for DEMO-FNS, three circuits are distinguished: (i) for the rough processing of the exhaust gases from the tokamak pumping system, (ii) for tritium extraction from the blanket, and (iii) for processing of the tritium-containing waste, the capture of tritium from technological flows (including air from working rooms in emergencies) and the extraction of gases added for better plasma performance (impurity seeding).

A conventional block diagram of the FC systems, including all three contours, is shown in Fig. 1. The systems that form the contours are highlighted in one color. The colored arrows indicate the fuel isotope fluxes. In general, the structure chosen is typical for the majority of fusion reactor projects [11—13]. However, the presence in the device of the breeding blanket unit and the steady-state NBI system with a gas composition significantly different from the gas combination in the primary circuit required a fundamentally new approach to the FC architecture and composition of the technological systems, necessary for their integration [5].

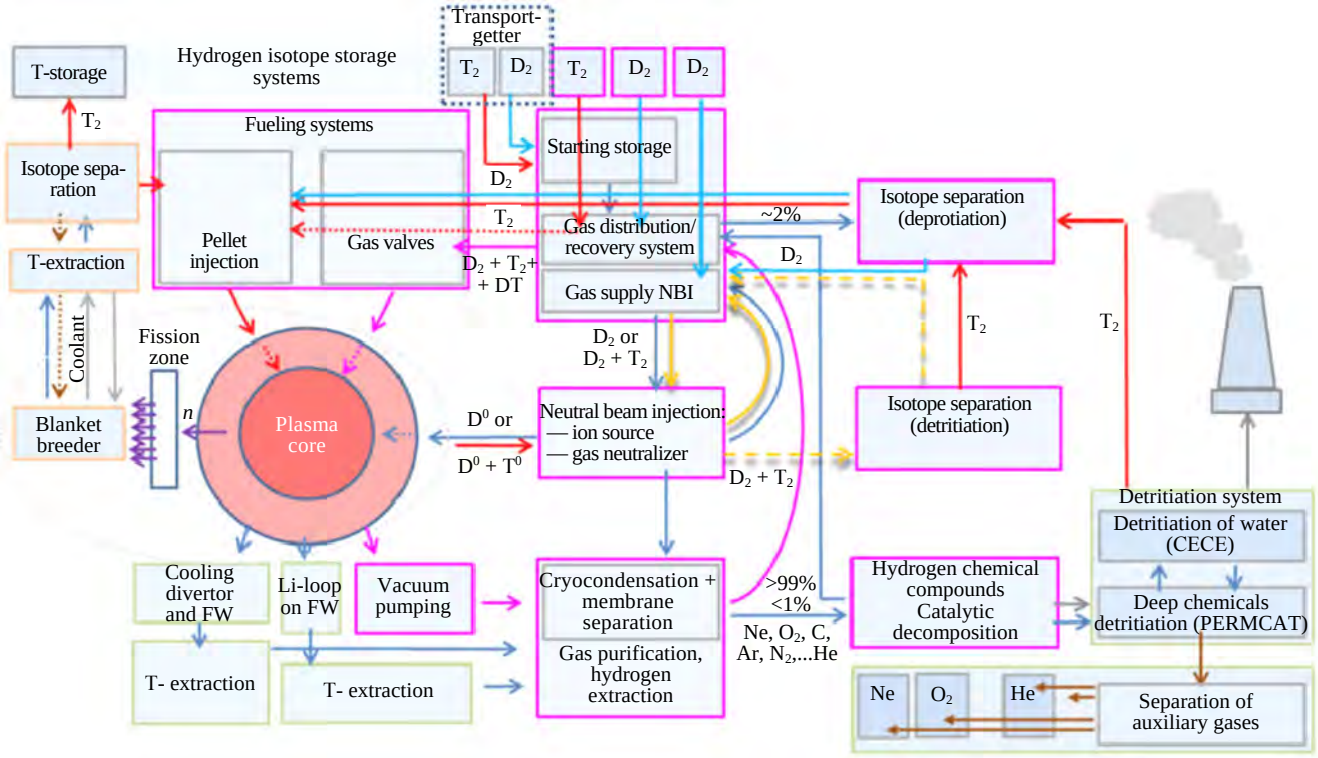

Fig. 1. Block diagram of FC systems. The systems of the first, second, and third contour are conventionally shown in different colors (according to the functions described in the text). Colored arrows show the fluxes of the fuel isotopes. For the NBI system, three gas supply cases are shown

The FC systems of DEMO-FNS must maintain a steady-state operation mode of fuel mixture processing and supply (for fuelling). To create and maintain the plasma discharge with a power amplification factor (the ratio of the fusion power to the additional heating power) $Q \sim 1$, a relatively low fuel (T and D) flow, ~0.08 g/s, is required. Therefore, it was proposed to circulate the hydrogen isotopes mixture in the FC DEMO-FNS without separating isotopologues (H_2, HD, D_2, DT, T_2), but with re-balancing the D-T isotopic composition in the gas injection system. Isotope separation will be performed for a flow (less than 5% of the total) sufficient to provide the required amount of the isotopes in the injection systems, where it is necessary to use a predominantly single isotope (D_2 with T minority for NBI and T_2 with D minority for pellet injection). Processing such a flow is sufficient to control the H fraction in the plasma by its removal in the isotope separation system [5]. The critical (required) degree of the fuel isotope purity should be determined in the further process of in-depth modeling of the individual FC systems (including injection) and optimization to reduce the tritium content in all FC systems, as well as to meet the safety and compatibility requirements of the systems.

The DEMO-FNS project is based on the FC technologies that have already been used in JET and TFTR tokamaks and are being developed for the ITER project. The significant progress achieved in recent decades in the fuel cycle technologies for the fusion reactors CFETR and DEMO is also taken into account when considering the technical proposals for the FC technological systems and their integration [5, 6].

The FC-FNS code was modified to comply fully with the FC architecture that had previously been selected by the analysis of the candidate technologies [5]. One of the changes concerned the gas supply to the NBI system. The FC scenarios in the model were supplemented with a new case using the injection of a mixed, $D^0 + T^0$, NBI (which had previously been considered in [2, 6, 10, 14, 15] at a concept level) realized by a closed gas cy-

cle. This solution will avoid loading the tokamak fuel reprocessing system (the rough and membrane gas separation, isotope separation) with additional gas flows while providing the required injection of the fuel isotopes into the plasma core with a minimum change in the isotopic composition of the injector gas [14]. This case is modeled similarly to the closed cycle for the D^0 beam, taking into account the control of the isotopic gas composition through the isotope separation system included in the loop [5, 14]. Thus, all the scenarios modeled in FC-FNS rely on concrete technological solutions. This renders the results obtained more reliable and allows us to calculate the isotope inventories in the FC systems, taking into account the peculiarities of the physical and chemical processes occurring there.

INTEGRATED MODELING OF CENTRAL AND DIVERTOR PLASMA

For integrated modeling of the core and divertor plasma, the mediated coupling of the ASTRA [9] and-SOLPS4.3 [8] codes is used — an approach developed earlier for the ITER project [16, 17]. In this approach, the one-dimensional modeling of the plasma core by the ASTRA code is supplemented by the boundary conditions and constraints represented in the form of scalings obtained from two-dimensional modeling results of the edge plasma using the SOLPS4.3 code. As a result, an efficient algorithm is built, which provides a simultaneous description of plasma regions with strongly differing timescales and makes it possible to calculate the parameters of the plasma core that are consistent with the constraints for the divertor (heat loads, gas flows). In this work, for all FC systems, the deuterium and tritium fluxes are calculated, corresponding to the plasma parameters obtained in [3].

The principal technical parameters of DEMO-FNS, as well as the main plasma parameters obtained from the coupled modeling of the core and divertor plasma using this code combination [3], are shown below:

R/a, m . . .	3.2/1
B, T . . .	5
I_p, MA . . .	4—5
Auxiliary heating (NBI) power P_{NBI}, MW . . .	30
Beam atom energy E_{NBI}, keV . . .	500
Auxiliary heating (ECRH) power P_{ECRH}, MW . . .	6
The core plasma volume inside the separatrix V_{pl}, m^3 . . .	121
Fusion power P_{fus}, MW . . .	30
Isotopic composition of plasma core fuel components f_{core}^{T} . . .	0.5
Ne fraction in the plasma at the separatrix f_{Ne} . . .	0.02
Average plasma density $<n_e>$, m^{-3} . . .	$7 \cdot 10^{19}$
Electron density at the separatrix $n_{sep\,(e)}$, m^{-3} . . .	$4.67 \cdot 10^{19}$
Power supplied to SOL P_{SOL}, MW . . .	37.4
DEMO-FNS parameters for FC-FNS code simulation:	
Reduced neutral pressure in the divertor p_n, Pa . . .	2.0
Pumping speed from the divertor c_p, m^3/s . . .	30
Energy confinement time τ_E, s . . .	0.737
Particle confinement time τ_p, s . . .	2.95
Effective plasma charge Z_{eff} . . .	2.74
He density at the separatrix n_{sep}^{He}, m^{-3} . . .	$0.11 \cdot 10^{19}$
He atom influx across the separatrix S_{sep}^{He}, 1/s . . .	$6.12 \cdot 10^{19}$
Pellet injection (HFS/LFS) frequency, Hz . . .	0—1.5/0—100
Pellet size (LFS, HFS), mm^3 . . .	0.05/7
Fueling efficiency:	
k, % $k_{eff\,(NB)}$ . . .	90
$k_{eff\,(pel)}$HFS/LFS . . .	90/50
Fusion neutron flux, 1/s . . .	$1.08 \cdot 10^{19}$
Max. duration of T breeding interruption, days (T from getter)* . . .	20

*The acceptable time for which the tritium breeding in the blanket can be paused — the T reserve to meet the facility's demand for this period is stored in the getter [7].

In calculations using the ASTRA and SOLPS codes, the hydrogen isotopes are not distinguished. The calculations are carried out for fuel particles with atomic weight 2.5 (ASTRA) or 2 (SOLPS). Therefore, to estimate the fluxes of deuterium and tritium, we introduce additional assumptions. We assume that the transport coefficients of the D and T particles in the plasma are equal. Then the relative concentration of tritium in the core plasma $f_{\text{core}}^{\text{T}}$ is determined by the ratio of the strength of the sources of D and T and by their distribution over the plasma core cross-section. For our estimates, we assume that the contributions from various sources to the density of the corresponding plasma species are additive. Then global particle balance in the plasma core can be written in the form

$$N_{\text{core}} = N_{\text{sep}} + S_{\text{NB}}\tau_{\text{NB}} + S_{\text{pel}}\tau_{\text{pel}} + S_{\text{sep}}\tau_{\text{sep}} - S_{\text{fus}}\tau_{\text{tot}}, \quad (1)$$

where $N_{\text{core}} = n_{\text{core}} V_{\text{pl}}$ is the total number of the D and T particles in the plasma core, $N_{\text{sep}} = n_{\text{sep}} V_{\text{pl}}$ (we assume no pinch for the hydrogen components), n_{sep} is the plasma density at the separatrix obtained from the scaling fit to the SOLPS data, and V_{pl} is the volume of the core plasma inside the separatrix. Here S_{NB}, S_{pel}, S_{sep}, and S_{fus} are the source intensities of the D and T ions related to injection of neutrals, injection of pellets, gas supply from the edge (determined from the SOLPS scaling), and fusion reactions, whereas τ_{NB}, τ_{pel}, τ_{sep}, and τ_{tot} are the corresponding confinement times for these ions. All these N and S values are calculated in the ASTRA code, and the values of τ are determined by numerical differentiation of Eq. (1) with respect to the corresponding variable S. The profiles of the sources and density obtained from the modeling [3] are shown in Fig. 2. Fig. 3 shows the evolution of the total particle, in this case, electron, inventory in the plasma after a minor, about 10%, artificial reduction of the individual sources. The ratio of the difference between the particle inventory at two corresponding source values to the difference of these values gives the estimate of the particle confinement times τ_{NB}, τ_{pel}, τ_{sep} and τ_{tot} for different sources.

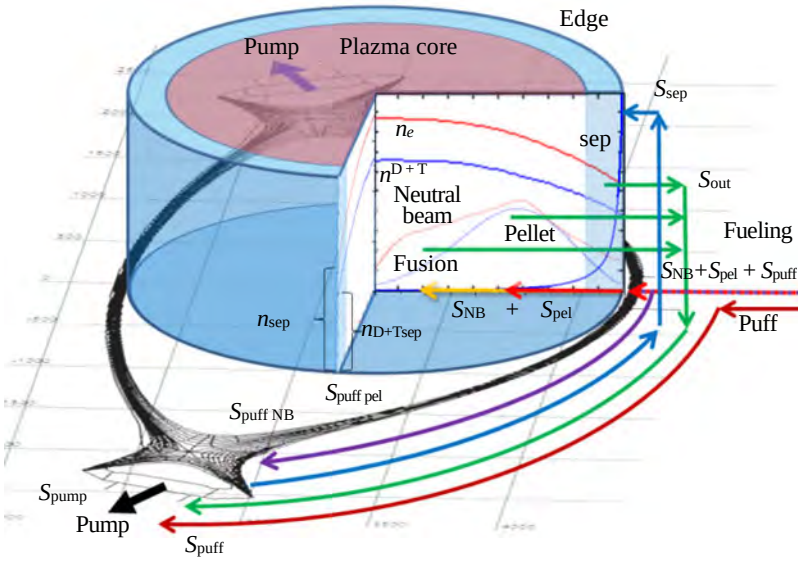

Fig. 2. Cartoon of the flows that appear in Eqs. (1)—(5). Indicated are the plasma fueling flows, as well as the gas puff into the vacuum chamber and pumping. The electron (n_e) and fuel (n_{D+T}) density profiles in the plasma core are calculated by ASTRA. The profiles of the ion sources of different nature (NBI, pellet injection, and gas injection) in the core plasma are shown. Flows that penetrate into the plasma core S_{NB}, S_{pel}, S_{sep} are shown as well as those that do not reach there, $S_{\text{puff NB}}$ and $S_{\text{puff pel}}$. They are directed to the pumping port. The particle loss from the plasma core S_{out} equals the sum of the fluxes generated by all sources (see Eqs. (3), (5)). Also shown is the computational grid of the SOLPS covering the region of the edge plasma and divertors

In Eq. (1), the τ_{NB}, τ_{pel}, τ_{sep}, and τ_{tot} parameters are the diffusion times characterizing the escape rate of ions originated from the corresponding source to the separatrix. The effective slowing of the density decay in the plasma core due to recycling is described here by the non-zero plasma density at the separatrix n_{sep} and the neutral flow into the core S_{sep}, which are calculated in the SOLPS code and are approximated by the scalings.

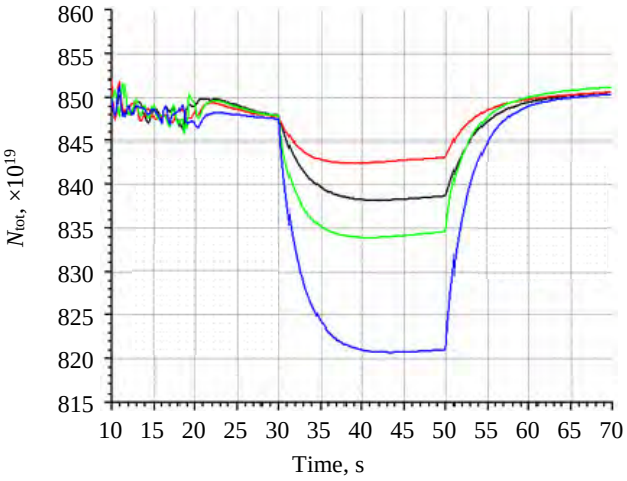

Fig. 3. Evolution of the total particle (in this case, electrons) content after a 10% artificial decrease (at 30 ms) in individual sources: neutral beam (—), pellet-injection (—), neutrals flux from divertor (—), and all of them (—)

Note that the particle transport equations in the ASTRA code are written for electrons and impurity ions. The density of the hydrogen isotopes in the core plasma is calculated from quasi neutrality $<n^{T+D}> = <n_e> - \sum(Z_i<n_i>)$, where i is the impurity index (in our case, He, Ne, Be). Here $<n_e>$ is the average concentration of electrons, Z_{He}, Z_{Ne}, Z_{Be} are the average ion charges of the corresponding impurity (for the light impurities considered here, we assume their complete ionization in the core plasma), and $<n_i>$ is the average impurity concentration obtained in the ASTRA code.

USING CONSISTENT PLASMA PARAMETERS FOR CALCULATING FUEL FLOWS IN THE FC

Let us write the balance equation system for tritium. Particle retention in the core plasma:

$$f^{T}_{core} N_{core} = f^{T}_{div} N_{sep} + S^{T}_{NB} \tau_{NB} + S^{T}_{pel} \tau_{pel} + f^{T}_{div} S_{sep} \tau_{sep} - S_{fus} \tau_{tot}. \quad (2)$$

Balance of tritium particle sources in the plasma core:

$$S^{T}_{out} = S^{T}_{NB} + S^{T}_{pel} + f^{T}_{div} S_{sep} - S^{T}_{fus}. \quad (3)$$

Their balance in the divertor:

$$f^{T}_{div} c_p p_n + f^{T}_{div} S_{sep} = S^{T}_{puff} + S^{T}_{out}. \quad (4)$$

Here f^{T}_{div} is the tritium fraction in the divertor plasma fuel components, which we consider constant, so the tritium fraction in the flows to the pumping system and the plasma core is the same:

$$f^{T}_{div} = S^{T}_{sep}/S_{sep} = S^{T}_{pump}/S_{pump} \equiv S^{T}_{pump}/(c_p p_n), \quad (5)$$

and

$$S^{T}_{puff} = S^{T}_{NB}(1 - k_{eff\,(NB)})/k_{eff\,(NB)} + S^{T}_{pel}(1 - k_{eff\,(pel)})/k_{eff\,(pel)} + S^{T}_{GIS}. \quad (6)$$

Here f^{T}_{core} and f^{T}_{div} are the T fractions in the core and divertor plasma, respectively. S^{T}_{out} is the tritium flux from the core plasma across the separatrix and S^{T}_{GIS} the tritium gas puff into the vacuum chamber, which provides the required pressure (reduced to the normal conditions [20]) p_n in the divertor at a given pumping speed c_p (p_n is determined in the coupled ASTRA + SOLPS calculation from the condition of the acceptable heat load on the divertor targets [16]). $k_{eff\,(NB)}$ and $k_{eff\,(pel)}$ are the efficiencies of fueling the plasma core by the beam and pellets. The coefficients $(1 - k_{eff\,(NB)})$ and $(1 - k_{eff\,(pel)})$ describe the fraction of particles that do not reach the plasma core upon injection of the neutral beams and pellets (the accompanying gas, ionizing in the divertor layer). Since these particles are injected into the tokamak chamber, they must be pumped out and therefore appear in the particle balance in the divertor plasma. The set of 5 Eqs (2)—(6) has 5 unknowns S^{T}_{out}, S^{T}_{pel}, S^{T}_{puff}, S_{puff}, S^{T}_{GIS} and is solved for the given 4 parameters S^{T}_{NB}, f^{T}_{div}, c_p, p_n, which are varied in our model. The tritium fraction in the plasma core f^{T}_{core} is fixed equal to the value adopted in the corresponding ASTRA calculation, where it is used to calculate the fusion power [3]. The following, additional equations allow one to find the fluxes of deuterium and include also the values of the total fluxes S_{pel} and S_{out}, which are calculated by ASTRA [3]:

$$S^{D}_{out} = S_{out} - S^{T}_{out}; \quad (7)$$

$$S^{D}_{pel} = S_{pel} S^{T}_{pel}; \quad (8)$$

$$S^{D}_{puff} = (1 - f^{T}_{div})(S_{puf} + S_{out}) - S^{D}_{out}; \quad (9)$$

$$S^{D}_{GIS} = S^{D}_{puff} - S^{D}_{NB}(1 - k_{eff\,(NB)})/k_{eff\,(NB)} - S^{D}_{pel}(1 - k_{eff\,(pel)})/k_{eff\,(pel)}. \quad (10)$$

The working pressure in the divertor p_n at a given pumping speed c_p [3, 6] is maintained by gas puff into the vacuum chamber S_{puff}. This flow is formed by the gas injected through the gas valves S_{GIS} and by the gas flows from the $S_{puff\,(NB)}$ and $S_{puff\,(pel)}$ injection systems that did not enter the plasma core (due to the fueling

efficiency <100% [18]).The actual particle fluxes from the injection systems for each (D and T) isotope are $S_{\mathrm{NB}}^{\mathrm{total\,(T;\,D)}} = S_{\mathrm{NB}} + S_{\mathrm{puff\,(NB)}} = S_{\mathrm{NB}}/k_{\mathrm{eff\,(NB)}}$ and $S_{\mathrm{pel}}^{\mathrm{total\,(T;\,D)}} = S_{\mathrm{pel}} + S_{\mathrm{puff\,(pel)}} = S_{\mathrm{pel}}/k_{\mathrm{eff\,(pel)}}$ [6, 10]. Therefore, these particle fluxes affect the divertor pressure (and thus reduce the required gas puffing rate). These fluxes have also an important role in the simulation of the injection systems, pumping, and fuel mixture processing in the FC. The tritium source balance in the core plasma, Eq. (3), determines the tritium flow rate across the separatrix into the divertor $S_{\mathrm{out}}^{\mathrm{T}}$ and the $f_{\mathrm{div}}^{\mathrm{T}}$ value is the parameter determining the tritium flow rate $S_{\mathrm{GIS}}^{\mathrm{T}}$ through the gas valves (6).

Fig. 2 shows the plasma fueling flows, the gas puff into the vacuum chamber and the pumping flow, the electron density (n_e), and the fuel isotope density ($n^{\mathrm{D+T}}$) profiles. Different zones of fueling by the NBI, pellet injection, and gas injection sources are also shown. Flows that penetrate into the plasma core, $S_{\mathrm{NB}}^{\mathrm{T+D}}$, $S_{\mathrm{pel}}^{\mathrm{T+D}}$ and $S_{\mathrm{sep}}^{\mathrm{T+D}}$, are shown, as well as those that do not reach there, $S_{\mathrm{puff\_NB}}^{\mathrm{T;\,D}}$ and $S_{\mathrm{puff\_pel}}^{\mathrm{T;\,D}}$. The particle losses from the plasma core $S_{\mathrm{out}}^{\mathrm{T+D}}$ are equal to the sum of the fluxes generated by all sources.

The total gas flow rates and intensities of the various sources are determined by the ASTRA + SOLPS codes, ensuring that they match the selected operating mode of the reactor. Thus, in FC-FNS, we assume that the $S_{\mathrm{pel}}^{\mathrm{T;\,D}}$ fluxes provide the required D and T densities in the plasma core for various NBI cases ($S_{\mathrm{NB}}^{\mathrm{T}}$ and $S_{\mathrm{NB}}^{\mathrm{D}}$). By changing the ratio of $S_{\mathrm{puff}}^{\mathrm{T}}/S_{\mathrm{puff}}^{\mathrm{D}}$ (while maintaining the total S_{puff}), the T fraction $f_{\mathrm{div}}^{\mathrm{T}}$ can be changed. Selection of the optimal values for the fuel fluxes in the injection system should ensure particle balance in the core and divertor plasma, Eqs. (2)—(6), for D and T, providing plasma burning and neutron production.

Since the total number of D and T particles in the plasma core is specified by the ASTRA code, a condition for the range of the fuel isotope injection fluxes can be obtained. Writing Eq. (2) in the form

$$N_{\mathrm{core}}^{\mathrm{T,\,D}} = f_{\mathrm{div}}^{\mathrm{T,\,D}} N_{\mathrm{sep}}^{\mathrm{D+T}} + S_{\mathrm{NB}}^{\mathrm{T,\,D}} \tau_{\mathrm{NB}} + S_{\mathrm{pel}}^{\mathrm{T,\,D}} \tau_{\mathrm{pel}} + f_{\mathrm{div}}^{\mathrm{T,\,D}} N_{\mathrm{sep}}^{\mathrm{D+T}} \tau_{\mathrm{sep}} - S_{\mathrm{fus}}\tau_{\mathrm{tot}},$$ we obtain

$$N_{\mathrm{core}}^{\mathrm{T,\,D}} = f_{\mathrm{core}}^{\mathrm{T,\,D}} N_{\mathrm{core}} = f_{\mathrm{div}}^{\mathrm{T,\,D}} N_{\mathrm{sep}} + S_{\mathrm{NB}}^{\mathrm{T,\,D}} \tau_{\mathrm{NB}} + S_{\mathrm{pel}}^{\mathrm{T,\,D}} \tau_{\mathrm{pel}} + f_{\mathrm{div}}^{\mathrm{T,\,D}} S_{\mathrm{sep}}^{\mathrm{D+T}} \tau_{\mathrm{sep}} - S_{\mathrm{fus}}\tau_{\mathrm{tot}},$$ or

$$(n^{\mathrm{T+D}} V_{\mathrm{pl}} f_{\mathrm{core}}^{\mathrm{T,\,D}} + S_{\mathrm{fus}}\tau_{\mathrm{tot}} - S_{\mathrm{NB}}^{\mathrm{T,\,D}} \tau_{\mathrm{NB}} - S_{\mathrm{pel}}^{\mathrm{T,\,D}} \tau_{\mathrm{pel}})/(V_{\mathrm{pl}} n_{\mathrm{sep}}^{\mathrm{D+T}} + S_{\mathrm{sep}}\tau_{\mathrm{sep}}) = f_{\mathrm{div}}^{\mathrm{T,\,D}}.$$

This equation limits injection into the plasma to maintain its density for the given confinement times. Since it contains the $f_{\mathrm{core}}^{\mathrm{T,\,D}}$ and $f_{\mathrm{div}}^{\mathrm{T,\,D}}$ terms, it can be used as a condition for the fraction of the isotopes in the divertor $f_{\mathrm{div}}^{\mathrm{T,\,D}}$ depending on the required $f_{\mathrm{core}}^{\mathrm{T,\,D}}$ value:

$$(n^{\mathrm{T+D}} V_{\mathrm{pl}} f_{\mathrm{core}}^{\mathrm{T,\,D}} + S_{\mathrm{fus}}\tau_{\mathrm{tot}} - S_{\mathrm{NB}}^{\mathrm{T,\,D}} \tau_{\mathrm{NB}})/(V_{\mathrm{pl}} n_{\mathrm{sep}}^{\mathrm{D+T}} + S_{\mathrm{sep}}\tau_{\mathrm{sep}}) > f_{\mathrm{div}}^{\mathrm{T,\,D}}, \qquad (11)$$

with a non-negative value of $S_{\mathrm{pel}}^{\mathrm{T,\,D}}$.

Substituting the values for the consistent stationary solution in the core and divertor plasma into Eq. (11), one can find the boundaries of the admissible range of $f_{\mathrm{div}}^{\mathrm{T}}$. This limitation has a simple nature — when the T fraction in the divertor is changed, the deuterium fraction is changed too, but in the opposite direction. As a result, $S_{\mathrm{sep}}^{\mathrm{D}}$ is changed. This, in turn, leads to a change of $f_{\mathrm{core}}^{\mathrm{T,\,D}}$. Therefore, to ensure particle balance in the plasma core, the necessary $f_{\mathrm{div}}^{\mathrm{T,\,D}}$ value must be provided by the fueling gas puff $S_{\mathrm{puff}}^{\mathrm{T,\,D}}$ and pumping $S_{\mathrm{pump}}^{\mathrm{T,\,D}}$. We'll take a closer look at this in the next section.

The FC-FNS code implements a numerical method for solving the set of Eqs. (2)—(6) by an iteration method, which calculates the fluxes of the fuel isotopes required to feed the plasma and calculates the gas flows in the systems of pumping, hydrogen extraction, isotope separation to the required concentrations, and their injection in various forms (gas, neutral beams and cryogenic pellets). Using the equations described in [6, 10], for specified values of $S_{\mathrm{pump}}^{\mathrm{T,\,D}}$ and $S_{\mathrm{core}}^{\mathrm{T,\,D}}$ fluxes in the FC systems and the relative tritium concentrations, the corresponding values of f_i^{T} in these systems are determined. The isotopic composition index together with the flux of one fuel isotope in the FC system makes it possible to calculate the flux of the other if not specified otherwise. The FC diagram (see Fig. 1) shows that some systems have several input and/or output flows, and they do not necessarily have the same isotopic composition. For example, monoisotopic mixtures are characteristic for the

output of the systems for breeding T, isotope separation, and injection. As a rule, the input flow to a system (for example, isotope separation) is set from the condition of ensuring the required product flow at the output — in this case, the f_i^{T} values allow one to calculate correctly the input and output flows of the fuel mixture components.

RESULTS AND DISCUSSION

Using the ASTRA code, a stationary solution was found and the particle confinement times $\tau_{\mathrm{tot}\,(e)}$, $\tau_{\mathrm{NB}\,(e)}$, $\tau_{\mathrm{pel}\,(e)}$, $\tau_{\mathrm{sep}\,(e)}$ were calculated instead of a single τ_{p} that we used earlier for all sources. Table 1 shows the characteristic particle retention times from the various sources, as calculated with ASTRA.

T a b l e 1. **Characteristic particles retention times from various sources, calculated by ASTRA**

Parameters	Value	Parameters	Value (10^{19})
Particle confinement time $\tau_{\mathrm{NB}\,(e)}$, s	2.69	Total particles N_{core}	630
Particle confinement time $\tau_{\mathrm{pel}\,(e)}$, s	2.5	Particle source from NB injectors S_{NB}, 1/s	37.5
Particle confinement time $\tau_{\mathrm{sep}\,e}$, s	0.63	Pellet particle flow S_{pel}, 1/s	28.5
Particle confinement time $\tau_{\mathrm{tot}\,(e)}$, s	0.96	Particle flow from the divertor S_{sep}, 1/s	222
		Total particle source S_{tot}, 1/s	288

For the stationary solution found by ASTRA + SOLPS4.3 codes for the core and divertor plasma with corresponding He balance and Ne seeding gas in divertor (see Table 1), the FC-FNS code calculations were performed for three cases of gas supply to the heating injectors [10, 19]: (i) using $D_2 + T_2$ mixture with the isotope ratio close to the plasma composition; (ii) with a closed gas supply loop (described in section 1) and using the $D_2 + T_2$ mixture; and (iii) with a closed gas supply loop and D_2 as the working gas (in this case, the T fraction is controlled by the purification system). As a result of the numerical solution of the set of equations, the absolute values of the flows in various FC systems were obtained for the given values of $f_{\mathrm{core}}^{\mathrm{T}}$ and $f_{\mathrm{div}}^{\mathrm{T}}$.

Plasma scenario calculations in ASTRA were performed for $f_{\mathrm{core}}^{\mathrm{T}} = 0.5$. The working range of $f_{\mathrm{div}}^{\mathrm{T}}$ from Eq. (11) turns out to be different for different cases of NBI gas supply. For example, for the $D^0 + T^0$ beam, we get $f_{\mathrm{div}}^{\mathrm{D}} < 0.53$ and $f_{\mathrm{div}}^{\mathrm{T}} < 0.53$, which will result in the working range of $0.47 < f_{\mathrm{div}}^{\mathrm{T}} < 0.53$. For the D^0 beam, the working range for the T fraction in the divertor is $0.54 < f_{\mathrm{div}}^{\mathrm{T}} < 0.60$. Therefore, for the $D^0 + T^0$ beam case the variant $f_{\mathrm{core}}^{\mathrm{T}} = f_{\mathrm{div}}^{\mathrm{T}}$ can be realized, but for the D^0 beam this condition $f_{\mathrm{core}}^{\mathrm{T}} = f_{\mathrm{div}}^{\mathrm{T}}$ cannot be met.

The option of $f_{\mathrm{core}}^{\mathrm{T}} = 0.5$ was considered for $f_{\mathrm{div}}^{\mathrm{T}} = 0.47, 0.50, 0.53, 0.54, 0.60$. The first three modes are only realizable for the $D^0 + T^0$ beam cases, and the last two for the D^0 beam case. Fig. 4 shows the isotopic composition f_i^{T} in the key FC systems, depending on $f_{\mathrm{div}}^{\mathrm{T}}$. The plots for $0.47 < f_{\mathrm{div}}^{\mathrm{T}} < 0.53$ correspond to the

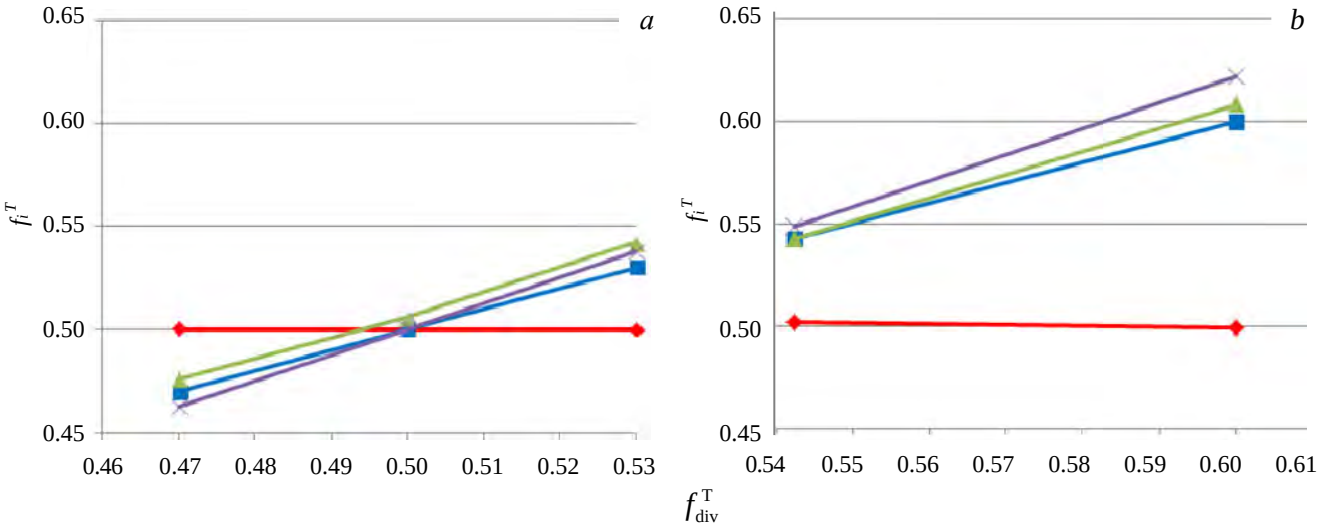

Fig. 4. Isotopic composition f_i^{T} in the key FC systems: core plasma (——), purification system (——), flow distribution (——), and gas injection (——) vs. $f_{\mathrm{div}}^{\mathrm{T}}$, for the $D^0 + T^0$ beam scenarios ($0.47 < f_{\mathrm{div}}^{\mathrm{T}} < 0.53$) (*a*), for the D^0 beam ($0.54 < f_{\mathrm{div}}^{\mathrm{T}} < 0.60$) (*b*)

$D^0 + T^0$ beam cases, and $0.54 < f_{div}^T < 0.60$ to the D^0 beam. It can be seen that $f_{core}^T = 0.5$ is kept for all f_{div}^T. For $f_{div}^T = 0.5$, the f_i^T values for the systems of purification, flow distribution (to restore the isotopic composition [6, 7]) and gas puff differ in the absolute value within 5%. Changing f_{div}^T in one direction or another leads to the change of f_i^T in the same direction. The largest f_i^T deviation from f_{core}^T is observed for the gas puff system into the vacuum chamber/divertor, and $f_{puff}^T < f_{div}^T < f_{core}^T$ or $f_{core}^T < f_{div}^T < f_{puff}^T$, which allows providing the required f_{div}^T value.

The condition $f_{core}^T \sim 0.5$ is provided by the fuel injection regime (the pellet size and the injection frequency), at which Eq. (2) is satisfied. In all cases considered, the FC-FNS model assumed the fuel injection from the HFS (high field side) by cryogenic fuel pellets D_2 and T_2 of a cylindrical shape with d = 2.0 mm and the length equal to the diameter. In this case, the selected injection frequencies do not exceed 1.5 Hz. The injection from the LFS (low field side) was considered similarly, but with the smaller size, d = 0.5 mm, D_2 pellets. Its frequency depends substantially on the f_{div}^T operating point. Due to ablation, the LFS pellet loses particles at the plasma periphery, which decreases the f_{div}^T value because of the increase of their (D) amount in the divertor plasma. This reduces the S_{puff}^D flow required to maintain f_{div}^T at the required level. Nevertheless, some of the particles from the pellets fuel the plasma core. Accordingly, to maintain the balance of fluxes, Eq. (3), it is necessary to reduce the S_{pel}^D flux from the HFS. Obviously, the closer to the border of the operating window, Eq. (11), the T fraction in divertor f_{div}^T is chosen, the less margin for the $S_{pel\,(LFS)}^D$ flow (so that particle balance, Eq. (3), for D + T is not violated) remains. In this regard, if D pellet injection for ELM mitigation is foreseen, then the frequency of this injection can be limited depending on the operating point in f_{div}^T considering NBI gas supply and the expected $S_{pel\,(LFS)}^D$ flow. So, at the low end of the range (at $S_{pel\,(HFS)}^D = 0$), the available injection frequency with LFS is 5 and 10 Hz for $D^0 + T^0$ and D^0 beams, respectively. At the same time, at the high end of the range, these values reach 105 and 110 Hz.

Here, the ELMs and the associated particle loss from the plasma core were not taken into account. The particle loss due to ELMs should be compensated by HFS fuelling. This will lead to an increase in the flow of $S_{pel\,(HFS)}$ and will require re-balancing of all the flows (including a decrease in S_{puff}). This assessment is underway and will be reported separately in the future.

Fig. 5 shows the dependences of fuel particle fluxes from different sources on the T fraction in the divertor f_{div}^T for the $D^0 + T^0$ and D^0 NBI cases (see. Fig. 4) and Table 2 shows their values. The plots on the left ($0.47 < f_{div}^T < 0.53$) correspond to the $D^0 + T^0$ beam case and those on the right ($0.54 < f_{div}^T < 0.60$) to the D^0 beam. One can see that the corresponding fluxes D and T for all sources have the opposite dynamics, thereby providing the conditions for maintaining the total fluxes $S_i^{T,D}$. The horizontal dotted lines in Fig. 5 show the average values of the total flow S_i^{T+D}, relative to which $S_i^{T,D}$ change their values. The particle fluxes from the NBI, $S_{NB}^{T,D}$, for the $D^0 + T^0$ beam are equal, and for the D^0 beam, while maintaining the total ion source current,

T a b l e 2. **The D and T particle source intensity (10^{19} 1/s) for different values of f_{div}^T**

Beam	f_{div}^T	S_{NB}^T	S_{NB}^D	S_{pel}^T	S_{pel}^D	S_{sep}^T	S_{sep}^D	S_{out}^T	S_{out}^D
$D^0 + T^0$	0,47	17,6	19,9	26,7	1,26	104	118	147	137
	0,5	18,7	18,7	13,9	13,9	111	111	142	142
	0,53	20,2	17,3	0,84	27,1	117	104	137	147
$D^0 + T^0$	0,47	18,7	18,7	25,0	2,95	104	117	147	138
	0,5	18,7	18,7	13,9	13,9	111	111	143	143
	0,53	18,7	18,7	2,86	25,1	117	104	138	147
D^0	0,54	0	37,5	25,3	2,66	120	102	144	141
	0,60	0	37,5	2,97	25,0	133	89	135	150

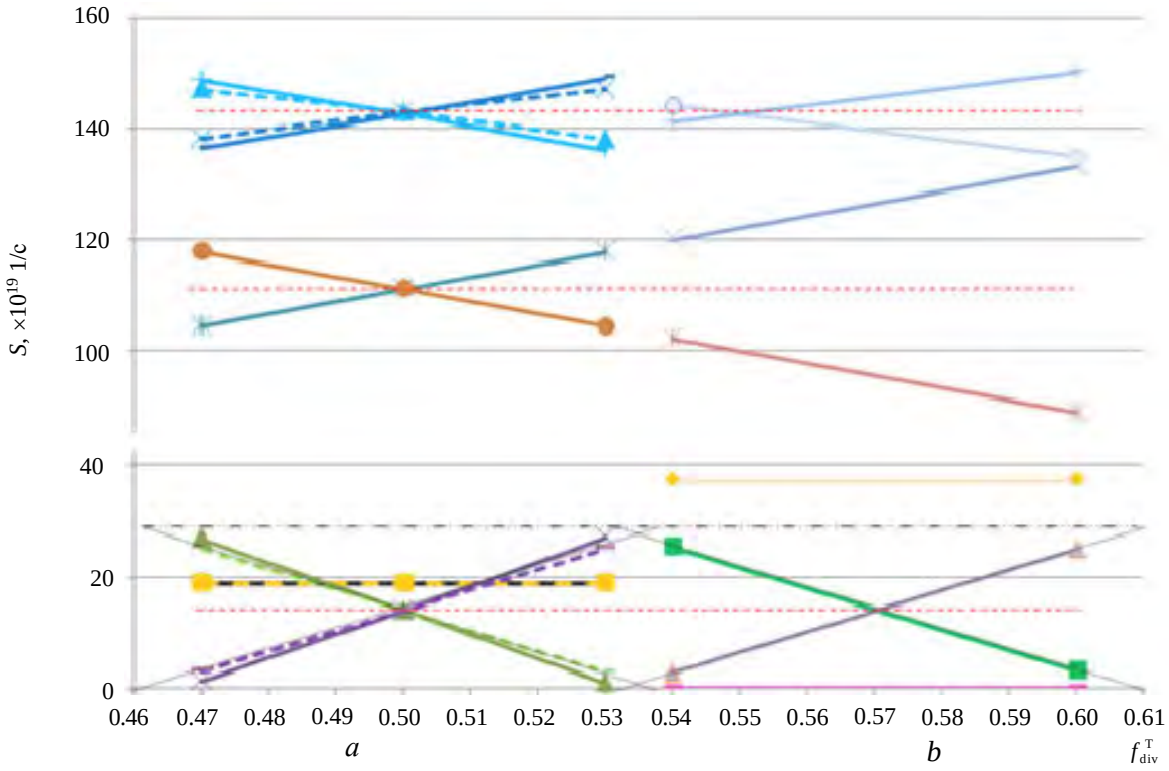

Fig. 5. Particle flu xes (for D and T) from sources vs. $f_{\text{div}}^{\text{T}}$ for the cases of the $D^0 + T^0$ and D^0 beams considered above. The plots for $0.47 < f_{\text{div}}^{\text{T}} < 0.53$ correspond to the scenarios for the $D^0 + T^0$ beam (*a*), and $0.54 < f_{\text{div}}^{\text{T}} < 0.60$ for the D^0 beam (*b*). The horizontal dashed lines (---) show the average values of the total flow $S_i^{\text{T+D}}$, relative to which $S_i^{\text{T, D}}$ change their values. The dash-dotted line shows the S_{pel} value (-·-·-): ◆ — S_{NB}^{T} ($D^0 + T^0$); ● — $S_{\text{sep}}^{\text{D}}$ ($D^0 + T^0$); ■ — $S_{\text{pel}}^{\text{T}}$ (D^0); + — $S_{\text{out}}^{\text{D}}$ (D^0); -·-■-·- — S_{NB}^{D} ($D^0 + T^0$); + — $S_{\text{out}}^{\text{T}}$ ($D^0 + T^0$); ▲ — $S_{\text{pel}}^{\text{D}}$ (D^0); - - - — $S_{\text{pel}}^{\text{T}}$ ($D^0 + T^0$); ▲ — $S_{\text{pel}}^{\text{T}}$ ($D^0 + T^0$); — — $S_{\text{out}}^{\text{D}}$ ($D^0 + T^0$); × — $S_{\text{sep}}^{\text{T}}$ (D^0); - - - — $S_{\text{pel}}^{\text{D}}$ ($D^0 + T^0$); × — $S_{\text{pel}}^{\text{D}}$ ($D^0 + T^0$); — — S_{NB}^{T} (D^0); ✱ — $S_{\text{sep}}^{\text{D}}$ (D^0); ▲ — $S_{\text{out}}^{\text{T}}$ ($D^0 + T^0$); ✱ — $S_{\text{sep}}^{\text{T}}$ ($D^0 + T^0$); ◆ — S_{NB}^{D} (D^0); ○ — $S_{\text{out}}^{\text{T}}$ (D^0); × — $S_{\text{out}}^{\text{D}}$ ($D^0 + T^0$)

respectively, twice as large. Thus, for this particle source, the total $S_{\text{NB}}^{\text{T+D}}$ value is also retained in the entire range considered (see the flow values in Table 1). The D_2 pellet flux $S_{\text{pel}}^{\text{D}}$ values rise from 0 (at the high end of the $f_{\text{div}}^{\text{T}}$ range) to the maximum value, while the T_2 pellet flux $S_{\text{pel}}^{\text{T}}$ reflects the opposite dynamics. The intersections of the $S_{\text{pel}}^{\text{T}}$ and $S_{\text{pel}}^{\text{D}}$ curves with the 0 level line and the total flux $S_{\text{pel}}^{\text{T+D}}$ correspond to the working range boundaries, Eq. (11), for $f_{\text{div}}^{\text{T}}$. The dotted lines in the figure show the $S_i^{\text{T, D}}$ plots for the $D^0 + T^0$ beam case with the closed gas supply cycle. For this case, the dependencies are flatter than for the second case (the $D^0 + T^0$ beam with the open gas cycle). Table 3 shows the D and T particle fluxes in the divertor for different values of $f_{\text{div}}^{\text{T}}$.

T a b l e 3. **D and T particle fluxes (10^{19} 1/s) in the divertor for different values of $f_{\text{div}}^{\text{T}}$**

Beam	$f_{\text{div}}^{\text{T}}$	$S_{\text{puff (NB)}}^{\text{T}}$	$S_{\text{puff (NB)}}^{\text{D}}$	$S_{\text{puff (pel)}}^{\text{T}}$	$S_{\text{puff (pel)}}^{\text{D}}$	$S_{\text{GIS}}^{\text{T}}$	$S_{\text{GIS}}^{\text{D}}$	$S_{\text{puff}}^{\text{T}}$	$S_{\text{puff}}^{\text{D}}$
$D^0 + T^0$	0,47	2,08	2,08	2,97	0,14	859	1000	865	1004
	0,50	2,08	2,08	1,55	1,55	931	931	934	934
	0,53	2,08	2,08	0,09	3,10	1000	858	1004	865
$D^0 + T^0$	0,47	2,08	2,08	2,78	033	861	1000	865	1003
	0,50	2,08	2,08	1,55	1,55	931	931	934	934
	0,53	2,08	2,08	0,32	2,79	1000	861	1003	865
D^0	0,54	0	4,17	2,81	0,29	1020	846	1019	850
	0,60	0	4,17	0,33	2,78	1160	706	1159	713

A detailed description of the flows in the injection and pumping systems in DEMO-FNS is necessary to refine the parameters of the fuel cycle systems, which must have the appropriate performance for processing the incoming flows. The flow map of the fuel isotopes in the FC allows optimizing both the architecture of the systems and the technologies used to reduce the processing time of the tritium-containing gas flows, reducing the

total T inventory on the site. Table 4 shows the gas flows through the main FC systems for various NBI cases: $D^0 + T^0$ and D^0 ($f_{core}^T = 0.5$). As already mentioned, the candidate technologies for hydrogen extraction, isotope separation, and pumped (from the vacuum chamber) gas detritiation were considered earlier [5] based on similar

T a b l e 4. **Gas flows through the main FC systems for various NBI cases: $D^0 + T^0$(closed gas supply loop) and D^0($f_{core}^T = 0.5$) (in mol/s; 1 mol = $2 \cdot 6.022 \cdot 10^{23}$ nuclei for gases with diatomic molecules, such as H_2, D_2, T_2).**

NBIcases	Pumping	Cleanup, Gas separation	Isotope Separation	Isotope Rebalancing	Fueling:			Blanket
					PIS	NBI	GIS	
$D^0 + T^0_{NB}$	0.010/0.008	0.030/0.029	$3 \cdot 10^{-4}/3 \cdot 10^{-4}$	0.030/0.029	$6 \cdot 10^{-6}/3 \cdot 10^{-4}$	0.021/0.021	0.009/0.008	$1.2 \cdot 10^{-5}/0$
D^0_{NB}	0.010/0.008	0.010/0.008	$9 \cdot 10^{-4}/4 \cdot 10^{-4}$	0.009/0.008	$6 \cdot 10^{-6}/3 \cdot 10^{-4}$	$2 \cdot 10^{-6}/0.042$	0.009/0.008	$1.2 \cdot 10^{-5}/0$

flow calculations in the FC (including [6]). By considering this refined data, further optimization can be carried out.

Table 5 shows the T inventory in the FC systems considered, estimated from isotope flux modeling with the FC-FNS code. As noted in [10, 14, 15], the $D^0 + T^0$ beam case with the open cycle of the NBI gas supply corresponds to the largest T amount in the entire system (this case is not shown separately here). From a technological point of view, the closed fuel cycle is more attractive. Here many of the FC systems can have lower productivity, although for the $D^0 + T^0$ beam, it has little advantage in the T inventory. For the D^0 beam, the T inventory in the FC is reduced by more than a factor of 1.5. With T inventories in the backup storage and the long-term storage, the total T inventory at the site will be from 850 to 1150 g, which is lower than the estimates made earlier [6]. First of all, this is explained by the decrease of the fusion power and, consequently, the T breeding rate in the hybrid blanket of the machine. Other reasons include the change in the flux ratio in the core and divertor plasma, as well as optimization of the FC architecture and refinement of the plasma parameters simulated by the ASTRA + SOLPS4.3 codes.

T a b l e 5. **T/D inventories in the main FC systems as calculated by FC-FNS code. Values in brackets taking into account T inventories in backup storage and in long-term storage**

DEMO-FNS FC systems	$D^0 + T^0$ beam, g	D^0 beam, g
Gas supply to heating injectors	300/200	1/1380
Pellet fuel injection	25/35	25/35
Gas puff	17/12	17/12
Pumping	48/28	48/28
T breeding and extraction	56	56
Li-loop on the FW and/or in divertor	<1	<1
FW and divertor cooling and T extracting	<1	<1
Membrane permeation	1/1	1/1
Chemical H-compounds decomposition	20/64	6/18
Isotope separation	100/40	100/40
Detritiation of gas in heating injectors	—	<1
Plasma core	<0.1	<0.1
Backup storage	95	95
Long-term storage (after a year)	290	305
Manifolds, receivers, etc.	70/50	70/50
In construction materials	110/70	110/70
Total amount	840(1150)/500	530(850)/1600

CONCLUSION

The paper presents a zero-dimensional model of the FC complex of the DEMO-FNS tokamak, which includes the FC systems as well as the core and edge tokamak plasmas. An approach to modeling the core plasma is developed, considering different fuel retention times for particles originating from different fueling sources. The working range of the isotopic composition in the divertor plasma is found, at which the required fraction of tritium in the core plasma is provided. For various cases of the NBI gas supply scheme, the fueling parameters were selected, which are necessary to ensure the specified isotopic composition in the core and divertor plasma. The selected in-

jection frequencies of cryogenic D_2 and T_2 fuel pellets do not exceed 1.5 Hz for all cases considered (without ELM-induced particle loss from the core). Scenarios with $f_{\text{core}}^{\text{T}} = 0.5$ in the range $0.47 < f_{\text{div}}^{\text{T}} < 0.53$ for the $D^0 + T^0$ beam and $0.54 < f_{\text{div}}^{\text{T}} < 0.60$ for the D^0 beam were found. It is shown that for LFS (D_2) pellet injection, it will be necessary to select the $f_{\text{div}}^{\text{T}}$ operating value taking into account the beam isotope composition and the expected $S_{\text{pel (LFS)}}^{\text{D}}$ flux. The closer $f_{\text{div}}^{\text{T}}$ value is chosen to the edge of the working window, the lower $S_{\text{pel (LFS)}}^{\text{D}}$ flux can be allowed without negatively affecting the plasma core parameters. The permissible injection frequency depends significantly on the value of $f_{\text{div}}^{\text{T}}$ (from 5 to 110 Hz for the specified size of LFS pellets), which can limit the working area of parameters when mitigating ELMs this way.

The FC-FNS code has been modified to fully match the architecture chosen in the course of the analysis of the DEMO-FNS candidate fuel cycle technologies. The model is supplemented with a new scenario of the NBI gas supply for $D^0 + T^0$ beam injection with a closed gas cycle. The gas flows through the main FC systems were calculated for various NBI gas supply schemes and the T inventories in the FC systems are obtained as the isotope flux simulation result. The $D^0 + T^0$ beam case with the open NBI gas supply cycle requires the largest T amount in the FC systems (850 g). From the technological point of view, a closed fuel cycle is more justified, in which many FC systems can have lower productivity (however, for the $D^0 + T^0$ beam, it gains little in T content (840 g)). For the D^0 beam, the T content in the FC decreases by more than a factor of 1.5. The whole T inventory in the backup storage, the long-term storage, and in the FC is expected to range from 850 g to 1150 g (for the D^0 and $D^0 + T^0$ beam scenarios, respectively), which is lower than the estimates made earlier [6].

This work was supported by the National Research Center «Kurchatov Institute». The SOLPS calculations were performed using computing resources of the federal collective usage center Complex for Simulation and Data Processing for Mega-science Facilities at NRC «Kurchatov Institute», http://ckp.nrcki.ru/.

REFERENCES

1. **Kuteev B.V., Shpanskiy Y.U.S., and DEMO-FNS project team.** Progress in the design of the DEMO-FNS hybrid facility. — Nucl. Fusion, 2019, vol. 59, 076014; https://doi.org/10.1088/1741-4326/ab14a8.
2. **Ananyev S.S., Dnestrovskij A.Yu., Kukushkin A.S., Spitsyn A.V., Kuteev B.V.** Integration of coupled modeling of the core and divertor plasmas into «FC-FNS» code and application to DEMO-FNS project. — Fusion Engineering and Design, 2020, vol. 155, 111562; https://doi.org/10.1016/j.fusengdes.2020.111562.
3. **Dnestrovskij A.Yu. et al.** Integrated modelling of core and divertor plasmas for the DEMO fusion neutron source hybrid facility. — Nucl. Fusion, 2019, vol. 59, 096053; https://doi.org/10.1088/1741-4326/ab3075.
4. **Kukushkin A.S. et al.** Physics requirements on fuel throughput in ITER. — J. Nucl. Mater., 2011, vol. 415, S497; https://doi.org/10.1016/j.jnucmat.2010.08.050.
5. **Ananyev S.S., Ivanov B.V., Kuteev B.V.** Analysis of promising technologies of DEMO-FNS fuel cycle. — Fusion Engineering and Design, 2020, vol. 161, 111940; https://doi.org/10.1016/j.fusengdes.2020.111940.
6. **Ananyev S.S., Dnestrovskij A.Yu., Kukushkin A.S., Spitsyn A.V., Kuteev B.V.** Simulation of fuel flows in injection systems of DEMO-FNS hybrid facility involving coupled modeling of the core and divertor plasmas. — VANT. Ser. Thermonuclear Fusion, 2019, vol. 42, № 2; https://doi.org/10.21517/0202-3822-2019-42-2-5-21.
7. **Ananyev S.S., Spitsyn A.V., Kuteev B.V.** Electronic model FC-FNS of the fusion neutron source DEMO-FNS fuel cycle and modeling hydrogen isotopes flows and inventories in fueling systems. — Fusion Eng. Des., 2019, vol. 138, p. 289; https://doi.org/10.1016/j.fusengdes.2018.12.003.
8. **Kukushkin A.S., Pacher H.D., Kotov V. et al.** Finalizing the ITER divertor design: the key role of SOLPS modeling. — Fusion Eng. Des., 2011, vol. 86, p. 2865—2873; http://dx.doi.org/10.1016/j.fusengdes.2011.06.009.
9. **Pereverzev G.V., Yushmanov P.N.** ASTRA: Automated System for Transport Analysis in a Tokamak. Report ID 282186, Max-Planck-Institut fuer Plasmaphysik, 2002.
10. **Ananyev S.S., Dnestrovskij A.Yu., Kukushkin A.S., Spitsyn A.V., Kuteev B.V.** Architecture of fuel systems of hybrid facility DEMO-FNS and algorithms for calculation of fuel flows in the FC-FNS model. — Fusion Science and Technology, 2020, vol. 76, p. 503—512; https://doi.org/10.1080/15361055.2020.1718855S.
11. **Ni M., Song Y., Jin M., Jiang J., Huang Q.** Design and analysis on tritium system of multi-functional experimental fusion–fission hybrid reactor (FDS-MFX). — Fusion Eng. Des., 2012, vol. 87, № 7—8, p. 1004—1008.
12. **Di Pace L., Rizzello C., Natalizio A., Kalyanam K., Matsugu R., Caporali R.** Analysis of the SEAFP reactor fuel cycle. — J. Fusion Energy, 1997, vol. 16, № 1—2, p. 55—65.
13. **Kuan W., Abdou M.A., Willms R.S**. Time-dependent tritium inventories and flow rates in fuel cycle components of a tokamak fusion reactor. — Fusion Eng. Des., 1995, vol, 28 (C), p. 329—335.

14. **Ananyev S., Spitsyn A.V., Kuteev B.V.** Concept of DT fuel cycle for a fusion neutron source DEMO-FNS. — Fusion Eng. Des., 2016, vol. 109—111, p. 57; https://doi.org/10.1016/j.fusengdes.2016.03.053.
15. **Ananyev S.S., Spitsyn A.V., Kuteev B.V.** Hydrogen isotopes distribution modeling by FC-FNS code in fuel systems of fusion neutron source DEMO-FNS. — Fusion Eng. Des., 2019, vol. 146, p. 582; https://doi.org/10.1016/j.fusengdes.2019.01.028.
16. **Pacher H.D. et al.** Impurity seeding in ITER in a carbon-free environment. — J. Nucl. Mater., 2015, vol. 463, p. 591; https://doi.org/10.1016/j.jnucmat.2014.11.104.
17. **Pacher H.D., Kukushkin A.S., Pacher G.W., Janeschitz G.** Scaling of ITER divertor parameters — interpolation from 2D modelling and extrapolation. — J. Nucl. Mater., 2003, vol. 313—316, p. 657—663; https://doi.org/10.1016/S0022-3115(02)01374-0.
18. **Abdou M. et al.** Blanket/first wall challenges and required R&D on the pathway to DEMO. — Fusion Eng. Des., 2015, vol. 100, p. 2—43; https://doi.org/10.1016/j.fusengdes.2015.07.021.
19. **Ananyev S.S., Dlougach E.D., Krylov A.I., Kuteev B.V., Panasenkov A.A.** Concept of plasma heating and current drive neutral beam system for fusion neutron source DEMO-FNS. — Physics of Atomic Nuclei, 2019, vol. 82, № 7, p. 981—990; https://doi.org/10.1134/S1063778819070020.
20. **Kukushkin A.S., Pacher H.D., Kotov V., Reiter D., Coster D.P., Pacher G.W.** Effect of the dome on divertor performance in ITER. — J. Nucl. Mater., 2007, vol. 363—365, № 1—3, p. 308—313; https://doi.org/10.1016/j.jnucmat.2007.01.094.

AUTHORS

Sergey S. Ananyev, Leading Researcher, PhD in physics and mathematics, NRC «Kurchatov Institute», 1, Academika Kurchatova sq., Moscow, 123182, Russia, Ananyev_SS@nrcki.ru

Alexey Yu. Dnestrovsky, Leading Engineer, PhD in physics and mathematics; NRC «Kurchatov Institute», 1, Academika Kurchatova sq., Moscow, 123182, Russia, Dnestrov0@gmail.com

Andrey S. Kukushkin, Leading Researcher, PhD in physics and mathematics; NRC «Kurchatov Institute», 1, Academika Kurchatova sq., Moscow, 123182, Russia, ank755@gmail.com

Статья поступила в редакцию 15 января 2021 г.
После доработки 16 марта 2021 г.
Принята к публикации 25 марта 2021 г.
Вопросы атомной науки и техники.
Сер. Термоядерный синтез, 2021, т. 44, вып. 2, с. 65—77.

UDC 621.039.623:533.9.082

DIAGNOSTICS AND CONTROL OF FUSION-FISSION HYBRID TOKAMAK-BASED REACTORS: THE TECHNOLOGY FOR MEASUREMENT SYSTEMS

F.P. Orsitto[1], M. Angelone[1], M. Tardocchi[2]

[1]ENEA Department for Fusion and Nuclear Safety, Frascati, Italy
[2]Istituto per la Scienza e Tecnologia dei Plasmi CNR, Milano, Italy

A fusion-fission hybrid (FFH) reactor is a complex machine, which includes a tokamak fusion neutron source and two blankets: the tritium regeneration and the actinide burner zones. These three systems need their own diagnostics and controls. Problems associated with the implementation and integration of control systems call for a simplified technology. In this paper, the criteria determining the diagnostics needs of FFH reactors are reviewed bearing in mind the requirement that the measurements systems should be simple and robust, and their number be limited, considering the space occupied by the blankets. The diagnostics for the tokamak neutron source, including the machine protection and burn control are among the basic equipment. As the fusion and fission blankets can be integrated in a single subsystem their diagnostics must be conceived as an integrated package that includes the means for measuring isotope content, neutron multiplication and effective reactivity of the fission blanket, as well as tritium regeneration in the breeding blanket. The most recent technological developments the field of neutron spectroscopy for fusion and fission blankets are presented, including the diamond and self-powered neutron detectors technology.

Key words: fusion-fission reactors, diagnostics, blankets.

DOI: 10.21517/0202-3822-2021-44-2-78-85

ДИАГНОСТИКА И УПРАВЛЕНИЕ ГИБРИДНЫМИ РЕАКТОРАМИ СИНТЕЗА-ДЕЛЕНИЯ НА ОСНОВЕ ТОКАМАКА: ТЕХНОЛОГИЯ ИЗМЕРИТЕЛЬНЫХ СИСТЕМ

Ф.П. Орситто[1], М. Анджелоне[1], М. Тардокки[2]

[1]Национальное агентство по новым технологиям, энергии и устойчивому экономическому развитию (ENEA), Отделение термоядерной и ядерной безопасности, Фраскати, Италия
[2]Институт научных и технологических проблем плазмы, Милан, Италия

Гибридный реактор синтеза-деления (ГРСД) представляет собой сложную установку, которая включает в себя токамак, являющийся источником термоядерных нейтронов, и два бланкета: зоны воспроизводства трития и сжигания актинидов. Эти три системы нуждаются в собственной диагностике и своих системах управления. Проблемы, связанные с внедрением и интеграцией специализированных систем управления, требуют упрощённой технологии. В настоящей статье рассматриваются критерии, определяющие потребности в диагностике ГРСД, с учётом требования, чтобы измерительные системы были простыми и надёжными, а их количество было ограничено, учитывая пространство, занимаемое бланкетами. Диагностика источника нейтронов — токамака, включая защиту установки и управление термоядерной реакцией, входит в число основного оборудования. Поскольку бланкеты, в которых будут происходить реакции синтеза и деления, могут быть интегрированы в единую подсистему, их диагностика должна быть спроектирована как интегрированный пакет, включающий средства измерения содержания изотопов, размножения нейтронов и эффективной реактивности бланкета деления, а также воспроизводства трития. Представлены самые последние технологические разработки в области нейтронной спектроскопии для бланкетов, в которых будут осуществляться реакции синтеза и деления, включая технологию алмазных и автономно обеспечивающихся энергией детекторов нейтронов.

Ключевые слова: гибридные реакторы синтеза-деления, диагностика, бланкеты.

INTRODUCTION

The fusion-fission hybrid (FFH) reactor can be viewed as an attractive actinide burning or fusion-assisted transmutation system for the elimination of transuranic nuclear waste [1, 2]. The FFH has three subsystems: i) a breakeven ($Q \sim 1$—3) tokamak, as a source of 14 MeV neutrons, ii) a fission blanket acting as a transuranic burner, and iii) a tritium breeding fusion blanket. A hybrid load assembly used as a reference in this study, employs a $Q \approx 2$ spherical tokamak [2] as neutron source. FFH diagnostic equipment must complement tokamak measurement systems plus blanket diagnostics, including those used for tritium regeneration and fission characterization. Tokamak diagnostic equipment generally falls into the following subgroups: i) machine protection, ii) basic plasma control, iii) advanced control, iv) physics evaluation and advanced control [3]. Due to the space constraints associated with the fusion and fission blankets, the tokamak of a FFH must have simple equipment for basic plasma control, machine protection and fundamental plasma measurement. In the present study, systems related to the above diagnostics subgroups are discussed: some basic plasma measurements like electron

temperature are considered as well. The paper introduces the reference tokamak model and summarizes the FFH environmental constraints. It also provides the definitions of terms, such as neutron fluence and damage, and presents the criteria for determining the diagnostic needs of a hybrid reactor: DEMO-like diagnostics and controls (D&C) for the tokamak neutron source (machine protection and burn control), and the D&C for both fission and fusion blankets; introduces the diagnostic technology needed for a tokamak neutron source and presents measurements of 14 MeV neutrons, produced by the tokamak neutron source, as well as by single crystal diamond and/or SiC detectors. Furthermore it deals with the diagnostics for the FFH fusion and fission blankets; and presents the conclusions.

REFERENCE TOKAMAK MODEL AND ENVIRONMENTAL CONSTRAINTS

The diagnostics needs for a FFH can be more precisely determined using models as a reference for the evaluation of systems to be implemented. Table 1 shows the main parameters of FFH models compared with the ITER design.

T a b l e 1. **Parameters of tokamaks proposed as FFH neutron sources vs ITER parameters**

Parameter	FDS-I (China)	SABR (USA)	CFNS (USA)	FNS (RF)	ITER
Major radius, m	4	3.75	1.35	3.2	6.2
Aspect ratio, (R/a = major radius/minor radius)	4	3.4	1.8	3.2	3.1
Magnetic field, T	6.1	5.7	2.9	5	5.3
Q (P_{fus}/P_auxiliary heating)	3	3	2	2	10.0
P_{fus}, MW	150	180	100	60	400.0
Average neutron wall loading, MW/m^2	0.5	0.6	0.9	0.2	0.57
Plasma elongation	1.78	1.7	3	2	1.7
Triangularity	0.4			0.5	0.33
q, safety factor	3.5	3	2.5	4.4	3
Plasma current, MA	6.3	8.3	10	5	15

We can use the Kadomtsev similarity parameter, S_k [10—12] to define similar plasmas, i.e. plasmas with the same confinement properties (R is the tokamak major radius, B is the on-axis toroidal magnetic field, A is the aspect ratio R/a: $S_k = RB^{4,5}A^{-3/2}$. Fig. 1 shows S_k for the devices included in Table I.

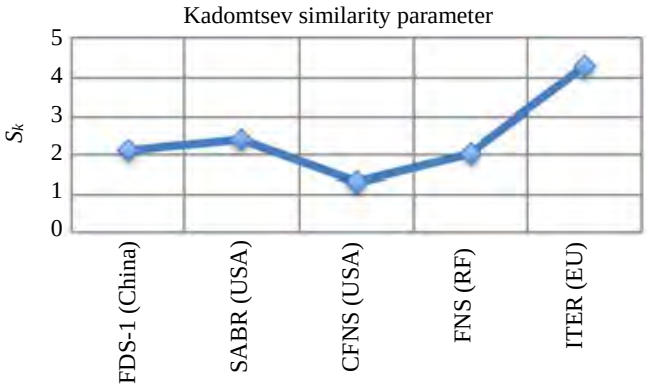

Fig. 1. Similarity parameters evaluated for FFH reactors models considered in Table 1

It is clear from Fig. 1 that FDS-I, SABR and FNS parameters are more or less similar. All have an either 2 or 3 fusion gain Q. The difference between the above FFH models and ITER lies in the level of their availability and the pulse length, which must be of the order of 75% and at least 3 hrs, respectively, for a tokamak neutron source useful for FFH. These characteristics are there in the DEMO tokamak reactor. In fact, some guidelines applied to DEMO diagnostics can be also useful for determining FFH diagnostic systems, if we regard a FFH tokamak neutron source as a low power/low gain DEMO-like reactor. The following criteria can be identified as a basis for determining the FFH diagnostic systems [4]:

— a plasma scenario is available (assessed): no specific measurements are made in respect to a physics scenario evaluation, the physics scenario model is assumed known;

— measurements are needed for: assessing the machine protection and safety, including the divertor and PWI (plasma wall interaction); controlling the plasma scenario (including DT-reactions/burn control and neutron production): controlling tritium production; controlling the fission blanket;

— in particular, since available space will be used primarily to maximize the fusion and fission blankets, diagnostics for machine protection and plasma scenario/burn control should be minimal.

Evaluating the magnitude of a FFH tokamak neutron fluence (neutrons/m^2 or MW·a/m^2) would be useful. To this end, the CFNS machine (internal surface, $S \approx 100$ m^2), producing 100 MW of DT (deuterium-tritium) fusion power with availability of 50% in one year will be used as a reference. Assuming that 100 W fusion cor-

responds to 80 MW of 14 MeV (14 MeV = $2.24 \cdot 10^{-12}$ J) neutron power, this gives a neutron flux, $\varphi = 80.0 \cdot 10^6/(100\ m^2 \cdot 2.24 \cdot 10^{-12}\ J) = 3 \cdot 10^{17}\ n/(s \cdot m^2)$. Integrating this flux over 120 days (i.e., one year = 240 days) of operation per year, we obtain a neutron fluence of $3 \cdot 10^{24}\ n/m^2$. The ITER neutron fluence (assuming that 400 MW fusion power corresponds to 320 MW of 14 MeV — neutron fusion power, the ITER availability is 7% a year and inner surface of the ITER vessel, S_ITER ≈ 200 m^2) is $1 \cdot 10^{24}\ n/m^2$ for 16.8 effective day reactor operation. The CNFS fluence is three times as large as that of ITER for one year of operation and is therefore well sustainable even with currently available FW materials.

Minimum machine protection diagnostic set. Table 2 shows a possible minimum diagnostic set for the tokamak machine protection (see [4] for additional details of the DEMO diagnostic systems and [5] and [6] for those of FFH).

T a b l e 2. **Minimum machine protection diagnostic set**

Magnetics	Sensors: hall probes
Runaway electrons and control by Cherenkov radiation detection	
IR cameras	W or Mo mirrors
Polarimetry (poloidal and toroidal)	W or Mo mirrors)
Plasma position reflectometry (waveguides to be tested)	
Fission chambers and diamond detectors	—
X-ray spectroscopy	—
VUV and V spectroscopy	—

In general, the machine protection diagnostics already studied for the ITER case can be used as a template for a FFH reactor: however, as suggested above, the neutron damage of the diagnostic system components, such as the Hall sensors, the waveguides or the first mirrors, can be higher for a FFH than for ITER. That is why for a FFH reactor, R and D of the neutron damage for the diagnostic system components should be set at the level of fluence evaluated above. A minimum machine protection diagnostic set should include the following:

— magnetics for equilibrium evaluation: the Hall probes measure the magnetic flux. They are very useful for measuring long pulses and are resistant to high neutron fluxes;

— combined polarimetry/interferometry tools to measure the DL line integrated density and determine, through Faraday rotation and Cotton-Mouton phase shift measurements, the equilibrium with internal (relative to the plasma) constraints. Polarimetry can also allow a rough evaluation of electron temperature T_e averaged over the line of sight for $T_e \approx 10$ keV;

— IR cameras for measuring the temperature of the wall and divertor tiles;

— fission chambers, diamond/SiC detectors and activation foils for the measuring tokamak neutron yield;

— spectroscopy measuring plasma impurities;

— Cherenkov probes and hard X-ray spectrometers for measuring the runaways.

Burn Control in a plasma scenario on a tokamak-based FFH reactor. Burn control in plasma scenarios implies the use of a complex matrix, shown in Table 3.

T a b l e 3. **Burn control matrix for a plasma scenario**

Actuator	Plasma parameter controlled	Availability	Actuator output controlled	Latency	Hardware response time
ECRH, NBI	Temperature and density profiles	All scenarios	Angle of ECRH launcher	<1s	<1s
ECRH, NBI, Central solenoid	Conductivity profiles	Current rise	Angle of ECRH launcher	<1s	<5s
Impurity seeding (Ar, N)	Radiation profile (divertor detachment	All scenarios	Impurity flux and density, Z_{eff} (dilution, fusion power)	<0.1s	<1s
Deuterium gas injection	Density	All scenarios	Isotopic mix (fusion power)	<0.1s	<1s
Tritium (NBI or pellet)	Central fuelling	All scenarios	Isotopic mix (fusion power)	<1s	<1s
ESRH System	Parallel current	Steady state scenario	Angle ECRH launcher	<1s	<1s
NBI	Plasma rotation	All scenarios mainly steady state	NBI power	<1s	<1s
PF System	Plasma boundary	All scenarios	Higher ordet moment of boundary shape or gas	<1s	<1s

The burn control matrix includes a column for actuator as well as columns for plasma parameter controlled (and diagnostic system used), the scenario and actuator output to be controlled, the latency (maximum time delay of the actuator response from the sensor input), and hardware response time.

For example, an actuator in the form of a neutral beam injector (NBI) is used to control plasma rotation, while the sensor (diagnostic) would be the spectroscopy (active or passive), this control is needed mainly in the

advanced tokamak scenario, the power of the NBI controls the plasma rotation, and both the latency and the hard ware response time must be less than 1s.

From Table 3 it can be seen that the main burn control quantities are: temperature and density profiles resolved in time, impurity content, rotation spatial profiles, and radiation profiles. The neutronics is central to fusion power monitoring. Listed in Table 4 are potential neutron measurement high tech sensors.

T a b l e 4. **Neutron diagnostics versus measurements**

Parameter	Neutron camera	Fission chamber	Activation foils	Spectrometer
Fission power	Possible to measure parameter	Primary method	Provide supplementary/relate information	
Fission power density	Primary method	Provide supplementary/relate information	Provide supplementary/relate information	
Total neutron flux	Possible to measure parameter	Primary method	Provide supplementary/relate information	
1st wall fluence	Provide supplementary/relate information	Provide supplementary/relate information	Primary method	
Fuel ratio	Possible to measure parameter			Primary method
Runaway	Provide supplementary/related information			
MHD instabilities	Possible to measure parameter			
Ion temp distribution	Possible to measure parameter			Provide supplementary/relate information

Table 4 is set out to show what diagnostic system is appropriate and useful (and to what extent) in controlling a given parameter. For example, the fusion power is measured mainly by fission chambers giving the neutron yield (in neutrons/s); where as the fusion power density is measured primarily by a neutron camera, which allows neutron fluxes to be measured along different lines of sights (usually the same lines of sights are shared with gamma ray sensors to detect gamma ray emitted by interactions between fusion alpha particles and impurities). Fusion power and neutron flux feedback control is needed to keep constant the hybrid reactor's global power. The k_{eff} (effective criticality coefficient of the fission blanket) decreases with the fuel fissioning up, in which case the fusion power (the number of neutrons) needs to be increased. The main plasma parameters to be controlled are plasma density and dilution and T_e, consequently the main actuators are the NBI power and the gas injection valves.

DIAGNOSTIC TECHNOLOGY NEEDED FOR A TOKAMAK NEUTRON SOURCE: MEASURING 14 MEV NEUTRONS PRODUCED BY A TOKAMAK NEUTRON SOURCE USING SINGLE CRYSTAL DIAMOND AND/OR SIC DETECTORS

This section addresses recently developed neutron measurement technologies represented by single crystal diamond detectors (SCDDs) for quantifying DD (2.5 MeV) and DT (14 MeV) neutrons. A SCDD [7, 8] is a compact device, suited to harsh environments and characterized by high-intensity neutron fluxes and high temperature. The device is insensitive to magnetic fields and little sensitivity to gamma radiation background. Furthermore, SCDDs have high energy resolution (<1%). Their neutron detection technology relies on the collection of electrons and holes that are generated by charged particles in nuclear reactions induced by neutrons on carbon nuclei: an energy of 13 eV is needed to produce an electron-hole pair. The following neutron-induced nuclear reactions on ^{12}C are used to detect neutrons:

i) the n—α-reaction: $n + {}^{12}\text{C} = {}^{9}\text{Be} + \alpha$ (Q = –5.7 MeV, threshold energy 6.17 MeV);

ii) elastic neutron scattering on ^{12}C nuclei: $n + {}^{12}\text{C} = n' + {}^{12}\text{C}$;

iii) n—3α-reaction: $n + {}^{12}\text{C} = n' + 3\alpha$ (Q = –7.23 MeV, threshold energy 7 MeV).

For the 2.5 MeV DD-neutrons, the only detection path available is via elastic scattering, while for the 14 MeV DT-neutrons, i) reactions, ii) and iii) are available as well.

Fig. 2 shows a remarkable measurement of 14 MeV neutron calibration using the Frascati Neutron Generator (FNG).

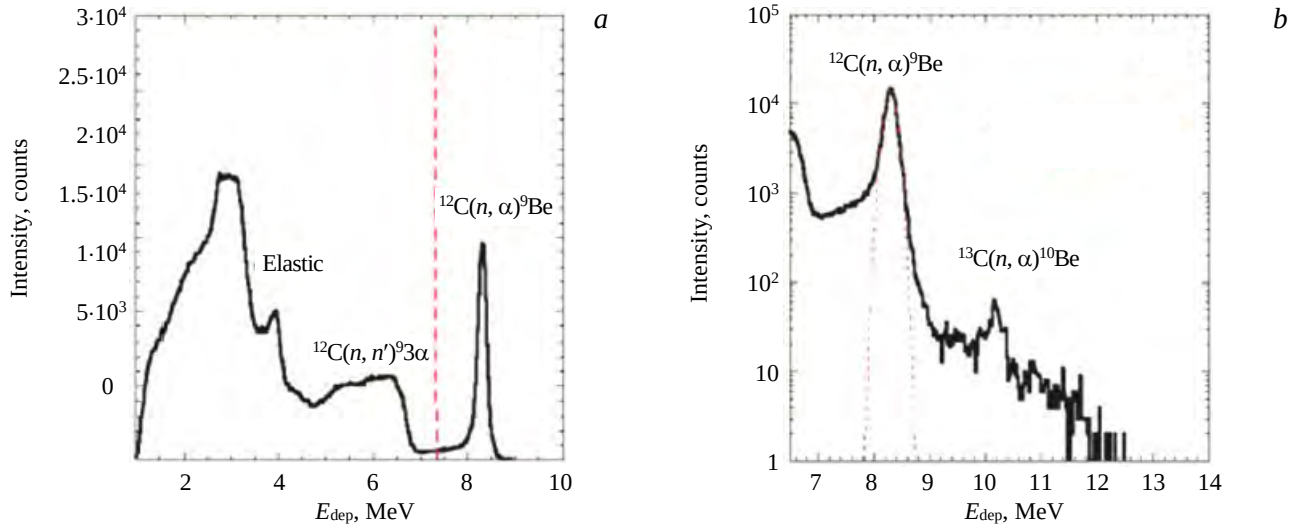

Fig. 2. Linear (*a*) and log-linear (*b*) signals measured with the single crystal diamond detector using the FNG 14 MeV neutron generator: —— — measurement, ····· — gauss fit

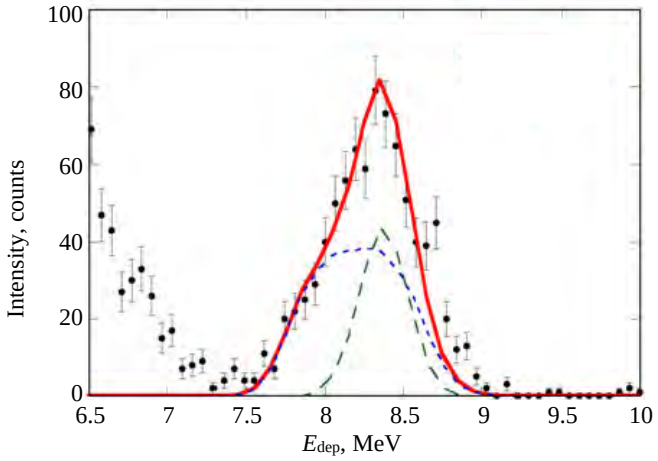

Fig. 3. 14 MeV neutron spectroscopy performed by SCDD; the components of neutrons produced in collisions of DT-reactions tritium beams with thermal ions and thermal deuterium and tritium nuclei: —— — fit, ----- — beam-th, – – – — th

Fig. 2 shows different SCDD signals indicative of the neutron-induced nuclear reactions; e.g., a good energy resolution (of the order of 1%) is found in the measurements, and the count rate capability is >1 MHz. Fig. 3 displays a very recent (October 2020) preliminary measurement produced in a DT calibration JET pulse: the plot shows a preliminary reconstruction of the various components of the neutron production.

The SiC detector has similar properties (one notable difference being a lower energy resolution), but is less susceptible to damage by neutrons that can distort detector response and worsen the energy resolution.

The technology for neutron measurements on a FFH prototype is similar to that developed for JET DT and that being designed for ITER. The role of neutron spectrometers is to monitor the real-time performance of fusion plasmas in selected robust plasma scenarios ($Q_{therm}/Q_{non\text{-}therm}$). A neutron monitor can be used to measure the overall neutron yield (including the multiplication factor due to the fission part). The ITER experience suggests that the diagnostics integration is a very challenging endeavour. Solutions studied for ITER, could be beneficial for FFH, although need to be FFH-specific.

FUSION-FISSION HYBRID'S FUSION AND FISSION BLANKET DIAGNOSTICS

The FFH reactor system consists of three subsystems: a tokamak neutron source, a tritium producing blanket, and a fission blanket. Measurements are therefore needed to monitor:

— the fission rate of main transuranic (TRU) elements;

— the secondary (relative to fission) neutron production;

— tritium production and the tritium breeding ratio.

Sensors can be inserted in the blankets to determine the status of tritium production and the fission of TRU elements.

Fusion blanket diagnostics. A first list includes both passive and active detectors: active detectors:

— (micro) fission chambers (FCs);

— self-powered neutron detectors (SPNDs) for total neutron/gamma flux measurements;

— diamond/SiC sensors (coated with ^{6}LiF films for tritium measurement) and SPNDs with $^{Nat.}$LiF coatings, used as emitters or lithium-based detectors (time dependent tritium production): (micro) ionization chambers (ICs) for gamma dose-rate measurements.

Passive detectors: nuclear activation system.

The SPNDs [9] are rugged miniature devices (Fig. 4) that have long been used for in-core fission reactor monitoring (for safety and neutron/gamma flux mapping purposes). SPNDs operate without any applied voltage, which enhances their reliability and resistance to radiation from the reactor core. The detectors are usually constructed in a *coaxial configuration,* in which the *central conductor* (called the emitter) material usually determines the device characteristics. The other electrode or metallic sheath is called the collector, and the two are separated by a (coaxial) mineral insulator.

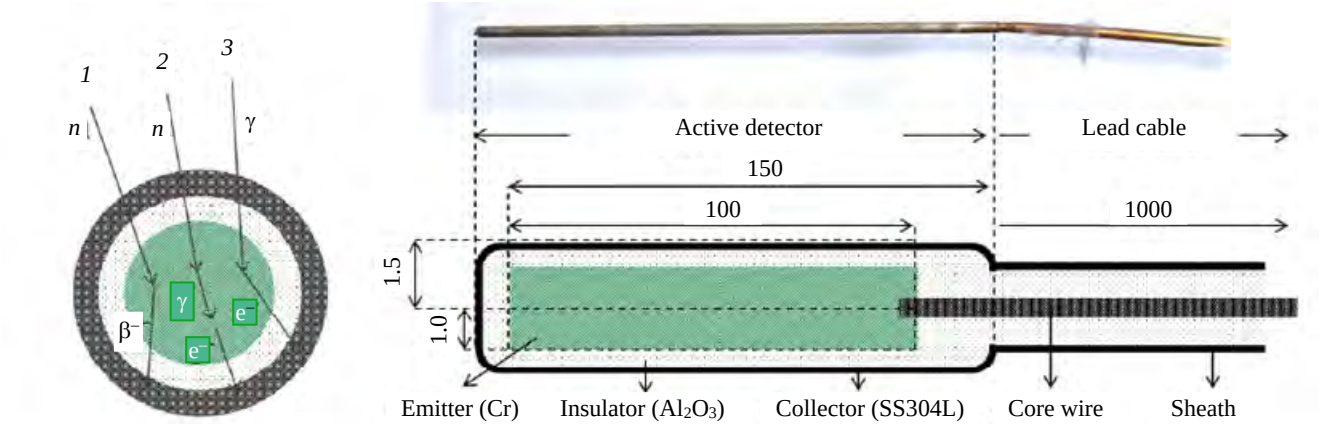

Fig. 4. Scheme of a SPND detector

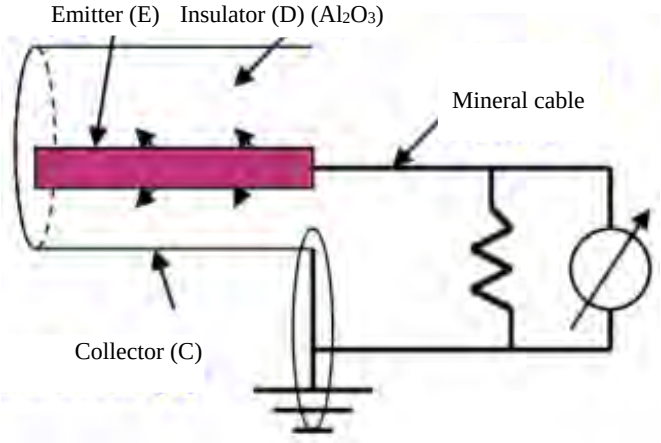

Fig. 5. SPND electrical circuit

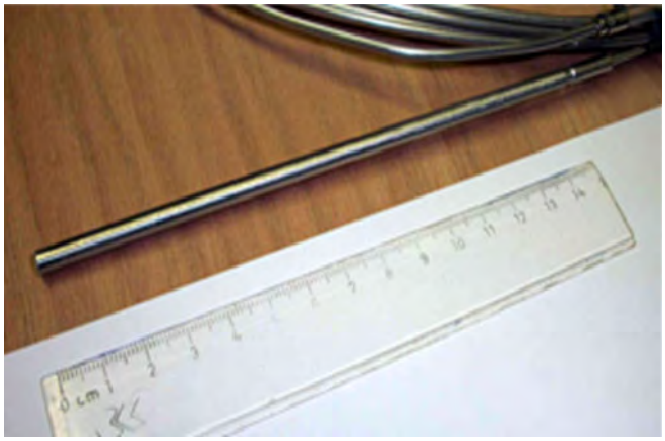

Fig. 6. ENEA CNPD prototype detector based on a Cr emitter

The SPND operates on the basis of measuring a beta decay (decay in electrons) related to a metastable state created by the interaction of the neutron with the emitter (in green in Fig. 4) which can essentially be either of the following materials: chromium, cobalt, vanadium or rhodium. Generated electric signal is compared to the collection on the 'collector' (in Fig. 4, one can see that the collector is made of stainless steel) of the electrons generated through the beta decay. The SPND electrical circuit is shown in Fig. 5.

In commercial SPNDs (used in fission reactors), the *emitter* (*metal*) material has at least a moderate neutron capture cross-section at *thermal neutron energy* allowing activation products to decay through *beta_emission.* Because the neutron spectrum generated by a fusion FFH neutron generator has higher energy, *commercial emitters are not suitable.* Consequently, *prototype SPNDs* whose *emitters are* suitable for fast neutron spectrum (enough beta activation) are presently developed at ENEA and KIT. Two prototypes detectors fabricated (Cr and Be emitter) *ENEA developed the SPND_Cr, KIT the SPND_Be.* Fig. 6 shows a Cr-based prototype SPND implemented at ENEA: it is 10 cm long and has a 2 mm across Cr emitter (5.5 gr), and a 10 m-long mineral cable (SS-304 sheath and Al_2O_3 insulator).

Tests were performed on the SPND_Cr prototype using the FNG (frascati neutron generator, REF) 14 MeV neutron source and a strong ^{60}Co gamma-ray

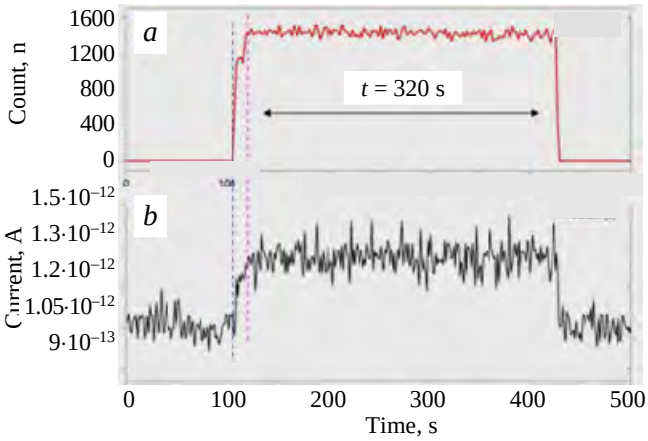

Fig. 7. 14 MeV neutron monitor (*a*); current signal generated by the SPND_Cr (*b*)

source. The signal detected by the SPND_Cr, when 14 MeV neutrons are injected, is shown in Fig. 7; Fig. 7, *a* presents the neutron monitor, while Fig. 7, *b* shows a measured current signal.

Fig. 8 shows the SPND_Cr detector calibration: the linearity of the signal generated by the SPND_Cr while changing the neutron dose rate is displayed.

The SPBD_Cr can also detect gamma rays: Fig. 9 shows a comparison between current signals generated by the SPND_Cr detecting neutrons and gamma rays. Note the opposite polarities of the current produced by 14 MeV neutrons and gammas. This could be predicted by a Monte-Carlo simulation.

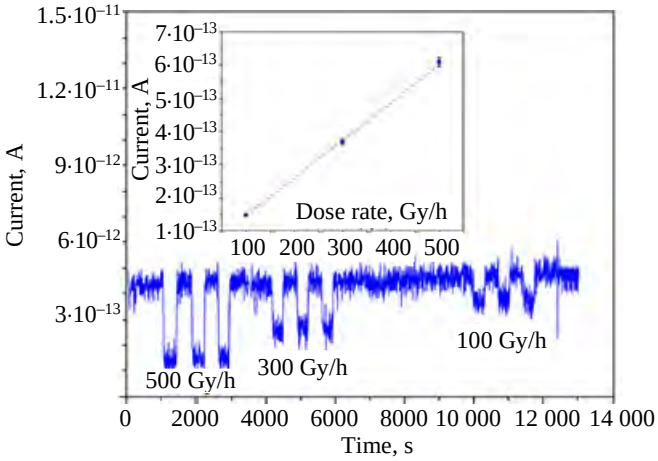

Fig. 8. Calibration of the SPND_Cr: linearity between the current signal and the neutron dose

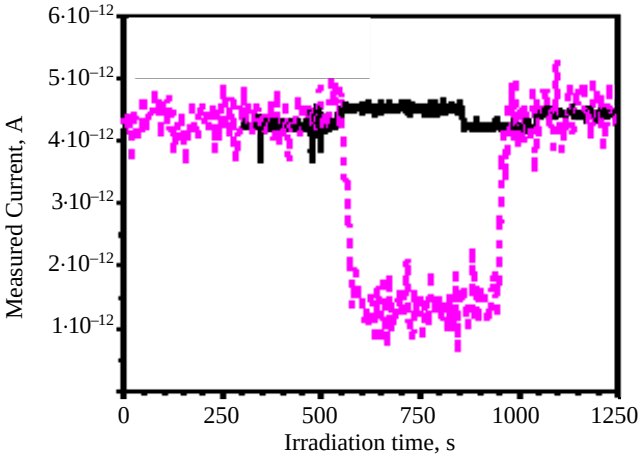

Fig. 9. SPND_Cr current signals generated with FNG 14 MeV neutrons and the CALLIOPE ENEA ^{60}Co gamma ray source (note the opposite polarity of the signals): —— — 14 MeV neutrons, - - - — gamma-rays

CONCLUSIONS

A tokamak-based FFH reactor is a complex system, which includes three subsystems: i) a tokamak neutron source, ii) a fusion blanket, iii) a fission blanket. These subsystems need their diagnostics and controls. The FFH reactor is a tokamak with low fusion gain, but working with very long pulses (at least 3 hrs) and high availability (75%); it is a low power DEMO-like device: the integrated in time neutron fluence ($3\cdot10^{24}$ n/m^2) is three times that of ITER, in one year. The evaluated neutron fluence means that from the point of view of diagnostic technology, the ITER system design can be used as a template, but some additional R&D on the damage of the main components like the mirrors and waveguides exposed to plasma are required. Tokamak plasma control includes the machine protection and plasma burn monitoring, which can be done using a minimum DEMO-like [6] set of diagnostics and actuators including plasma density and temperature diagnostics, as well as spectroscopy for plasma impurity detection. In this paper, the fusion and fission blanket diagnostic technology solutions are discussed and characterization measurements of 14 MeV neutron diamond detectors for fusion blanket and the SPND are given in detail. The diamond detectors are very promising as neutron sensors for DEMO-like devices i.e., high neutron flux environment. The SPND can be used or the neutron measurements on the fission blanket being very robust and compact: Chromuim-based SPND are currently studied and considered to be suited for the detection of high energy 14 MeV neutrons.

REFERENCES

1. **Stacey W.M.** — J. Fus. Eng., 2009, vol. 28, p. 328—333.
2. **Kotschenreuther M.K. et al.** — Fus. Eng. Des., 2009, vol. 84, p. 83—88.
3. **ITER** Physics Basis. — Nucl. Fusion, 1999, vol. 39, p. 2541, and ibid., 2007, vol. 47, p. 5337.
4. **Orsitto F.P. et al.** — Nucl. Fusion, 2016, vol. 56, p. 026009.
5. **Orsitto F.P.** Fusion for neutrons and subcritical nuclear fission. — AIP Conf. Proc. 2012, vol. 1442, p. 289.
6. **Orsitto F.P.** — In: FUNFI2 Proc. 2017 ENEA ISBN 978-88-8286-357-9, ed. A. Pizzuto and F.P. Orsitto; https://www.enea.it/it/seguici/pubblicazioni/edizioni-enea/2017/FUNFI2-2nd-International-Conference-on-Fusion-Fission, p. 131.
7. **Cazzaniga C. et al.** — Rev. Sci. Instr., 2014, vol. 85, p. 11E101.
8. **Giacomelli L. et al.** — Rev. Sci. Instr., 2016, vol. 87, p. 11D822.
9. **Goldstein N.P., Todt W.H.** — IEEE Trans Nuclear Science, 1979, vol. NS-26, p. 916.
10. **Kadomtsev B.B.** — Fiz. Plazmy, 1975, vol. 1, p. 531 [Sov. J. Plasma Phys., 1975, vol. 1, p. 295].
11. **Orsitto F.P. et al.** — In: 39th EPS/ICPP, 2012. Stockholm, paper 2.154 — Physics driven scaling laws for similarity experiments.
12. **Romanelli M., Romanelli F., Zonca F.** On the optimal choice of the dimensionless parameters of burning plasma physics experiments. — In: 28th EPS Conference on Contr. Fusion and Plasma Phys. Funchal, 18—22 June 2001, ECA 2001, vol. 25A, p. 697—700.

AUHTORS

Francesco Paolo Orsitto, ENEA Department for Fusion and Nuclear Safety, C.R. Frascati, v E. Fermi 45, 00044 Frascati, Italy, francesco.orsitto@enea.it

Maurizio Angelone, ENEA Department for Fusion and Nuclear Safety, C.R. Frascati, v E. Fermi 45, 00044 Frascati, Italy

Marco Tardocchi; Istituto per la Scienza e Tecnologia dei Plasmi CNR, Milano, Italy

Статья поступила в редакцию 15 января 2021 г.
После доработки 16 марта 2021 г.
Принята к публикации 25 марта 2021 г.
Вопросы атомной науки и техники.
Сер. Термоядерный синтез, 2021, т. 44, вып. 2, с. 78—85.

UDC 621.039

ANALYSIS OF THE SETUP AND PARAMETERS OF THE FNS-ST TOKAMAK FAST ATOM INJECTOR

A.A. Panasenkov, S.S. Ananyev, E.D. Dlougach, B.V. Kuteev

NRC «Kurchatov Institute», Moscow, Russia

A Fusion Neutron Source (FNS) based on Spherical Tokamak (ST), now being developed, is expected to produce a high-yield (up to 10^{18} s^{-1}) neutron flux via in-plasma stationary current generation with a beam of fast atoms [1—3]. This study is concerned with the selection of the setup and parameters of a fast deuterium atom injector for the FNS-ST neutral injection system. Fast atom energy is important for determining the efficiency of current generation in tokamak plasma and estimating the neutron yield. Different injector setup versions based on positive- and negative-ion sources were tested, and the one selected based on sources of positive deuterium ions with energies ≤140 keV. An injection module allowing the delivery of 3.5 MW deuterium neutral beam power to plasma is considered.

Key words: fusion neutron source, tokamak, injector, ion source, neutral beam.

DOI: 10.21517/0202-3822-2021-44-2-86-99

АНАЛИЗ СХЕМЫ И ПАРАМЕТРЫ ИНЖЕКТОРА БЫСТРЫХ АТОМОВ ДЛЯ ТОКАМАКА ТИН-СТ

А.А. Панасенков, С.С. Ананьев, Е.Д. Длугач, Б.В. Кутеев

НИЦ «Курчатовский институт», Москва, Россия

В разрабатываемом проекте термоядерного источника нейтронов на основе сферического токамака ТИН-СТ предполагается возможность стационарной генерации тока в плазме с помощью пучка быстрых атомов, что обеспечивает высокий уровень (до 10^{18} $с^{-1}$) потока нейтронов [1—3]. Данная работа посвящена выбору схемы и параметрам инжектора быстрых атомов дейтерия для системы нейтральной инжекции токамака ТИН-СТ. Энергия быстрых атомов является важным параметром, определяющим эффективность генерации тока в плазме токамака и нейтронный выход. Рассмотрены схемы инжекторов на основе источников пучков положительных и отрицательных ионов и выбран вариант с использованием источников положительных ионов дейтерия с энергиями до ≤140 кэВ. Рассмотрен вариант инжекторного модуля с мощностью вводимого в плазму пучка атомов дейтерия на уровне 3.5 МВт.

Ключевые слова: термоядерный источник нейтронов, токамак, инжектор, источник ионов, пучок быстрых атомов.

INTRODUCTION

Fusion neutron sources (FNS) are considered promising for applications, such as testing of struc-tural materials for future nuclear and thermonuclear reactors, nuclear waste disposal research, fuel production and testing of hybrid reactor technologies. Spherical tokamaks have better plasma stability and confinement characteristics than their classical counterparts. They can be used as a template for smaller neutron sources capable of providing a high stationary neutron flux at a lower cost [1—3].

A FNS-ST (Spherical Tokamak)-based thermonuclear neutron source project, now being designed, is anticipated to produce a high-yield (up to 10^{18} s^{-1}) neutron flux via in-plasma stationary current generation with a beam of fast atoms [1—3]. This study is concerned with the selection of the setup and parameters of a fast deuterium atom injector for the FNS-ST neutral injection system. Fast atom energy is important for determining the efficiency of current generation in tokamak plasma and estimating the neutron yield. It has been shown in [2] that in the 100—200 keV range, the fraction of neutrons generated via D—T reactions in the thermal component of the plasma decreases with increasing beam energy, while the total neutron yield grows due to rising intensity of D—T reactions associated with the beam-plasma interaction. Another effect of beam energy increase is a noticeable enhancement of plasma current generation efficiency. How-ever, beam energy increase is capped by the relatively small plasma size. In fact, a neutral beam (NB) fraction passing through the plasma without being captured also grows with increasing energy, im-parting a significant power load onto the tokamak first wall.

FNS-ST's key characteristics are as follows:

Large radius R, m . . .	0.5
Small radius a, m . . .	0.3
Elongation k . . .	2.75
Toroidal magnetic field B_T, T . . .	1.5

Plasma current I_P, MA . . . 1.5 MA

Average plasma density, m^{-3} . . . $(0.5—1)10^{20}$

The NB power, P_{inj} = 6—10 MW, is delivered to the plasma by three operating injectors. The NB enters the tokamak chamber through a 0.3×0.6 m entrance window.

Selection of the ion types and energy. From the viewpoint of the NB injection efficiency, the 100—200 keV beam energy range, proposed for FNS-ST, is an intermediate case, where both positive and negative ion technology (PI and NI, respectively) may be used. This is due to the neutralization efficiency of deuterium ions in the gas target with energy increasing, which remains at a level of about 60% for NI and rapidly decreases for PI. Fig. 1 demonstrates the equilibrium yield (Φ_0) of D^0 atoms as a function of energy released in the D^+ neutralization of in a «thick» deuterium target [4] (target thickness: $\tau = \int n_o(x)dx$). In fact, this dependence reflects the efficiency of PI neutralization in the beam current ($\Phi_I = \Phi_0$). By multiplying Φ_0 by corresponding ion energy value we obtain a curve representing neutralization efficiency in terms of power (Φ_P), where power is expressed in terms of atoms obtained per ampere of source ion current at different energies. For deuterium PI case, this dependence has a maximum of about 52 kW/A at an energy of around 100 keV (Fig. 2). In the NI case, the Φ_P value grows almost linearly by a factor of around 0.6 with increasing ion energy. Consequently, with the rise of the ion energy, to obtain a neutral beam of a given power with the PI technology a significant increase in the current and power of the beam from the source is required, while in the NI case the required ion current decreases noticeably at an almost constant beam power (Fig. 3).

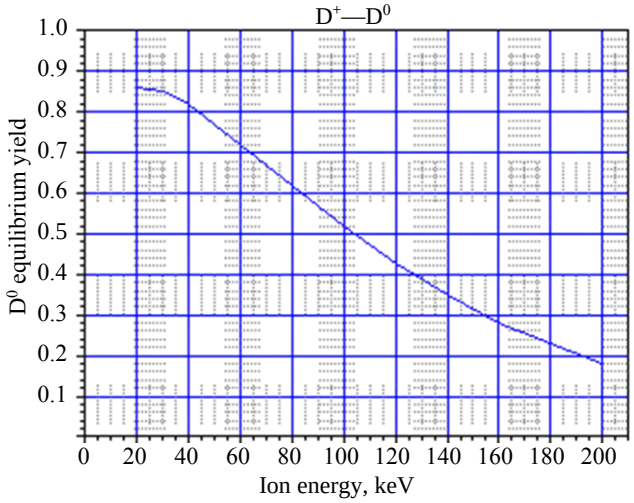

Fig. 1. Equilibrium yield of D^0 atoms upon neutralization of D^+ ions in a «thick» gas target

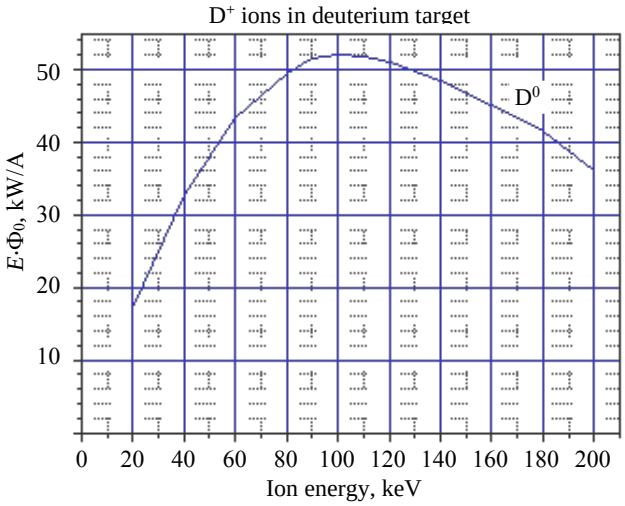

Fig. 2. Efficiency of neutralization by power (Φ_P) of D^+ ions in a «thick» gas target

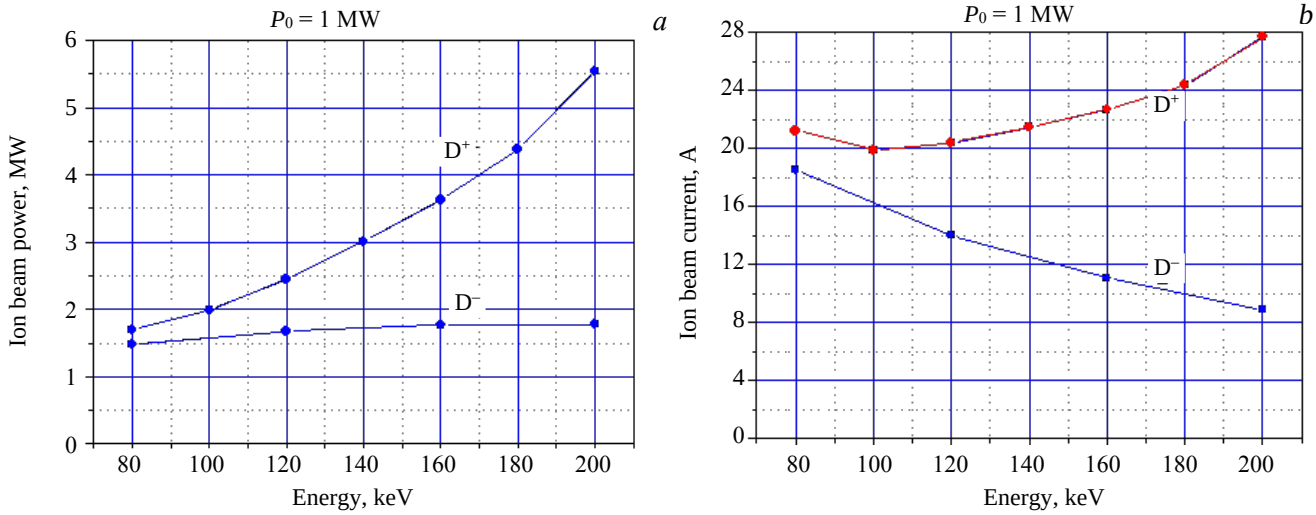

Fig. 3. Energy dependence of the power (*a*) and current (*b*) of source ion beams D^+ or D^- required to obtain a 1 MW neutral beam

An example of the beam composition changes in 120 keV PI and NI beams undergoing neutralization in a deuterium target is shown in Fig. 4. One can see that with positive ions being neutralized, the equilibrium yield of fast atoms is achieved in an «infinitely thick» target, while for negative ions there is a thickness optimum (τ_{opt}) associated with a maximum atomic yield, and a further τ increase leads to the same yield as in the PI case. Accordingly, in the NI case, τ_{opt} is always taken, and for PI, in order not to let too much gas flow into the neutralizer, τ is usually chosen to ensure an atomic yield of 95% of the equilibrium value ($\tau_{0.95}$, $\Phi_{0.95}$). In the 100—200 keV energy range, the τ_{opt} value is practically independent on ion energy when using the NI technology, while in the case of PI, the $\tau_{0.95}$ dependence is quite strong (Fig. 5) and exceeds the optimal value for the NI technology 2—5 times (100 to 200 keV, respectively).

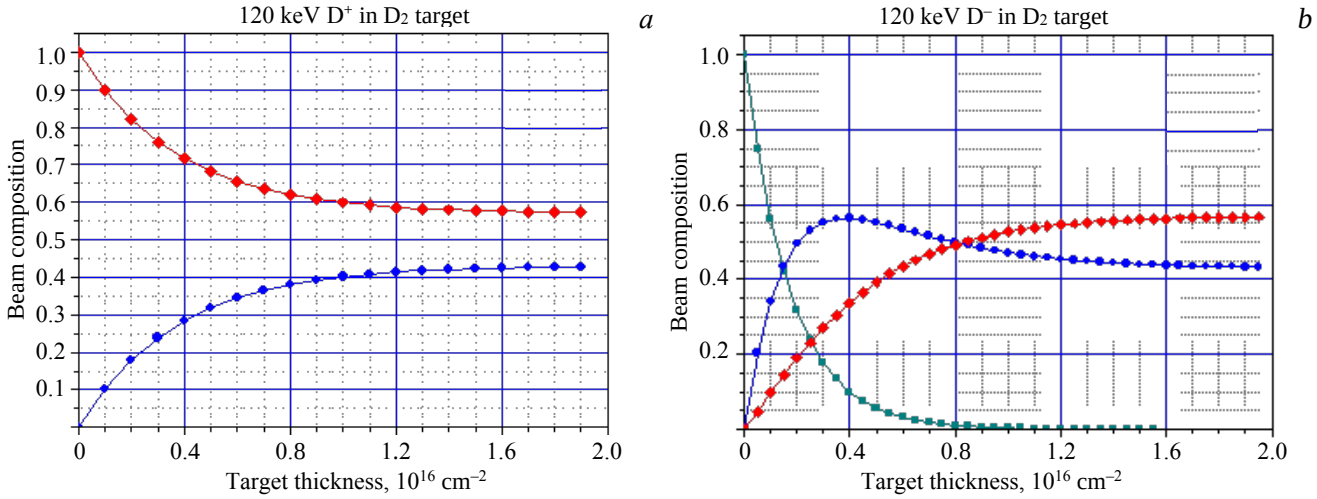

Fig. 4. Evolution of beam composition upon the passage of D^+ (◆) (*a*) and D^- (■) (*b*) ions of a 120 keV energy through the D_2 gas target, ● — D^0

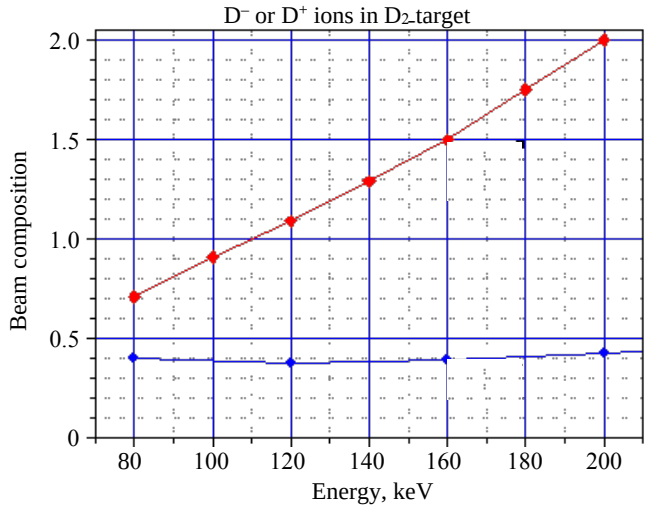

Fig. 5. Energy dependence of the required deuterium target thickness: optimal for the initial ion beam D^- and $\tau_{0.95}$ for the D^+ beam: ◆ — $D^+ \rightarrow D^0$, ◆ — $D^- \rightarrow D^0$

Thus, the above data point to the advantages of the NI technology, which become decisive at energies above ~150 keV. The NI beam's small average divergence angle is an additional case in favor of the NI. For example, in ITER's NBI system, based on negative ion neutralizers, the beam divergence operating angle of 7 mrad determines the high efficiency of beam transportation to plasma [5].

That said, the following NI weaknesses should be noted:

— about 15% of the NI current is contained in a «halo» with a divergence angle of up to 30 mrad, and more than a half of this current may be lost on the injector components, which increases power deposition along them and reduces the injector's power efficiency;

— D^- ion current density is low (20 mA/cm^2 at the ion source exit); as a result, a current of several tens of amperes can only be obtained, if the plasma emission surface is uniform and measures more than 0.5 m^2 in the gas-discharge chamber of the ion source;

— to date, for the nominal current density, a high degree of uniformity of the plasma emitter of an NI source with a large emission surface, which is necessary for the formation of a beam with a low angular divergence, has yet to be demonstrated;

— to reduce the losses of NI inside the ion-optical system (IOS) of the ion source (IS) owing to their stripping on the background gas, a vacuum gap is provided between the IS and the neutralizer to evacuate the gas; as a result, gas feeding into the neutralizer increases several times due to its outflow in both directions.

The PI technology (for ion energies less than 150 keV) has the following strengths:

— an order of magnitude higher D^+ current density is achieved at the PI source exit, allowing the area of the uniform plasma emitter and electrodes of the IS IOS to be reduced approximately 3—4 times even if the PI current is twice as large as that required. At the same time, the neutralizer dimensions are decreased, and the flow of gas fed to the neutralizer and needed to achieve required target thickness is reduced;

— in addition, in the PI scheme, the neutralizer is attached to the ion source and gas exiting the source participates in the creation of the target, making the gas load on the injector's cryogenic pumping system appreciably less than with the NI technology;

— PI-based beam injectors are compact and extensively tested in different fusion machines.

The PI technology disadvantages include:

— an approximately twice as wide divergence angle compared with the NI technology, the result being a weaker beam transmission efficiency;

— presence of D_2^+ and D_3^+ molecular ions (15—20% and 7—10%, respectively) in the IS beam, from which atoms with energies $E/2$ and $E/3$ originate in the neutralizer as a result of dissociation and neutralization. Ionized and captured at the tokamak plasma periphery, these atoms contribute little to the in-plasma current generation;

— the system of magnetic deflection of residual ions exiting the neutralizer must have a large size beam receiver to ensure the interception of ions with three energy fractions;

— because the residual ion beam power can be ~1.5 times greater than the NB power (see Fig. 3, *a*), this receiver appears to be the most energy-stressed component of the injector.

The analysis of an injected NB ionization in the FNS-ST plasma and in-plasma current generation is discussed in [6]. It is shown that in a small-sized FNS-ST with a plasma concentration of $\sim 1 \cdot 10^{20}$ m^{-3}, up to 5% of delivered NB power passes through the plasma if particle energy is higher than ~150 keV. Such a load on the FNS-ST chamber wall is regarded as critical, and the upper acceptable NB energy level is estimated at 140 keV.

Setup and parameters of the D^+ ion-based FNS-ST injector. A FNS-ST injection module configuration allowing the delivery of a 3.5 MW deuterium atomic beam power is considered with a view of using a PI source with a deuterium ion energy in the range of 100—140 keV. A 3.5 MW power should ensure the tokamak operation during the injection of a 10 MW NB using four alternately enabled injectors, of which three are in operation, and one is in the cryopump regeneration mode (or setting, preparation, etc.). The IS geometry and parameters, as well as the components of the beam path from the IS output electrode to the tokamak chamber entrance window are specified. The injector schematic is shown in Fig. 6.

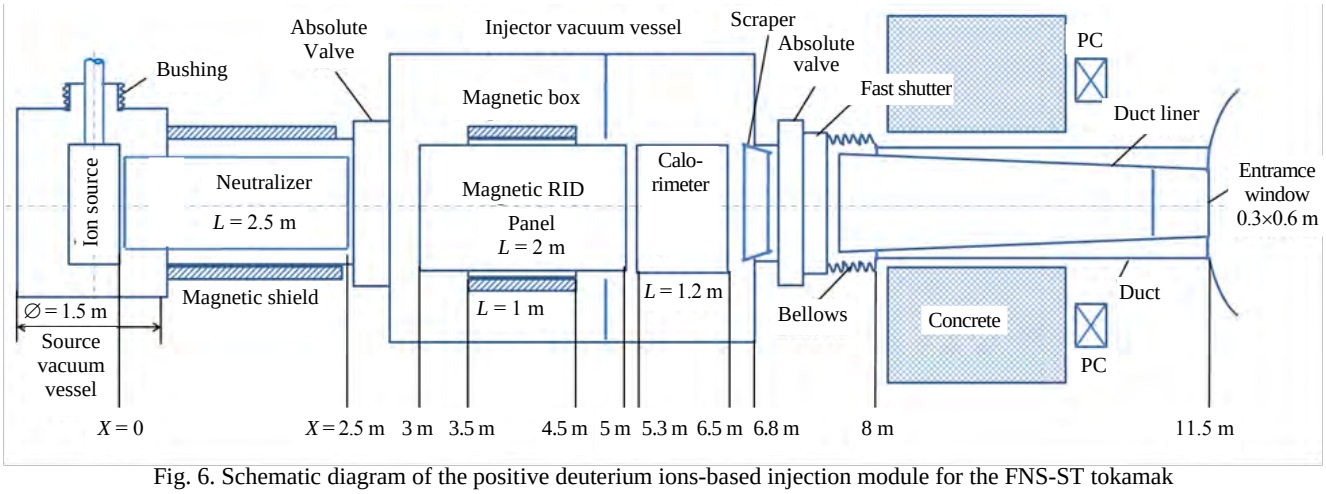

Fig. 6. Schematic diagram of the positive deuterium ions-based injection module for the FNS-ST tokamak

Injector main components. An ion source producing a positive deuterium ion beam with a 80 A current. A vertically elongated uniform plasma emitter of ions with emission current density = 0.2 A/cm^2 on an area of 18×115 cm is formed in the gas-discharge chamber (GDC). An ion beam with a divergence angle of ±15 mrad is extracted from the plasma and shaped using a four-electrode multi-aperture IOS. Each electrode has five sections, each containing 8×10 profiled apertures, so that each section produces 80 elementary beams («beamlets»), whose axes are focused horizontally on the center of the tokamak entrance window. With their axes separated

by 220 mm, these sections are inclined vertically, so that their center lines are also directed at the center of the entrance window. To ensure a stationary operation, the electrodes have channels in their bodies, intended for forced water cooling. The IS is placed inside a source vacuum vessel (SVV) 1.5 m in diameter and 2.2 m high. All IS communications kept at high potential (e.g., the GDC, emission and extracting electrodes) are admitted into the SVV through a ceramic bushing 0.5 m in diameter and 0.4 m high.

The neutralizer is a 2.5 m long water-cooled copper liner with a 18×120 cm passage window, installed inside the tube connecting the SVV with the injector's vacuum vessel (VV). The gas target is formed by a deuterium flow injected into the liner near the IS, whose flow rate is adjusted with regard to the gas flow from the source GDC. A magnetic shield, fixed on the connecting tube, is designed to reduce the tokamak's scattered magnetic field inside the neutralizer to within 1 G. The front end of the liner is inserted into the SVV close to the IOS output (grounded) electrode (the «adjusted» neutralizer).

An absolute vacuum valve is at the entrance of the injector VV, it separates the SVV and the rest of the beam path by vacuum when the SVV needs to be opened for repair or IS replacement.

The injector VV contains: a magnet to deflect residual positive ions leaving the neutralizer onto a residual ion dump, a movable diagnostic NB calorimeter, and cryosorption pumps with a $1 \cdot 10^6$ l/s pumping speed. The VV is 2×2.5×4 m (W×H×L), with panels of cryopumps fixed on its side walls.

Magnetic system for residual ion deflecting and dumping (MRID). A post neutralizer beam consists of NB and residual ions, whose power significantly exceeds the NB power, and on-axis power density (PD) reaches 70—80 MW/m^2. To ensure a stationary reception of such a PD, the residual ion beam must strike the dump surface at a less than 10º angle, meaning that a large space within the injector VV should be provided for dumping the residual ions — especially with account of components with energies E/2 and E/3. Therefore, here we consider a small-sized version, in which ions are horizontally deflected by a vertical magnetic field (MF) onto a dump panel built into the magnetic deflection system. A schematic view of the magnetic system, in which the MF horizontal profile is uniform inside the deflecting volume, is shown in Fig. 7, *a*, and a photo of the experimental device is given in Fig. 7, *b*.

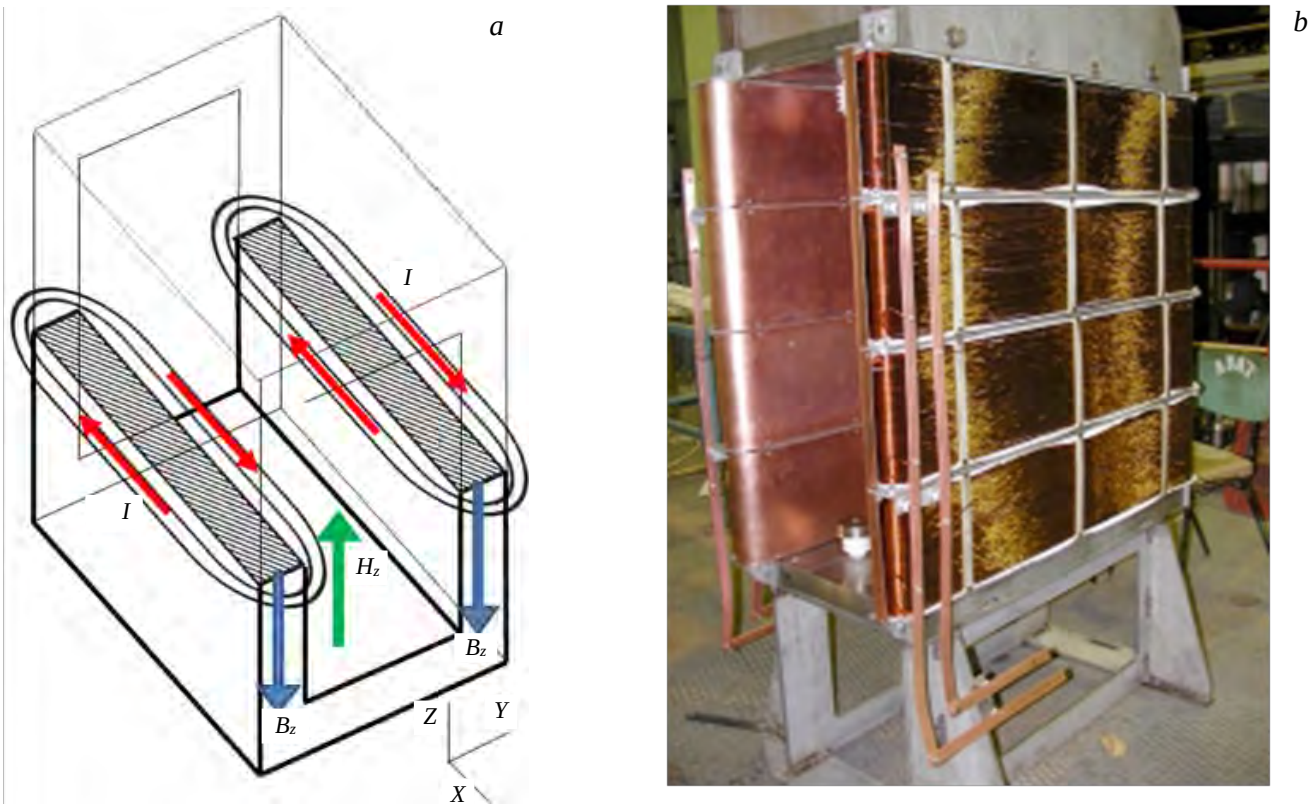

Fig. 7. Schematic view of the magnetic system (I — magnetic coil current) (*a*) and a photo of the experimental device (*b*), whose «magnetic steel box» has a length of 1 m, an opening of 0.4×1 m and a magnetic steel thickness of 6 mm

The magnet system is a «magnetic steel box» whose side walls (cores) carry coils, which allow identically directed current to be distributed over a height of 1 m. A MF created inside the box is in opposition to induction B_z of the steel cores. Fig. 8 shows the measured profiles of the vertical MF inside and outside the experimental

device (in the local coordinate system) at currents of 115 A in each coil. Inside the «box», the field horizontal uniformity is acceptable, but along the MF system axis it falls more than 10 times at a distance of about 1 m from the «box» edge.

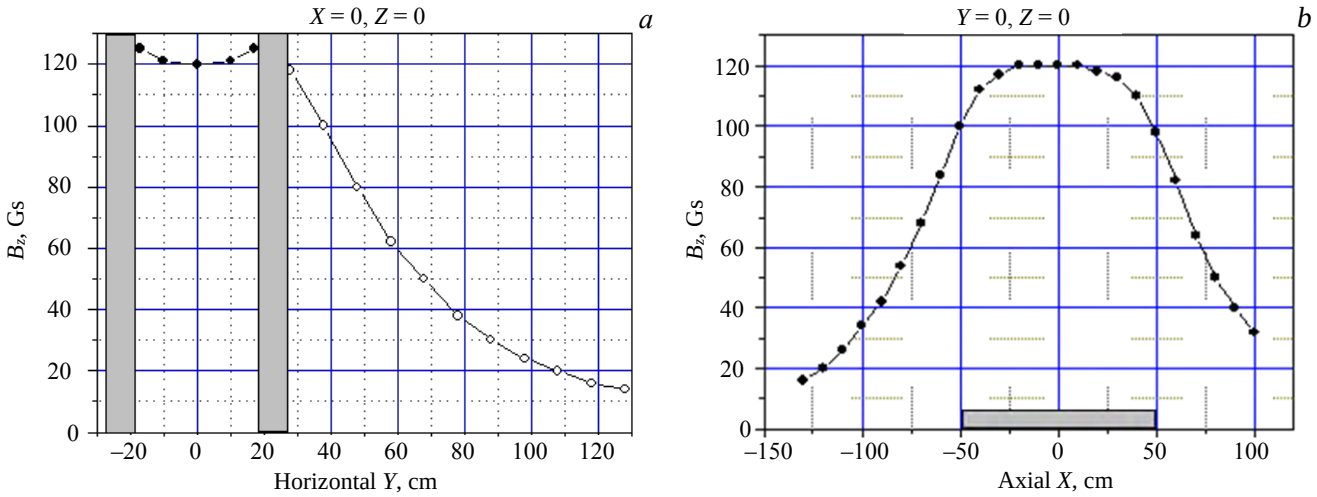

Fig. 8. Experimental profiles of the vertical magnetic field along the horizontal (*a*) and axial (*b*) coordinates of the MRID (in the local coordinate system) at current of 115 A in each of the coils

The vertical panel collecting the residual ions is placed inside the deflection system (Fig. 9). It consists of two layers of horizontal tubes made of hardened chromium-zirconium bronze with swirl heat removal intensifiers (swirl tube elements STEs, similar to the dumps of the ITER injectors) [5]. The STEs are of 20 mm in outer diameter and have 2 mm-thick walls. They remove heat loads with heat flux densities up to ~10 MW/m^2 when a water velocity in one STE is 2 m/s and up to 15 MW/m^2 with the velocity of 3.5 m/s is provided [7]. In each layer, the pitch between the tube axes is 34 mm, the tubes of the back layer are shifted relative to the front layer by half pitch, providing full interception of the beam even in a case of mutual vertical displacement of the tubes by ~2 mm. There are altogether 65 tubes, each with a working length of 2 m.

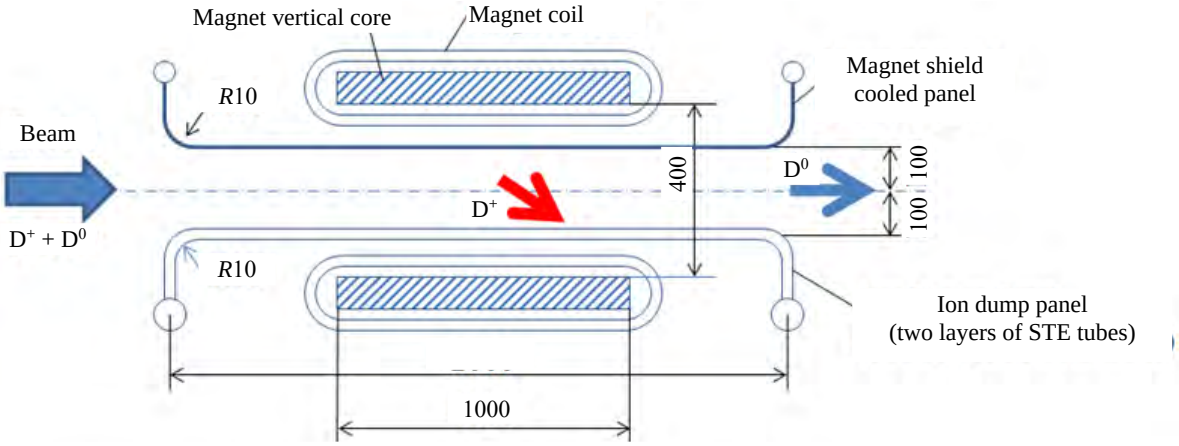

Fig. 9. Plan view of the MRID magnetic system and the ion dump panel position

The calorimeter is a device unit for receiving NB during training of an ion source and bringing its parameters to the operating mode during the period when this injector does not inject NB into the tokamak. It is equipped with diagnostic devices for measuring the NB power and the beam profile over its cross section to determine its divergence and sight accuracy. The calorimeter consists of two movable panels, which for this period move, forming a V-shaped configuration with an opening angle of 20°, which provides a decrease in the peak PD on the panels by about 5 times. Each panel, similarly to the MRID, consists of two layers of chrome-zirconium bronze tubes, the only difference is in the working length of the tubes — in the calorimeter it is 1.2 m, the number of tubes in each panel is 65. The panels open when the injector operates on the tokamak, the width of the corridor between the panels is 0.4 m.

Other units along the injection path are:

— scraper in the form of a truncated pyramid ($6.7 < X < 7.1$ m), designed to cut off the beam «wings» to reduce the load on the elements of the connecting duct line;

— absolute vacuum valve that cuts off the injector from the tokamak during work with opening the volumes of either the injector or the tokamak;

— fast shutter that only opens up when the NB is injected into the plasma. In the closed state, it has insignificant gas conductivity both from the injector to the tokamak and vice versa, and provides a small leakage of gas into the tokamak chamber while the cryopanels are being regenerated in the injector VV;

— bellows connecting unit, designed to compensate the injector and the tokamak's thermo-mechanical displacements relative to one another, when the system is in operation;

— NB duct with a water-cooled liner inside that takes on the neutrals not passing into the tokamak entrance window, as well as ions formed along the path due to re-ionization of beam atoms in collisions with background gas molecules and deflected to the liner walls by the tokamak stray magnetic field.

Efficiency of the NB transport and power loads onto the beam path components. Calculations were carried out using the PDP and BTR beam codes (see [8] for details). Data on the geometry of the injection path and the beam parameters were obtained from a series of optimization calculations using the following criteria: NB power delivered to the plasma: 3.5 MW, loads on the components along the beam path have power density within 500 kW/m^2, and for dumps of NB and residual ions not more than 15 MW/m^2.

As mentioned above, the IS output electrode has five sections, arranged vertically and inclined in such a way that their centerlines are directed at the center of the tokamak window. They are distanced 11.5 m away from the IS output electrode. Each section has 8×10 apertures, from which beamlets are extracted and focused horizontally at 11 m. The source produces a vertically elongated narrow beam with an initial size of 15×110 cm, this configuration was chosen to minimize the beam width in the region of the tokamak entrance window and in the plasma. In addition, the minimum gas inflow into the neutralizer is achieved, since its conductivity is proportional to the square of its liner width.

The deuterium ion beam current is 80 A at a current density on the plasma emission surface in the GDC of 0.2 A/cm^2. With such the current density, the composition of the beam ions is approximately $D^+ : D_2^+ : D_3^+ = 0.75:0.15:0.10$. The thickness of the deuterium target in the neutralizer appears to be sufficient to dissociate molecular ions almost entirely. For originating ions and atoms with energies (E/2 or E/3), the efficiency of their neutralization is determined in accordance with the dependence shown in Fig. 1. The composition of the mixed beam at the exit from the neutralizer is given in Table 1. It can be seen that in comparison with Fig. 1, the average efficiency of neutralization of the initial ion beam increases due to the appearance of particles with energies E/2 and E/3 due the dissociation of molecular ions.

T a b l e 1. **Beam composition at the neutralizer exit, at a 80 A source ion current, with D^+, D_2^+ and D_3^+ being in the 0.75:0.15:0.10 ratio, and ion current components in the 60:12:8 A ratio**

Energy of ions from the source E, keV	100	120	140
Ion beam power, MW	8	9.60	11.20
D^0 atoms current after 95% neutralization with dissociation of molecular ions, A			
E	29.64	23.94	19.95
E/2	17.56	16.42	15.28
E/3	19.15	18.70	18.01
Total D^0 current, A	66.35	59.05	53.24
Neutralization efficiency Φ_{0I} (in current)	0.83	0.74	0.67
Power in atoms, MW			
E	2.96	2.87	2.79
E/2	0.88	0.98	1.07
E/3	0.64	0.75	0.84
Total D^O power, MW	4.48	4.61	4.70
Neutralization efficiency Φ_{0P} (in power)	0.56	0.48	0.42
Residual ion current, A			
E	30.36	36.06	40.05
E/2	6.44	7.58	8.72
E/3	4.85	5.30	5.99
Total D^+ current, A	41.65	48.95	54.76
Residual ion power, MW			
E	3.04	4.33	5.61
E/2	0.32	0.46	0.61
E/3	0.16	0.21	0.28
Total D^+ power, MW	3.52	4.99	6.50

Calculations of the beam transport and loads on the beam path components were carried out for a 140 keV D^+ ion beam energy extracted from the IS. The beam geometry on the path from the IS exit to the MRID exit and the cross-section of the mixed beam at the neutralizer exit with a maximum PD of 140 MW/m^2 are shown in Fig. 10.

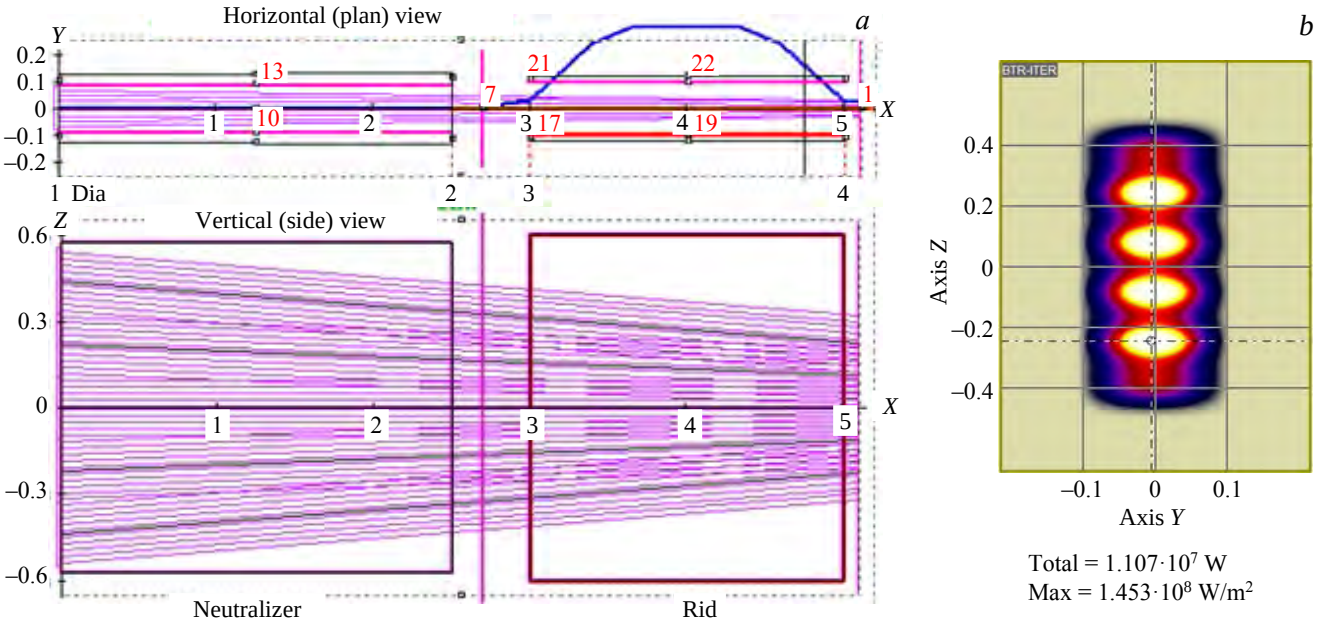

Fig. 10. Beam geometry in the path from the IS exit to the MRID exit. The axial lines of the output electrode sections and beamlets are shown, the right (№ 10) and left (13) walls of the neutralizer, the residual ions dump panel (19) and the screen plate (22) of the MRID, the axial profile of the model magnetic field are marked (*a*). Section of the beam at the exit from the neutralizer at a beam energy of 140 keV and an average angle of divergence $\theta_b = \pm 15$ mrad (*b*)

Neutralizer loads. Loads coming from the beam on the neutralizer side walls depend on the accuracy of the IS beam axis horizontal angular alignment relative to the injection axis. Calculation result for an ideal setting is shown in Fig. 11: PD peaks at the neutralizer exit, and four peaks emerge vertically due to the overlapping of beams starting from adjacent sections of the IS electrodes.

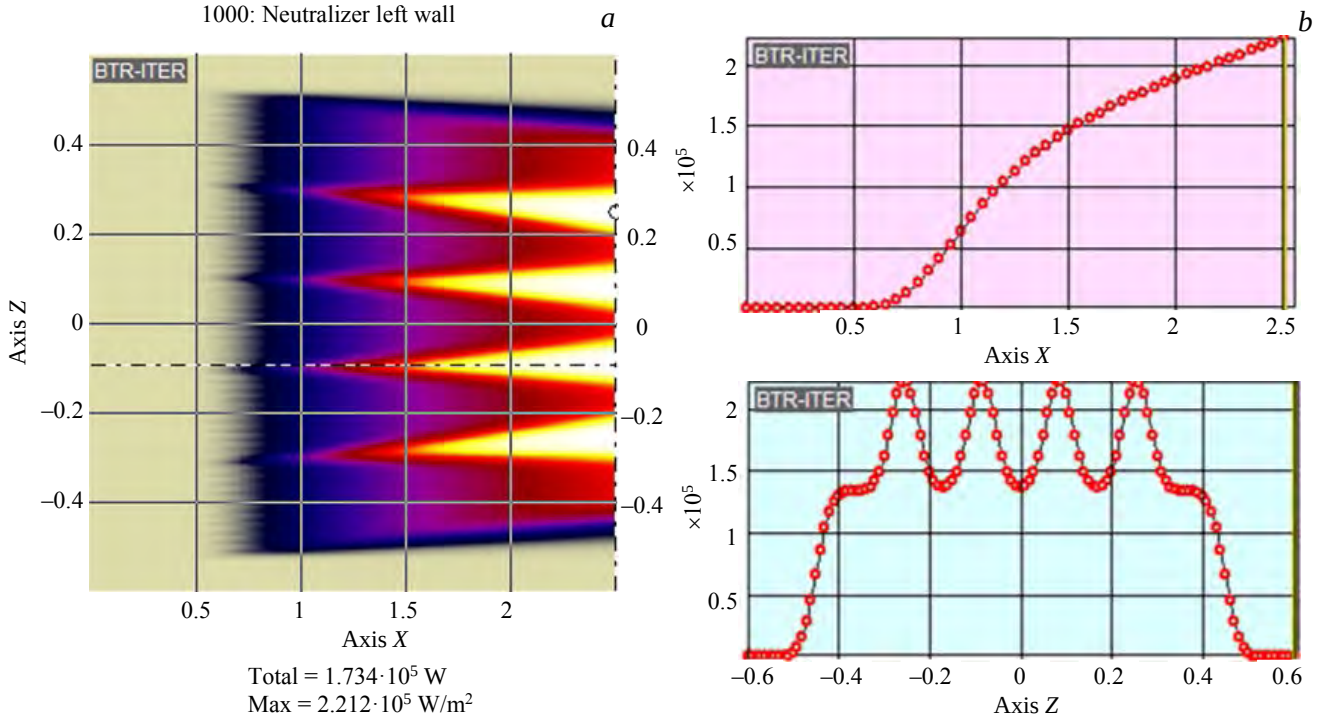

Fig. 11. Load coming from the beam on the neutralizer left wall with the beam axis ideally fixed between the IS and injection path axis: beam footprint (*a*), axial and vertical power density profiles (at $X = 2.5$ m) (*b*)

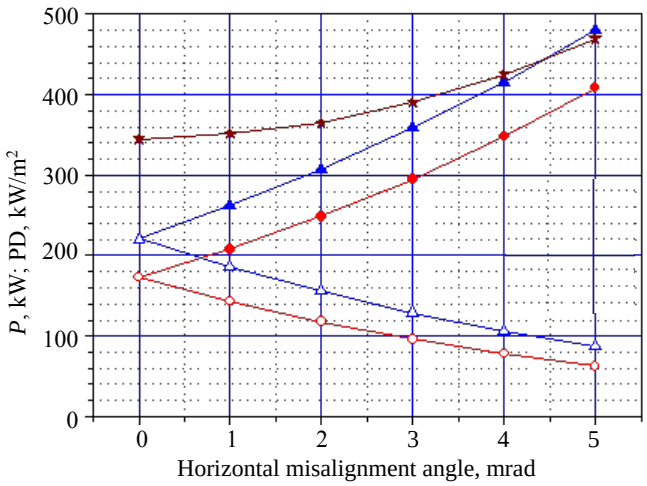

Fig. 12. Power (P), maximum PD and total power (P_{tot}) on the neutralizer right and left walls as functions of the misalignment angle in the beam axis setting: ◆ — P left, ◇ — P right, ▲ — PD left, △ — PD right, ★ — P tot

An appreciable load asymmetry can be observed on the right and the left walls, even with relatively small misalignment angles resulting from a horizontal beam axis adjustment (α_h) and likely due to inaccuracies both in the IOS electrodes assembly and the IS installation in the SVV (Fig. 12).

As can be seen from the figure, the ratio of both powers and PD on the left/right sides grows 4-fold already at α_h = 4 mrad, P_l reaches 350 kW, and PD_l is more than 400 kW/m^2, while the total beam power losses in the neutralizer increases almost by 25% to 425 kW. It should be noted that the ratio of loads on the neutralizer walls can serve as a good diagnostic tool for determining α_h when tuning the injector.

MRID loads. To completely intercept the beam of residual D^+ ions with energy E = 140 keV on the MRID receiving panel (19 in Fig. 10), a deflecting vertical magnetic field of 130 Gs is required. The beam footprint, and axial and vertical PD profiles on the panel are shown in Fig. 13.

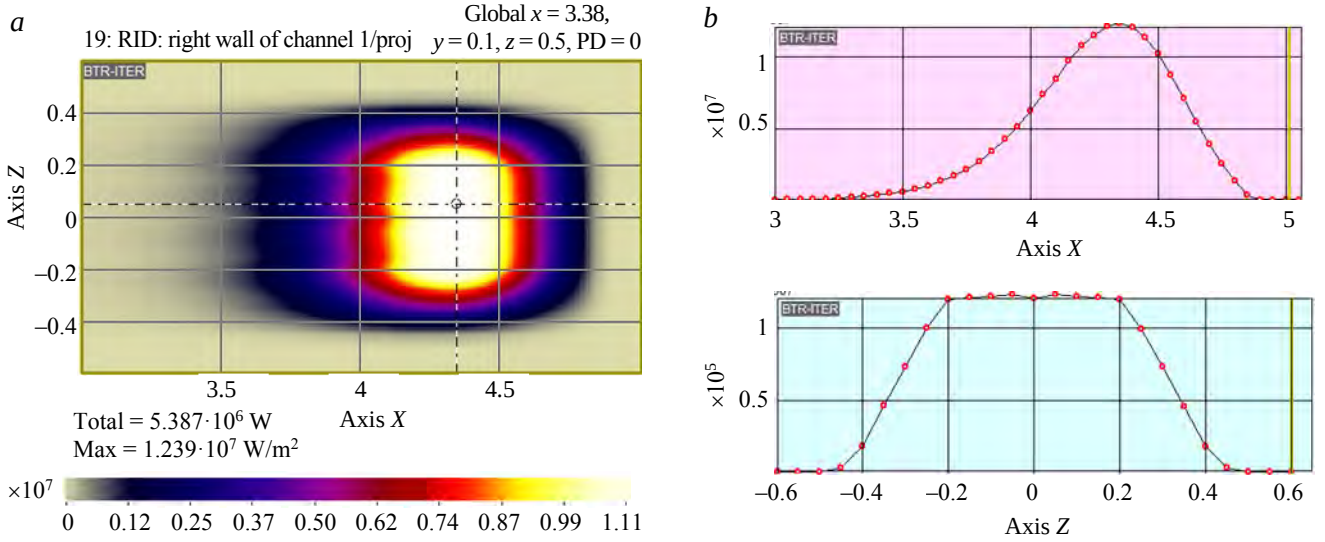

Fig. 13. Footprint of the deflected beam of 140 keV residual D^+ ions on the MRID dump panel (*a*), and power density axial and vertical profiles (*b*)

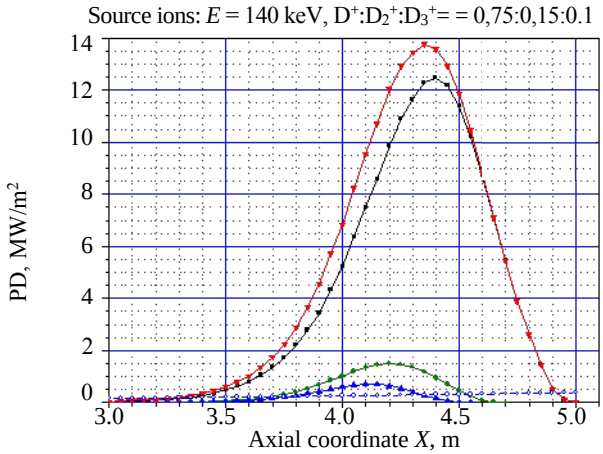

Fig. 14. PD axial profiles on the MRID dump panel of the residual ion beam components with energies of 140, 70, and 46.7 keV, deflected by a 130 Gs magnetic field; the total PD profile; and load profile from the NB for the case of the ion beam axis angular misalignment, α_h = –4 mrad (to the right), E, keV: ■ — 140, ● — 70, ▲ — 46, ▼ — sum PD, ○ — NB PD

Beams of residual D^+ ions with energies $E/2$ (70 keV) and $E/3$ (~47 keV) are dumped onto the same panel with small shifts and with significantly lower PD. The total PD reaches a value close to 14 MW/m^2 (Fig. 14).

The calorimeter load. The calorimeter operates when it is necessary to get the IS into working order and check the adjustment of the beam parameters. During this period its panels are shifted, forming a V-shape configuration. The junction of the panels is at X = 6.5 m. With an ideal beam axis setting, the PD profiles on the right and the left panels are symmetrical. The calorimeter receives a neutral beam with three atomic components energies E, $E/2$ and $E/3$, the footprints of which are superimposed

on each other. Fig. 15 shows the footprint, and axial and vertical profiles of the NB on the left panel at the energy E = 140 keV of D^+ ions from the source and a beam axis ideally aligned to the injection axis. The power of ~2.2 MW received by the panel is half the NB power with a PD up to ~10 MW/m^2.

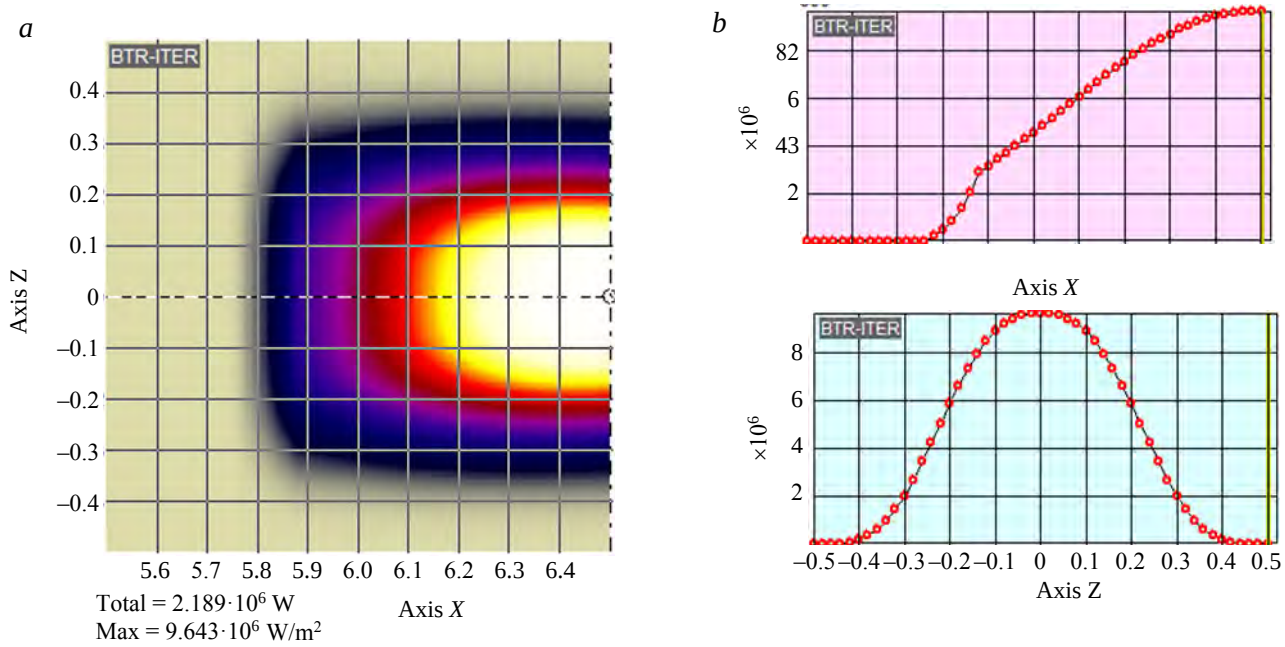

Fig. 15. Footprint of the neutral beam on the calorimeter left panel (*a*), and beam power density axial and vertical profiles (*b*) at the energy of D^+ ions from the source, E = 140 keV

Scraper loads. The scraper geometry should provide a NB «cutoff» to prevent the PD loads coming from the beam on the walls of the NB duct liner and the scraper itself from exceeding ~500 kW/m^2. This requirement has to do with the technological difficulties of cooling the walls. Maximum permissible misalignment angles resulting from horizontal and vertical beam axis adjustment, α_h and α_v, were calculated as ±4 and ±6 mrad, respectively, relative to the injection axis. This allowed appropriate configuration of these components to be selected. Figs 16, 17 shows the scraper dimensions and the maximum power and PD profiles of the loads on its left and bottom walls.

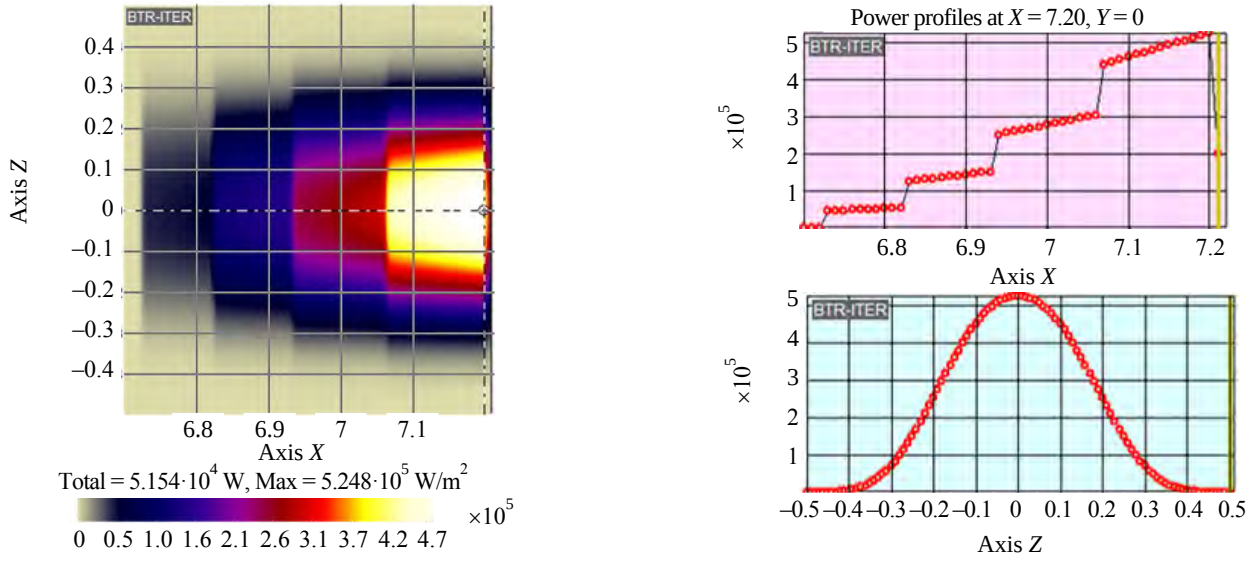

Fig. 16. Scraper dimensions (X_8 = 6.7 m, W/H = 0.32/1.0 m; X_9 = 7.2 m, W/H = 0.28/0.8 m) and maximum power loads and PD, α_h/α_v = 4/0 mrad

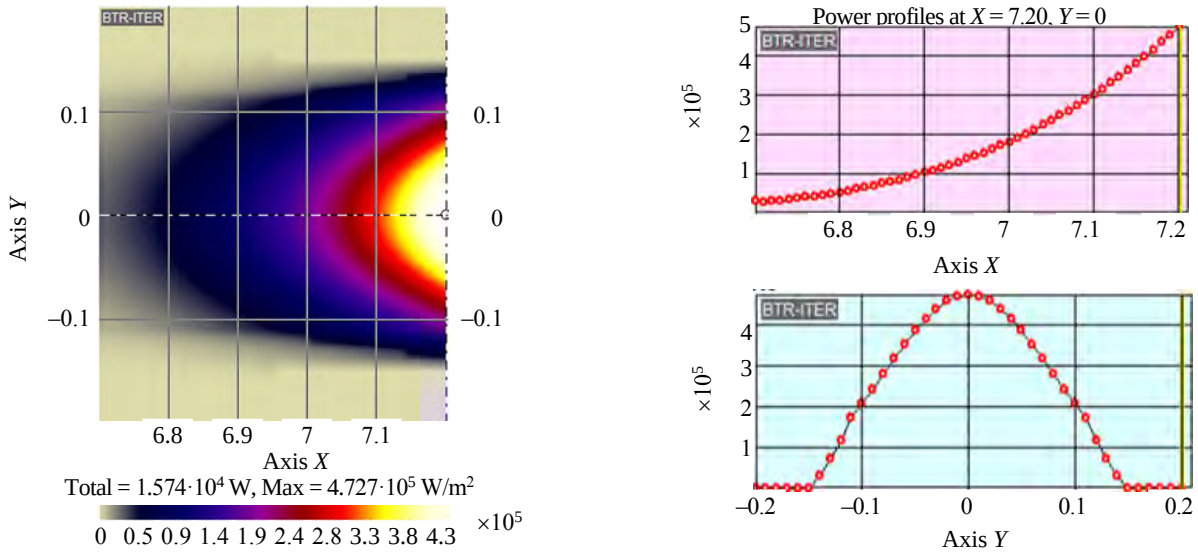

Fig. 17. Scraper dimensions (X_8 = 6.7 m, W/H = 0.32/1.0 m; X_9 = 7.2 m, W/H = 0.28/0.8 m) and maximum power loads and PD profiles and bottom, α_h/α_v = 0/–6 mrad walls of the scraper at the maximum permissible misalignment angles of the beam axis relative to the injection axis

NB duct liner loads. The liner is divided into two sections, and has a constant channel width of 0.3 m along its entire length, while the sections' upper and lower walls have different slopes to equalize PD peak values, as shown in Fig. 18. A PD peak of about 500 kW/m^2 is obtained at the liner downstream end.

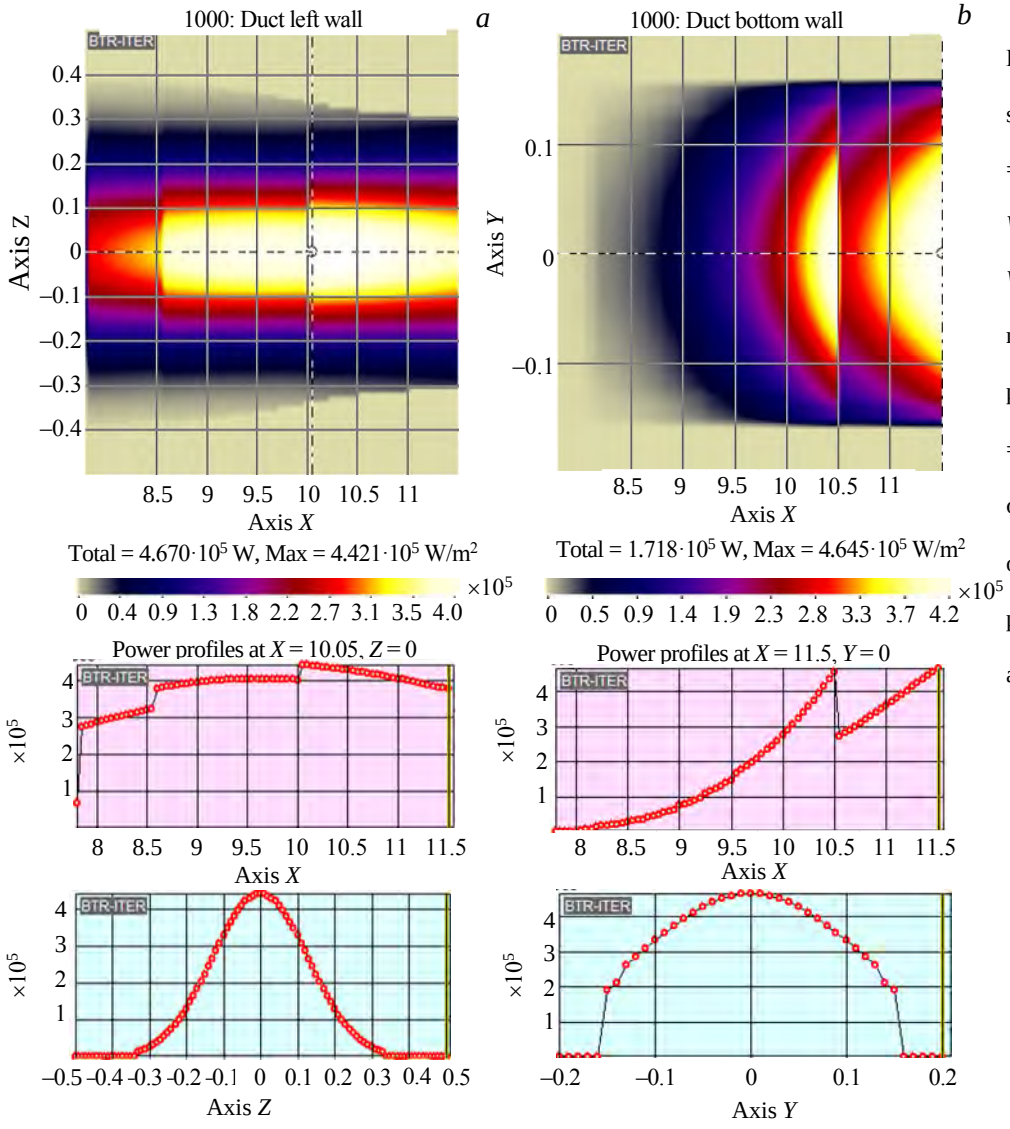

Fig. 18. NB duct liner dimensions (X_{10} = 7.8 m, W/H = = 0.3/0.85 m; X_{11} = 10.5 m, W/H = 0.3/0.63 m; X_{12} = 11.5 m, W/H = 0.3/0.6 m) and the maximum load power and PD profiles on the left, α_h/α_v = = 4/0 mrad (*a*) and bottom, α_h/α_v = 0/–6 mrad (*b*) walls of the liner at the maximum permissible misalignment angles

Fig. 19 shows the PD profiles and the power values of the neutral beam entering the FNS-ST chamber for the ideal and the worst-case beam axis alignment. One can see that with an imperfect beam axis alignment, input power falls from 3.58 to 3.36 MW, while PD remains at its maximum of ~44 MW/m^2.

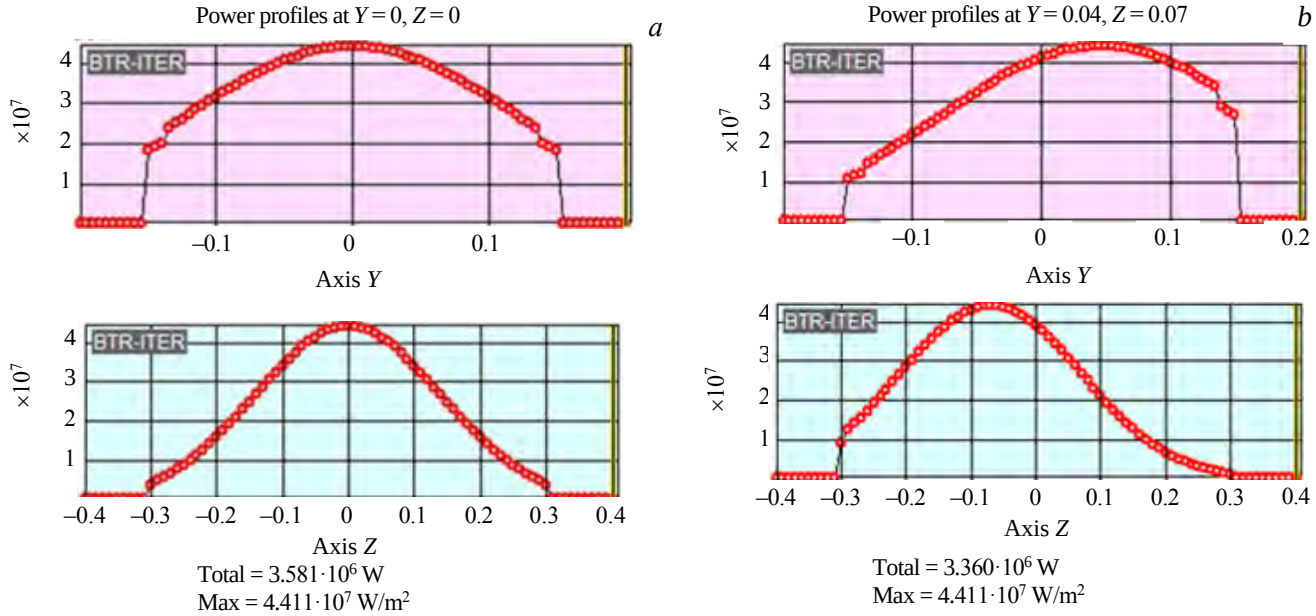

Fig. 19. Power density profiles of the neutral beam injected into the FNS-ST plasma for cases of ideal beam axisaligning, α_h/α_v = 0/0 mrad (*a*) and for maximum values of misalignment angles, α_h/α_v = 4/–6 mrad (*b*)

Table 2 shows the change in the beam power along the injection path and the distribution of loads to the path components, when the IS beam energy is 140 keV, for the ideal beam axis alignment to the injection axis and for the worst-case misalignment angles, α_h/α_v = ±4/±6 mrad. As one can see from the table, the efficiency of NB transmission from the neutralizer to the tokamak plasma entrance, is 76% in the «ideal» case and drops to acceptable 71% in the «worst misalignment» case.

T a b l e 2. **Change in the beam power along injection path and load distribution to the path components (positive deuterium ions beam current from the ion source of 80 A; D^+:D_2^+:D_3^+ ionic makeup: 0,75:0,15:0,10; divergence angle: ±15 mrad)**

IS beam energy, keV	140	
IS beam power, MW	11.2	
Beam axis horizontal/vertical misalignment angle, mrad	0/0	±4/±6
Beam power load in the neutralizer, MW	0.34	0.42
Neutral beam power at the neutralizer exit, MW	4.57	4.53
Ion beam power at the neutralizer exit, MW	6.29	6.25
Power of the neutral beam load in the MRID, MW	0.27	0.33
Total power released in MRID (atoms + ions), MW	6.56	6.58
NB power at the exit from the MRID, MW	4.30	4.20
NB power intercepted by the scraper, MW	0.05	0.07
NB power load on the duct liner walls	0.67	0.77
NB power injected into the plasma, MW	3.58	3.36
Efficiency of NB transport to the plasma	0.76	0.71

Injector vacuum conditions. The gas (deuterium) flow rate in the injector VV is determined by required thickness, τ, of the neutralizer gas target. As mentioned earlier, when neutralizing positive ions, the equilibrium yield of fast atoms is achieved at «infinite» τ; therefore, τ is usually chosen that provides the atoms yield of 95% of the equilibrium one. The value of τ increases with increasing beam energy and for an energy of 140 keV $\tau_{0.95} = 1.26\cdot10^{20}$ m^{-2} (see Fig. 5). A neutralizer liner 2.5 m long connects two volumes: the SVV and the injector VV, while the change in gas concentration/pressure along its axis is almost linear, and the pressure in the VV is negligible compared to the pressure in the SVV. Accordingly, the gas concentration in the SVV volume should be about $1\cdot10^{20}$ m^{-3}, i.e., pressure ~0.37 Pa (at a room temperature). With a liner section of 0.18×1.2 m and a length of 2.5 m, its conductivity is about 15 m^3/s and the gas flow, providing the required $\tau_{0.95}$, will be Q_N = 5.6 Pa·m^3/s. The gas escaping from the ion source passes through the neutralizer, its flow will be about

1.6 Pa·m^3/s. Accordingly, an additional gas feed into the SVV is required at the level of 4 Pa·m^3/s. In addition, a residual ion beam with a current of about 55 A is dumped in the VV, which, after neutralization on the MRID panel, gives a molecular deuterium flux of 0.65 Pa·m^3/s; so the total flow in the VV is about 6.3 Pa·m^3/s.

The pumping in the VV of the deuterium molecules at a rate of about $1.1\cdot10^3$ m^3/s is carried out by cryosorption panels with a total area of ~14 m^2, located on the side walls of the VV. To reduce the NB loss in the region after the MRID due to the re-ionization of atoms due their collisions with the background gas molecules, the VV is divided into two parts using a vacuum baffle located in the MRID region. In this case, differential pumping is provided, which reduces the pressure in this section to $\sim2.5\cdot10^{-3}$ Pa. According to estimates, the re-ionization losses of the NB will be ~7% (about 0.24 MW).

The duration of the injector continuous operation is limited on account of the explosion hazard. Gas evacuated from the VV freezes on cryopanels, and a critical value may be reached, in which event an atmospheric air breakthrough into the VV and the cryopanels rapid warming may occur, giving rise to an «explosive mixture». In accordance with explosion safety provisions, deuterium content in the mixture under normal conditions must not exceed 2% ($2\cdot10^3$ Pa). Considering that the VV and SVV total volume is 25 m^3, gas accumulated on cryopanels must not exceed $5\cdot10^4$ Pa·m^3. Consequently, at a gas flow of 6.3 Pa·m^3/s, the injector must be brought to a halt after 2.2 hours of operation to regenerate the cryopanels, and must be ready to resume operation in ~45 min to make sure that NB power injection into the tokamak is uninterrupted.

CONCLUSION

Strengths and weaknesses of positive- or negative-ion-based fast deuterium neutral beam injectors for FNS-ST have been analyzed and compared with the assumption of their applicability to the «intermediate» beam energy range of 100—200 keV. It has been shown that a negative- deuterium-ion-based system has significant advantages over the positive ion technology at ion energies above 150 keV, whereas at lower energies the situation is vice versa.

As is shown in [6], in the case of a small-sized FNS-ST, the attenuation of an >140 keV neutral beam during its moving in the tokamak plasma is insufficient in terms of its power release on the first wall. Consequently, the injection module for the FNS-ST should be a positive- deuterium-ion-based system allowing the delivery of 3.5 MW deuterium neutral beam power to plasma at an ion source energy of 100—140 keV and source ion current of 80 A.

Calculations of the efficiency of beam transmission to the tokamak plasma were done for different beam geometries. The ion beam configuration at the IS exit was chosen in the form of a five-section vertically elongated 0.15×1.15 m «ribbon» with each section focused onto the tokamak 0.3×0.6 m entrance window. Power loads on the beam path components were calculated, and the efficiency of NB transport was found to be 75%.

A compact system of residual ion beam horizontal deflection by a vertical magnetic field onto a dump panel inside the magnetic system is considered. At a 140 keV source ion energy, the fraction of residual ions is about 60%, therefore, peak power density, PD_{max}, at the dump panel reaches 15 MW/m^2.

The dump panel, as well as calorimeter panels with a PD_{max} of 10 MW/m^2, falls into the class of receivers with critical heat fluxes (CHF), whose design uses hardened chrome-zirconium bronze tubes with twisted tape heat removal intensifiers. The configurations of the other injector components are selected such that PD_{max} is within 0.5 MW/m^2.

The working gas (deuterium) supplied to the neutralizer and the ion source is pumped at a rate of about $1\cdot10^3$ m^3/s using cryopanels, placed inside the injector vacuum vessel. The duration of the injector continuous operation is limited on account of the explosion hazard. At a gas flow of 6.3 Pa·m^3/s, the amount of gas accumulated on the cryopanels should not exceed $5\cdot10^4$ Pa·m^3, i.e. the injector must stop operation after 2.2 hours to regenerate the cryopanels. If NBIS FNS-ST uses four injectors, they should be enabled alternately, so that with three units in operation one is in the cryopump regeneration mode. The latter should be ready to resume operation in ~45 minutes to make sure that NB power injection into the tokamak is uninterrupted.

This work was supported by the National Research Center «Kurchatov Institute» (28.09.2020 № 1934a).

REFERENCES

1. **Kuteev B.V. et al**. Steady state operation in compact tokamaks with copper coils. — Nucl. Fusion, 2011, vol. 51, p. 073013.
2. **Гончаров П.Р. и др.** Сопоставление нейтронного выхода классических и сферических токамаков. — ВАНТ. Сер. Термоядерный синтез, 2011, вып. 2, с. 36—43.
3. **Днестровский А.Ю., Голиков А.А., Кутеев Б.В. и др.** Исследование стационарного режима работы нейтронного источника на основе токамака. — ВАНТ. Сер. Термоядерный синтез, 2010, вып. 4, с. 26—35.
4. **ORNL** «Red Book», 1977.
5. **ITER** Final Design Report, DDD 5.3, 2001.
6. **Dlougach E.D. et al.** Neutral beam current ratio in the neutron source FNS-ST. — ВАНТ. Сер. Термоядерный синтез, 2021, т. 44, вып. 1, с. 68—79.
7. **Naumov V.K., Semashko N.N., Komov A.T. et al.** Method of adiabatic cross-section and its application for estimating of thermo-physical and thermo-strength parameters of high density beam dumps. — Plasma Devices and Operations, 1999, vol. 8, p. 39—65.
8. **Ananyev S.S., Dlougach E.D. et al.** Modeling and optimization of the neutral beam line for plasma heating and current drive for the DEMO-FNS fusion neutron source project. — Fusion Engineering and Design, 2020, vol. 161, p. 112064.

AUTHORS

Alexander A. Panasenkov, PhD head scientist, NRC «Kurchatov Institute», 1, Academika Kurchatova sq., Moscow, 123182, Russia, Panasenkov_AA@nrcki.ru

Sergey S. Ananyev, Leading Researcher, PhD in physics and mathematics, NRC «Kurchatov Institute», 1, Academika Kurchatova sq., Moscow, 123182, Russia, Ananyev_SS@nrcki.ru

Eugenia D. Dlougach, senior scientist, NRC «Kurchatov Institute», 1, Academika Kurchatova sq., Moscow, 123182, Russia, edlougach@gmail.com

Boris V. Kuteev, Professor, Deputy Head Tokamak Department Fusion Research Centre; NRC «Kurchatov Institute», 1, Academika Kurchatova sq., Moscow, 123182, Russia, Kuteev_BV@nrcki.ru

Статья поступила в редакцию 15 января 2021 г.
После доработки 16 марта 2021 г.
Принята к публикации 25 марта 2021 г.
Вопросы атомной науки и техники.
Сер. Термоядерный синтез, 2021, т. 44, вып. 2, с. 86—99.

UDC 621.039.616

NEUTRAL BEAM CURRENT RATIO IN THE NEUTRON SOURCE FNS-ST

E.D. Dlougach, A.A. Panasenkov, B.V. Kuteev, E.A. Filimonova

NRC «Kurchatov Institute», Moscow, Russia

The FNS-ST spherical tokamak [1] is of particular interest for development as a neutron source, since it can provide higher steady-state neutron flux densities than *classical* tokamaks [2]. When choosing the device operation parameters, it is assumed that the non-inductive current drive in FNS-ST may be achieved with an energetic neutral beam injection (NBI). The choice of a neutral beam (NB) production scheme is mainly determined by beam energy; neutral beams with energy E_b > 140 keV can be more effective in plasma heating and current drive, while they can be efficiently produced only from negative ions. For small tokamak reactors, positive-ion-based injectors with smaller dimensions seem more attractive, thus the lower energy interval of 100—140 keV is considered too, and the final choice of operating energy will be based on the total NBI efficiency optimization. In the framework of this study, injection efficiency was estimated in terms of *current ratio*, i.e. the ratio between the beam current output in plasma and the beam source current input. The analysis is done by a simple approach (*LNB, light neutral beam*), used for the direct estimation of fast ion (FI) current. The LNB technique has much in common with the model presented in [3], but allows for NB energy optimization *without* recourse to any scaling laws. It leverages the analytical expressions from [4] to calculate FI thermalization and phase space distributions, and obtain FI current profiles. It has proved to be applicable to selecting the injected beam energy — with account of the NB production scheme, and in agreement with the shine-through losses reduction.

Key words: fusion neutron source, spherical tokamak, neutral beam, injector, beam current, shine-through, light model, LNB, FNS.

DOI: 10.21517/0202-3822-2021-44-2-100-106

ГЕНЕРАЦИЯ ТОКА НЕЙТРАЛЬНЫМ ПУЧКОМ В НЕЙТРОННОМ ИСТОЧНИКЕ ТИН-СТ

Е.Д. Длугач, А.А. Панасенков, Б.В. Кутеев, Е.А. Филимонова

НИЦ «Курчатовский институт», Москва, Россия

Сферический токамак FNS-ST [1] представляет особый интерес для разработки источника нейтронов, поскольку может обеспечить более высокую стационарную плотность потока нейтронов по сравнению с классическими токамаками [2]. При выборе параметров работы установки предполагается возможность неиндуктивной генерации тока в ТИН-СТ пучком быстрых атомов (NBI). Выбор схемы инжекции нейтрального пучка (NB) определяется энергией пучка. Нейтральные пучки энергией E_b > 140 кэВ более эффективны с точки зрения нагрева и генерации тока, но технология их получения основана на ускорении отрицательных ионов. Что касается компактных токамаков, то инжекторы на положительных ионах, которые имеют более скромные габариты, более привлекательны, поэтому для них также рассматривается более низкий интервал энергии 100—140 кэВ, и окончательный выбор энергии будет сделан с учётом оптимизации совокупной эффективности инжекции пучка. В данной работе эффективность инжекции оценивается в терминах *усиления токов*, т.е. в виде отношения между результирующим током пучка в плазме и током, извлекаемым из ионного источника. Анализ выполнен с помощью простой модели пучка (*LNB, лучевой нейтральный пучок*), который позволяет быстро получать ток быстрых ионов в процессе их торможения в плазме. Указанная модель имеет много общего с моделью [3], но позволяет оптимизировать энергию пучка без использования скейлингов. Модель LNB использует аналитические выражения [4] для расчёта термализации быстрых ионов (FI) и их распределения в фазовом пространстве, а также для получения профилей тока. Указанная методика применена для выбора энергии инжектируемого пучка с учётом эффективности его производства и в пределах допустимой нагрузки от пучка на первой стенке.

Ключевые слова: термоядерный источник нейтронов, сферический токамак, нейтральный пучок, инжектор, генерация тока, сквозные потери, лёгкая лучевая модель, LNB, ТИН-СТ.

INTRODUCTION

Spherical tokamaks (ST) can provide higher neutron flux density and better compatibility with fission blankets than classical tokamaks, and at a much lower cost. However, heating and current drive (CD) systems can increase the entire device cost essentially and should be designed with maximum care.

The FNS-ST [1] tokamak is supposed to provide a high steady-state neutron flux of about ~10^{18} n/s. The machine operation parameters are selected from the assumption that non-inductive current drive is achieved in FNS-ST using energetic atoms injection. Fast neutral beam is the most efficient current source, as the generated fast ions directly produce the current parallel to the magnetic field. The beam driven current together with bootstrap current can fully replace the inductive current in plasma, making steady-state operation possible.

In a nominal operation mode, nuclear fusion reactions from high-energy ions slowing down in plasma should contribute up to 90% to overall neutron generation. In other words, FNS-ST neutrons are expected to

originate mainly from D—T-fusion reactions between hot injected beam particles (or high-energy *tails*) and core plasma ions that form the Maxwell background [2]. An example of NB optimization for FNS-ST steady-state operation is given in [3], where a *system* (*zero-dimensional*) approach is proposed for scanning the machine parameters; and ITER scaling laws are used to assess CD and plasma heating. Fusion power gain (Q_{fus}) proved to be highly sensitive to deuterium beam energy, due to the beam-plasma interaction. It reaches a ~0.8 peak at E_b = 300 keV, and falls down to ~0.5 at E_b = 100—150 keV. Because the production of neutral beams with E_b > 140 keV from positive ions is ineffective, the decreased energy range is considered as well [3]. Finally, the interval of injected deuterium beam energy optimization is E_b = 100—300 keV.

The best CD *efficiency* is typically achieved at higher electron temperatures and lowest plasma density in order to maximize the fast ion slowing down time, and by choosing the beam energy is close to the so-called critical energy [4]. All beam-driven effects including current generation, beam-plasma fusion, plasma heating and rotation, are very sensitive to the initial deposition of fast ions (FI), the latter being mainly defined by the beam penetration path in plasma. In short, the beam penetration depth, fast ion current amplification in plasma, and shine-through losses are the principal figures of merit when choosing the operation gap for beam-plasma system.

The spatial and angular structure of the injected beam can smear the beam deposition shape, which normally results in the beam capture and CD decrease as compared to pencil beam models. In compact tokamak systems the beam width is comparable with the plasma core radius, and the beam geometry is even more critical as the combination of distorted FI distributions across magnetic surfaces with wider pitch-angle and ions energy profiles essentially reduce the expected beam current gain and neutron output. A way to measure these 3D effects is to use a beam-plasma model that would account for the entire geometry of a given beam-plasma system, including the source beam detailed specification and plasma magnetic configuration.

The NBI total efficiency can be estimated in the terms of *Current ratio*, i.e. the beam output in plasma (or current circulating around the torus) referred to the beam source input, in current, so that the total NBCD efficiency is calculated as a product of the injector yield in neutralized current, the beamline transmission coefficient, and the beam current amplification in plasma. The beamline transmission is beyond the scope of this paper and is assumed to be constant regardless of beam energy. The focus of this paper is more on the enhancement of neutral beam injection performance and beam energy optimization with a view to maximizing plasma current output.

A simple technique (LNB, light neutral beam) is proposed for the beam current direct and fast estimation; it has much in common with the model presented in [3], but enables the calculation of beam-driven quantities without recourse to ITER scaling laws for NBCD (the reliance on those laws may not deliver accurate results in the case of compact devices). The LNB method is also useful in the sensitivity analysis of beam deposition in plasma, as it allows a comprehensive evaluation of beam geometry and spectra effects on CD (however, this is outside the scope of this paper). The LNB technique is based on the analytical expressions for neutral beam heating [4], and allows calculation of beam ion thermalization and current, spatial distributions and energy profiles directly by the beam bunch tracing through 3D plasma. The technique is applied to evaluate the compound beam current from all the injected beam fractions (energy groups), and to select optimum operation range with account of the NB production scheme.

Due to FNS-ST device rather small size, the beam capture in plasma should be not less than 95% within the range of plasma density considered. Therefore, prior to optimizing the injection geometry, we lowered the upper value of the injected beam energy to ensure that the beam capture efficiency is high enough for the designed range of plasma densities and that the lost beam fraction (shine-through) does not damage the plasma facing surfaces.

NBI SCHEME FOR FNS-ST

The NBI system for FNS-ST will include 3 or 4 injectors, each delivering ~3.5 MW power to FNS-ST plasma (deuterium + tritium), so that the total steady-state beam power injection is 10 MW (in deuterium). The beam port size is 0.3×0.6 m. The injection axis is horizontal (Z = 0), the positions of tangential injection points are variable: R = 0.4—0.6 m. The system's main parameters are summarized below:

Aspect ratio R/a, m . . .	0.5/0.3
Elliptic elongation k . . .	~3 (2.75)
Toroidal magnetic field, T . . .	1.5
Electron temperature T_e, keV . . .	1—5

Average plasma density n_e, 10^{20} m^{-3} . . .	0.5—1
Plasma current I_p, MA . . .	0.8—1.5
NB tangential injectors . . .	3—4
NB total power P_b, MW . . .	10
D^0 atoms energy, keV . . .	100—200
Ion source current I_s^+, A . . .	80
NB port size $W \times H$, m . . .	0.3×0.6

The choice of the beamline design for the NB injection is based on the following considerations. There are two possible design solutions, one based on a *positive ion source* (PIS), the other on a *negative ion source* (NIS). A PIS-based injector neutral output in current decreases rapidly with increasing NB energy in the range of 100—300 keV, thus it is not so efficient to generate NB at $E_b > 140$ keV needed to reach the plasma core. A negative-ion-based NBI scheme offers the prospect of much higher neutral fractions for high-beam energy, with the neutral output remaining almost constant and close to ~60%. Also, a NIS-based injector enables a better beam transmission, with beam divergence being twice as small as that observed with the PIS beam technology. On the other hand, the PIS-based NBI provides higher (by at least an order of magnitude) densities of extracted ion current and features a more compact beamline setup. In addition, the positive-ion technology has been extensively studied and used.

A detailed performance analysis and comparison of the two NB production schemes have been performed, and the following conclusions have been made:

— the choice of the NBI scheme depends on the energy of injected atoms: for $E_b > 140$ keV, the NIS is preferable. For lower energy, a detailed analysis of beamline efficiency will tell;

— whatever the NBI design, the NBI vacuum vessel (VV) should be mounted horizontally. The VV, together with the beamline components, is more than 100 MT in weight; its fastening and alignment, as well as remote maintenance are difficult if the platform is inclined;

— the NIS-based injector has the advantages of a highly efficient atom production, regardless of atom energy, beam higher transmission to plasma, and a more compact electrostatic residual ion dump (ERID);

— the drawbacks of the negative-ion technology include lower D^- current density (~20 mA/cm^2) at the source exit, the neutral beam halo fraction (15% of beam particles), which decreases NBI performance and raises power loads, plasma emitter non-uniformity across large emissive surface leading to higher beam divergence;

— the advantages of a PIS-based injector (for $E_b < 140$ keV) are: high D^+ current density (200 mA/cm^2) at the source exit (i.e. lower emitter area), smaller neutralizer dimensions, reduced gas flow (target thickness), the neutralizer can be attached to the ion source (reduced gas load for cryopanels, as compared with NIS);

— the drawbacks of the PIS-based NBI include: a 2-fold lower power efficiency, molecular ion fractions in the source — D_2^+ (15—20%) and D_3^+ (10%) which produce due to dissociation and neutralization the lower-energy atoms ($E/2$ and $E/3$), the latter are ionized and captured by plasma periphery reducing resultant NBCD; compact electrostatic RID deflection and dumping system cannot be used (due to the high current density and volume charge), instead, magnetic deflection is employed, with dumping surfaces fitting all energy fractions; for E_b ~140 keV, the residual power in ions can be twice as high as the neutral power, hence the magnetic RID becomes the most power loaded component of the injector.

Given the small size and relatively wide plasma density range in FNS-ST, the beam energy interval was checked to meet the >95% capture criterion to prevent the shine-through damage of the camera first wall. According to preliminary shine-through estimations, a deuterium beam with E_b ~ 200 keV can produce ~5 MW/m^2 peak power density at the first wall, for mean plasma density 1×10^{20} m^{-3}. Thus, the operation with 200 keV beams will only be possible at a plasma density exceeding 1.5×10^{20} m^{-3}, and E_b ~ 300 keV beams — from 2×10^{20} m^{-3}. Plasma operation at lower densities will only be safe with the NB energy below E_b ~ 150 keV and provide the expected shine-through of <2 MW/m^2.

With all these considerations in mind it was finally decided to use the PIS based scheme with deuterium beam energy 100—140 keV, and with ~3.5 MW power injected by each NB module. In this scheme, beam content (D^+ and D^0) in a thick gas target is defined by the ratio of cross-sections of two competing processes — charge exchange and ionization, and achieves equilibrium when the gas target is infinitely thick. This ratio (as well as the maximum atomic yield, F^0) is a function of the beam energy, E_b, and the equilibrium neutral fraction decreases rapidly with increasing

energy, as shown in Fig. 1. To provide an infinitely thick target, for which equilibrium is attainable, one needs a very long neutralizer and extremely large gas flow. Therefore, in a PIS-based injector, a nominal gas thickness point is chosen for 95% of the maximum atomic yield. The optimum target thickness (F_{95} = 0.95F^0) in a PIS-based NBI rises almost linearly with the beam energy. Power contained in the residual charged part of the beam after neutralization is comparable with the neutral power injected to plasma. For E_b ~ 140 keV, the dumped residual power can be twice as high as the neutral beam power, making RID the most loaded NBI component.

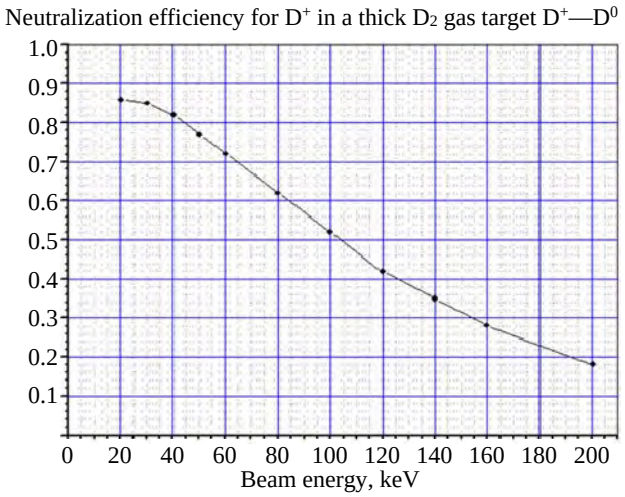

Fig. 1. Energy dependence of the equilibrium neutral fraction in a deuterium beam

The ion beam extracted from a positive ion source contains three particle species: D^+, D_2^+ (15—20%), and D_3^+ (~10%). Molecular ions, while passing through a gas cell, dissociate and after neutralization produce atoms with lower energies $E_{1/2}$ and $E_{1/3}$. The lower-energy beam fractions are ionized and captured at the plasma periphery; hence CD calculations should account for the injected beam spectral content.

The neutral beam content was calculated for the 100—140 keV range of injected beam energies — taking into account the source beam species percentage and the neutral yield for each source species (F_{95}). The results

T a b l e 1. **Neutral beam fractions (F) and effective neutral yield in current for I_s^+ = 1 A**

Parameter	E_b, keV					
	100		120		140	
	I_n, A	$F(I_s^+)$	I_n, A	$F(I_s^+)$	I_n, A	$F(I_s^+)$
E_{full}	0.49	0.37	0.40	0.30	0.33	0.25
$E_{1/2}$	1.46	0.22	1.37	0.21	1.27	0.19
$E_{1/3}$	2.39	0.24	2.34	0.24	2.25	0.23
Injected NB current D_1^0 I_b, A		0.83		0.74		0.67
Effective neutral yield I_b/I_s^+	0.83		0.74		0.67	

Comments to Table 1: Atoms D_1^0 current, [A] — after 95% neutralization with molecular ions dissociation; I_n, A — neutralized D_1^0 output, *normalized* to 1 A of each beam fraction; $F(I_s^+)$, A — specific contribution to the neutralized current, for 1 A of the total ion source current; the source beam content is: D^+: D_2^+ : D_3^+ = 0.75:0.15:0.10.

are shown in Table 1. The source beam fractions ratio D^+: D_2^+: D_3^+ = 0.75:0.15:0.10 in all cases. All the values are normalized to the source beam current (either specific or total) I_s^+ = 1 A. The injected beam energy corresponds to the basic (full) energy fraction: $E_b = E_{full}$.

The results of Table 1 are illustrated as a chart in Fig. 2. Based on the neutral yield values, the NB energy 100 keV looks the most attractive for the beamline design.

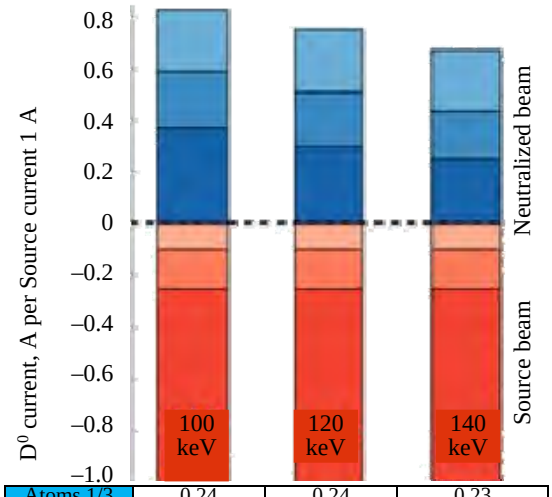

Atoms 1/3	0.24	0.24	0.23
Atoms 1/2	0.22	0.21	0.19
Atoms full	0.37	0.30	0.25
Atoms 1/3	0.10	0.10	0.10
Atoms 1/2	0.15	0.15	0.15
Atoms full	0.75	0.75	0.75

Fig. 2. The neutral beam output fractions E_{full}, $E_{1/2}$, $E_{1/3}$ (blues) for NB energy of 100, 120, and 140 keV, respectively. The source beam contents (D^+: D_2^+: D_3^+) are shown in red colors

LNB MODEL FOR BEAM PENETRATION AND IONIZATION

The NB total efficiency can be defined as a product of total neutralized yield in current, beamline transmission, and fast ion current multiplication in plasma. Although a lower energy beam seems to be more efficient from the NBI perspective, current produced by the beam in plasma can be of higher priority. As a neutral beam produced with PIS technology has three energy fractions, all of them contribute to the beam penetration, ionization and slowdown, pro-

ducing their own fast ion current fraction in plasma. Current drive calculations take into account the actual NB content measured in Fig. 2.

The injected atoms produce a current of fast ions (FI) circulating around the torus. The FI current stacks up during the injection period, and a steady state is reached when the build-up rate of current due to stacking is balanced by the loss rate due to slowing down through collisions with plasma electrons and bulk ions, or to charge exchange of the fast ions with neutral atoms [4].

To calculate beam deposition and CD directly, a simple *LNB model* (*light neutral beam*) is used. From the LNB's viewpoint, the beam consists of a large number of rays (or test atoms), whose input structure is predefined (calculated by specialized NBI codes). The direct tracing procedure for each beam ray is discrete and deterministic; it applies analytical expressions [4] and allows beam-driven quantities calculation without recourse to scaling laws (which may be not quite applicable to small devices). Although LNB accepts the detailed beam configuration and spectra effects, these are beyond the scope of this paper. The results shown are obtained for a *thin beam* (single ray) direct tracing in a plasma toroidal target with elliptical cross-section of FNS-ST plasma.

The NB penetration and ionization are calculated using analytical fits of cross-sections proposed by Janev [5]; the procedure scheme and the resulting plot for E_b = 120 keV are shown in Fig. 3. The three energy fractions of the beam are marked in the plot, making clear the significant difference in ionization rates between the fractions. The cross-section for the lower-energy beam fraction ($E_{1/3}$) is almost 3 times higher than that for the E_{full} beam fraction.

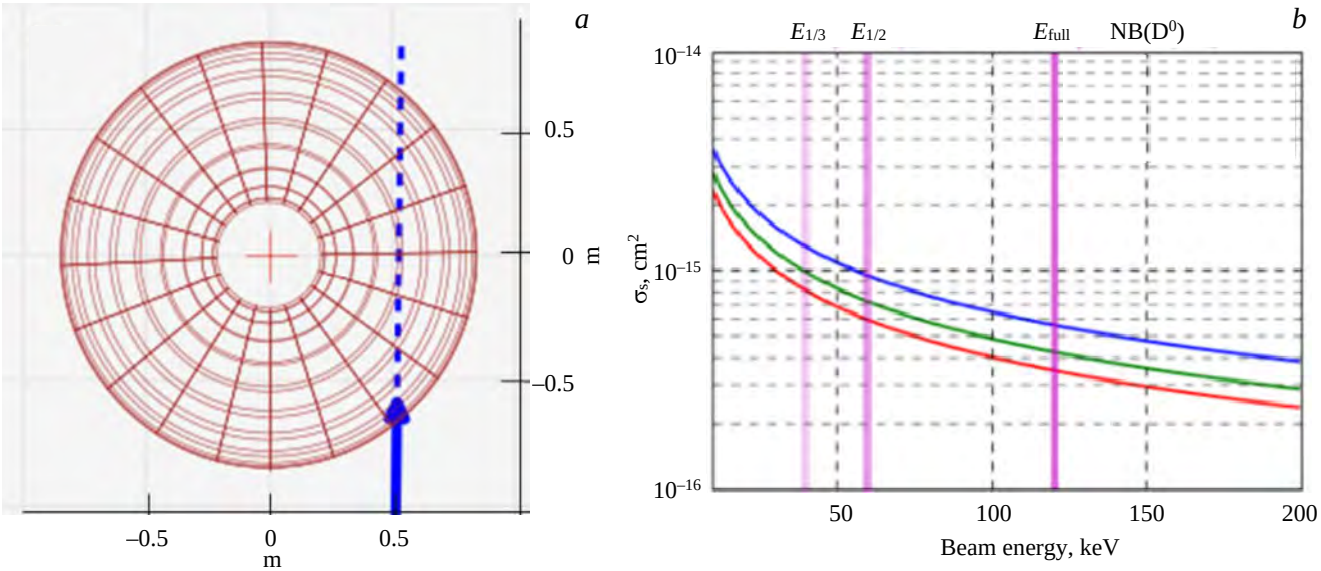

Fig. 3. The LNB scheme of single ray injection to FNS-ST (*a*), and energy dependence of beam-stopping cross-sections (*b*) calculated for D-beam E_{full} = 120 keV for plasma temperature T_e = 1 keV and for plasma densities n_e = 0.1×10^{20} m^{-3} (—), 1×10^{20} m^{-3} (—), 10×10^{20} m^{-3} (—)

FAST IONS SLOWING-DOWN AND CURRENT GENERATION

The NBI fast ions distribution in phase space can be calculated by solving the kinetic equation with a beam produced source term and the collision operator, which includes fast ion slowing-down and pitch angle scattering. As opposed to the Fokker-Planck equation numerical solution for reduced phase space, LNB directly calculates the NB slowing down path in plasma toroidal geometry — from the instant the FI source distribution generated along each beam ray. The fast ion toroidal current is supposed to be produced by the ions velocity component parallel to the magnetic field. The plasma is assumed to be steady-state and unaffected by the beam. The charge-exchange FI losses are ignored, as are the electron screening of FI current, radial diffusion, and orbit effects. The net CD value is calculated as: $I_{NB\,CD} = I_{FI}$. Due to these approximations, LNB model allows the evaluation of the beam-driven quantities upper bounds, with the geometry optimization.

The characteristic time for the beam ions slowing down to the thermal energy including the drag force on plasma ions and electrons, is taken from [4] as: $\tau_s = \frac{\tau_{se}}{3} \ln\left[1+\left(\frac{E_b}{E_c}\right)^{3/2}\right]$. Here $\tau_{se} \propto (T_e^{3/2}/n_e)$ is the Spitzer ion-electron slowing-down time, see 5.4.3 in [4], $\propto$ — means «proportional», and $E_c = 14.8(A_b/A_i^{2/3})\,T_e$ — the *critical energy*. The critical energy for a D-beam in a D-plasma at T_e = 5 keV is ~93 keV (~19T_e).

The FI toroidal current from the NB, normalized by 1 A injected is shown in Fig. 4 as a function of NB energy. The plot is calculated for mono-energetic deuterium beam (LNB) injected to FNS-ST plasma with T_e = 5 keV, n_e = $1 \cdot 10^{20}$ m^{-3}. The beam is injected in equatorial plane, the target radius is R_t = 0.5 m. The plasma kinetic profiles (T_e, n_e) are assumed parabolic with maximum at the magnetic axis.

Clearly, the energy dependence of the beam current is quite strong — 2-time energy rise results in threefold increase of NB current. It means that the total NB ratio can be more affected by the FI efficiency, than by neutralization yield in the injector.

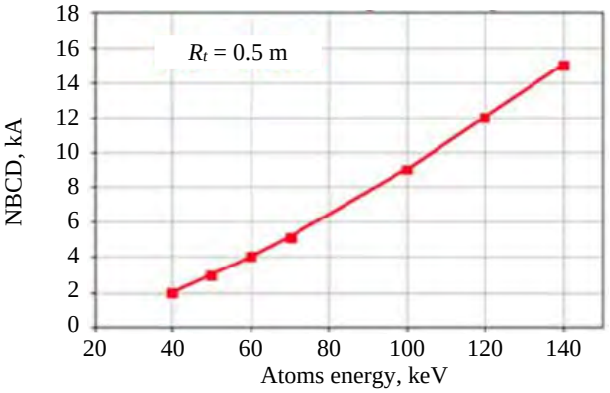

Fig. 4. LNB normalized toroidal current in FNS-ST due to fast ions slowing-down within the energy range selected for PIS-scheme

NBI TOTAL EFFICIENCY IN CURRENT

As the injected beam in PIS scheme comes with three energy fractions (E_{full}, $E_{1/2}$ and $E_{1/3}$), the cumulative ionization and current drive are calculated with the weight of each fraction. The calculations are made for the following values of NB energy: E_b = E_{full} = 100, 120, 140 keV. The neutral beam content is taken from Table 1, calculated for the source beam ratio $D^+ : D_2^+ : D_3^+$ = 0.75:0.15:0.10. The results of the specific FI current fractions and total FI current per 1 A injected are shown in Table 2. All the values are normalized to the injected current (specific or total) I_b = 1 A. The last row of the table shows the total NB efficiency in current (I_{CDtot}/I_s^+), represented as a product $F(I_s^+) \times G(I_b)$.

T a b l e 2. **Fast ions current (kA), efficiency, and total FI current in plasma for I_b = 1 A**

Parameter	E_b, keV					
	100		120		140	
	I_{CD}, kA	$G(I_b)$	I_{CD}, kA	$G(I_b)$	I_{CD}, kA	$G(I_b)$
E_{full}	9	4.05	12	4.87	15	5.61
$E_{1/2}$	3	0.8	4	1.13	5.2	1.47
$E_{1/3}$	1.7	0.5	2	0.66	2.5	0.87
NBCD $I_{CD\,tot}$, kA		5.35		6.66		7.95
Effective NB ratio $I_{CD\,tot}/I_s^+$	4.43		4.93		5.34	

Comments to Table 2: I_{CD}, kA — FI current, *normalized* to 1 A injected in a beam fraction; $G(I_b)$, kA — specific fraction contribution to the FI current, for 1 A current injected.

Data from Table 2 are presented as a chart in Fig. 5. It can be seen that for the energy range selected, the neutralization yield is the highest at E_b = 100 keV, but the overall NBI efficiency is the best at the upper limit E_b = 140 keV, so that the current gain I_{CDtot}/I_s^+ hits the maximum and can be about 5.34 kA per 1 A delivered by the ion source. For example, the NB source current 80 A would produce the output FI current: $I_{CD\,tot}$ = 354 kA — for E_b = 100 keV (the ion beam source power is P_0 = 8 MW); $I_{CD\,tot}$ = 430 kA — for E_b = 140 keV (and P_0 = 11.2 MW).

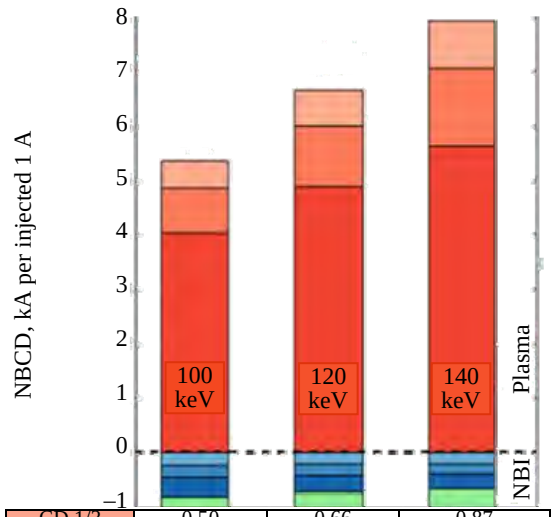

CD 1/3	0.50	0.66	0.87
CD 1/2	0.80	1.13	1.47
CD full	4.05	4.87	5.61
Atoms 1/3	0.24	0.24	0.23
Atoms 1/2	0.22	0.21	0.19
Atoms full	0.37	0.30	0.25
Residuals	0.17	0.26	0.33

Fig. 5. The neutral beam current gain for NB energy 100, 120, and 140 keV (red colors). The neutral beam fractions (E_{full}, $E_{1/2}$, $E_{1/3}$) are shown in blues, the residual ions fraction — in greens

CONCLUSION

NBI shows the best current generation performance among various plasma heating and CD systems. NBI is particularly important for fusion neutron sources design, as it makes the largest contribution to neutron production. In FNS-ST tokamak the beam-

plasma fusion is expected to be the main source of neutrons, so the neutral beam should be effectively captured by plasma and produce the high-energy tails in the ions spectra needed for beam-plasma fusion and neutron generation. As the fusion rates in the two-component system (beam + plasma) highly depend on the fast ions current and energy distributions, NBI shall be optimized to provide a reliable mechanism of steady-state current drive and fusion rate control.

The NB efficiency in current grows with the beam energy due to the beam higher penetration to the plasma core and longer ion relaxation time. However, the shine-through fraction increases with the beam energy as well, and both effects are measured when deciding on a particular energy value. The radial profiles of beam current generation strongly depend on the beam 3D deposition in plasma, the latter being sensitive to the beam structure, beam energy, the injection geometry (tangent point and tilting), plasma density and temperature profiles. All these effects have to be accounted for in the NBI optimization based on the beam efficiency study.

Initial assessment of beam deposition and slowing-down with LNB technique has proved, that for the energy range of 100—140 keV, a neutral beam with a nominal energy of ~140 keV is the best performer in terms of current drive. Although the neutral beam of 140 keV is produced with lower efficiency in current (67%), the current gain in plasma referred to the beam source current is the best (with multiplication factor ~8000), due to the longest path of the hot ions thermalization. For a beam source current of 80 A it provides a ~430 kA current of fast ions driven by the beam.

The work is supported by NRC «Kurchatov Institute».

REFERENCES

1. **Kuteev B.V. et al.** Steady state operation in compact tokamaks with copper coils. — Nucl. Fusion, 2011, vol. 51, p. 073013.
2. **Гончаров П.Р., Кутеев Б.В., Голиков А.А., Лукаш В.Э., Хайрутдинов Р.Р., Шпанский Ю.С., Сергеев В.Ю., Быков А.С., Грязневич М.П.** Сопоставление нейтронного выхода классических и сферических токамаков. — ВАНТ. Сер. Термоядерный синтез, 2011, вып. 2, с. 36—43.
3. **Голиков А.А., Кутеев Б.В.** Выбор параметров режима стационарного разряда в компактном токамаке. — ВАНТ. Сер. Термоядерный синтез, 2010, вып. 2, с. 50—58.
4. **Wesson J.** Tokamaks, 4th Edition 2011, Oxford: Oxford University Press.
5. **Janev R.K. et al.** Penetration of energetic neutral beams into fusion plasmas. — Nucl. Fusion, 1989, vol. 29, p. 2125.

AUTHORS

Eugenia D. Dlougach, senior scientist, NRC «Kurchatov Institute», 1, Academika Kurchatova sq., Moscow, 123182, Russia, edlougach@gmail.com

Alexander A. Panasenkov, PhD Head scientist, NRC «Kurchatov Institute», 1, Academika Kurchatova sq., Moscow, 123182, Russia, Panasenkov_AA@nrcki.ru

Boris V. Kuteev, Professor, Deputy Head Tokamak Department Fusion Research Centre; NRC «Kurchatov Institute», 1, Academika Kurchatova sq., Moscow, 123182, Russia, Kuteev_BV@nrcki.ru

Elena A. Filimonova, scientist, VANT assistant editor; NRC «Kurchatov Institute», 1, Academika Kurchatova sq., Moscow, 123182, Russia, alb@fc.iterru.ru

Статья поступила в редакцию 15 января 2021 г.
После доработки 16 марта 2021 г.
Принята к публикации 25 марта 2021 г.
Вопросы атомной науки и техники.
Сер. Термоядерный синтез, 2021, т. 44, вып. 2, с. 100—106.

UDC 621.039.673

ST40 PROGRESS TOWARDS OPTIMIZED NEUTRON PRODUCTION

M. Gryaznevich., A. Nicolai, V. Chuyanov and Tokamak Energy Ltd. Team

Tokamak Energy Ltd., United Kingdom

ST40 tokamak, which is now operational, can be used as a prototype of a Compact Fusion Neutron Source. Such (CFNS) can be optimized for tritium production and complement a modular Fusion Power Plant. Recent results from ST40 are presented and options to optimize ST40 for neutron production are discussed.

Key words: spherical tokamak ST40, compact fusion neutron source (FNS).

DOI: 10.21517/0202-3822-2021-44-2-107-110

ПРОГРЕСС ОПТИМИЗАЦИИ ПРОИЗВОДСТВА НЕЙТРОНОВ В СФЕРИЧЕСКОМ ТОКАМАКЕ ST40

М. Грязневич, А. Николаи, В. Чуянов и команда ООО «Токамак Энерджи»

ООО «Токамак Энерджи», Великобритания

Токамак ST40, который сейчас находится в эксплуатации, может быть использован в качестве прототипа компактного источника термоядерных нейтронов (КИТН). Такие КИТН могут быть оптимизированы для производства трития и стать частью модульной термоядерной электростанции. Представлены и обсуждаются последние результаты оптимизации ST40 по генерации нейтронов.

Ключевые слова: сферический токамак ST40, компактный источник термоядерных нейтронов.

INTRODUCTION

Tokamak Energy Ltd. is developing a modular approach to a fusion power plant [1]. In this new alternative route to fusion power, the economically feasible fusion power plant will consist of several low power modules. In all modular approaches, regular necessary maintenance is done offline in a module-to-module way, providing high availability of the power plant and lower maintenance cost. The approach saves time and resources needed for development, to improve reliability by the cheap reservation, to use economy of mass production. Our modular fusion plant will consist of several compact, low-power high-field spherical tokamak (ST) modules and auxiliary systems shared between them. This decreases the prototype costs (one module is actually a DEMO) and the fusion development risk [2]. The modular approach combines the advantages of the economy of scale for the conventional part of the plant and those of the economy of mass production for the fusion core and does not increase the plant's capital cost. At the same time, it permits to design a very efficient ST-based fusion power plant that allows for:

— high availability, due to reduced duration of the first wall change and maintenance. Modules can be serviced in turn, so electricity supply can be maintained;

— possibility for its units to share start-up (e.g., gyrotrons) and remote access facilities, as well as the hot cell for maintenance;

— establishing a sustainable supply chain, because the production of many small units is attractive to manufacturers.

Modules with acceptable fusion power and neutron wall loading should be in a narrow range of aspect ratios between $1.65 < R/a < 1.9$ [2]. Demonstration fusion module would aim to have a long pulse plasma operation with required fusion power and possible demonstration of tritium breeding, so it will be a compact ST FNS. The fusion module is not expected to be fully self-sufficient in tritium, and even in a full-scale power plant, the tritium self-sufficiency issue may be eased, as one of the modules will be customized to meet the tritium production need. A CFNS based on a compact ST may act as a tritium breeder, if neutron output is maximized. Neutrons can also be produced via DD- and D—^{3}He- (beam-plasma and beam-beam) reactions [3, 4], so there are ways to increase neutron production minimizing tritium consumption or even in DD. A CFNS based on a high-field ST may be also used for other non-electrical applications of fusion.

ST40 TOKAMAK AS A CFNS PROTOTYPE

ST40 (design parameters: R = 0.4—0.6 m, R/a = 1.6—1.8, I_{pl} = 2 MA, B_t = 3 T, k = 2.5, τ_{pulse} ~ 1—2 s, 3 MW NBI, 2 MW ECRH/EBW, DD/DT operation) is a currently operational compact spherical tokamak (Fig. 1), proposed as a CFNS test prototype.

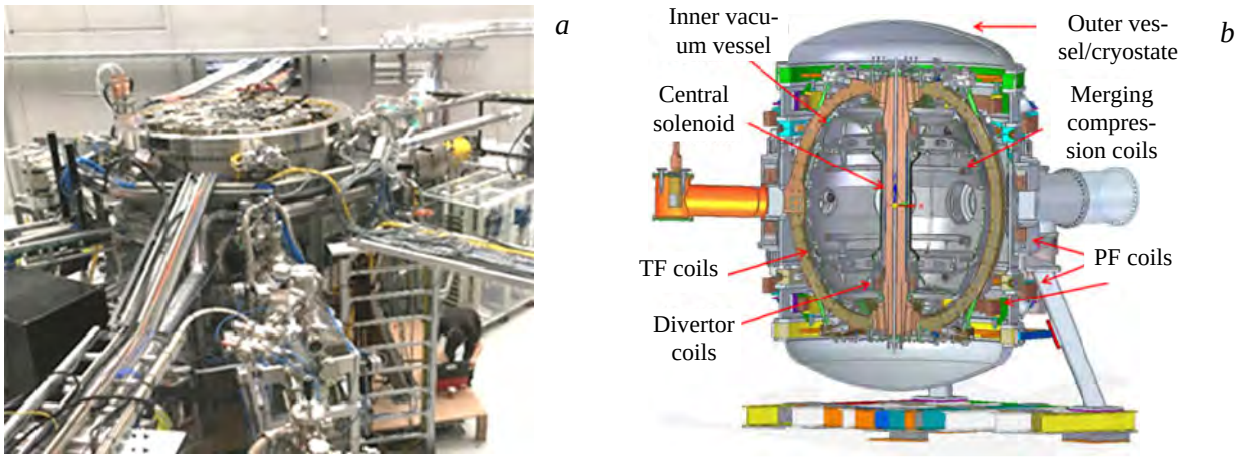

Fig. 1. ST40 tokamak: photo (*a*) and sectional drawing (*b*)

Waveforms for a typical discharge, obtained in 2018 during initial operations, are presented in Fig. 2. A CCD visible light image and EFIT reconstruction at 30 ms are also shown. Plasma current >0.5 MA at 2 T TF, electron and ion temperatures in a several — keV range produced using merging-compression formation, solenoid-assisted ramp-up and 1 MW of 25 kV NB heating, and densities up to 2×10^{20} m^{-3} have been achieved in later experimental campaigns in 2019—2020. At the flat-top, measured T_i increases with TF, in agreement with observations on other STs. However, on ST40, a sharp T_i and W_{EFIT} increase is observed at TF > 1—1.1 T (Fig. 3), which may suggest transition to a better confinement at higher TFs.

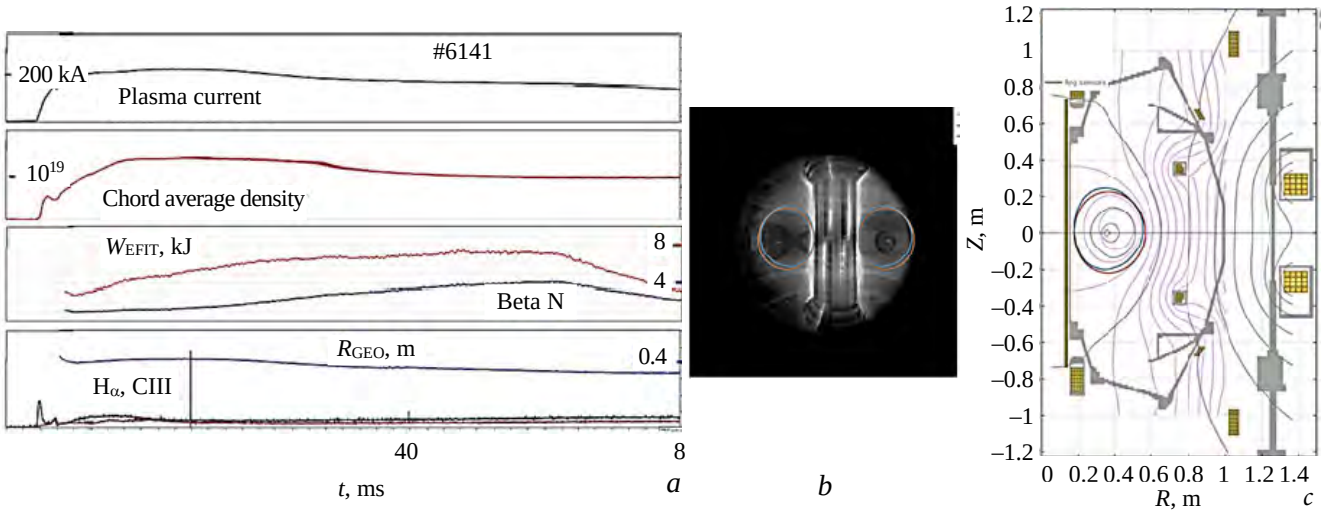

Fig. 2. Waveforms for a typical discharge with B_t = 1.3 T (*a*), CCD image (*b*) and EFIT reconstruction at t = 30 ms (*c*)

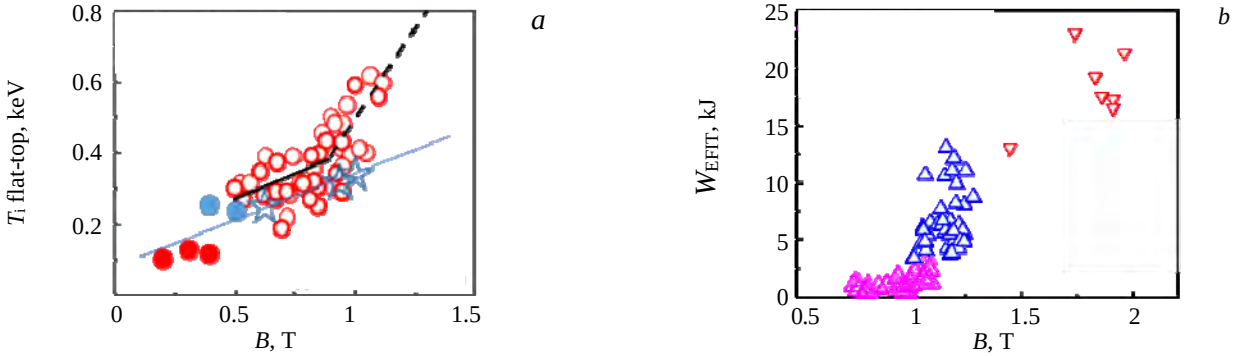

Fig. 3. T_i measured with Doppler spectroscopy on ST40 in 2018 (○ — T_i end of flat-top; ○ — T_i mid of flat-top), and with NPA on START (●) and Globus-M (●) against toroidal field, along with a predicted ion temperature assuming the Artsimovich formula (☆) (*a*); thermal energy W_{EFIT} against toroidal field: △ — W_{EFIT} 2018 Prog0; △ — W_{EFIT} 2019 Prog1; ▽ — W_{EFIT} 2019-20 Prog2 (*b*)

OPTIMIZATION OF CFNS NEUTRON PRODUCTION PERFORMANCE FOR

There are several ways to use ST40 for optimizing neutron production. One is to optimize beam-plasma and beam-beam reactions to enhance the neutron yield. This can be done by accelerating fast ions injected by NBI to a significantly higher energy, increasing the efficiency of beam reactions to make neutron production more efficient [3]. The cross-section of these reactions increases strongly with fast ion energy, and if the latter grows to a mega-electron-volt level, neutron production from some reactions may increase many fold compared to reactions that occur in pure thermal Maxwellian plasma of a 10 keV temperature range, Fig. 4.

In a high-field ST, the confinement of such high-energy ions may be significantly better than in conventional aspect ratio tokamaks or in STs with a low toroidal field, Fig. 5. The figure shows ion orbits for both trapped (1 MeV) and freely passing cases, observed in a ST. It is clear from Fig. 5 that fast ions have smaller orbits and spend more time at the high-field side. These effects help reduce fast ion losses and enhance the efficiency of reactions on fast particles. Fig. 6 shows the results of ion distribution and neutron yield simulation with the NFREYA full-orbit Monte-Carlo code and the FIFPC Fokker-Planck code [5]. We use a 1 MW, 50 keV beam and accelerate D ions by ICRH to 1 MeV. High neutron yield of up to 3.5×10^{17} n/s can be expected, summarising DD beam-beam, beam-plasma, DD-thermal and DT-thermal (tritium produced in the DD-reaction). Several other approaches for fast ion acceleration using ICRH can be considered [4].

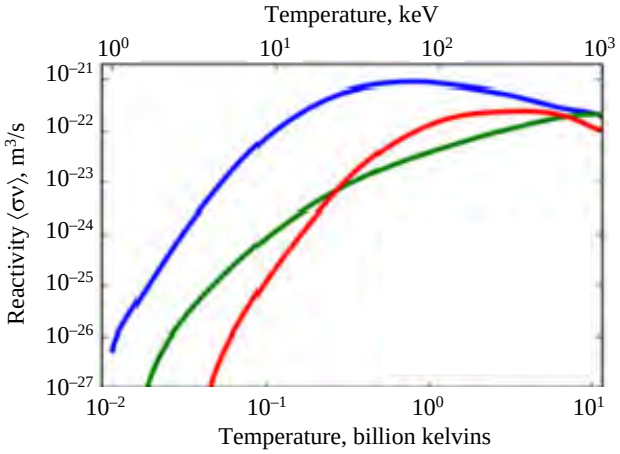

Fig. 4. Cross-sections of the primary fusion reactions: — D—T; — D—D; — D—He_3

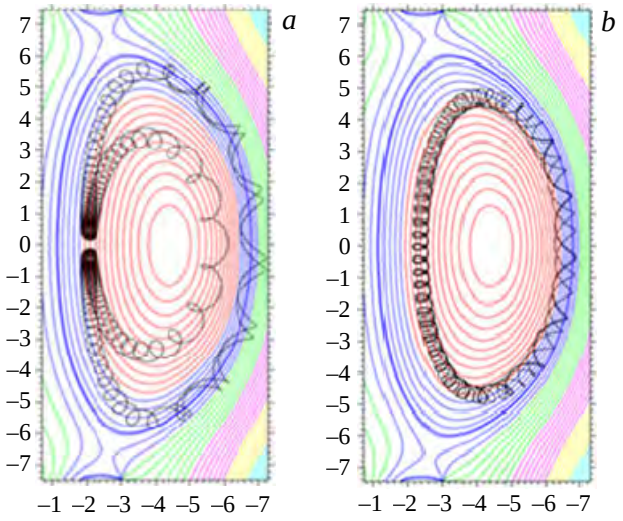

Fig. 5. Example of 1 MeV trapped (*a*), and passing, ion orbits in a ST (*b*)

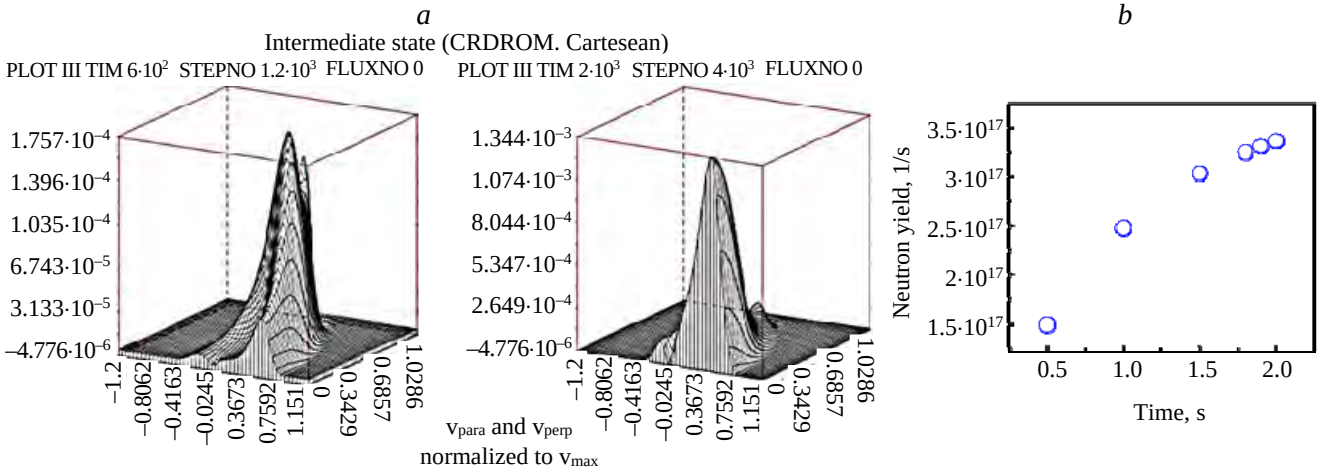

Fig. 6. Initial and final distribution of ions in velocity space: the background temperatures are T_e/T_i = 8.6 keV/6.4 keV, the density is $8\cdot10^{19}$ m^{-3} (*a*); neutron yield in time (*b*)

Acceleration of the fast ion tail by ECRH with beating ECR waves has been attempted on tokamaks and other plasma devices [6]. While the ratio of each EC wave frequency to the ion cyclotron frequency is large (100 GHz range), the frequency difference can be near the ion cyclotron frequency (tens of MHz), allowing the

IC wave to heat plasma. The waves interact in a region close to ECR, where the efficiency is at its maximum. It may also be possible to transfer microwave power to energetic ions by parametric decay near the upper-hybrid resonance [6]. High-field side launch of EBW will be used on ST40 to test this in a spherical tokamak.

If D and T nuclei are polarized parallel to magnetic field and to each other, fusion reactivity may be increased by 50% [7]. Calculations suggest that deuteron polarization can enhance the DD-reaction by a factor of between 1.5 and 2. Time to depolarize them by binary collisions is at least 5 times longer than the nuclear burning time. This will be of interest when a pure DD-fusion device is considered. The nuclei can be introduced into the fusion device by standard means, such as gas puffing, injection of energetic neutral beams or pellet injection.

CONCLUSIONS

Enhanced confinement of fast particles in STs opens up opportunities for boosting a high-field ST's neutron production efficiency. A CFNS based on a high-field ST may be used for tritium production and other non-electrical applications of fusion. ST40 experiments contribute to the assessment of a high-field ST as a CFNS prototype.

REFERENS

1. **Gryaznevich M. et al.** — J. of Physics: Conference Series, 2015, vol. 591, p. 012005.
2. **Chuyanov V.A., Gryaznevich M.P.** — Fusion Engineering and Design, 2017, vol. 122, p. 238.
3. **Mantsinen M.J. et al.** — Plasma Phys. Control. Fusion, 2003, vol. 45, p. A445.
4. **Kirov K.K. et al.** — AIP Conference Proceedings, 2020, vol. 2254, p. 030011.
5. **Gryaznevich M., Nicolai A., Buxton P.** — Nuclear Fusion, 2014, vol. 54, p. 104005.
6. **Hansen S.K. et al.** — Phys. Plasmas, 2019, vol. 26, p. 062102.
7. **Kulsrud R.M. et al.** — Nuclear Fusion, 1986, vol. 26, p. 1.

AUTHORS

Mikhail Petrovich Gryaznevich; mikhail. gryaznevich@tokamakenergy.co.uk

V. Chuyanov; Tokamak Energy Ltd. 173 Brook Drive, Milton Park, Oxon, OX14 4SD, United Kingdom
valery.chuyanov@tokamakenergy.co.uk

A. Nicolai; Tokamak Energy Ltd. 173 Brook Drive, Milton Park, Oxon, OX14 4SD, United Kingdom

Статья поступила в редакцию 15 января 2021 г.
После доработки 16 марта 2021 г.
Принята к публикации 25 марта 2021 г.
Вопросы атомной науки и техники.
Сер. Термоядерный синтез, 2021, т. 44, вып. 2, с. 107—110.

UDC 621.039.574.3

DEVELOPMENTS FOR STELLARATOR-MIRROR FUSION-FISSION HYBRID CONCEPT

V.E. Moiseenko[1], S.V. Chernitskiy[1], O. Ågren[2], N.B. Dreval[1], A.S. Slavnyj[1], Yu.V. Kovtun[1], A.V. Lozin[1], R.O. Pavlichenko[1], A.N. Shapoval[1], V.B. Korovin[1], M.M. Kozulya[1], N.V. Zamanov[1], A.Yu. Krasiuk[1], Y.V. Siusko[1], I.E. Garkusha[1]

[1]*NSC Kharkiv Institute of Physics and Technology, Kharkiv, Ukraine*
[2]*Uppsala University, Ångström laboratory, Uppsala, Sweden*

Conceptual development activities on a stellarator-mirror-based fission-fusion hybrid system (SM hybrid) are reviewed. Intended for transmutation of spent nuclear fuel and safe fission energy production, SM hybrid consists of a fusion neutron source and a powerful subcritical fast fission reactor core. Its fusion component is a stellarator with an embedded magnetic mirror. The stellarator allows for the confinement of a moderately hot (1—2 keV) deuterium plasma. In the magnetic mirror, the hot sloshing tritium ions are trapped and fusion neutrons are generated. The magnetic mirror is surrounded by a fission mantle, where transmutation of minor actinides and energy generation take place. One candidate magnetic confinement device for the SM hybrid is the advanced DRACON magnetic trap system, which, unlike the «classical» DRACON version, has one short, rather than two longer mirrors with a relatively short size of 3—6 m. A comparative numerical analysis of collisionless losses occurring in the magnetic trap part of the single-mirror DRACON leads to a conclusion about the possibility for high-energy tritium ions to be fairly well confined in the magnetic trap area. The Uragan-2M (U-2M) stellarator is used to test the SM hybrid concept with experiment. To fit a magnetic trap into U-2M system, one of the toroidal coils had to be switched off. A radial escape of charged particles may spontaneously give rise to a weak radial electric field, which may result in closing the particles' drift trajectories and thereby substantially improve their confinement. Background plasma confinement without destructive instabilities is demonstrated in the stellarator-mirror regime of U-2M) operation. The sloshing ions driven by radio-frequency heating are detected in the mirror part of the device with NPA diagnostics. A novel fission mantle design for the SM hybrid is proposed.

Key words: fusion-fission hybrid, stellarator, magnetic mirror, nuclear transmutation.

DOI: 10.21517/0202-3822-2021-44-2-111-117

РАЗРАБОТКА КОНЦЕПЦИИ СТЕЛЛАРАТОРНО-ПРОБКОТРОННОЙ ГИБРИДНОЙ УСТАНОВКИ СИНТЕЗА-ДЕЛЕНИЯ

В.Е. Моисеенко[1], С.В. Черницкий[1], О. Агрен[2], Н.Б. Древаль[1], А.С. Славный[1], Ю.В. Ковтун[1], А.В. Лозин[1], Р.О. Павличенко[1], А.Н. Шаповал[1], В.Б. Коровин[1], М.М. Козуля[1], Н.В. Заманов[1], А.Ю. Красюк[1], Е.В. Сюсько[1], И.Е. Гаркуша[1]

[1]*Национальный научный центр «Харьковский физико-технический институт», Харьков, Украина*
[2]*Упсальский университет, лаборатория Ангстрем, Упсала, Швеция*

Рассматривается концептуальный проект стеллараторно-пробкотронной гибридной системы синтеза-деления (СП-гибрид). Предназначенный для трансмутации отработавшего ядерного топлива и безопасного производства энергии при делении тяжёлых ядер СП-гибрид состоит из источника термоядерных нейтронов и мощной подкритической активной зоны реактора деления, работающего на быстрых нейтронах. Его термоядерный компонент является стелларатором со встроенным пробкотроном. Стелларатор позволяет удерживать умеренно горячую (1—2 кэВ) дейтериевую плазму. В пробкотроне горячие плещущиеся ионы трития захватывают и генерируют термоядерные нейтроны. Пробкотрон окружён мантией, в которой происходят деление тяжёлых ядер, трансмутация минорных актиноидов и генерация энергии. Одним из возможных устройств магнитного удержания для СП-гибрида является усовершенствованная система магнитной ловушки ДРАКОН, которая в отличие от «классической» версии ДРАКОНА имеет один короткий пробкотрон, а не два более длинных, имеющий размер в пределах 3—6 м. Сравнительный численный анализ бесстолкновительных потерь, возникающих в той части пробкотрона, где находится магнитная ловушка ДРАКОН, позволяет сделать вывод о возможности достаточно хорошо удерживать высокоэнергетические ионы трития в области этой магнитной ловушки. Стелларатор «Ураган-2М» (U-2M) используется для экспериментальной проверки концепции гибридной стеллараторно-пробкотронной системы. Для установки магнитной ловушки в систему U-2M необходимо было отключить одну из тороидальных катушек. Радиальный выход амбиполярных частиц может спонтанно вызвать слабое радиальное электрическое поле, которое может замкнуть траектории дрейфа частиц и тем самым существенно улучшить их удержание. Удержание плазмы без разрушительных неустойчивостей продемонстрировано в стеллараторно-пробкотронном режиме работы U-2M. Горячие ионы, появившиеся в результате радиочастотного нагрева, регистрируются в пробкотронной части этого устройства с помощью анализатора нейтральных частиц. Предложена новая конструкция ядерной части для СП-гибрида, в которой будет происходить деление ядер.

Ключевые слова: гибридная система синтеза-деления, стелларатор, пробкотрон, трансмутация ядер.

INTRODUCTION

Current nuclear power plants rely mainly on ^{235}U fission for power generation. The ore reserves of this uranium isotope are not large, and the future of nuclear power production is associated with utilizing ^{238}U

and ^{232}Th, which are abundant. This situation has three implications. Number one is that the large amount of spent nuclear fuel already generated by the nuclear industry continues to grow. Today, the preferred option for nuclear waste management is long term geological storage with a view to keep the wasteisolated until the radionuclides have decayed to acceptable levels. However, the decay may last thousands of centuries, which is hardly acceptable. Therefore, geological storage should be looked upon as a way to gain some time before a full-scale incineration of spent nuclear fuel is in place. Unlike geological storage, incineration is consistent with the sustainability concept.

Number two is the inevitable need for introducing a new fuel cycle to allow ^{238}U and ^{232}Th to be used as a fuel. Both isotopes cannot be directly burned, and the first stage of this fuel cycle includes breeding of ^{239}Pu and ^{233}U. The fission of these isotopes, as well as many others, results in a twice as small fraction of delayed neutrons as the fission of ^{235}U. This seriously hinders the controllability of critical reactors. Another need is for introducing a closed fuel cycle, in which, in the best-case scenario, waste would only consist of fission products. Such waste could be stored in a geological repository for a much shorter time of about 300 years. In the closed fuel cycle, all fissionable isotopes involved in the nuclear chain must be burned. This is only possible in fast reactors. Unfortunately, many fast reactor concepts are difficult to implement due to the positive reactivity accompanying a temperature increase. This, coupled with the shortage of delayed neutrons, has a serious impact on reactor safety. Implication number three is that ^{235}U cannot be easily synthesized. If we burn it up completely, there will be no ^{235}U left for future generations.

A solution is a subcritical fast reactor driven by an external neutron source. Inherently safe, it can be used for burning fertile components of spent nuclear fuel, nuclear breeding and energy generation under the closed fuel cycle. The neutron source for this reactor must be powerful and efficient. Two obvious candidates for the role of drivers of a sub-critical fast reactor are the spallation and fusion neutron sources, of which the latter are more compact, more feasible and less costly. In turn to, there are three major lines of fusion-fission hybrids (subcritical fission reactors driven by a fusion neutron source), i.e. tokamak, mirror and stellarator-mirror based hybrids.

Tokamak [1] offers the best plasma confinement. However it allows an acceptable neutron budget to be only achieved with an excessive neutron production. Tokamak's another inherent weakness is the pulsed-mode operation with a long (~100 s) duty cycle.

In a mirror-based hybrid [2], plasma confinement is poor, which translates into the machine's low energy efficiency and huge size.

The SM hybrid [3, 4] has an acceptable plasma confinement, stationary operation and a very compact design.

THE SM HYBRID

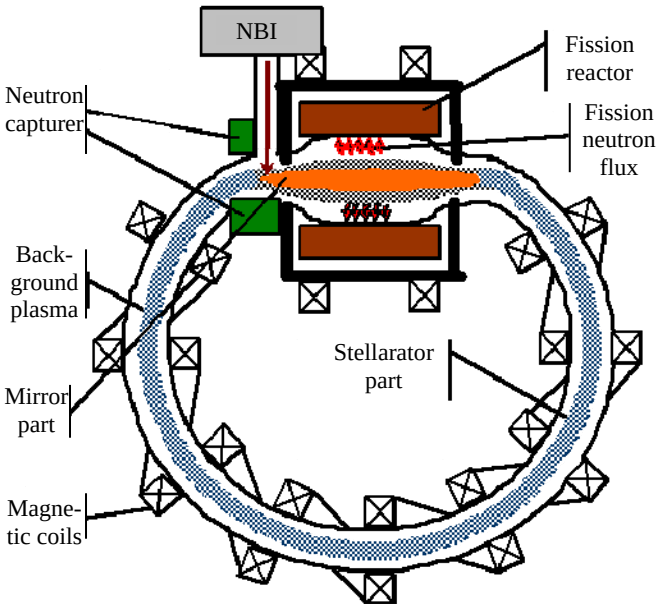

Fig. 1. Sketch of the fission-fusion hybrid

In the SM hybrid, fusion neutrons are generated in a deuterium-tritium plasma, confined magnetically in a stellarator-type system (Fig. 1). The plasma contains a warm electron component, and the majority of deuterium ions are in thermal equilibrium with electrons. The stellarator provides a steady-state operation and offers a relatively good confinement for such a warm Maxwellian plasma. Hot minority tritium ions are sustained in the plasma by a radio-frequency (RF) heating [5—8]. Considering the stellarator's inferior ability to confine high energy ions, it is proposed in [3] to integrate it with a magnetic trap with lower field. Hot ions mostly have perpendicular to the steady magnetic field kinetic energies. Because of the trapping effect, the hot (sloshing) ions' motion is restricted to the mirror part of the

device. The containment of hot sloshing ions and, therefore, contraction the neutron production zone to the mirror part is favorable, as it makes it sufficient to only have the mirror part surrounded with a fission mantle. Furthermore, all sensitive plasma diagnostics and plasma control devices could be located at the stellarator part, but at a distance of the fission reactor zone, where the neutron flux is reduced.

It is not only RF heating that can sustain hot sloshing ions, but also a continuous neutral beam injection (NBI). The latter is implemented in both stellarators [9] and mirror machines [10].

For mirror-based hybrids, a quasi-tangential injection to the mid plane is typical. In comparison with normal injection, it allows the injection energy to be increased. However, a mid plane injection can seriously affect the reactor design, requiring either the reactor division into two independent nuclear reactor cores [11] or, in the case of a single reactor core, introduction of beam lines within the reactor core. Each of those modifications is a major engineering challenge.

Normal injection seems preferable, as it implies a smaller neutron loss from fission core and allows beam lines to be placed out side of the reactor core. To avoid beam shine-through, the shorter beam-plasma interaction distance is offset with a tolerable plasma density increase. The configuration with an NBI at the mirror ends, presented here, is similar to the scheme reported in [12]. The NBI is normal to the magnetic field and targets plasma just near the fission mantle border (see Fig. 1). Shined-through atoms, outnumbered by injected atoms, hit the armor made of refractory material (tungsten) and placed opposing to the NBI port.

The first step in the study of the SM hybrid is to analyze the power balance [4, 13] and thereby estimate the plasma machine size, the magnetic field strength, power needed for the sustain of hot ions and the overall power efficiency. The analysis used the results of the ISS04 stellarator scaling [14] and kinetic calculation. The calculations resulted in a compact device with achievable characteristics. The parameters of the device chosen as a demo machine are given in [3]. They are as follows:

Stellarator beta . . .	0.01
Mirror beta . . .	0.15
Tritium injection energy, keV . . .	150
Beam shine-through parameter (ratio of ion mean-free path to plasma radius) . . .	1.5
Background plasma temperature, keV . . .	1.6
Stellarator part magnetic field, T . . .	4.1
Mirror ratio . . .	1.7
Angle of rotational transform . . .	0.8
Inverse aspect ratio . . .	0.05
Plasma density, cm^{-3} . . .	$1.5 \cdot 10^{14}$
Tritium concentration (in mirror part)	0.11
Heating power, MW . . .	20
Fission power, MW . . .	570
Plasma minor radius, cm . . .	20
Torus major radius, m . . .	4
Mirror length, m . . .	3.2
Electric efficiency Q_{el} (for nuclear mantle with $k_{\text{eff}} = 0.95$) . . .	4.8
Estimated cost, M$ . . .	500

This SM hybrid version is used for neutronic calculations and cost estimates.

FUSION PART OF THE SM HYBRID

The SM hybrid's magnetic system is a combination of a stellarator and a mirror. It was first implemented as part of the U-2M stellarator at the Kharkiv Institute of Physics and Technology in Ukraine. There are two big questions about this magnetic system, viz. (i) whether it can have magnetic surfaces, and (ii) whether it can confine hot ions in its mirror part.

Studies at U-2M. Stellarator U-2M was involved in modeling such system, [15]. It has the advantage of a winding availability, which allows using an additional toroidal magnetic field. The winding accommodates

16 separate magnetic coils. The switching off of one of them produces a local mirror inside it with a proper mirror ratio of 1.5 [16].

First Biot-Savart magnetic calculations were done to model the field with the coil switched off. Several practically important cases were identified, where the field lines formed nested magnetic surfaces in the device. Next, experiments to measure the magnetic configuration had been performed [17], which verified the theoretical data and demonstrated the magnetic configurations of U-2M with an embedded magnetic mirror.

A theoretical study was carried out to analyze the behavior of fast ions in the mirror part of U-2M [18]. It involved Biot-Savart magnetic calculations and drift surface calculations based on motion invariants. The study confirms poor confinement properties of the magnetic mirror created in the U-2M stellarator by means of switching off one toroidal field coil. The created magnetic mirror had a flaw, namely, a curved magnetic axis. Calculated drift surfaces were not closed, hence, there was no radial confinement. Such a situation can be avoided if the embedded mirror would have a straight magnetic axis. Unfortunately, this cannot be realized in U-2M. Meanwhile, the radial electric field can improve the situation substantially in U-2M. It causes a particle drift in the poloidal direction which competes with the vertical magnetic drift. Above a certain value of the electric field, mean drift surfaces become closed, and particle confinement improves. This value can be obtained from $e\varphi \sim \mu\Delta B$, where φ is the electric potential, μ is the magnetic moment and ΔB is the variation of the magnetic field across the confinement volume. To establish the electric potential in the plasma column, a very small amount of lost ions is sufficient. The electric potential seems to be small enough to perturb the diffusive character of confinement of the bulk plasma.

Such an opportunity to confine fast ions is checked experimentally at U-2M (see below). Since the RF heated ions are confined at the mirror part of U-2M, one can suggest that the regime with the radial electric field is realized in that case.

Plasma generation in U-2M in SM hybrid regime. The U-2M — based experiments proved the possibility of background plasma production and confinement. A discharge was initiated by a RF pulse of a crankshaft antenna [19]. The discharge start-up was successful, as produced a ~10^{12} cm^{-3} plasma. The OV and CV lines showed up in the discharge. Their intense emission, especially that of the CV line, indicates an electron temperature of at least 100 eV. The parameters of the stellarator-mirror discharge are lower, but compatible with those of regular discharges.

Experimental study of fast ion generation in the embedded mirror. An experiment to generate sloshing ions in an embedded mirror was carried out on the U-2M stellarator. The magnetic beach approach was employed. A compressional Alfven wave was launched with a two-strap (W7-X like) antenna operated in monopole phasing. It is expected [5] that on the way to the embedded mirror, at a lower magnetic field, the wave reaches the ion cyclotron layer and accelerates the trapped ions. The neutral particle analyzer is used to detect high-energy ions.

The U-2M stellarator was recently equipped with a passive single-energy channel electrostatic small-angle 30° CX neutral particle analyzer (NPA) without mass separation similar to that described in [20]. Sweeping voltage NPA operating regimes [21] were used. A 2—5 ms analyzing voltage with triangular temporal shape was applied to electrostatic plates to enable a fast (2—5 ms) measurement of energy distribution using a single-energy channel analyzer. An additional 15 keV acceleration of ions after the electrostatic separation and ion-electron conversion allowed the suppression of the NPA collector energy sensitivity [21]. The NPA was located close to the switched off toroidal field coil and not far away from the W7-X like RF antenna, used for the ion cyclotron heating. Nitrogen was used in the NPA gas stripping cell. The 10—100 eV energy range was not covered by the NPA. Variations of line of sight angle allow us measuring the CX flux distribution from the plasma center to the edge. Very high CX fluxes in U-2M RF discharges allowed an analog NPA signal to be obtained. The NPA signal integration time was 0.1 ms, and its sampling rate was about 50 000 samples/s. Substantial CX flux as well as fraction of fast ions with perpendicular energy characterized by temperature of 400—500 eV was observed in pure hydrogen RF discharges in the U-3M stellarator [21], as well as in recent experiments invol-

ving the U-2M stellarator. Here we are demonstrating the strong transient CX flux in a «hybrid» configuration discharge, as shown in Fig. 2.

The CX flux radial distribution indicates that the energetic ions are localized in the centre of the plasma column. It should be admitted that the sweeping voltage of 1 kV corresponds to ion energy of 4.5 keV due to the NPA calibration coefficient [21, 22]. Ions with energies of 4.5 keV in the U-2M hybrid configuration are clearly seen in Fig. 2. Here we report the first experimental evidence of fast ions in a hybrid system. Although the presence of 0.5—4.5 keV ions is evident, some unclear points, e.g., different mechanisms of energetic ion generation in conventional stellarator and hybrid configurations are yet to be addressed.

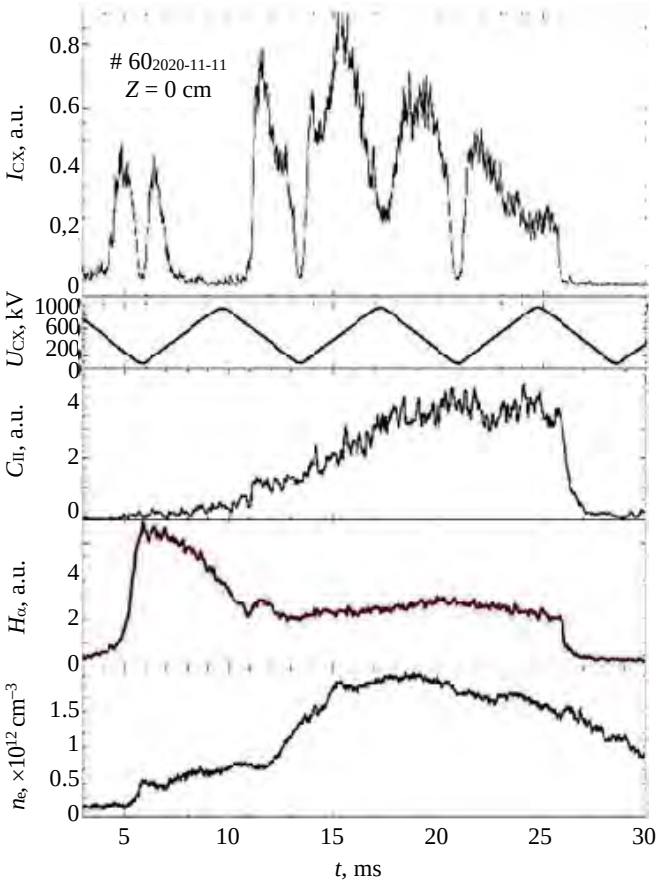

Fig. 2.Waveforms of the row NPA signal, NPA sweeping voltage, spectral lines C_{II} and H_α emission and line-averaged density in hybrid configuration pure H discharge: $p = 2.4\times10^{-3}$ Pa, $B_0 = 0.38$ T, 2.5 ms (start of the pre-ionization with K-2 RF generator), 12.5 ms (shutdown) K-2: $f_2 = 5.36$ MHz, $U_a = 4$ kV, RF power ~30 kW, 12.5 ms (start of main pulse with K-1 RF generator), 27.5 ms (shutdown) K-1: $f_1 = 4.9$ MHz, $U_a = 5.5$ kV, RF power ~80 kW

DRACON as a plasma confinement component of the SM hybrid. One candidate magnetic confinement device for the SM hybrid is the DRACON magnetic trap system, which, unlike the «classical» DRACON version, has one short, rather than, two longer mirrors. The equilibrium stellarator configuration DRACON (see [18] and references therein) consists of two rectilinear regions and two curvilinear elements (known as CREL), which close the magnetic system and whose parameters are chosen so as to keep the Pfirsch—Schluter currents within the CREL and to prevent them from penetrating into the rectilinear sections. In order to improve plasma confinement, the magnetic field in the CRELs is higher than the field in the rectilinear parts. So, in fact the rectilinear parts represent two mirror traps, which are closed by the CRELs. Fusion reactions in such a device can be realized in the mirror parts, which help to confine the hot ion component (tritium) with high perpendicular energy. A comparative numerical analysis of collision less losses occurring in the magnetic trap part of the single-mirror DRACON [18] leads to a conclusion about the possibility for high-energy tritium ions to be fairly well confined in the magnetic trap area.

FISSION PART OF THE SM HYBRID

The acquired knowledge of the fusion neutron source parameters can be used to obtain the initial conditions for a preliminary design of the hybrid's fission mantle part. The mantle design is mostly based on the results of engineering research described in [23].The cylindrical reactor is compact, with a 1.6-m radius and a 4-m length. Its major parts (Fig. 3), moving from the axis to the major radius, are the inner opening for the plasma column, the first wall, the LBE (lead-bismuth eutectic) buffer, the metal fuel-loaded, LBE-cooled active zone, the core extension zone (filled by LBE), and the reflector. Fuel for the fission

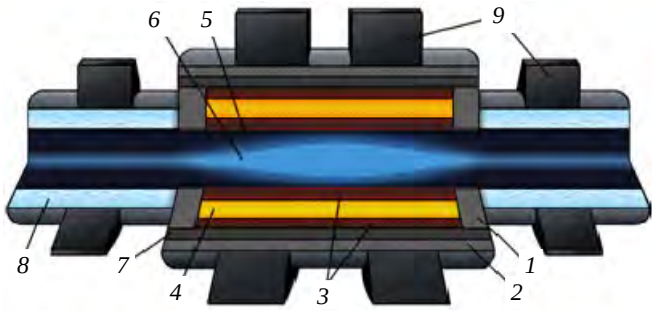

Fig. 3. Reactor part of the SM hybrid: *1* — axial reflector (HT-9 steel 70% and LBE 30%); *2* — 60:40 Vol.% mixture of the stainless steel S30467 tipe 304B7 with water, the steel contains 1.75% wt of natural boron; *3* — coolant (lead and Bismuth eutetic); *4* — fission blanket; *5* — first wall; *6* — neutron souce (D—T-plasma); *7* — radial reflector (HT-9 steel 70% and $Li_{17}Pb_{83}$ 30%, enrich 20% ^{6}Li); *8* — borated water with B, 10 g/kg; *9* — magnetic coils

component is produced by separating uranium and fission products from spent nuclear fuel. Actual fuel material is an alloy (TRU—10Zr) consisting of transuranic elements with 10% wt zirconium [24]. The active zone size is chosen using MCNPX calculations to achieve the effective neutron multiplication factor $k_{\text{eff}} \approx 0.95$. For the discussed reactor, the calculated fusion power multiplication factor is 65. There are only 5 t of transuranic elements in the fuel. This suggests that a nuclear plant operated at full capacity will need to refuel every 1—2 years.

PRELIMINARY COSTS ESTIMATES

There is no point in doing the required experiments based on a downscaled prototype, as the hybrid machine itself is quite small. Taking the Wendelstein7-X stellarator's cost, EUR 1 billion (https://en.wikipedia.org/wiki/Wendelstein_7-X), as a reference and considering that:

— the SM machine is smaller;

— the diagnostic equipment is less advanced;

— the coils and the vacuum chamber are much simpler (in DRACON's case);

— the cost could be decreased to EUR 0.2—0.3 billion.

The fission mantle is expected to be installed after the completion of the «plasma part» test. Its cost can be put at EUR 0.2 billion based on the cost of the BREST-OD-300 (EUR 0.3 billion), the project carried out by Russia's Rosatom (https://www.riatomsk.ru/article/building_%20reactor_seversk). The total cost estimate for a hybrid with a fission mantle is then in the range of EUR 0.4—0.5 billion. This is less than the cost of the accelerator-driven MYRRHA system (around EUR 1.6 billion (https://en.wikipedia.org/wiki/MYRRHA)).

DEMO MACHINE OPERATION PROSPECTS

The DEMO device needs 20 MW of RF power, which is high, but not exceptional: such a power is available, for instance, at the JET tokamak. Power supply could be provided by 1—2 MW modules and enlarged step by step to a total of 5 MW, needed for initial experiments. Frequency could be set at 27.2 MHz, the standard industrial value. It makes sense to start those experiments using the ^{3}He—H mixture, a halved magnetic field and low power (5 MW). For a 3/4 magnetic field, the D—^{3}He mixture could be used. The fission mantle can be installed after the completion of the «plasma part» test.

With around EUR 0.5 billion of investment, the SM hybrid based on the spent fuel incineration technology could be developed in 10—15 years.

SUMMARY AND CONCLUSIONS

The U-2M experimental studies suggest that the SM hybrid key properties are achievable. This machine offers the prospect of a successful implementation of the stellarator-mirror plasma trap technology. It is designed in such a way that the desired properties, including background plasma confinement and generation/confinement of hot ions at the mirror part are fully feasible. There is reason to be hopeful that developing an appropriate device is a realistic undertaking.

Calculations suggest that the plasma part of the SM hybrid could be a DRACON-like device with a single embedded mirror as short as needed.

The MCNPX calculations for the fission mantle are in line with a robust device design and operation, with no major engineering challenges looming.

The fuel mass is small enough, and refueling is needed every 1—2 years.

The estimated cost of the DEMO device for the SM hybrid is just EUR 500 million, which is the lowest for hybrid devices. It is just twice as large as the cost of a critical reactor of the same power. But the safety advantage could be a decisive argument in favor of hybrids to be used for regular power production under the closed fuel cycle.

REFERENCES

1. **Kuteev B.V. et al.** — Nucl. Fusion, 2011, vol. 51, p. 073013.
2. **Ågren O., Moiseenko V.E., Noack K.** — Fusion Science and Technology, 2010, vol. 57, № 4, p. 326.

3. **Moiseenko V.E., Noack K., Ågren O.** — J. Fusion Energy, 2010, vol. 29, p. 65.
4. **Moiseenko V.E., Kotenko V.G., Chernitskiy S.V. et al.** — Plasma Phys. Control. Fusion, 2014, vol. 56, p. 094008 (11p.).
5. **Moiseenko V.E., Ågren O.** — J. of Physics: Conference Series, 2007, vol. 63, p. 012004.
6. **Moiseenko V.E., Ågren O.** — Phys. Plasmas, 2005, vol. 12, p. 102504.
7. **Moiseenko V.E., Ågren O.** — Phys. Plasmas, 2007, vol. 14, p. 022503.
8. **Moiseenko V.E., Ågren O.** — AIP Conf. Proc., 2012, vol. 1442, p. 199. doi:http://dx.doi.org/10.1063/1.4706869.
9. **Yamada H. et al.** — Nucl. Fusion, 2003, vol. 43, p. 749.
10. **Zuev A.A. et al.** — Plasma Phys. Rep., 2002, vol. 28, p. 268.
11. **Noack K. et al.** — Annals of Nuclear Energy, 2008, vol. 35, p. 1216.
12. **Ryutov D.D., Molvik A.W., Simonen T.C.** — J. Fusion Energy, 2010, vol. 29, p. 548.
13. **Moiseenko V.E., Ågren O.** — Fusion Science and Technology, 2013, vol. 63, № 1T, p. 119.
14. **Yamada H. et al. —** Nucl. Fusion, 2005, vol. 45, p. 1684.
15. **Bykov V.E. et al.** — Fusion Technology, 1990, vol. 17, p. 140.
16. **Kotenko V.G., Moiseenko V.E., Ågren O.** — AIP Conf. Proc., 2012, vol. 1442, p. 167.
17. **Lesnyakov G.G. et al.** — Problems of Atomic Science and Technology. Series: Plasma Physics, 2013, vol. (83), № 1, p. 57.
18. **Moiseenko V.E. et al.** — Plasma Phys. Control. Fusion, 2016, vol. 58, p. 064005 (8 p.).
19. **Moiseenko V.E. et al.** — Nukleonika, 2016, vol. 61(2), p. 91.
20. **Afrosimov V.V. et al.** — Soviet Phys. Tech. Phys., 1961, vol. 5, p. 1378.
21. **Dreval M., Slavnyj A.S.** — Plasma Phys. Control. Fusion., 2011, vol. 53, p. 065014.
22. **Slavnyj A.S. et al.** — Problems of Atomic Science and Technology. Series: Plasma Physics, 2021, vol. 131, № 1, p. 25.
23. **Chernitskiy S.V. et al.** — Annals of Nucl. Energy, 2014, vol. 72, p. 413.
24. **Stacey W.M. et al.** — Fusion Science and Technology, 2002, vol. 41, p. 116.

AUTHORS

Uppsala University, Ångström laboratory, Box 534, SE 751 21 Uppsala, Sweden
Olov Ågren, Olov.Agren@angstrom.uu.se

Institute of Plasma Physics, National Science Center «Kharkiv Institute of Physics and Technology», 61108 Kharkiv, Ukraine

V.E. Moiseenko, moiseenk@ipp.kharkov.ua; S.V. Chernitskiy; M.B. Dreval; A.S. Slavnyj; Yu.V. Kovtun; A.V. Lozin; R.O. Pavlichenko; A.N. Shapoval; V.B. Korovin; M.M. Kozulya; N.V. Zamanov; A.Yu. Krasiuk; Y.V. Siusko; I.E. Garkusha

Статья поступила в редакцию 15 января 2021 г.
После доработки 16 марта 2021 г.
Принята к публикации 25 марта 2021 г.
Вопросы атомной науки и техники.
Сер. Термоядерный синтез, 2021, т. 44, вып. 2, с. 111—117.

UDC 621.039.624

3D COILS FOR A COMPACT MIN *B* MIRROR FIELD WITH MINIMAL FLUX TUBE ELLIPTICITY

O. Ågren[1], V.E. Moiseenko[2]

[1]*Uppsala University, Uppsala, Sweden*
[2]*Institute of Plasma Physics, National Science Centre Kharkiv Institute of Physics and Technology, Kharkiv, Ukraine*

We determine coil arrangements for reproducing a minimum-*B* mirror magnetic field, optimized with respect to plasma stability, plasma cross-section ellipticity and particle drift surfaces. The reproduction has to be done with precision, as field errors may give rise to plasma instabilities or collisionless plasma losses due to the guiding centres' drift away from the confinement region. We have developed a set of twisted «fishbone» coils to allow an array of coils to be flexibly stacked, as required for a precise magnetic field reproduction. Results suggest that high mirror ratios of around 10 can be obtained using a fishbone coil arrangement. The mirror ratio can be further increased by finite plasma beta. Parameters representative of a compact 10 MW fusion neutron source have been derived.

Key words: biasing end plates, magnetic mirror, mirror machine, hybrid reactor, fusion neutron source, minimum *B*.

DOI: 10.21517/0202-3822-2021-44-2-118-123

ТРЁХМЕРНЫЕ КАТУШКИ ДЛЯ ПОЛУЧЕНИЯ КОМПАКТНОГО МАГНИТНОГО ПОЛЯ С МИНИМАЛЬНОЙ ИНДУКЦИЕЙ И МИНИМАЛЬНОЙ ЭЛЛИПТИЧНОСТЬЮ ТРУБОК МАГНИТНОГО ПОТОКА ПЛАЗМЫ В ТЕРМОЯДЕРНЫХ УСТАНОВКАХ С МАГНИТНЫМИ ПРОБКАМИ

О. Агрен[1], В.Е. Моисеенко[2]

[1]*Университет Уппсалы, Уппсала, Швеция*
[2]*Институт физики плазмы, Национальный научный центр «Харьковский физико-технический институт», Харьков, Украина*

Мы определяем расположение трёхмерных катушек в пробкотроне с минимум *B*, оптимизированного с точки зрения стабильности плазмы, эллиптичности поперечного сечения плазмы и поверхностей дрейфа частиц. Воспроизведение должно быть выполнено с большой точностью, так как ошибки поля могут привести к нестабильности плазмы или бесстолкновительным потерям плазмы из-за дрейфа направляющих центров из области удержания плазмы. Мы разработали твистированные катушки «фишбон», которые позволяют гибко укладывать массив катушек в соответствии с требованиями точного воспроизведения магнитного поля. Результаты расчётов показывают, что высокие пробочные отношения около 10 могут быть получены с помощью катушек «фишбон». Пробочное отношение может быть дополнительно увеличено за счёт конечного значения бета плазмы. Получены параметры, характерные для компактного источника термоядерных нейтронов мощностью 10 МВт.

Ключевые слова: смещающие торцевые пластины, пробкотрон, установка с магнитными пробками, гибридный реактор, источник термоядерных нейтронов, минимальная индукция магнитного поля.

INTRODUCTION

A minimum-*B* mirror field, optimized with respect to plasma stability, plasma cross-section ellipticity and particle drift surfaces has been derived in [1], Fig. 1 (the confinement region has essentially straight and nonparallel magnetic field lines). The shape of the magnetic surface cross section evolves from circular at the mid plane to elliptical near the magnetic field maximum and regains a circular shape at the expander tank wall, where ring-shaped end plates biased to different voltages could be placed. The plot is for a case, where a = 40 cm (plasma radius), c_L = 4 m (longitudinal scale length), R_m = 4 (mirror ratio) and M = 3 (magnification of the flux tube cross sectional area at the end tank). In the present paper, we investigate how such a target field can be reproduced by some appropriate arrangement of superconducting 3D-coils. The reproduction of the magnetic field

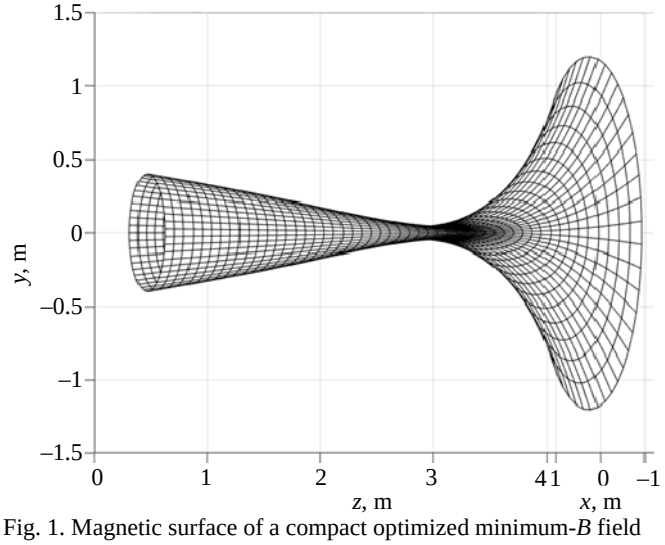

Fig. 1. Magnetic surface of a compact optimized minimum-*B* field

needs to be quite precise, since field errors may trigger plasma instabilities or cause collisionless plasma losses by guiding centers drifting away from the confinement region. Straight Ioffe bars and variants of baseball coils and ying-yang coils have been used to create a quadrupolar mirror magnetic field, but the flexibility to shape the magnetic field in more detail is limited, if the coil design does not permit a flexible stacking of many coils. This study is an extension of the research reported in [2], where a special set of «fishbone coils» was introduced for a quadrupolar minimum-*B* field. We will use a slight modification of those coils in the present study, and expand the parameter range for the reproduction of magnetic field and present a convenient way to make a good precision fit to the target field. Some tasks of interest are constraints set by the coils on device size and the mirror ratio. The mirror ratio should preferably be as high as possible within tolerable limits for the flux tube cross section ellipticity.

COIL MODEL

The magnetic field from filamentary currents is determined by the Biot-Savart's law:

$$\mathbf{B}(\mathbf{x}) = \frac{\mu_0 I}{4\pi}\oint \frac{d\mathbf{l}'\times\mathbf{R}}{R^3},$$

where $\mathbf{R} = \mathbf{x} - \mathbf{x}'$ is the relative vector between the field point and filament source point. Consider first a single filamentary current with line element $d\mathbf{l}' = d\varphi'\left(\hat{\boldsymbol{\varphi}}' r' + \hat{\mathbf{z}}\frac{dz'}{d\varphi'}\right)$ wound on a round cylinder at distance r' from the z axis with a line element: $d\mathbf{l}' = \hat{\boldsymbol{\varphi}} r' d\varphi' + \hat{\mathbf{z}} dz' = (-y' d\varphi',\, x' d\varphi',\, dz')$, $z'(\varphi') = z_0' + h\cos 2\varphi'$, $dz' = \frac{dz'}{d\varphi'} d\varphi' = -2h\sin 2\varphi' d\varphi'$. Here $x' = r'\cos\varphi'$, $y' = r'\sin\varphi'$ and $(r',\, \varphi',\, z')$ are the cylindrical coordinates for source points on the magnetic axis of the linear device. A finite h gives a quadrupole field component. Compared to the coil set in [2], the straight parts connected by curved elements in [2] are here replaced by the wiggle $z' = z_0' + h\cos 2\varphi'$, which can be anticipated to give a similar contribution to the quadrupolar field. Near the magnetic axis, the Cartesian magnetic field components from this current loop are determined by

$$B_z = f(z) + \mathrm{O}(r^2),\quad B_x = \frac{x}{2}\left[-\frac{df}{dz} + g(z)\right] + \mathrm{O}(r^3),\quad B_y = \frac{y}{2}\left[-\frac{df}{dz} - g(z)\right] + \mathrm{O}(r^3) \quad (1a, b, c).$$

For a single filament we obtain $f(z) = \frac{\mu_0 I}{4\pi} r'^2 \oint \frac{d\varphi'}{R_0^3} g(z) = \frac{\mu_0 I}{4\pi} r'^2 \oint \left(-3h\frac{1-\cos 4\varphi'}{R_0^5} - \frac{\partial}{\partial z}\frac{\cos 2\varphi'}{R_0^3}\right) d\varphi'$.

A simple check confirms that these formulas yield $\nabla\cdot\mathbf{B} = 0$. The special case of $g(z) = 0$ corresponds to an axisymmetric field.

We extend these calculations to a set of filamentary currents I_{jk} wound on cylinders, where j enumerates the cylinder radii and k counts the filament coils on each cylinder surface, compare Fig. 2. Separation distance r_j' between the cylinder surfaces and the z axis can be written as $r_j' = a_0 + j\Delta r',\ j = 0, 1, 2, ..., N_r$, where a_0 is

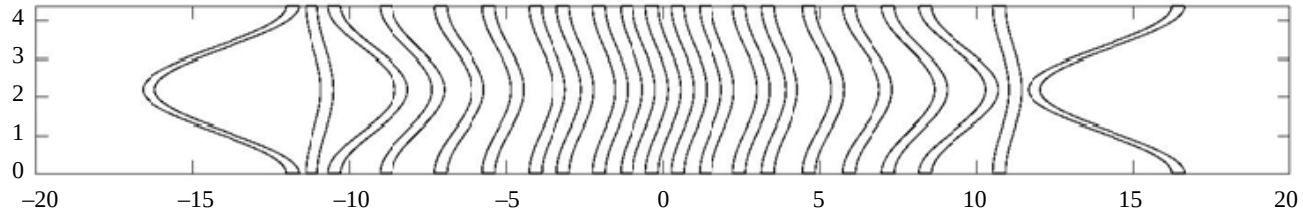

Fig. 2. Coil boundaries versus arc length $a_0\varphi'$ at the inner coil radius, which is the radius where the filament curvatures are at their maximum. Measurement units are meters. The complete coil winding includes analogous layers of wire currents at constant external radii r_j' wound with the same variation with φ', which facilitates convenient stacking of the coils. Each coil layer at a constant radius has a width L_z along z, and a package is formed by adding such layers in the interval of $a_0 \le r_j' \le a_1$, where a_1 is the outer coil radius. The coil set consists of a sequence of pair of identical coils on the opposite sides of the mid plane at $z = 0$. The figure is for the case, where a coil pair closest to the mid plane has coalesced in to a single coil

the inner radius and $a_1 = a_0 + N_r\Delta r'$ is the outer radius of the coil package. Filamentary currents with currents I_{jk} are wound at the cylindrical radius r'_j with the axial source coordinates (compare Fig. 2): $z'_k(\varphi') = z'_{0,k} + h_k \cos 2\varphi'$, $k = \pm1, \pm2, \ldots, k_{\max}$. Here $z'_{0,k}$ determines the axial center of the filamentary current. For simplicity, we take $I_{jk} = I_k$ for all j values (for convenient stacking of the coils, we will arrange packages, where all filamentary currents in a given package have the same $z'_{0,k}$, h_k and I_k values). The described winding results in l, $g(z) = \sum_{j,k} B_k \cdot \frac{g_{j,k}(z)}{a_0}$, where $B_k = \mu_0 I_k/(2a_0)$ and $f_{jk}(z) = \frac{a_0 r'^2_j}{2\pi}\oint \frac{d\varphi'}{R^3_{0,jk}}$, $g_{j,k}(z) = \frac{a_0^2 r'^2_j}{2\pi}\oint\left(-3h_k \frac{1-\cos 4\varphi'}{R^5_{0,jk}} - \frac{\partial}{\partial z}\frac{\cos 2\varphi'}{R^3_{0,jk}}\right)d\varphi'$. With $z'_{0,-k} = -z'_{0,k}$, $h_{-k} = h_k$ and $I_{j,-k} = I_{j,k}$, we have a symmetric quadrupole field satisfying $f(-z) = f(z)$ and $g(-z) = g(z)$.

Details of the coil arrangement will be presented elsewhere. As indicated in Fig. 2, for convenient stacking, we collect filaments into paired packages, where parameters for the current I_i the quadrupolar parameters h_i are identical. Each package, which models a multi-turn winding in a cryogenic coil, has width L_z along the z direction, compare Fig. 2, and identical inner and outer coil radii. With an arrangement where identical coils are placed on opposite sides of the mid plane, a symmetric minimum-B field is formed, satisfying $f(-z) = f(z)$ and $g(-z) = g(z)$. Overlapping between the coils must be avoided.

TARGET MAGNETIC FIELD PROPERTIES

With $B_0 = f(0)$, we introduce $u_e(z)$ and $\gamma_o(z)$ by $u_e(z) = \sqrt{\frac{B_0}{f(z)}}\cosh\left(\int_0^z \frac{g}{2f}dz\right)$, $\gamma_o(z) = \sqrt{\frac{B_0}{f(z)}}\sinh\left(\int_0^z \frac{g}{2f}dz\right)$, where $u_e(z) = u_e(-z)$, and is an even function and $\gamma_o(z) = -\gamma_o(-z)$ is an odd function. In the equatorial plane, these functions satisfy the Cauchy conditions, namely, $u_e(0) = 1$, $\gamma_o(0) = 0$, $u'_e(0) = 0$ and $\gamma'_o(0) = 1/c_L$, where $c_L = 2f(0)/g(0)$ is a parameter, which determines the longitudinal length scale for the quadrupolar field (axisymmetric fields correspond to $c_L \to \infty$). The Cartesian components of the field are in the paraxial approximation determined by $B_z = \frac{B_0}{u_e^2 - \gamma_o^2}$, $B_x = x\frac{B_0}{u_e^2 - \gamma_o^2}\frac{u'_e + \gamma'_o}{u_e + \gamma_o}$, $B_y = y\frac{B_0}{u_e^2 - \gamma_o^2}\frac{u'_e - \gamma'_o}{u_e - \gamma_o}$.

Near $z = 0$ this reduces to $B_x \to (x/c_L)B_0$ and $B_y \to (y/c_L)B_0$. The formulas show that the shape of the magnetic field near the z axis is determined by $u_e(z)$ and $\gamma_o(z)$. Our goal is to fit $u_e(z)$ and $\gamma_o(z)$ to the target functions $u_e^{(SF)}(z)$ and $\gamma_o^{(SF)}(z)$, , derived in [1] for an optimized minimum-B field. The target functions correspond to an extended SFLM (straight field line mirror) field with a minimal flux surface ellipticity for a given mirror ratio, which will be connected to expanding flux tubes beyond the mirror throats. Over most of the confinement region, apart from a close vicinity to the location for the maximal magnetic field strength, the corresponding target functions are accurately described by the simple SFLM expressions $u_e^{(SF)}(z) = 1$ and $\gamma_o^{(SF)}(z) = z/c_L$, which simplifies the fitting in that region. This ideal SFLM field results in: $B \to \frac{B_0}{1 - z^2/c_L^2}$, allowing desirable properties for a region with a finite mirror ratio to be obtained, although this simple solution cannot be directly extended to the expander region beyond the mirror throats due to singularities that show up at $z = \pm c_L$. The extended SFLM field derived in [1] is somewhat (but importantly) deviated from the ideal SFLM solution in the confinement region, which enables a smooth transition into the end tank region. The magnetic field from the coils should also provide suitable properties on the path to the expander tank region.

We use the SFLM target functions derived in [1]: $\gamma_o^{(SF)}(z) = \frac{z}{c_L}\left[1 - \frac{1}{4(1+\varepsilon_N)}\left(\frac{\kappa_0 z}{c_L}\right)^{2N}\right]$, $u_e^{(SF)}(z) = 1 + \frac{1}{4(1-\varepsilon_N)}\left(\frac{\kappa_0 z}{c_L}\right)^{2N}$. Here $\varepsilon_N = 1/(2N)$, integer N determines how close the target function is to the idealised SFLM field, and mirror ratio R_m determines the κ_0 parameter. With $R_m = 4$ and $N = 4$, $\kappa_0 = 0.839$, and parameter values for other cases can be found in [1]. The above target functions are only applicable to confinement region $-z_B \le z \le z_B$, where the magnetic field strength is at its maximum at the end points. Apart from the small, but important, deviations, we have $u_e^{(SF)}(z) = 1$, and $\gamma_o^{(SF)}(z) = z/c_L$ in the confinement region. The coil parameters should demonstrate a proper magnetic field evolution into the end tank region beyond the mirror throats. Our goal is to provide desired flux tube magnification M at the end tank wall with nearly circular flux surface footprints at the end tank to avoid short circuiting between the end plates, which are biased to different voltages. Nearly circular shapes will certainly appear far enough beyond the mirrors, since the vacuum field asymptotically approaches an axisymmetric dipole field.

To generate the magnetic field, we first select parameters for mirror ratio R_m and longitudinal scale length c_L, together with coil parameters for the inner coil radius a_0, the outer coil radius a_1, and their axial length, L_z. We then do the fitting by selecting i_{max}, i.e. the number of coil package pairs, and adjusting the coil parameters to match current I_i, wiggling h_i and central coil position $z_{0,i}$ for each coil, so that apart from very small field errors, we end up with $u_e(z) = u_e^{(SF)}(z)$, and $\gamma_o(z) = \gamma_o^{(SF)}(z)$ in the confinement region. An almost exact agreement with the target function assures that the coils produce a magnetic field satisfying the minimum-*B* criterion near the axis, which corresponding MHD stability for the flute and ballooning modes, accompanied with favourable properties for flux tube ellipticity and suppression of neoclassical transport effects.

RESULT FOR A FUSION NEUTRON SOURCE

As an example, we have considered a case which could be representative for a fusion neutron source with a fusion power in the range of 10 MW. In Figs. 2 and 3, plasma dimension parameters are a = 0.35 m and c_L = 10 m. The coil parameters are a = 1.4 m, and L_z = 0.4 m. The available width for shielding and other arrangements can be estimated from $\Delta a_{shyield} \approx a_0 - 2a$ = 70 cm. For this case, the reproduction was made using mirror ratio R_m = 6 and parameter value a_0/c_L = 0.14. To match the strong gradients of the target functions for this rather high mirror ratio, it was necessary to consider a low value of a_0/c_L. The target functions (with N = 3) and the coil fitting give a good agreement in the confinement region as seen in Fig. 3.

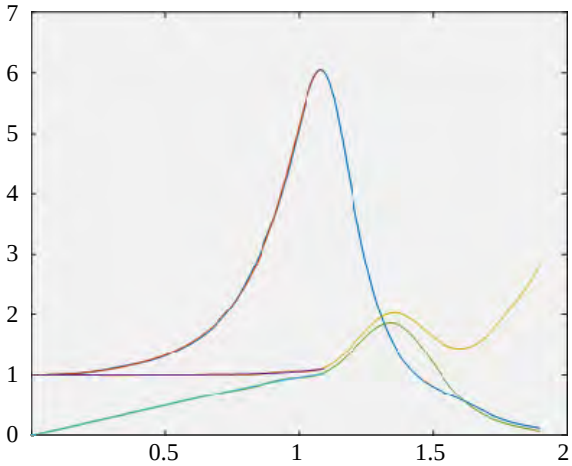

Fig. 3. The $u_e(z)$, $\gamma_o(z)$, functions (yellow and green, respectively) and the corresponding mirror ratio $R_m(z) = 1/(u_e^2 - \gamma_o^2)$ (blue) generated by the coil set versus z/c_L is shown. The plots demonstrate accurate reproductions of the SFLM field in the confinement region

The coil parameters

i	1	2	3	4	5	6	7	8	9	10	11
$z'_{0,i}/c_L$	0	0.081	0.17	0.28	0.37	0.51	0.65	0.8	0.94	1.0946	1.41
h_1/a_1	–0.252	–0.252	–0.252	–0.272	–0.272	–0.322	–0.422	–0.592	–0.762	–0.18	1.63
$\Delta z'_i$, cm	—	41	49	67.2	50	93	86	86.2	76.2	33.12	22
$\tilde{I}_i$	0.1239	0.2767	0.3346	0.3139	0.4543	0.5369	0.7022	0.5782	2.3336	6.3276	0.9491

(Note that separations $\Delta z'_i$ between neighbouring coils provide space for the structural support and openings to the vacuum chamber. The $\tilde{I}_i$ parameters represent dimensionless coil currents.)

The ellipticity at a maximum B strength is reasonably well described by a simple estimate $\varepsilon_{ell}(R_m) \approx 4R_m$. Because the target vacuum field is close to a marginal minimum-B field, we need to assure that field errors do not give rise to plasma instabilities. The small field errors obtained here are unlikely to pose any problem for flute stability, since they would be surpassed by several other stabilizing effects. Although the gas-dynamic regime may, in principle, provide stabilization for an expander with its favourable curvature, other mechanisms of stability control should be identified, if we aim for a more collision-free regime. Line tying could be one such mechanism. Wall stabilization is present since a plasma displacement induces image currents in a conducting vacuum vessel. Most importantly, a finite beta deepens the magnetic well and is therefore expected to strongly improve flute stability. Small field errors also are not expected to have any dramatic effect on the confinement, if a radial electric field is applied, since the **E**×**B** rotation tends to smear out guiding centre excursions caused by the field errors. There are therefore reasons to anticipate a robust confinement in the magnetic field with favourable MHD-stability properties.

We have also computed the representations of a more compact test device with a 6-m long confinement region, as well as a full scale stand-alone fusion reactor with a 100-m long confinement region. The 6-m long device could be of interest for testing purposes, if optimal confinement properties could be demonstrated in a real-life device, and such a device could also be designed for investigations of centrifugal confinement, where a controlled **E**×**B** rotation provides a plasma heating source. Apparently, centrifugal confinement schemes [4, 5] have not yet been tested on a device with superior MHD-stability properties, such as the SFLM field, where stability of flute and ballooning modes is predicted. An interesting possibility with the centrifugal confinement is the potential for counteracting pitch angle scattering, since it could provide a torque and a corresponding kinetic energy deposition into perpendicular velocity components. Since only a small tilt in pitch angle is required to prevent a particle from escaping into the loss cone, there may be a chance that the longitudinal confinement in mirrors is dramatically increased with a moderate power applied to the centrifugal confinement scheme. If so, a mirror may even be relevant as a stand-alone fusion reactor.

A 100-m long full scale device can be designed with a mirror ratio exceeding 10 for the vacuum field using our magnetic shaping method. Including a finite plasma β, there may be a possibility to reach a mirror ratio of around 20 [1]. A good confinement of energetic particles is anticipated in the SFLM field, while the confinement of tritium and Helium 3 particles from the D—D-fusion reaction is expected to substantially increase the power output from a D—D-plasma. Several crucial problems concerning tritium inventory and its breading ratio could be eased by a fusion device using the D—D-fuel, however that would require a by far higher confinement than achieved in any device developed so far. It seems plausible that commercial fusion energy development will be confined to one or another scenario involving only the D—D-fuel cycle.

Essentially, a target field can be reproduced to a certain maximal mirror ratio, where higher values for the mirror ratio are obtainable for long-thin systems. For a sufficiently long-thin system, mirror ratios in the range of 10 can be achieved. Finite plasma βcan be exploited to raise the mirror ratio to around 20.

SUMMARY AND DISCUSSION

A detailed reproduction of an optimized magnetic field is necessary to avoid plasma instabilities. MHD stability for both flute and ballooning modes with β ~ 1, combined with minimal ellipticity, are envisaged for the SFLM field. Arrangements can also be made to suppress the neoclassical transport effects. The objective of this study was to identify a practical and convenient coil set for the reproduction of a SFLM field, and to determine the limiting values of the mirror ratio for this coil set. Our fishbone coil arrangement can be applied to a wide range of sizes for a minimum-B mirror field.

The most critical parameter for accurate reproduction is ratio $\frac{a_0}{c_L} = \frac{\text{inner coil radius}}{\text{axial scale length}}$.

It determines the upper limit on the mirror ratio, and higher mirror ratios can be fitted with smaller values of a_0/c_L. For a sufficiently long-thin system, we can achieve $R_m \approx 10$ for the vacuum field, with tolerable values for the ellipticity. With a finite plasma beta, the mirror ratio can be increased further. In a minimum-B vacuum magnet field, a finite β would not trigger flute instability (because diamagnetic currents deepen the magnetic

well) or increase the ellipticity. For the optimised magnetic field, the largest flux tube ellipticity in the confinement region is estimated as $\varepsilon_{ell} \approx 4R_m(0)$, where $R_m(0)$ is the vacuum field mirror ratio.

The fishbone coils are smoothly twisted, which is favourable for superconductors [3]. Results representative for a 10 MW fusion neutron source are presented in this paper. A detailed reproduction of the target SFLM field is also possible for a wider parameter range.

A more compact magnetic field design may be appropriate for a 6-m long test device, where the existence of the radial invariant could be tested experimentally. The idea is that a quasi-neutral electric field, controlled by biased end plates, would act like a «glue» to force each guiding centre to move in close vicinity of its mean magnetic surface, which is connected with the radial constant of motion [1]. The latter prevents a collision-free radial leakage, allowing the neoclassical transport effects to be neglected.

With higher (around 100 kV) bias voltages, there may also be the possibility of testing the centrifugal confinement [4, 5], as well as plasma heating by a controlled **E**×**B** rotation. The point is to test this heating scenario for a magnetic field with superior MHD-stability properties. To the best of our knowledge, experiments performed so far on other devices have been using magnetic field designs prone to MHD-instabilities.

REFERENCES

1. **Ågren O., Moiseenko V.E.** — Fusion Engineering and Design, 2020, vol. 161, p. 111943.
2. **Hagnestål A., Ågren O., Moiseenko V.E.** — J. Fusion Energ., 2012, vol. 31, p. 379.
3. **Chaddah, P.** Critical current densities in superconducting materials. — Sadhana, 2003, vol. 28, p. 273—282; https://doi.org/10.1007/BF02717137.
4. **Ellis R.F., Hassam A.B., Messer S., Osborn B.R.** — Physics of Plasmas, 2001, vol. 8, p. 2057; https://doi.org/10.1063/1.1350957.
5. **Volosov V.I., Pekker M.S.** — Nucl. Fusion, 1981, vol. 21, p. 1275.

AUTHORS

O. Ågren; Uppsala University, Ångström Laboratory, Box 534, SE-751 21 Uppsala, Sweden, olov.agren@angstrom.uu.se
V.E. Moiseenko, Institute of Plasma Physics, National Science Center KIPT, 61108 Kharkiv, Ukraine, moiseenk@ipp.kharkov.ua

Статья поступила в редакцию 15 января 2021 г.
После доработки 16 марта 2021 г.
Принята к публикации 25 марта 2021 г.
Вопросы атомной науки и техники.
Сер. Термоядерный синтез, 2021, т. 44, вып. 2, с. 118—123.

UDC 621.039.54; 621.039.6

FUSION NEUTRON SOURCE AS AN EFFECTIVE PRODUCER OF NON-TRADITIONAL NUCLEAR FUEL

G.G. Kulikov, A.N. Shmelev, A.E. Kruglikov, V.A. Apse, E.G. Kulikov

National Research Nuclear University MEPhI, Moscow, Russia

The paper aims at studying peculiarities in isotope composition of thorium blanket under irradiation by fusion neutron source (FNS) in hybrid thermonuclear reactor (HTR). High-energy (14 MeV) component of neutron spectrum in thorium HTR blanket can produce non-traditional fissile mixture including not only ^{233}U, but also ^{231}Pa, ^{232}U and ^{234}U. The extraction of such non-traditional fuel from a spent Th-blanket and its utilization in traditional nuclear power reactors could increase fuel burnup and contribute to nuclear weapon non-proliferation. The results of a comprehensive investigation of the above positive effects, which included high-precision neutronics analyses of a HTR's Th blanket, are presented. The chosen model of HTR allowed the formation of high-energy neutron spectrum in Th-blanket with significant fraction of 14-MeV neutrons; it appeared that threshold (n, 2n)- and (n, 3n)-reactions are able to produce significant amounts of non-traditional target isotopes ^{231}Pa and ^{232}U; it was shown that accumulation of non-traditional target isotopes weakened substantially in depth of Th-blanket. It is therefore reasonable to look for optimal thickness of Th-blanket and optimal inventory of natural thorium.

Key words: hybrid thermonuclear reactor, fusion neutron source, thorium blanket, ^{231}Pa, ^{232}U, computer code SERPENT-2.

DOI: 10.21517/0202-3822-2021-44-2-124-132

ТЕРМОЯДЕРНЫЙ НЕЙТРОННЫЙ ИСТОЧНИК — ЭФФЕКТИВНЫЙ НАРАБОТЧИК НЕТРАДИЦИОННОГО ЯДЕРНОГО ТОПЛИВА

Г.Г. Куликов, А.Н. Шмелев, А.Е. Кругликов, В.А. Апсэ, Е.Г. Куликов

Национальный исследовательский ядерный университет «МИФИ», Москва, Россия

Анализируются особенности изотопного состава Th-бланкета при облучении в гибридном термоядерном реакторе (ГТР) на (D—T)-плазме. (D—T)-плазма была выбрана потому, что высокоэнергетическая (14 МэВ) составляющая нейтронного спектра в ториевом бланкете ГТР позволяет получать нетрадиционную делящуюся смесь, включающую не только ^{233}U, но и изотопы ^{231}Pa, ^{232}U и ^{234}U. Такие нетрадиционные топливные композиции могут представлять интерес для проектов АЭС с ядерными реакторами на тепловых нейтронах, поскольку они могут привести к более высокому выгоранию топлива и усилению режима ядерного нераспространения. Исследования этих положительных эффектов потребовали детального нейтронно-физического анализа ториевого бланкета ГТР. В статье представлены результаты, полученные в ходе этих исследований: выбранная модель ГТР позволила сформировать высокоэнергетический нейтронный спектр в Th-бланкете с значительной долей нейтронов с энергией 14 МэВ; пороговые (n, 2n)- и (n, 3n)-реакции способны производить значительные количества нетрадиционных изотопов ^{231}Pa и ^{232}U; накопление этих изотопов существенно ослабевает в глубине Th-бланкета. Поэтому нужно искать оптимальную толщину Th-слоя и оптимальное количество загружаемого в бланкет природного тория.

Ключевые слова: гибридный термоядерный реактор, термоядерный источник нейтронов, ториевый бланкет, ^{231}Pa, ^{232}U, компьютерная программа SERPENT-2.

MODEL OF FUSION NEUTRON SOURCE

High-energy (14 MeV) neutrons present in thorium HTR blanket can produce non-traditional mixes off issionable materials including not only ^{233}U, but also ^{231}Pa, ^{232}U and ^{234}U. The extraction of those non-traditional fuel sourced from a spent Th-blanket and their subsequent utilization in conventional nuclear power reactors could increase fuel burn up and enhance nuclear non-proliferation [1—4]. A one-dimensional cylindrical HTR model [5] was used in numerical analyses. Radial HTR zones were treated as infinitely long axial layers. An equi component D—T plasma ($n_T = n_D = 5\cdot10^{14}$ ion/cm^3) was taken to be the main neutron source. A basic layout of the HTR model is shown in Fig. 1.

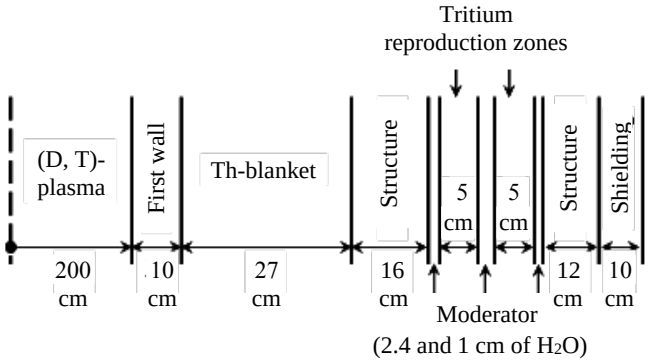

Fig. 1. Basic layout of the HTR model

The thorium blanket was place dimmediately behind the first wall, to allow high-energy 14-MeV neutrons to irradiate thorium and produce non-traditional

nuclides via certain threshold reactions. In front of the blanket, fusion neutrons are partially moderated by the first wall. The blanket is separated from the tritium reproduction zones (Li-containing zones) by structural materials. Light-water layers are set in front of, behind and between the tritium reproduction zones to intensify ^{6}Li(n, α)T reaction. Neutron senter the tritium reproduction zones after having passed through the tritium blanket and been slowed down. Theses low neutrons do not have the potential to initiate any threshold reaction and can be utilized in the tritium reproduction zones without decreasing the production of non-traditional nuclides.

NEUTRON ANALYSIS OF THORIUM HTR BLANKET

Time-dependent neutronics analyses of the isotopic content compositions in thorium HTR blanket were carried out using SERPENT-2 Monte Carlo [6—8] with continuous energy dependencies of evaluated nuclear data. The first wall neutron load was taken as 1 MW/m^2. This value is generally acceptable from the standpoint of the first wall strength properties.

SERPENT-2code. SERPENT-2 is the multi-purpose computer code based on Monte Carlo methodology. It applies continuous energy dependencies of evaluated micro cross-sections to the solution of three-dimensional transport equations. SERPENT-2 was initially created to solve nuclear reactor physics problems, but now its capabilities extend beyond this. Applications can be divided into the following three categories:

— traditional problems of the nuclear reactor physics: spatial homogenization, determination of reactor criticality, investigations of nuclear fuel cycle, simulation of nuclear research power reactors, validation of deterministic computer codes, etc.;

— multi-physical simulations: neutronics combined with thermal-hydraulic analyses, CFD-code computations, as well as computations that account for variations in fuel properties;

— neutron/photon transport modeling in the estimation of exposure dose — aimed at solving radiation shield problems and conducting nuclear power and medical research.

SERPENT-2 reads continuous energy micro cross-sections from ACE-formatted libraries. The interaction physicsis based on classical kinematics of inter-particle collisions, reaction cross-sections from evaluated nuclear data files (ENDFs) and probability table sampling in the unresolved resonance energy range. ACE-formatted cross-section libraries are based on JEF-2.2, JEFF-3.1, JEFF-3.1.1, ENDF/B-VI.8 and ENDF/B-VII evaluated nuclear data files. Data on radioactive decay and fission yield are taken from standard ENDF-formatted libraries.

Neutron spectrum in Th-blanket. The results of the Th-blanket neutron spectrum calculation are shown in Fig. 2. One can see two peaks, one close to 10 MeV, the other close to 0.4 MeV. While the former is directly related to fusion neutrons coming from the source, the latter is produced by neutrons that have passed through the first wall, undergone inelastic scattering and lost a significant portion of their initial energy. Neutrons with resonance, epithermal and even thermal energies can be found in deep inner layers of the Th-blanket. The proportion of these slow neutrons is substantially smaller than that of high-energy neutrons. As a result, a sufficiently high-energy neutron spectrum can be formed in the Th-blanket even with a thick (10 cm) first wall. The proportion of high-energy neutrons increases with decreasing blanket thickness.

Micro cross-sections and reaction rates in Th-blanket. This section deals with the basic characteristics that define the Th-blanket performance in terms of producing the important ^{231}Pa and ^{232}U isotopes. These characteristics are the micro cross-sections of ^{232}Th and neutron flux in different radial zones of Th-blanket at the beginning of irradiation (Fig. 3). Because the ^{232}Th burn up will be relatively low when the first wall neutron load sincrease (1 MW/m^2) at a certain level of engineering maturity, neutron reactions on ^{232}Th nuclei will define the neutron balance throughout the irradiation cycle.

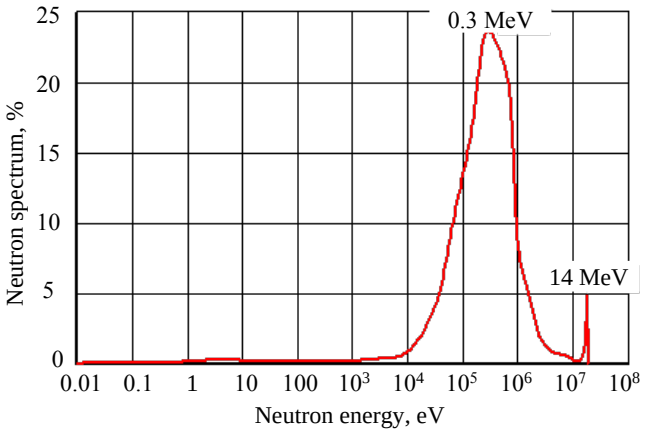

Fig. 2. Th-blanket neutron spectrum

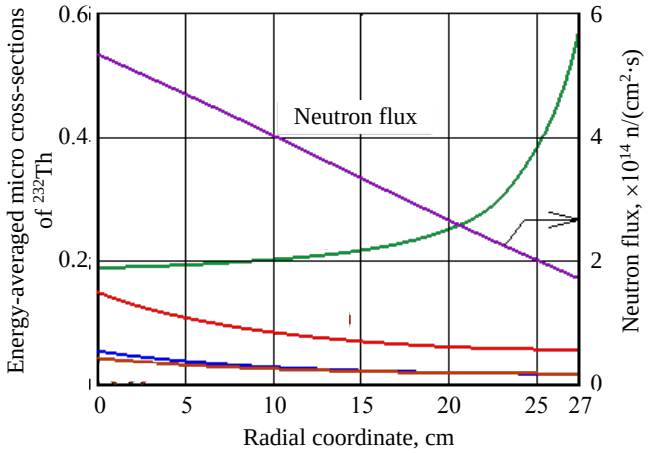

Fig. 3. Energy-averaged micro cross-sections of ^{232}Th and neutron flux in Th-blanket: —— — (n, γ), —— — $(n, 2n)$, —— — $(n, 3n)$, —— — (n, f)

As one can see, the probability of radiative neutron capture increases, while of the (n, f), $(n, 2n)$ and $(n, 3n)$ threshold reactions decreases with the depth of neutron penetration into the Th-blanket. This effect is caused by gradual neutron slowing down. The micro cross-sections of radiative neutron capture by ^{232}Th increase especially strongly in periphery of Th-blanket (in the last centimeters). At the same radial points the neutron flux falls roughly twice in an almost linear manner. Therefore, one can conclude that the intensity of ^{231}Pa and ^{232}U production in the Th-blanket peripheral areas is low. It diminishes both in absolute terms (kilograms per year) because of the low neutron flux, and in relative terms as compared against the production of ^{233}U because of the low ratios between the cross-sections of the threshold reactions and the radiative neutron capture. As a conclusion, the problem of optimizing the blanket thickness and thorium inventory should be set and solved.

The cross-section of ^{232}Th (n, f) reaction is more or less similar to the micro cross-section of the ^{232}Th $(n, 3n)$ reaction, meaning that the thorium fission reaction is weaker than reactions giving rise to the ^{233}U, ^{231}Pa and ^{232}U isotopes. This fact allowed us to expect modest heat generation rates in the Th-blanket that would simplify heat removal from it. Therefore, thermal energy release into the environment without utilization may be economically reasonable.

The balance of energy-averaged reaction rates in Th-blanket is presented in Fig. 4. The processes involved include radiative neutron capture by of ^{232}Th, fission reaction of ^{232}Th, ^{232}Th $(n, 2n)$ and ^{232}Th $(n, 3n)$ threshold reactions, radiative neutron capture reactions of structural materials (Fe, Mo) and neutron leakage. In fact, these reaction rates are appropriate micro cross-sections (see Fig. 3) multiplied by the neutron flux and by the ^{232}Th, Fe and Mo concentrations.

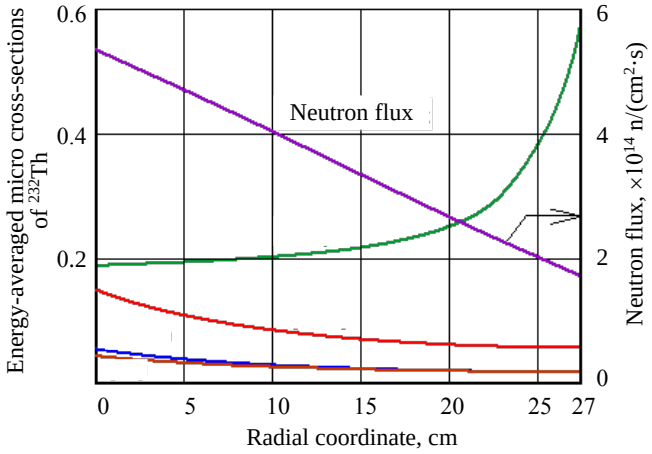

Fig. 4. Energy-averaged reaction rates and neutron leakage rate in Th-blanket: —— — (n, γ), —— — $(n, 2n)$, —— — $(n, 3n)$, —— — (n, f)

Neutron leakage rate is positive over the first 9 cm and negative further into the blanket. This suggests that neutrons coming from plasma through the first wall and getting multiplied in the upper 9 cm layer by ^{232}Th (n, f), ^{232}Th $(n, 2n)$ and ^{232}Th $(n, 3n)$ threshold reactions, irradiate the deeper blanket layers.

The following conclusions can be made. First, threshold ^{232}Th $(n, 2n)$ and ^{232}Th $(n, 3n)$ reactions give rise to the isotopes of interest, ^{231}Pa and ^{232}U and play a remarkable role in the balance of neutron reactions. However, it is the ^{232}Th (n, γ) ^{233}U-reaction that plays the main balancing role. Second, the ^{233}U production rate at the blanket periphery is substantially higher than the production rates of ^{231}Pa and ^{232}U isotopes. Therefore, enhancing the production of the desired isotopes may require a thinner blanket. Third, the ^{232}Th (n, f)-reaction is slow in all radial points of the Th-blanket. Then one may anticipate that heat could be dumped into the environment without the need to be utilized. Fourth, the neutron balance is strongly influenced by the rate of neutron leakage, especially that occurring deep in the blanket.

Rates ofreactions involved in the isotope decay chain. This section analyses the rates of neutron reactions involved in the chain of isotopic transformations in the Th-blanket. The rates of radioactive decay, radiative neutron capture reaction and fission reaction for some short-lived isotopes are presented in Table 1.

T a b l e 1. **Reaction rates (1/day) of short-lived isotopes from the decay chain of Th-blanket.**

Isotope	λ	$(\sigma_c \cdot \Phi)$	$(\sigma_f \cdot \Phi)$	$(\sigma_{cf} \cdot \Phi)$
^{231}Th	0.64	0.000206	0.000045	0.000251
^{233}Th	45.0	0.000174	0.000008	0.000182
^{232}Pa	0.53	0.000077	0.000230	0.000307
^{233}Pa	0.026	0.000125	0.000002	0.000127

One can see that radioactive decay rates are at least twice as high as the rate of radiative neutron capture. For this reason, the composition analysis of an isotope mix produced in the Th-blanket may neglect the radiative neutron capture and fission of those short-lived nuclides. If structural materials with an enhanced radiation resistance are used in the first wall, then the neutron load (and related neutron flux) can be increased, while the reaction rate difference can be decreased. However, a several-fold neutral flux increase is hardly practicable.

Next, we compared reaction rates obtained with different cross-sections, i.e. macro cross-sections multiplied on neutron fluxes. We omitted the same multiplier (neutron flux) and calculated the macro cross-sections using relative masses of the isotopes (kg per 1 MT ^{232}Th) produced, for example, by the end of the 1000-day irradiation cycle rather than isotope concentrations, considering the close atomic weights of nuclides involved in the chain.

The rates of ^{232}U production via the threshold ^{232}Th(n, 2n) ^{231}Pa(n, γ), ^{232}Th(n, 3n) ^{230}Th(n, γ) ^{231}Pa(n, γ) reactions and via ^{232}Th(n, γ)^{233}U(n, 2n) reaction were calculated. The threshold reactions are comparable in terms of their contributions to the ^{231}Th production (in the form of a direct (n, 2n) threshold reaction on ^{232}Th nuclei in one case and through neuron capture by ^{230}Th in the other case). The total rate of these threshold reactions was compared with rates of the ^{231}Pa(n, γ) reaction and rate of threshold ^{233}U(n, 2n) reaction. The micro cross-sections, relative masses and reaction rates at the end of irradiation time (1000 days) are presented in Table 2.

T a b l e 2. **The rate of ^{232}U production via different channels**

^{232}Th-reaction	Evaluated reaction	Micro cross-section, barn	Relative mass, kg/t	Reaction rate, barn·kg
(n, 2n)	^{232}Th(n, 2n)	0.082	988.6	80.9
(n, 3n)	^{230}Th(n, γ)	3.679	0.911	3.35
(n, 2n) + (n, 3n)	^{231}Pa(n, γ)	6.167	2.564	15.81
(n, γ)	^{233}U(n, 2n)	0.010	6.188	0.063

It is evident from this table that the total rate of the threshold reactions, is more than twice as high as the ^{232}Th(n, γ)^{233}U(n, 2n)-reaction rate. The ^{232}Th(n, 2n)-reaction is 24 times faster than the ^{232}Th(n, 3n)-reaction. As a result, the lion's share of ^{232}U is produced via the^{232}Th(n, 2n)-reaction. The contributions of the rest reactions are negligible.

Some parameters of heat generation rate at the end of irradiation time are presented in Table 3. Isotope ^{233}U is main contributor here while contribution of ^{232}Th is lower by two orders of magnitude. Taking into account the fact that ^{232}Th is a threshold-fissionable isotope, and that Th-blanket contains 99.86% ^{232}Th, one can conclude that total heat generation rate at the end of irradiation time remains insignificant. Therefore, heat removal does not represent a serious problem, as thermal energy may be released into the environment without the need to be utilized

T a b l e 3. **Fission reaction rates for different isotopes at the end of irradiation time (1000 days)**

Isotope	Micro cross-section of fission, barn	Relative mass, kg/t	Fission rate, barn·kg
^{232}Th	0.025	998.6	25.26
^{230Th}	0.057	0.911	0.052
^{231}Pa	0.256	2.564	0.656
^{232}U	3.429	0.089	0.305
^{233}U	7.477	6.188	46.27
^{234}U	0.455	0.072	0.033

Thus, one can conclude that contribution of short-lived isotopes is negligibly small. Among the threshold reactions, only the ^{232}Th(n, 2n) should be accounted for.

Thorium burnup. Time-dependent thorium burnup via different reactions (radiative neutron capture, fission, threshold (n, $2n$)- and (n, $3n$)-reactions) is shown in Fig. 5.

Naturally, all time dependencies are linear, because the rates of all burnup reactions are linear functions of the neutron flux and neutron spectrum. The neutron flux is determined by the FNS intensity which is fixed with respect to the first wall fusion neutron load (1 MW/m^2). Time-dependent variations of neutron spectrum are very small because of low thorium burnup and low accumulation of new isotopes. Only around 10 kg out of one initial ton ^{232}Th input are burned up during an irradiation cycle, meaning that ^{232}Th burnup is nearly 1% of heavy metal (HM) inventory. Mean fuel burnup in current light-water reactors of VVER-1000 type is close to 5% HM while maximal fuel burnup is about 7% HM. The ways towards intensification of thorium burnup and production of objective isotopes must include the attempts to provide higher values of neutron load on the first HTR wall and longer irradiation time of Th-blanket. Anyway, it is necessary to seek for new structural materials with upgraded radiation resistance.

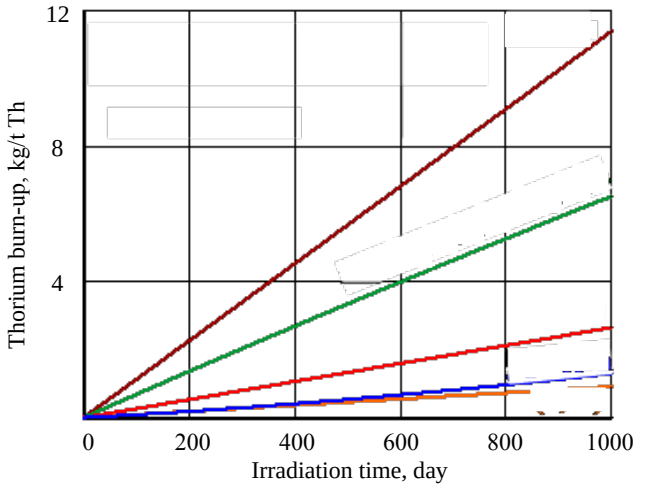

Fig. 5. Thorium burnup via different reactions as a function of irradiation time: —— total, —— radiative capture, —— (n, $2n$), —— fission, —— (n, $3n$)

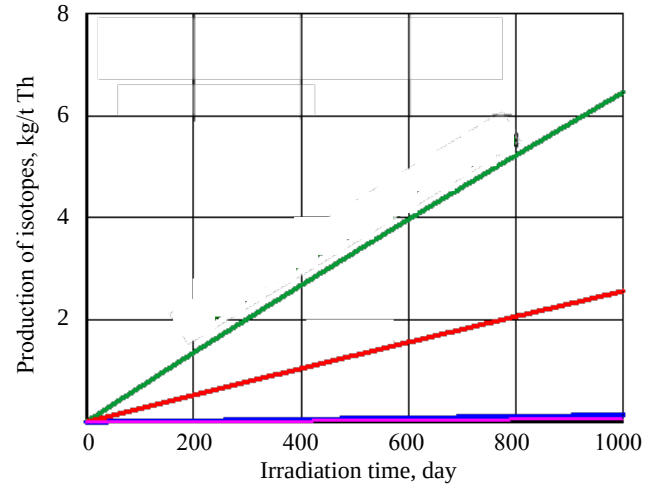

Fig. 6. Production of isotopes as a function of irradiation time: —— ^{233}U + ^{231}Pa ($T_{1/2}$ = 27 days), —— ^{231}Pa, —— ^{232}U, —— ^{234}U

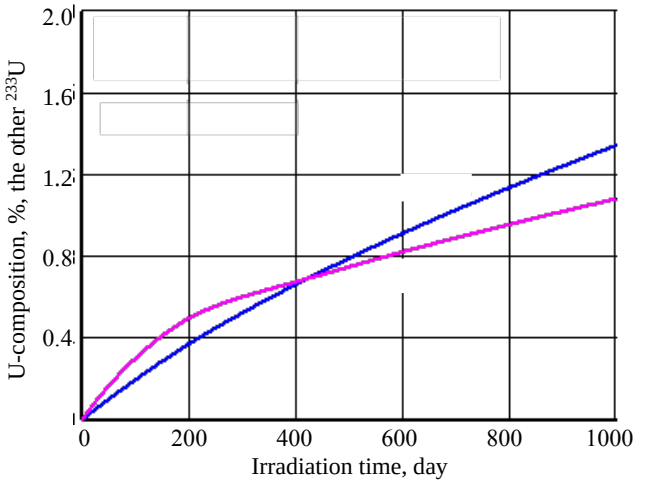

Fig. 7. Isotope composition of uranium as a function of irradiation time: —— ^{232}U, —— ^{234}U

As expected, the ^{232}Th(n, γ)-reaction is the main channel for thorium burnup. However, the ^{232}Th(n, $2n$) threshold channel is not negligibly weak, and slightly more intense than ^{232}Th(n, f) channel. These results allowed us to expect intense production of traditional isotope ^{233}U and non-traditional objective isotopes ^{231}Pa and ^{232}U.

Production of isotopes ^{233}U, ^{231}Pa and ^{232}U. Production of different isotopes in thorium blanket under irradiation by fusion neutrons is shown in Fig. 6 as a function of irradiation time.

We show ^{233}U and ^{233}Pa total production considering that ^{233}Pa decays into ^{233}U (half-life $T_{1/2}$ (^{233}Pa) = 27 days) almost fully. In fact, its radioactive decay is much faster than its radiative neutron capture and fission. As expected, the largest part of ^{233}U is produced via the ^{232}Th radiative neutron capture, followed by two rapid β-decays of ^{233}Th and ^{233}Pa. However, ^{231}Pa produced via the ^{232}Th(n, $2n$) threshold reaction constitutes a significant portion of the ^{233}U produced. The production of the «next in the line» isotopes ^{232}U and ^{234}U via the ^{231}Pa(n, γ)- and ^{233}U(n, γ)-reactions, respectively, is, of course, less substantial.

Isotopic composition of uranium produced. The ^{232}U and и^{234}U contentsin the uranium produced in Th-blanket are shown in Fig. 7 as functions of irradiation time.

One can see that the ^{232}U and ^{234}U contents increase almost linearly with time. At the end of the 1000-day irradiation time, they reach 1.6 and 1%, respectively.^{233}U represents the remaining 97.4%. In fact, highly-enriched weapon-grade uranium is produced in the irradiated thorium blanket. This material is very important for nuclear power reactors and re-

quires strict control (in the non-proliferation context) by the IAEA inspectorate. The produced weapon-grade uranium may be diluted by either natural or depleted uranium to a required concentration of fissile ^{233}U. In addition, such a dilution can provide proliferation resistance of the produced uranium at the highest isotopic level. In this case, main fissile isotope ^{233}U would be surrounded by the lighter ^{232}U and by the heavier ^{234}U and ^{238}U isotopes.

Now a question about the ^{234}U and ^{232}U contents of the uranium produced, 1 and 1.4%, respectively: are they large or small? Numerical evaluations suggest that these concentrations are negligible and unable to influence the neutron-physical properties of nuclear fuel in any significant way, as produced uranium would be diluted by ^{238}U. Moreover, with the uranium produced and diluted by natural / depleted uranium to 5% ^{233}U, the ^{232}U and ^{234}U concentrations fall ~25 times to 0.065 and 0.04%, respectively.

Presently, the glovebox approach is used to fabricate fresh nuclear fuel for light-water reactors from reprocessed uranium. According to the Russian technical regulations, the ^{234}U content in the reactor-grade uranium must be below 0.2%. The rationale behind this stringent requirement resides in the ^{234}U intense α-activity ($T_{1/2} = 2.45\cdot10^5$ years). If uranium is enriched using a gas-diffusion or gas-centrifuge technology, then α-particles emitted by ^{234}U are able to disorder the enriching process by the chemical dissociation of uranium hexafluoride UF_6 molecules accompanied by the formation of free fluorine and lower uranium fluorides (mainly, UF_5 and UF_4). These low-volatile uranium fluorides can disturb the uranium enriching process, as they can precipitate on the inner surfaces of process facilities (centrifuges, pipelines), while free fluorine can act as a strong corrosion-aggressive element.

As for ^{232}U, Russian technical regulations require that the ^{232}U content in uranium-bearing materials is below $2\cdot10^{-7}$%. The rationale is largely the same as that for ^{234}U, although a much stronger case can be considered for ^{232}U. Indeed, the ^{232}U half-live is significantly shorter than that of ^{234}U (69 years versus $2.45\cdot10^5$ years). The ^{232}U decay chain includes five additional α-emitters. Besides, one member of ^{232}U decay chain, namely isotope ^{208}Tl, is a source of high-energy (2.6 MeV) γ-rays. At the end of irradiation time (1000 days), the ^{232}U content in the uranium produced is ~10^7 times larger than the acceptable value for the glovebox technology of U-based fuel fabrication. Even if the uranium produced is diluted by ^{238}U, the ^{232}U content is at least ~10^5 times greater than acceptable value ($2\cdot10^{-7}$%)t. This means that remote technologies should be developed for nuclear fuel fabrication from uranium with such isotope composition. The intense emission of high-energy γ-rays can act as a strong deterrent for parties who might otherwise be willing to use uranium for non-peaceful applications. If such parties still go for the manufacturing of a nuclear explosive device (NED), they will have to carry out uranium pre-enriching with isotope ^{233}U in a cascade of gas centrifuges, for instance. In this case, intense α-activity of ^{232}U and its decay products could trigger a chemical dissociation of the UF_6 molecules. The separation of the ^{233}U isotope, surrounded by ^{232}U, ^{234}U и ^{238}U, is a much more intricate problem than the enrichment of natural uranium. To solve it, one would need a dedicated or a two-stage enrichment cascade to produce successively higher concentrations of the desired isotope. Besides, difference of ^{232}U, ^{233}U and ^{234}U atomic weights is only 1 a.m.u. while that in the process of natural uranium enrichment equals to 3 a.m.u. So small difference can complicate additionally the uranium enriching process and reduce efficiency of the process. If terrorists try to manufacture a NED without the ^{233}U separation, then intense heat generation by ^{232}U would melt down the chemical explosive, disabling the NED. The intense neutron emission by ^{232}U from spontaneous fission reactions can trigger a premature initiation of chain fission reaction in the NED and drastically reduce the energy yield of nuclear explosion. Thus, the large ^{232}U content is an extremely strong barrier against any unauthorized usage of the ^{233}U.

The technical capabilities of the government-owned industrial enterprises are evidently greater than those of terrorist organizations. Actually, we can always establish the ^{232}U content in uranium-bearing materials, which would allow the government-owned enterprises to work with these materials, but make them beyond the reach of non-state actors.

Production of ^{231}Pa. Ratio of ^{231}Pa-to-uranium content in Th-blanket is shown in Fig. 8 as a function of irradiation time.

One can see that the ^{231}Pa-to-U ratio is, in essence, a time-independent value (about 0.38). This

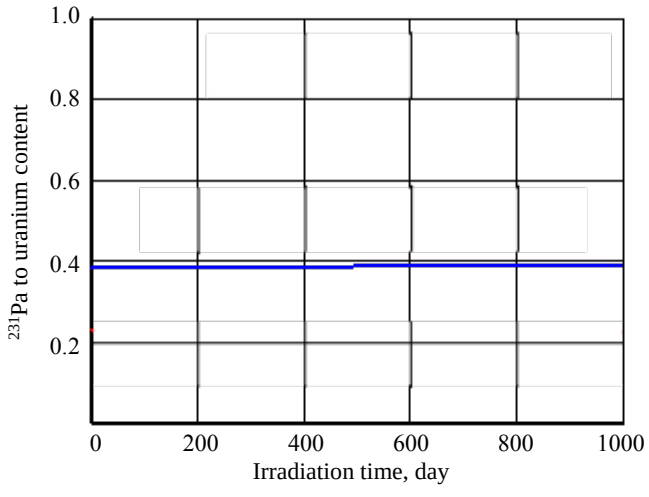

Fig. 8. Ratio of ^{231}Pa-to-U content as a function of irradiation time

means that with uranium enriched up to <5% ^{233}U the ^{231}Pa content in uranium-bearing materials will be 1.9%. We know that the neutron capture micro cross-section for ^{231}Pa is almost 75 times higher than for ^{238}U in the thermal energy range. Therefore, an intense neutron capture by ^{231}Pa can contribute to the neutron balance and stabilize neutron-multiplying properties of uranium-based fuels during irradiation time in a nuclear power reactor.

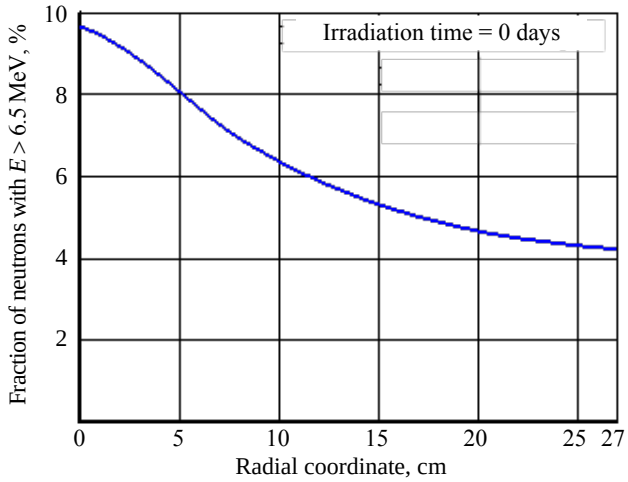

Fig. 9. Fraction of high-energy neutrons in thorium blanket (radial distribution)

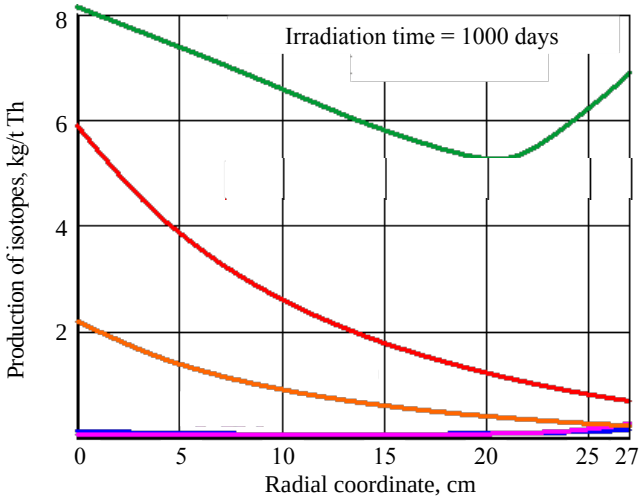

Fig. 10. Radial distributions of isotope production in thorium blanket: —— — ^{233}U + ^{231}Pa ($T_{1/2}$ = 27 days), —— — ^{231}Pa, —— — ^{230}Th, —— — ^{232}U, —— — ^{234}U

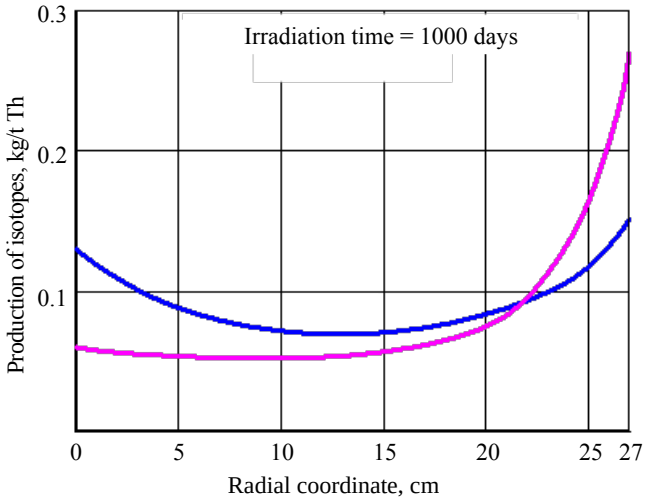

Fig. 11. Uranium isotope composition in Th-blanket: —— — ^{232}U, —— — ^{234}U

Fraction of high-energy neutrons in Th-blanket. Because the desired ^{231}Pa and ^{232}U isotopes are produced by threshold (n, 2n)- and (n, 3n)-reactions, it would be interesting to study the radial distribution of high-energy neutrons in thorium blanket. Only these high-energy neutrons are able to initiate threshold (n, 2n)- and (n, 3n)-reactions. As was shown in Fig. 5, the neutron spectrum does not change in any significant way during full irradiation time because of the ^{232}Th low burn-up (about 1.1% HM). For this reason, the radial distribution of high-energy neutrons in thorium blanket is shown in Fig. 9 for the beginning of irradiation.

Fraction of high-energy (E > 6.5 MeV) neutrons declines approximately twice as we move from the front edge of the Th-blanket (the plasma-blanket border) to its back edge (the blanket-structure border). The radial degradation of the high-energy neutron flux is due to the gradual neutron slowing down through elastic and inelastic scattering. Therefore all relevant isotopes, including those desired, will be accumulated in thorium blanket in a non-uniform spatial manner. This conclusion is confirmed by numerical results presented below.

Isotope production in thorium blanket. The radial distributions of isotope production in thorium blanket are shown in Fig. 10.

One can see that the production of the desired ^{231}Pa and ^{230}Th isotopes, which is only achievable with high-energy neutrons via threshold (n, 2n)- and (n, 3n)-reactions, is substantially (~by a factor of 6) more intense at the front edge than at the back edge of thorium blanket. This can be due to the neutron spectrum softening (see Fig. 9), i.e. slowing down of high-energy neutrons in the energy range below 6.5 MeV. The production of the «traditional» ^{233}U isotope initially declines, but ultimately starts rising. Such an irregular trajectory of the ^{233}U production may be due to the fact that moderated neutrons enter an energy range (1—100 eV), where the ^{232}Th neutron capture cross section is low, which is favorable to the production of ^{233}U (1 eV to 100 eV). However, this effect calls for further investigations.

The production of ^{232}U and ^{234}U is so small that the radial distributions of these isotopes are almost indistinguishable in Fig. 10. These distributions are treated separately in the next section.

Radial distribution of uranium isotope composition in Th-blanket. The radial distributions of uranium isotopes (^{232}U and ^{234}U) production in Th-blanket are presented in Fig. 11.

The ^{232}U production minimum in the middle of thorium blanket is due to the neutron spectrum softening. However, the ^{232}U production begins to increase in the peripheral layers of thorium blanket. This may be attributed, first, to the intense production of ^{233}U at the blanket periphery (see Fig. 10), second, by the initiation of threshold ^{233}U(n, 2n)^{232}U-reaction. The production of ^{234}U increases substantially closer to the blanket back edge. This can also be due to the vigorous generation of ^{233}U and the ^{233}U(n, γ)^{234}U-reaction.

COMPARISON WITH OTHER CALCULATIONS

Production of various isotopes in Th-blanket of HTR on D—T-plasma has been also investigated in papers [9, 10]. Experimental and computational data on reaction rates per one fusion neutron (E = 14 MeV) are presented in Table 4. These results demonstrate sufficiently good agreement.

T a b l e 4. **Reaction rates of ^{232}Th per one 14-MeV neutron**

^{232}Th reactions	Experiment [9]	Calculation [10]
(n,γ)	1.63 ± 0.10	1.58
(n,2n)	0.42 ± 0.04	0.58
(n,3n)	0.30 ± 0.05	0.15
(n,f)	0.17 ± 0.01	0.19
Neuron leakage	0.78 ± 0.04	0.76

The time-dependent variations of isotopic mixes produced in a thorium HTR blanket are shown in Fig. 12 [10]. They show a good qualitative agreement with the results published in [10]. Small discrepancies may be due to dissimilar HTR types, HTR blanket designs, different ENDF libraries and numerical approximations.

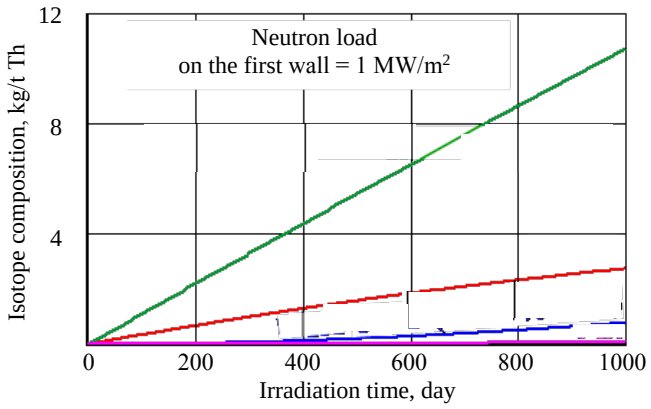

Fig. 12. Isotope composition of Th-blanket as a function of irradiation time: —— — ^{233}U + ^{321}Pa ($T_{1/2}$ = 27 days), —— — ^{231}Pa, —— — ^{232}U (1.5—6.7% in U), —— — ^{234}U

CONCLUSION

The proposed model of fusion neutron source makes it possible to form high-energy neutron spectrum in Th-blanket with sufficient fraction of 14-MeV neutrons.

It was demonstrated that non-traditional target isotopes ^{231}Pa and ^{232}U can be produced insignificant quantities via threshold (n, 2n)- and (n, 3n)-reactions.

A possibility was shown to use simplified chain of isotope transformations without taking short-lived isotopes into consideration. Only one ^{232}Th(n, 2n)-reaction should be accounted for.

The production of the desired isotopes was shown to reduce significantlyas it goes deeper into thorium blanket. It therefore seems reasonable to look for an optimal blanket thickness and the natural thorium inventory in the blanket.

Acknowledgments

The reported study was funded by RFBR, project № 19-29-02006.

REFERENCES

1. **Kulikov G.G., Shmelev A.N., Geraskin N.I., Kulikov E.G., Apse V.A.** Advanced nuclear fuel cycle for the RF using actinides breeding in thorium blankets of fusion neutron source. — Nuclear Energy and Technology, 2016, vol. 2, p. 147—150.
2. **Shmelev A.N., Kulikov G.G.** On the role of fusion neutron source with thorium blanket in forming the nuclide composition of the nuclear fuelcycle of the Russian Federation. — Physics of Atomic Nuclei, 2016, vol. 79, p. 1508—1512.
3. **Baatar T., Kulikov E.G.** Justification of VVER-1000 safety when using fuel compositions doped by protactinium and neptunium. — Izv. Wysshikh Uchebnykh Zawedeniy. Yad. Energ., 2020, vol. 1, p. 26—36.

4. **Kulikov G.G., Shmelev A.N., Kulikov E.G., Apse V.A.** Proliferation-protected, ultra-high burnup reactor fuel produced in the thorium blanket of a fusion neutron source Global. — In: International Nuclear Fuel Cycle Conference and TOP FUEL 2019. Light Water Reactor Fuel Performance Conference, p. 1088–1092.
5. **Orlov V.V., Shatalov G.E., Marin S.V.** Evolution of fuel isotope composition in thorium blanket of hybrid thermonuclear reactor. — Report of Kurchatov Institute on Nuclear Energy, 1979, p. 29—30.
6. **Leppänen J., Kaltiaisenaho T.** Expanding the use of serpent 2 to fusion applications: shut-down dose rate calculations. — In: International Conference on the Physics of Reactors PHYSOR 2016.
7. **Yudong L., Guangming Z., Francisco A.H., Pavel P., Jaakko L., Minyou Y.** Benchmark of Serpent-2 with MCNP. — Application to European DEMO HCPB Breeding Blanket, 2020, vol. 155**,** p. 111583.
8. **Riku T., Ville V., Jaakko L.** New energy deposition treatment in the Serpent-2 Monte Carlo transport code. — Annals of Nuclear Energy, 2019, vol. 129, p. 224—232.
9. **Shief H.E. J. et al.** Measurements of the Reaction Rate Distributions Produced in a Large Thorium Cylinder by a Central Source of DT Neutrons. — United Kingdom Atomic Energy Authority, 1977.
10. **Krumbein A., Lemanska M., Segev M., Wagschal J.J., Yaari A.** Reaction rate calculations in uranium and thorium blankets surrounding a central deuterium—tritium neutron source. — Nuclear Technology, 1980, vol. 48, p. 110—116.

AUTHORS

Gennadij Genrichovich Kulikov. leading engineer, PhD in Physics & Mathematics; National Research Nuclear Univ. MEPhI, 115409 Moscow, Kashirskoe sh. 31, Russia, ggkulikov@mephi.ru

Anatolij Nikolaevich Shmelev, professor, Dr. of Science Degree in Engineering; National Research Nuclear Univ. MEPhI, 115409 Moscow, Kashirskoe sh. 31, Russia, shmelan@mail.ru

Anton Evgenievich Kruglikov, engineer; National Research Nuclear Univ. MEPhI, 115409 Moscow, Kashirskoe sh. 31, Russia**,** aekruglikov@mephi.ru

Vladimir Aleksandrovich Apse, engineer, PhD in Engineering; National Research Nuclear Univ. MEPhI, 115409 Moscow**,** Kashirskoe sh. 31, Russia, apseva@mail.ru

Evgenij Gennadievich Kulikov, Associate Professor, PhD in Engineering; National Research Nuclear Univ. MEPhI, 115409 Moscow**,** Kashirskoe sh. 31, Russia, egkulikov@mephi.ru

Статья поступила в редакцию 15 января 2021 г.
После доработки 16 марта 2021 г.
Принята к публикации 25 марта 2021 г.
Вопросы атомной науки и техники.
Сер. Термоядерный синтез, 2021, т. 44, вып. 2, с. 124—132.

UDC 621.039.75

AMERICIUM AND CURIUM BURNUP IN A FUSION REACTOR

V.E. Moiseenko[1], S.V. Chernitskiy[2], O. Ågren[3]

[1]*Institute of Plasma Physics, National Science Center «Kharkiv Institute of Physics and Technology», Kharkiv, Ukraine*
[2]*«Nuclear Fuel Cycle» Research and Technology Division, National Science Center «Kharkiv Institute of Physics and Technology, Kharkiv, Ukraine*
[3]*Uppsala University, Ångström laboratory, Uppsala, Sweden*

A large amount of spent nuclear fuel (SNF) from nuclear power plants has been accumulated globally to date, and there is still no established strategy for handling it. While SNF can be partitioned, the predominant isotope Uranium-238 can be used to produce secondary fuel in fast nuclear reactors, and plutonium be burned in thermal nuclear reactors as a part of MOX fuel. Fission products can be disposed in geological repositories, as they decay in 200—300 years — much sooner than SNF. A major challenge is to handle minor actinides (MAs), particularly americium and curium, which are long-lived elements and are currently not recycled. They have different nuclear properties and cannot be treated like plutonium. It is possible to have americium and curium effectively burned up (fissioned) through irradiation with fusion neutrons. This paper explores the idea of employing fusion power plants for recycling those elements. An appropriate model was generated, which used americium and curium quantities small enough to avoid any strong impact on the reactor systems and operation. At the same time, the model allowed for high MA burnup rates. Nuclear facility used in the model was a torus-shaped thermonuclear reactor with plasma major and minor radii of 1000 and 300 cm, respectively. Such facility could take up additional 10 t of fuel (americium plus curium) with no significant impact on its physical characteristics. The americium and curium burnup rates, calculated with the MNCPX code, were within acceptable limits. Fission neutrons were found to contribute to the production of tritium, which may be important from the standpoint of the reactor's self-sufficiency in tritium supply. Calculations proved that the reactivity of the reactor as a fission burner was low, enabling a safe operation. In addition to the MA incineration and tritium breeding capacities, fission reactions provided for a moderate (tens of percent) power gain.

Key words: fast reactors, spent nuclear fuel, fusion installations, MCNPX.

DOI: 10.21517/0202-3822-2021-44-2-133-138

ВЫГОРАНИЕ АМЕРИЦИЯ И КЮРИЯ В ТЕРМОЯДЕРНОМ РЕАКТОРЕ

В.Е. Моисеенко[1], С.В. Черницкий[2], О. Агрен[3]

[1]*Институт физики плазмы, Национальный научный центр «Харьковский физико-технический институт», Харьков, Украина*
[2]*Научно-технический отдел «Ядерный топливный цикл», Национальный научный центр «Харьковский физико-технический институт», Харьков, Украина*
[3]*Университет Упсалы, лаборатория Ангстрема, Уппсала, Швеция*

В настоящее время во всём мире накоплено большое количество отработавшего ядерного топлива (ОЯТ) с атомных электростанций, и до сих пор нет установленной стратегии обращения с ним, в то время как ОЯТ может быть сепарировано, преобладающий изотоп ^{238}U может быть использован для получения вторичного топлива в быстрых ядерных реакторах, а плутоний может сжигаться в ядерных реакторах в качестве части МОКС-топлива. Продукты деления можно утилизировать в геологических хранилищах, так как они распадаются через 200—300 лет, гораздо раньше, чем ОЯТ. Основная проблема заключается в обработке минорных актинидов (МА), особенно америция и кюрия, которые являются долгоживущими элементами и в настоящее время не перерабатываются. Они обладают различными ядерными свойствами и не могут использоваться так же, как плутоний. Можно эффективно сжигать америций и кюрий (расщеплять) путём облучения термоядерными нейтронами. В настоящей статье исследуется идея создания термоядерных электростанций для переработки этих элементов. Была создана соответствующая модель, в которой использовались количества америция и кюрия, достаточно малые, чтобы избежать какого-либо сильного воздействия на реакторные системы и их работу. В то же время модель допускала высокие показатели выгорания МА. Ядерная установка, используемая в модели, представляла собой термоядерный реактор в форме тора с большим и малым радиусами плазмы 1000 и 300 см соответственно. Такая установка могла бы потреблять дополнительно 10 т топлива (америций плюс кюрий) без существенного влияния на её физические характеристики. Скорости выгорания америция и кюрия, рассчитанные с помощью кода MNCPX, находились в требуемых пределах. Было обнаружено, что нейтроны деления способствуют производству трития, что может быть важно с точки зрения самодостаточности реактора в поставках трития. Расчёты показали, что реактивность реактора была низкой, что обеспечивало безопасную эксплуатацию. В дополнение к мощностям сжигания МА и размножения трития реакции деления обеспечивали умеренный (десятки процентов) прирост мощности.

Ключевые слова: быстрые реакторы, отработавшее ядерное топливо, термоядерные установки, MCNPX.

INTRODUCTION

A large number of nuclear power reactors operating in the world require uranium «enriched» in the ^{235}U isotope for their fuel. This is not the case of research reactors and reactors used in watercraft, including submarines. The operation of thermal nuclear power plants results in large amounts of spent nuclear fuel (SNF), which conti-

nue to grow. Nuclear power development in different countries and globally depends on approach adopted with respect to the SNF management. This paper addresses approaches already in place and those that are yet in the works and believed to be promising, with a particular focus on SNF management using thermonuclear facilities.

Nuclear power plays an important role in the world's energy supply. Its growth prospects are directly linked to the availability of proven uranium reserves. [1]. Electricity from nuclear power plants is one of the cheapest [2]. That said nuclear power is fraught with a variety of problems, including the radiotoxic nuclear waste. At present, SNF is isolated in geological repositories, where it can be stored for hundreds of thousands of years. However, SNF contains valuable chemical elements, whose extraction can potentially deliver economic benefits [3].

The incineration of transuranic elements at different levels of burnup depth is only possible in a fast neutron spectrum, because not all transuranics can be fissioned by thermal neutrons. However, this technology has some limitations that can be summarized as follows:

— transuranics contained in SNF and undergoing fission cause a deficit of delayed neutrons, which decreases the reactor controllability [4, 5];

— in a fast reactor, the Doppler-effect is reduced, which can be a major safety issue in the case of an accident, such as the fuel heating up in the reactor core;

— fast reactors are critical.

From the above one can conclude that transuranic elements make up only a small fraction of fast reactor fuel, which significantly reduces the rate of their transmutation. What is more, the prospect of using the scarce ^{235}U as a major fuel component is highly undesirable.

Another method to obtain high-energy neutrons is to use an accelerator driven system (ADS) [6—9]. This electronuclear breeder facility, created as an alternative to fast neutron reactors, (Fig. 1) uses a subcritical nuclear reactor coupled with a particle accelerator and a neutron producing target, which eliminates the risk of power excursion accidents. In this method, MAs, placed in the core along with ^{235}U, are expected to gradually burn up. It is important to note the significant conceptual advantage of electronuclear units over traditional fast neutron reactors. In addition to being deterministically safer due to the subcritical core, an ADS allows a harder neutron spectrum to be achieved. As a result, the amount of all MAs is reduced (albeit with varying efficiency).

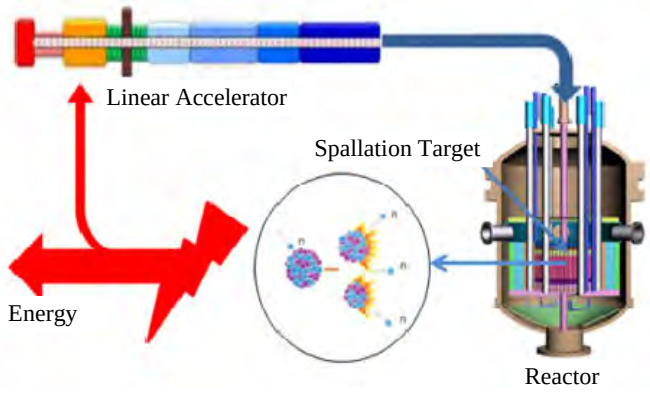

Fig. 1. Concept of electronuclear technology

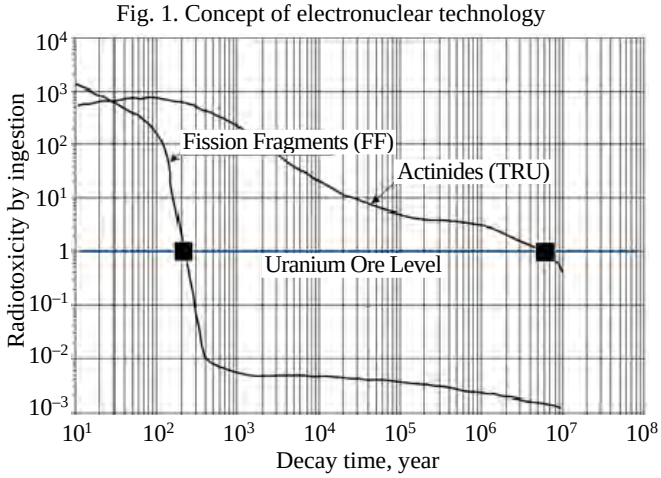

Fig. 2. Time evolution of the potential radiotoxicity (relative to uranium ore) of the two main components of nuclear waste for PWR spent fuel

The electronuclear technology has a greater degree of engineering complexity than the traditional reactor technology, as it combines accelerator technology and reactor physics, not to mention a number of related applied science disciplines.

Another technology that provides a harder neutron spectrum than the fast reactor is the fusion-fission hybrid reactor [10—12]. However, the disadvantages inherent in the ADS technology are also encountered in hybrid reactors.

One SNF management technology that is extensively used worldwide is temporary storage. This is relatively cheap compared to the above options, as the fuel (17 or 24 fuel assemblies) is stored in concrete containers at nuclear power plant sites. However, storage in interim on-site facilities is limited to 100 years, and options concerning further disposing of SNF are to be decided upon at a later stage.

Spent fuel can be partitioned. The majority isotope, ^{238}U, is not radioactive. Plutonium can be burned in thermal nuclear reactors as part of MOX fuel. Fission products can be disposed in geological repositories, as they decay in 200—300 years [13], much sooner than SNF (Fig. 2). A major challenge is to handle MAs, particularly americium and curium.

The aim of the study was to analyze the possibility of burning significant quantities of americium and curium isotopes in a tokamak-type fusion reactor with dimensions close to DEMO and figure out whether fusion power plants can be utilized for a deep burnup of americium and curium isotopes. The amounts of americium and curium isotopes to be present in the reactor were chosen to be small enough to avoid any strong impact on the reactor systems and operation.

FUSION REACTOR MODEL

Computer simulations were performed with the Monte—Carlo N-Particle extended (MCNPX) code [14], which supports problems involving the transport of radiation from a volumetric source of arbitrary spectral composition in complex three-dimensional models. It uses the Monte—Carlo method for the solution of radiative transfer equations and allows for continuous-energy treatment and flexible geometry modelling.

Our neutronic model has a two-dimensional cylindrically symmetric geometry. Its radial structure is shown in Fig. 3. The model dimensions are close to those of the future DEMO reactor. The vacuum chamber contains a D—T-plasma which is the source of fusion neutrons. The first wall, chosen to be 3 cm thick, was assumed to be made of HT-9 steel with a mass density of 7.7 g/cm^3. Its isotopic composition was taken from the ORNL Fusion materials data bank [15]. The HT-9 steel is a candidate structural material for the first wall of the ITER experimental thermonuclear reactor.

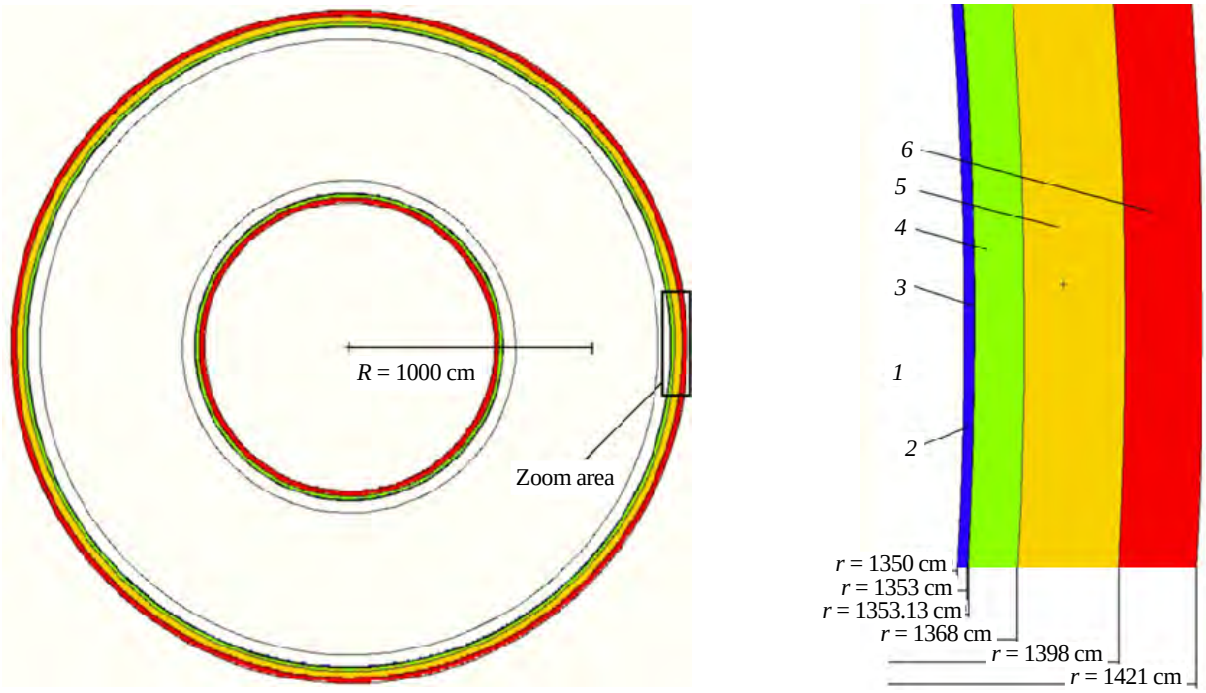

Fig. 3. Radial cross-section of the model: *1* — vacuum chamber; *2* — first wall; *3* — Am + Cm; *4* — LBE; *5* — natural lithium; *6* — shield

The thickness of the reactor core (blanket) containing the americium and curium isotopes was determined from critically calculations. A thickness of 0.13 cm was found to provide the effective multiplication factor $k_{\text{eff}} \approx 0.1$. Behind the blanket, there is a lead-bismuth-eutectic (LBE) system, which is 15 cm thick. The LBE system is assumed to be made of 44.5% wt. lead and 55.5% wt. bismuth and have a mass density of 10.17 g/cm^3 [16]. In addition to its primary role in the LBE system, lead acts as a fast neutron flux amplifier due to the neutron propagation threshold reaction ^{208}Pb(n, 2n)^{207}Pb. The buffer zone was chosen to be 15 cm thick for the reason that a fast neutron's free path within the LBE is 15 cm long. In general, using liquid metal as a coolant in a high-temperature reactor has many advantages. High boiling point, significant heat capacity, and good thermal conductivity are more or less inherent in liquid metals. Bismuth and lead have melting points of 271 ºC and 327 ºC, respectively, whereas the eutectic lead-bismuth alloy melts at 125 ºC. Therefore, LBE is less prone to solidify in the reactor cooling circuit, than pure lead.

Continuous tritium reproduction is very important to maintain a self-sufficient operation of the plasma neutron source. Due to tritium's low (~20 keV) beta decay energy [17], particles emitted from this decay are easily stopped by ordinary clothing or rubber surgical gloves. However, this isotope presents a radiation hazard when inhaled and ingested with food [18]. Therefore, tritium transportation may be dangerous. In addition, tritium is an expensive material (around USD 30 000 per gram) [19]. For this reason, it is worthwhile to arrange for tritium reproduction inside the hybrid reactor and on-site handling in addition to ensuring the plasma source self-sufficiency.

Tritium is produced through the following four reactions:

1. $^{6}Li + n \rightarrow {}^{4}He + T$;
2. $^{10}B + n \rightarrow 2\,{}^{4}He + T$;
3. $^{14}N + n \rightarrow {}^{12}C + T$;
4. $^{7}Li + n \rightarrow {}^{4}He + T + n$.

The cross-section of the thermal neutron reaction for ^{6}Li is about 940 barn, 70 barn for natural lithium and only $5\cdot10^{-3}$ barn for ^{10}B. The reaction $^{14}N(n, T)^{12}C$ is a threshold reaction (requiring a minimum energy of incident neutrons >4 MeV), and for neutron energies E_n = 5—7 MeV, the reaction cross section is only $2\cdot10^{-2}$ barn. The reaction $^{7}Li(n, n'T)$ is a threshold one and requires >2.8 MeV of incident neutron energy to start. Thus, the predictable and optimal way to produce tritium is through the ^{6}Li (n, T) reaction. The tritium breeding zone is 30 cm thick and filled with natural lithium. Calculations suggest that no additional lithium 6 enrichment is required.

A 23 cm-thick shield is used to reduce the neutron and gamma loads of the tokamak magnetic coils needed for the plasma confinement. The shield contains 304B7 alloy (UNS S30467) stainless steel [20] and water, 60:40 vol. %. The steel component has 1.75% wt. of natural boron. The protection zone is also used to provide supplementary external cooling for the entire installation.

All volumetric elements of the fusion reactor were modeled as a homogeneous mixture of its component materials. Because of the neutrons' long mean free path, such modeling is acceptable for fast systems and does not distort the result, and also significantly reduces the calculation time.

CALCULATION RESULTS

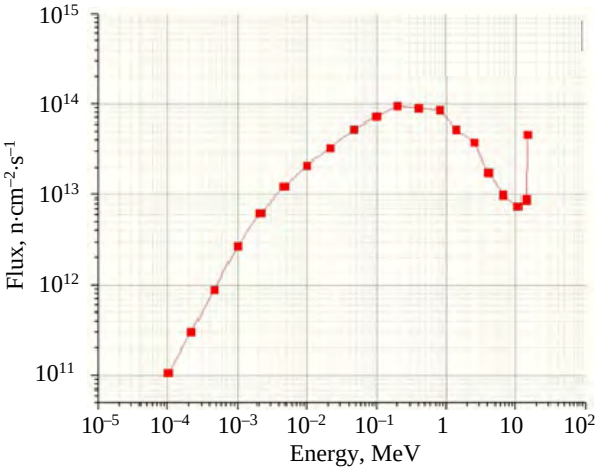

Fig. 4. Neutron spectrum at the blanket

The probability of any reaction depends on incident particle's energy. In our case, knowing the neutron spectrum in the vicinity of the americium and curium isotopes' location is important, as this allows the burnup rates for those isotopes to be estimated.

Americium and curium isotopes can be effectively fissioned by neutrons with energies higher than 0.5 MeV, especially those falling under the «thermonuclear» spectrum. As can be seen from Fig. 4, the number of neutrons with energies above 0.5 MeV is significant. It is interesting to compare the number of source neutrons and their energy for the discussed tokamak model and, for example, for a PWR-type thermal reactor (Table 1).

T a b l e 1. **Source neutron comparison**

Reactor type	Numbers of neutrons	Neutron energy, MeV
Fusion (DEMO)	1.0E21	14
PWR	3.0E19	0.7

As one can see from Table 1, a fusion reactor is a sound candidate for the role of a burner system for americium and curium. Column 2 in Table 2 shows the percent content of americium and curium in SNF extracted from PWR reactors. Column 3 shows the mass of each isotope loaded in a fusion reactor. When the specified amounts are loa-

ded, it appears that the reactor is deeply subcritical (k_{eff} = 0.091), with the thermal fission power at 0.425 GW_{th}, that is, about 15% of the fusion power (2.7 GW_{th} in our model). Such a low subcriticality makes the reactor safe. The additional fission power is not large and does not require big changes to the cooling system. Column 4 in Table 2 shows how the concentration of a given isotope in fuel decreases after one year of the facility continuous operation.

T a b l e 2. **Source neutron comparison**

Element	Wt.%	Fuel load, kg	Burnup after one year of operation, %	Fusion neutron source intensity, s^{-1}
^{241}Am	88.796	9390	7.0	$1.0 \cdot 10^{21}$
^{242}Am	0.06478	6.85	70	
^{243}Am	9.87	1040	6.2	
^{243}Cm	0.0174	1.83	12.8	
^{244}Cm	1.12	118	3.7	
^{245}Cm	0.121	12.7	8.2	
^{246}Cm	0.00967	1.01	1.9	

The model used natural lithium for the tritium breeding zone, which allowed a tritium breeding ratio of 1.34 to be obtained. This should be enough to produce tritium needed for the plant's own needs.

CONCLUSIONS

So far, about 400 000 t of SNF have been discharged from commercial nuclear power reactors, of which 100 000 t have been reprocessed. Considering that americium and curium account for about 0.1% of SNF, some 300 t of these materials should be available for transmutation purposes. The proposed method for americium and curium incineration in tokamaks does not seem to be about to perturb the operation of future tokamak-based fusion reactors in any significant way. The fusion reactor fleet should digest and remove part of SNF that is, accomplish something that other facilities are unable to do.

REFERENCES

1. **Sukhodolov A.P.** World's supply of uranium: prospects for primary provision of atomic energy industry. — Izvestiya of Irkytsk State Economics Academy, 2010, № 4, 72 p.
2. **Глухов В.В., Барыкин С.Е.** Экономика электроэнергетического комплекса. — СПб: Издательство СПбГПУ, 2003. 206 с.
3. **Kolarik Z., Renard E.V.** Potential applications of fission platinoids in industry. — Platinum Metals Review. 2005, vol. 49, p. 79—90.
4. **Sandmayer A.G.** Kinetics and stability of fast neutron reactors. — M.: «Publishing by atom. Science and Technology», 1963.
5. **Toshinskiy G., Bulavin P.** — Nuclear Energy, 1967, vol. 23, Iss. 2, p. 146—149.
6. **Барашенков В.С.** Проблемы электроядерной технологии. Препринт ОИЯИ Р2-94-56. — Дубна, 1994.
7. **Барашенков В.С.** Ядерно-физические аспекты электроядерного метода. — ЭЧАЯ, 1978, т. 9, вып. 5.
8. **Васильков Р.Г., Гольданский В.И., Орлов В.В.** Об электрическом бридинге. — УФН, 1983, т. 139, вып. 3.
9. **Васильков Р.Г., Гольданский В.И., Джелепов В.П., Дмитриевский В.П.** Электроядерный метод генерации нейтронов. — Атомная энергия, 1970, т. 29, вып. 3.
10. **Qiu L.J., Yang Y.W., Wu Y.C.** A compact tokamak transmutation reactor for treatment of high level wastes. — Plasma Physics and Controlled Nuclear Fusion Research. Proceedings of the Fifteenth International Conference, 1994, vol. 2.
11. **Stacey W.M., Hoffman E.A.** Tokamak transmutation facility studies. — Fusion Technology, 2001, vol. 39(2P2), p. 525—529.
12. **Azizov E.A., Gladush G.G., Lopatkin A.V., Lukasevich I.B.** Tokamak based hybrid systems for fuel production and recovery from spent nuclear fuel. — Atomic Energy, 2011, vol. 110(2), p. 93—98.
13. **Ishkhanov B.S.** Radioactivity. — M.: Publishing University Book, 2011.
14. **For the U.S.** Department of Energy. Monte-Carlo N-Particle Transport Code System for Multiparticle and High Energy Applications, Version 2.4.0. Los Alamos National Laboratory, Los Alamos report LA-CP-02-408, 2002.
15. **ORNL**, Fusion Materials, 1999; http://www.ms.ornl.gov/programs/fusionmtlspdf/june1999/hashimoto1.pdf.
16. **OECD** NEA, 2007; http://www.nea.fr/html/science/reports/2007/pdf/chapter2.pdf.
17. **Audi G., Wapstra A.H., Thibault C.** The AME2003 atomic mass evaluation (II). Tables, graphs and references. — Nuclear Physics A, 2003, vol. 729, p. 337—676.
18. **Osborne R.V.** Tritium Hazard Report: Pollution and Radiation Risk from Canadian Nuclear Facilities. Canadian Nuclear Association, 2007.
19. **Rogers Abby.** The 16 Most Expensive Substances in the World. URL: www.businessinsider.com/most-valuable-substances-by-weight-2011-11?op=1.
20. **Fix D.V. et al.** LLNL report UCRL-PROC-202920, 2004.

AUTHORS

Vladimir E. Moiseenko, Institute of Plasma Physics, National Science Center «Kharkiv Institute of Physics and Technology», Akademichna st. 1, 61108 Kharkiv, Ukraine, moiseenk@ipp.kharkov.ua

S.V. Chernitskiy, «Nuclear Fuel Cycle» Research and Technology Division, National Science Center «Kharkiv Institute of Physics and Technology», Akademichna st. 1, 61108 Kharkiv, Ukraine

O. Ågren, Uppsala University, Ångström laboratory, Box 534, SE 751 21 Uppsala, Sweden

Статья поступила в редакцию 15 января 2021 г.
После доработки 16 марта 2021 г.
Принята к публикации 25 марта 2021 г.
Вопросы атомной науки и техники.
Сер. Термоядерный синтез, 2021, т. 44, вып. 2, с. 133—138.

UDC 621.039.674.3

APPLICATIONS OF FUSION-FISSION HYBRID SYSTEMS FOR NUCLEAR FUEL CYCLE

M.N. Shlenskii[1, 2], B.V. Kuteev[2]

[1]*National Research Nuclear University Moscow Engineering Physics Institute, Plasma Physics Department, Moscow, Russia*
[2]*NRC «Kurchatov Institute», Tokamak Division, Moscow, Russia*

This paper comprises results presented at the FUNFI4 conference. The reported research focuses on the prospective utilization of a fusion-fission hybrid system (FFHS) as a powerful neutron source capable of transmuting minor actinides (MAs; Np, Am, Cm) from spent nuclear fuel (SNF). Calculations simulating nuclide kinetics in MA-bearing metal fuel were performed for three 40-MW fusion power FFHS reactors, intended for different purposes (demonstration, pilot-industrial, and industrial). In addition, the research assessed potential requirements for FFHSs and their role in Russia's nuclear power program. A model created by AO «Proryv» was used to analyze the development of the Russian nuclear power system with integrated FFHSs. MA quantities expected to be produced and transmuted in the integration scenario were estimated. The results suggest that just one hybrid facility's capacity would be enough to achieve a ~28% MA decrease in the Russian power system by 2130.

Key words: fusion-fission hybrid system (FFHS), fusion neutron source (FNS), minor actinides (MAs), partitioning and transmutation (P&T), closed nuclear fuel cycle.

DOI: 10.21517/0202-3822-2021-44-2-139-144

ПРИМЕНЕНИЕ ГИБРИДНЫХ СИСТЕМ СИНТЕЗА-ДЕЛЕНИЯ В ЯДЕРНОМ ТОПЛИВНОМ ЦИКЛЕ

М.Н. Шлёнский[1, 2], Б.В. Кутеев[2]

[1]*Национальный исследовательский ядерный университет «Московский инженерно-физический институт», Кафедра физики плазмы, Москва, Россия*
[2]*НИЦ «Курчатовский институт», Отдел токамаков, Москва, Россия*

Эта статья содержит представленные на конференции FUNFI4 результаты исследований возможного использования перспективных гибридных систем синтеза-деления (ГССД) в качестве мощного источника нейтронов, способного трансмутировать минорные актиниды (МА) Np, Am, Cm из отработавшего ядерного топлива (ОЯТ). Расчёты, моделирующие кинетику нуклидов в металлическом топливе, содержащем МА, были выполнены для трёх ГССД мощностью 40 МВт, предназначенных для различных целей (демонстрационной, опытно-промышленной и промышленной). В ходе исследования были оценены потенциальные потребности в ГССД и их роль в российской ядерной энергетике. Модель, созданная АО «Прорыв», была использована для анализа развития российской атомной энергетики с интегрированными в неё ГССД. Были оценены количества МА, которые, как ожидается, будут получены и трансмутированы в сценарии, охватывающем все три рассмотренных вида ГССД. Результаты расчётов показывают, что трёх ГССД (по одной установке каждого вида) будет достаточно для снижения количества МА, наработанных российской энергосистемой к 2130 г., на ~28%.

Ключевые слова: гибридная система синтеза-деления, термоядерный источник нейтронов, минорные актиниды, разделение и трансмутация нуклидов, замкнутый ядерный топливный цикл.

INTRODUCTION

One of the most crucial issues for the nuclear engineering community is to develop a closed nuclear fuel cycle that would extend the use of nuclear energy to more than 1000 years and make nuclear technologies more environmentally acceptable, cost-effective and safe. A further aspect of this issue is the management of SNF and radioactive waste (RW).

As reported in [1, 2] SNF from a light water reactor (LWR) typically contains more than 95% of U, about 1% of Pu, 0.1% of MAs and around 3—4% of fission products (FPs). Plutonium and MA, although present in low concentrations, are the main contributors to the SNF's long-term radiotoxicity [2]. The radiotoxicity of FPs declines much faster compared to that of actinides. It reaches radioactive equilibrium with respect to uranium ore in about 300 years [2]. If not reprocessed and transmuted, SNF reaches the natural radiotoxicity level only after 100 000 years [2].

In this context, SNF reprocessing via separation of minor actinides, Pu and U, seems to be a promising option for future nuclear energy production and SNF management [3]. Pu and U could be reused in fission reactors. FPs could be utilized as sources of radiation to reduce the amount of radioactive waste. As mentioned above, actinides are much slower than FPs in terms of radioactivity decay. This problem can be solved by transmuting MAs via fission reactions producing FPs. The strategy is known as partitioning & transmutation (P&T) [1].

Some of MAs' neutronics features make them less suited for transmuting with subcritical systems than with critical reactors. These include:

— a very hard spectrum required for the fission of most MAs due to the «threshold» character of their fission cross-sections;

— the capture-to-fission ratio, α (the ratio of the nonfission capture cross section to the fission cross section) for a given neutron spectrum is crucial to ensuring an effective transmutation [4];

— MA nuclides have small fractions of delayed neutrons (e.g., 0.00127 for ^{241}Am, 0.00214 for ^{239}Pu and 0.0172 for ^{238}U);

— the number of prompt neutrons per fission increases with initial neutron energy. Thus, the higher the initial neutron energy, the more effective the neutron utilization.

One of the most promising approaches to solving this problem is to use of a fusion reactor as a source of high energy neutrons. This is investigated, for example, in [1, 5—10].

Although the use of FFHSs for MA transmutation is subject of many research works, most of those works deal with early stages of designing a real-life facility or have no intention of designing a real-life facility at all. Furthermore, many studies lack a comprehensive analysis of the problem or overlook the fact that not only transmutation parameters are essential, but also the comparison with alternative transmutation techniques and the assessment of the impact, which the integration of FFHSs may produce on the nuclear power system.

METHODS, MODELS AND DATA

All three hybrid reactor types identified by the road map for the NRC «Kurchatov Institute» project are based on a tokamak with a blanket containing fissile materials and lithium. At present, the demo FFHS version (DEMO-FNS) is in the design stage. Two other hybrid reactors envisaged by the road map have a pilot-industrial and industrial designation (PIHR and IHR, respectively).

The DEMO-FNS features a high-end design, which is also more sophisticated and elaborate compared to the other two. PIHR and IHR have a similar build with slightly different parameters. Tokamaks used in the discussed hybrid systems have the following identical parameters: major plasma radius R_0 = 320 cm, minor plasma radius a = 100 cm, plasma current I_p = 5 MA, toroidal magnetic field B_{t0} = 5 T, fusion power P_{fus} = 40 MW (corresponding t_o ~$1.4 \cdot 10^{19}$ n/s for the D—T-reaction) and effective fuel irradiation time of 5 years. DEMO-FNS, PIHR and IHR are due to be started up in 2033, 2045 and 2055, respectively. Differences that are important for this study are listed in Table 1.

T a b l e 1. **Capacity factor and fuel loading with minor actinides**

Parameter	DEMO-FNS	PIHR	IHR
Capacity factor	0.3	0.8	0.95
Fuel loading (MA + Zr), t (H_2O as coolant)	26.24	26.24	41.68

DEMO-FNS's 3D-geometric model is shown in Fig. 1. Fig. 2 gives a cut of a 3D-geometric model for Monte-Carlo calculations of neutron transport. The blanket contains 18 MA-bearing fuel assemblies (the transmutation area), with lithium salt filling the remaining space (the tritium breeding area).

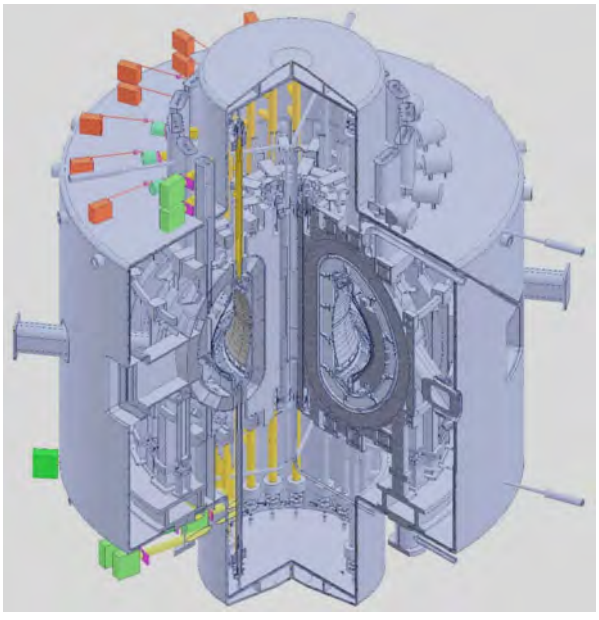

Fig. 1. 3D DEMO-FNS

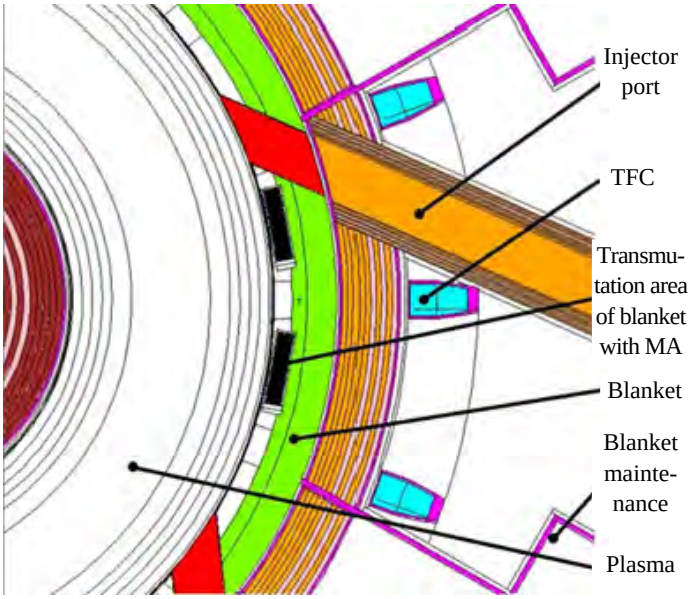

Fig. 2. Horizontal equatorial cut of DEMO-FNS model — transmutation area; TFC — Toroidal field coil

Two coolants for the transmutation area, CO_2 and H_2O, are considered. Whatever the coolant, it flows vertically, along the fuel rods and inside the assemblies' casings. H_2O is chosen as a basic coolant option for the blanket. Average coolant density inside the assemblies is 0.37 g/cm^3 for H_2O, and should be 0.14 g/cm^3, if CO_2 is employed. The use of CO_2 instead of H_2O encourages the k_{eff} to grow (up to 1.04). In that case, it is necessary to decrease the total fuel loading (to 19.7 t for DEMO-FNS).

A MA-Zr metal alloy was chosen as a fuel. This alloy has a theoretical density of 15 g/cm^3. Many researchers have considered this type of fuel [8, 11, 12], and it has even been utilized in a fast reactor [13]. Fuel inventory details are shown in Table 2.

T a b l e 2. **Fuel inventory (15 g/cm^3), % (mass)**

Nuclide	Fraction, %	Nuclide	Fraction, %
^{237}Np	28.67	^{90}Zr	2.05
^{241}Am	62.10	^{91}Zr	0.45
^{242m}Am	0.06	^{92}Zr	0.70
^{243}Am	4.63	^{94}Zr	0.72
^{244}Cm	0.49	^{96}Zr	0.12
MA	95.96	Zr	4.04

The FISPACT-II inventory code [17] was used to quantify nuclide kinetics using a constant neutron spectrum. The neutron spectrum for the transmutation area was obtained using Monte-Carlo calculations of neutron transport. The spectrum was volume-averaged for the whole transmutation area. The use of a constant neutron spectrum in the nuclide kinetics calculations skewed the results, because of the interplay between fuel inventory evolution and the spectrum. However, in the case of a subcritical system with an external neutron source, this error should not be significant. Some contradictions in the assessment of this error are addressed in different publications [9, 10].

The ENDF/B-VI neutron data file was used for neutron transport calculations. Data needed to quantify nuclide kinetics came from the TENDL_2014 nuclear data library (CCFE-709 group structure).

RESULTS AND DISCUSSION

Neutron transport and nuclide kinetics analysis. Other important parameters for the transmutation area were calculated via neutron transport modeling:

— with H_2O used as a coolant, volume-averaged total neutron flux $\bar{\Phi}_n = 2.88\cdot10^{14}$ (cm^2·s)$^{-1}$, average neutron energy $\bar{E}_n = 3.52$ MeV, and $k_{eff} = 0.95$;

— in the case of CO_2, $\bar{\Phi}_n = 3.02\cdot10^{14}$ (cm^2·s)$^{-1}$, $\bar{E}_n = 3.47$ MeV, and $k_{eff} = 0.91$.

From the obtained spectra it is deducted that 99% of neutrons have energies higher than 0.001 MeV, and 40% have energies higher than 1 MeV. In addition, when CO_2 is used as a coolant, the spectrum is harder and reflects greater quantities of fission and, to a lesser extent, fusion neurons, than in the water-cooling case.

The obtained spectra were used to calculate average cross-sections. As shown in Fig. 3, there are three important actinides (^{237}Np, ^{241}Am, ^{243}Am), whose capture-to-fission ratio, α, is higher than 1, despite a very hard neutron spectra inside the transmutation area ($\bar{E}_n > 3$ MeV). At the same time, it must be emphasized that this ratio is only slightly higher than 1, as opposed to α for light-water and fast reactors. As follows from Fig. 3, CO_2 is the best cooling option for the transmutation of MAs, as it allows all predominant actinides to have the lowest α value. There is, however, one problem with this coolant, to be discussed below.

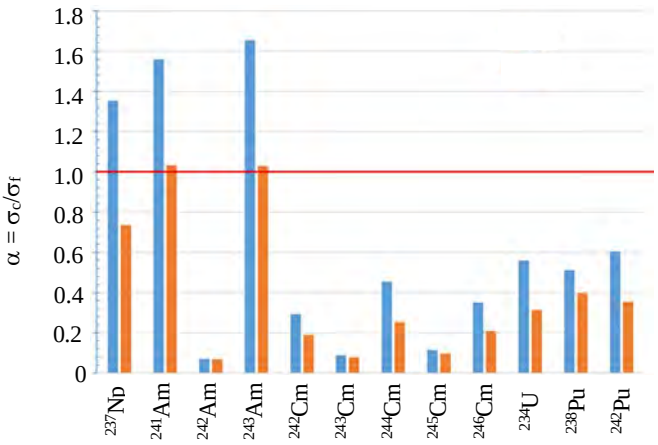

Fig. 3. Average capture-to-fission ratio, α, obtained with different coolants: ■ — H_2O; ■ — CO_2

Key transmutation characteristics observed in each of the reactors are listed in Table 3. Among other things, the table provides data on how the mass of the most important actinides changes during irradiation.

T a b l e 3. **Key MA transmutation characteristics observed in the FFHSs**

Parametr	DEMO-FNS (H_2O)	DEMO-FNS (CO_2)	PIHR	IHR
Total fuel loading, t	26.24	19.7	26.24	41.68
Irradiation + Idle, y	16.7	16.7	6.25	5.25
Change in actinide mass: accumulation (+); reduction (–), kg/t (per t of fuel)		Np		
	–9.9 (3.5%)	–5.2 (1.8%)	–19.1 (6.7%)	–100.3 (35.0%)
		Am		
	–70.2 (10.5%)	–63.2 (9.5%)	–60.8 (9.1%)	–241.8 (36.2%)
		Cm		
	–0.4 (7.7%)	–1.0 (21.2%)	+2.8 (57.5%)	+17.7 (358.1%)
		U		
	+2.4	+1.6	+0.9	+3.0
		Pu		
	+43.5	+29.5	+41.7	+174.0
Burnup of actinides, % (mass)	3.6	4.0	3.6	15.4
Total actinide incineration, kg	906.4	755.0	904.4	6148.0
Efficiency of actinide incineration, kg/year	54.3	45.2	144.7	1171.0
Time-averaged fission power, (thous. MW)	472	398	472	3100

A more detailed analysis of the final fuel inventory shows that the largest Pu fraction is comprised of ^{238}Pu (80%), ^{242}Pu (11%) and ^{240}Pu (6.5%). ^{234}U represents U almost entirely (99%). Although the total mass of Cm decreases, new isotopes ^{242}Cm (12%) and ^{245}Cm (2%) are produced due to neutron capture on Am and initial ^{244}Cm. ^{237}Np (37%) and ^{241}Am (60%) subjected to neutron capture generate a chain leading to ^{238}Pu. ^{234}U occurs as a product of ^{238}Pu α-decay.

As mentioned above, a simple change of the transmutation area coolant to CO_2 causes k_{eff} to grow to 1.04 and requires the total fuel loading to be decreased to 19.7 t. With CO_2, the qualitative change in actinides' combined mass is the same as with H_2O, but quantitative parameters are different. The burnup of actinides increases by 14.3%, however the total actinide incineration is less because of a lower fuel loading. The amount of transmuted Np and Am is smaller, as is the accumulation of U and Pu, while the amount of transmuted Cm is twice as large. This change is due to a greater hardness of the CO_2-associated spectrum, resulting in a neutron capture cross-section decrease that overrides the increase in the fission cross-sections. The result is the overall cross-section decrease, and the reduction of the transmutation rate. At the same time, due to the lower neutron capture rate, Cm is less than before, while its fission rate is very high (owing to its isotopes' low α). Consequently, the transmuted amount of Cm is larger than before.

Initially, fuel contains a small amount of Cm. For this reason, while its isotopes undergo fission at a high rate, new Cm isotopes emerge due to the neutron capture reaction on other actinides. The Cm amount may even increase (as reported in [15]): the neutron capture rate for other actinides is higher than the fission rate of Cm. This situation is typical for the operation of both the pilot industrial (PIHR) and industrial (IHR) reactors.

The ultimate purpose of the FFHS project is to create an industrial-scale hybrid reactor. The IHR will feature the same build as the DEMO-FNS and PIHR and similarly produce 40 MW of fusion power, but will have a larger fuel loading (40 t). This implies a more intense neutron flux in the transmutation area. For this study, it is assumed that the neutron flux will increase five times compared to the demo reactor using H_2O as a coolant. The high capacity factor (0.95) and large fuel loading should make for a good performance. Not only for MA transmutation, but also for electrical power production exceeding the reactor's operational consumption, so this facility will solve the problem of MA transmutation not only from a technical, but also from an economical, perspective.

For the IHR, fuel inventory evolution during the operating cycle is similar to that for the PIHR with the exception that the transmutation rate is higher due to a higher neutron flux. The IHR will be able to produce more than 3 GW (th) and ~1 GW (el), while its own electrical energy consumption will be about 200 MW.

FFHS integration in Russia's two-component nuclear power system and the potential for MA reduction. In the first part of this study, the potential of FFHSs for the MA transmutation was defined. However, what also matters is the impact of FFHSs' operation on the nuclear power system that reduces the total amount of MA. For this purpose, the Universal System Model designed by E.V. Muraviev [16] was used.

Fig. 4 shows the historic and prospective evolution of Russia's nuclear power net installed capacity. In 2100, the last thermal reactor will be decommissioned and only fast reactors will remain.

Nuclear power net installed capacity determines the production of SNF (and related MAs), as well as the total amount of MAs accumulated over a given year.

Fig. 5 shows the total amount of MAs in the system during successive five-year periods between 1970 and 2130. 287 t of MAs accumulate in SNF, if there is no fuel reprocessing, as shown with the blue curve. The orange curve is for actinides, whose inventory is scaled down with the help of hybrid reactors. The grey curve represents MAs managed through hybrid reactors' operation and initial fuel loadings in the blankets, so it is possible to reduce the total amount by 28% (82 t) or 43% (122 t), taking into account the initial fuel loadings.

The rate of MA production in the system was determined obtained based on information about MA accumulation during the assumed period of time. As follows from obtained data, it will be necessary to incinerate more than 4 t/year of MAs at the end of this timeline. This means that at least 4 facilities with IHR parameters will be needed. In the interim, two more IHRs can be put into service, in 2090 and 2120. In that case, the MA amount could be reduced by 48% (142 t) or 88% (262 t) taking into account the initial fuel loadings.

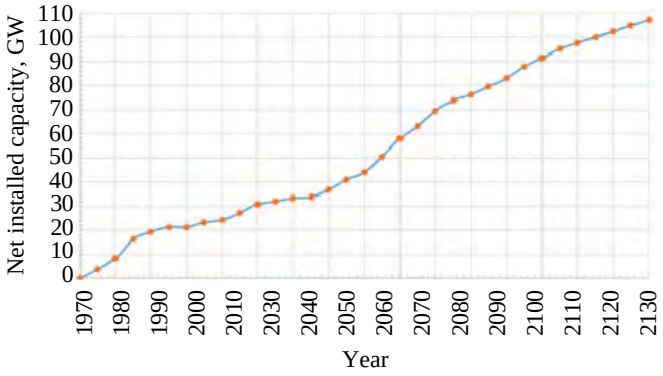

Fig. 4. Evolution of Russia's nuclear power the net installed capacity

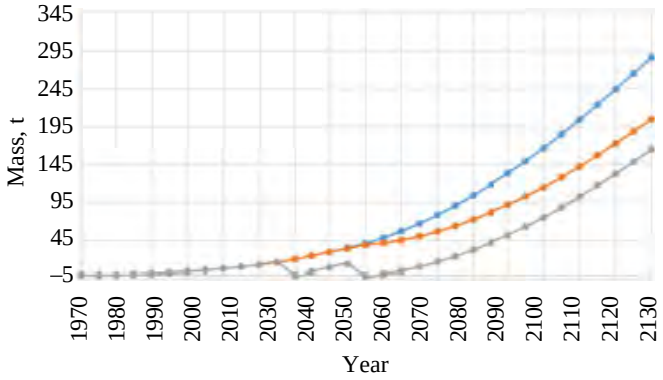

Fig. 5. Russian nuclear power system's total MA inventory: • — without PT; • — reduced amount by FFHR-operation; • — reduced amount by FFHR-operation and initial load

CONCLUSION

This research was performed as part of the Kurchatov Institute's project on the development of fusion-fission hybrid reactors in Russia. This study shows that the application of fusion-fission hybrid reactors possesses a promising application potential for the transmutation of minor actinides. Calculations on neutron transport and nuclide kinetics were performed for three reactor types intended for different purposes (demonstration, pilot-industrial, and industrial). The capture-to-fission ratio was found to be is less than 1 for most actinides, which should favor an effective MA transmutation. The exceptions are ^{237}Np (only if H_2O is used as a coolant), ^{241}Am and ^{243}Am, with α slightly higher than 1. The use of CO_2 as a coolant required the reduction of the total fuel load, thus the potential advantages of this coolant for transmutation are neutralized. This can be improved via optimization of the transmutation area for this coolant. During irradiation, new actinides emerge. This is important in light of the fuel potential multicycle reprocessing and reuse. Determining an equilibrium inventory for the FFHS's fuel is an objective for future research, as is the analysis of the inventory evolution and its influence on the neutron spectrum during irradiation and vice versa.

For effective MA transmutation, in terms of not only technical but also economical parameters, it is necessary to use a FFHS with a large fuel loading and high capacity factor, such as the IHR, which is able to incinerate more than 1 t of actinides per year and generate about 1 GW of electrical power.

A system analysis of nuclear power in Russia, performed with the involvement of the hybrid reactors, highlight the problems associated with the absence of MA transmutation and the potential of FFHSs to reduce these hazards.

As can be seen from the reported results, there is a deficit of extracted MA, even for optimized development scenarios. At the same time, it is necessary to decommission the DEMO-FNS and PIHR (at least as burner reactors), and to abandon one additional IHR, which is needed due to the rate of MA accumulation in the system. It is also necessary to delay the commissioning of 2 other additional IHRs.

For the scenarios considered in the study, the deficit problem of extracted MA may be overcome by around 2075. However, in the case of additional IHRs, the MA deficit takes place again at the time when the second and the third IHR is commissioned. This can be improved by using imported SNF, which can be considered a service of radioactive waste management. The results obtained also highlight the need to speed up the commissioning of SNF reprocessing plants to ensure the required amount of MAs for FFHS fuel manufacturing.

It follows from the analysis performed that, over the period of time considered, it is possible to decrease by 2130 the amount of MA in the system by ~28%, in the case of just 1 IHR, and by ~48%, in the case of two additional IHRs. If MAs loaded in the FFHS blankets are not treated as waste, then the amount of MAs isolated from the system may be up ~43% or, if two additional IHRs are there, up ~88%.

REFERENCES

1. **Salvatores M., Palmiotti G.** Radioactive waste partitioning and transmutation within advanced fuel cycles: achievements and challenges. — Prog. Part. Nucl. Phys., 2011, vol. 66, p. 144—166; doi:10.1016/j.ppnp.2010.10.001.
2. **Adlys G.** Sources of radiotoxicity in spent nuclear fuel. — In: Proc. of the Intern. Symposium on Biomedical Engineering and Medical Physics. Riga, Latvia, 10—12 October 2012; **Dekhtyar Y., Katashev A., Lancere L.** Eds. — Berlin: Springer, 2013, vol. 38, p. 213—216, ISBN 978-3-642-34196-0.
3. **Stacey W.** Transmutation missions for fusion neutron sources. — Fusion Eng. Des., 2007, vol. 82, p. 11—20; doi: 10.1016/j.fusengdes.2005.12.005.
4. **Adamov E.O., Vlaskin G.N., Lopatkin A.V., Rachkov V.I., Khomyakov Y.S.** Radiation equivalent treatment of radioactive nuclides in nuclear fuel cycle — effective alternative to the delayed solution of spent nuclear fuel accumulation problem. — News of the Russian Academy of Sciences, Energy, 2015, vol. 6, p. 15—25.
5. **Crossland I.** Nuclear Fuel Cycle Science and Engineering; Woodhead Publishing Limited. Cambridge, UK, 2012; ISBN 978-0-85709-073-7.
6. **Stacey W.M.** Solving the spent nuclear fuel problem by fissioning transuranics in subcritical advanced burner reactors driven by tokamak fusion neutron sources. — Nucl. Technol., 2017, vol. 200, p. 15—26; doi: 10.1080/00295450.2017.1345585.
7. **Wu Y., Jiang J., Wang M., Jin M., Team F.** A fusion-driven subcritical system concept based on viable technologies. — Nucl. Fusion, 2011, vol. 51, p. 103036; doi: 10.1088/0029-5515/51/10/103036.
8. **Yang C., Cao L., Wu H., Zheng Y., Zu, T.** Neutronics analysis of minor actinides transmutation in a fusion-driven subcritical system. — Fusion Eng. Des., 2013, vol. 88, p. 2777—2784; doi: 10.1016/j.fusengdes.2013.04.021.
9. **Ridikas D., Plukiene R., Plukis A., Cheng, E.** Fusion–fission hybrid system for nuclear waste transmutation (I): characterization of the system and burn-up calculations. — Prog. Nucl. Energy, 2006, vol. 48, p. 235—246; doi: 10.1016/j.pnucene.2005.09.004.
10. **Furudate Y., Shishido H., Yusa N., Hashizume H.** Construction of minor actinides reduction scenario in Japan utilizing fusion reactors. — Prog. Nucl. Energy, 2018, vol. 103, p. 28—32; doi: 10.1016/j.pnucene.2017.11.003
11. **Hong S.H., Kim M.H.** Neutronic investigation of waste transmutation option without partitioning and transmutation in a fusion-fission hybrid system. — Nucl. Eng. Technol., 2018, vol. 50, p. 1060—1067; doi: 10.1016/j.net.2018.06.008.
12. **Stacey W.M., Van Rooijen W., Bates T., Colvin E., Dion J., Feener J., Gayton E., Gibbs D., Grennor C., Head J. et al.** A TRU-Zr metal-fuel sodium-cooled fast subcritical advanced burner reactor. — Nucl. Technol., 2008, vol. 162, p. 53—79; doi: 10.13182/nt08-a3933.
13. **Capriotti L., Brémier S., Inagaki K., Pöml P., Papaioannou D., Ohta H., Ogata T., Rondinella V.** Characterization of metallic fuel for minor actinides transmutation in fast reactor. — Prog. Nucl. Energy, 2017, vol. 94, p. 194—201; doi: 10.1016/j.pnucene.2016.04.004.
14. **Sublet J.-C., Eastwood J., Morgan J., Gilbert M., Fleming M., Arter W.** FISPACT-II: an advanced simulation system for activation, transmutation and material modelling. — Nucl. Data Sheets, 2017, vol. 139, p. 77—137; doi: 10.1016/j.nds.2017.01.002.
15. **Wang M., Zeng Q., Jiang J., Wu Y.** Neutronics analysis and optimization for fusion driven subcritical spent fuel burning system. — J. Fusion Energy, 2015, vol. 34, p. 598—603; doi: 10.1007/s10894-015-9846-2.
16. **Muraviev E.V.** USM-1 System Model Generator. Preprint by FSUE RDIPE (NIKIET) № ET-08/75. Moscow, Russia, 2008.

AUTHORS

Mikhail Shlenskii, assistant-researcher, National Research Nuclear University Moscow Engineering Physics Institute, Plasma Physics Department, Kashirskoe Hwy 31, 115409 Moscow, Russia, shlenskiy_mn@nrcki.ru

Boris V. Kuteev, Professor, Deputy Head Tokamak Department Fusion Research Centre; NRC «Kurchatov Institute», 1, Academika Kurchatova sq., Moscow, 123182, Russia, Kuteev_BV@nrcki.ru

Статья поступила в редакцию 15 января 2021 г.
После доработки 16 марта 2021 г.
Принята к публикации 25 марта 2021 г.
Вопросы атомной науки и техники.
Сер. Термоядерный синтез, 2021, т. 44, вып. 2, с. 139—144.

UDC 621.384.65

HIGH FLUX ACCELERATOR-BASED NEUTRON SOURCE

T.A. Bykov[1, 2], A.A. Ivanov[1], D.A. Kasatov[1, 2], Ia.A. Kolesnikov[1, 2], A.M. Koshkarev[1, 2], G.M. Ostreinov[1, 2], A.N. Makarov[1, 2], I.M. Shchudlo[1, 2], E.O. Sokolova[1, 2], S.Yu. Taskaev[1, 2]

[1]*Budker Institute of Nuclear Physics, Novosibirsk, Russia*
[2]*Novosibirsk State University, Novosibirsk, Russia*

High-flux neutron sources are relevant to testing materials for thermonuclear facilities and hadron colliders, treating malignant tumors with boron neutron capture therapy, and other applications. An accelerator-based neutron source was proposed and implemented at the Budker Institute of Nuclear Physics in Novosibirsk, Russia. It comprises an originally designed tandem accelerator, a solid lithium target, and a neutron beam shaping assembly. The neutron source has been found capable of producing high neutron fluxes in different energy ranges, from thermal to fast. It is applicable to a wide range of research tasks, including the characterization of neutron detectors, intended for fusion studies, in-depth investigation of the promising ^{11}B(p, α)αα neutronless fusion reaction, etc.

Key words: neutron source, charge particle accelerator, lithium target.

DOI: 10.21517/0202-3822-2021-44-2-145-147

ИСТОЧНИК БОЛЬШИХ ПОТОКОВ НЕЙТРОНОВ НА ОСНОВЕ УСКОРИТЕЛЯ

Т.А. Быков[1, 2], А.А. Иванов[1], Д.А. Касатов[1, 2], Я.А. Колесников[1, 2], А.М. Кошкарёв[1, 2], Г.М. Остреинов[1, 2], А.Н. Макаров[1, 2], И.М. Щудло[1, 2], Е.О. Соколова[1, 2], С.Ю. Таскаев[1, 2]

[1]*Институт ядерной физики им. Г.И. Будкера СО РАН, Новосибирск, Россия*
[2]*Новосибирский государственный университет, Новосибирск, Россия*

Источники больших потоков нейтронов могут найти применение при исследовании материалов для термоядерных установок и адронных коллайдеров, лечении злокачественных опухолей методом бор-нейтронозахватной терапии и для других целей. В новосибирском Институте ядерной физики им. Г.И. Будкера был изобретён и изготовлен такой нейтронный источник на основе ускорителя, включающий впервые разработанный тандемный ускоритель оригинальной конструкции, твёрдую литиевую мишень и систему формирования пучка нейтронов. Было обнаружено, что разработанный нейтронный источник способен генерировать большие потоки нейтронов в различных диапазонах энергии — от тепловых нейтронов до быстрых. Он может применяться для многих целей, включая определение характеристик нейтронных детекторов, используемых в термоядерных исследованиях, а также при углублённом изучении перспективной безнейтронной термоядерной реакции ^{11}B(p, α)αα.

Ключевые слова: нейтронный источник, ускоритель заряженных частиц, литиевая мишень.

INTRODUCTION

A neutron source based on a charged particle accelerator and a lithium target has been proposed and developed for boron neutron capture therapy (BNCT) [1, 2] at the Budker Institute of Nuclear Physics (BINP) in Novosibirsk, Russia. This paper describes the said neutron source and summarizes relevant research. The neutron source applicability for the testing of fusion materials is discussed.

NEUTRON SOURCE

The BINP neutron source comprises a DC vacuum insulation tandem accelerator (VITA), a lithium target, and a neutron beam shaping assembly. A schematic diagram of the neutron source is shown in Fig. 1. The VITA is used to provide a high-current proton/deuteron beam of up to 2.3 MeV. Negative ions injected into the VITA are accelerated by applying a positive potential to the central electrode, then stripped to positive ions, and accelerated again by the same potential. The VITA has a special design that does not include accelerating tubes [3] present in conventional tandem accelerators. Instead, it

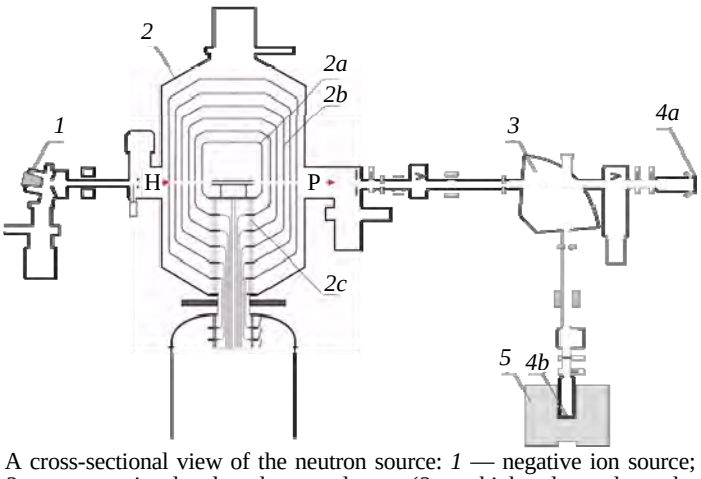

A cross-sectional view of the neutron source: *1* — negative ion source; *2* — vacuum insulated tandem accelerator (*2a* — high voltage electrode; *2b* — intermediate electrodes; *2c* — feedthrough insulator); *3* — bending magnet; *4* — lithium targets (*4a* — horizontally; *4b* — vertically); *5* — neutron beam shaping assembly

features intermediate nested electrodes (*2b*), fastened to a feedthrough insulator (*2c*), as shown in Figure. The advantage of this setup is that the ceramic parts of the feedthrough insulator are distanced well away from the ion beam, increasing the high-voltage strength of accelerating gaps given high ion beam current.

After acceleration, the ion beam is directed to the lithium target placed either horizontally (*4a*) or vertically (*4b*) behind the bending magnet. The low and high energy beam lines are equipped with diagnostics, such as retractable Faraday cups, beam current monitors, video cameras, beam profile scanner, stripping target efficiency monitor, and thermocouples installed on the beam apertures along its path. The lithium target (*4*) on a copper substrate is used to generate a neutron flux via the ^{7}Li(*p, n*)^{7}Be- or ^{7}Li(*d, n*)-reactions. The target assembly is water cooled [4].

RESULTS AND DISCUSSION

Proton beam energy varies in the range of 0.6—2.3 MeV with a high-energy stability of 0.1%. The beam current also varies in a wide range (from 0.5 to 10 mA) with a high current stability (0.4%) [5]. The VITA can generate a deuteron beam with similar characteristics.

A 2 MeV proton beam was used for an *in situ* observation of blisters growth in copper and tantalum [6]. The neutron yield behavior generated the ^{7}Li(*p, n*)^{7}Be-reaction was determined as a function of neutron fluence to identify the copper substrate's potential blistering effect on the efficiency of neutron production.

Table shows the yields and energies of reaction products generated by the device.

The yields and energies of reaction products generated by the device

Reaction	Incident ion energy, MeV	Product of reaction	Yield, 10^{11} mC^{-1}	Mean energy, keV	Maximum energy, keV	Ref.
^{7}Li(*p, n*)^{7}Be	2.0	Neutrons	1.1	75	230	[7]
	2.1		2.13	110	350	
	2.2		3.62	160	460	
	2.3		5.78	230	570	
^{7}Li(*d, n*)^{8}Be; ^{7}Li(*d, n*)2^{4}He	2.1		15	5600	15000	[8]
^{7}Li(*p, p'* γ)^{7}Li	1.85	Photons	0.9	478		[9]

In the device, the neutron flux is generated by the ^{7}Li(*p, n*)^{7}Be threshold reaction. A beam shaping assembly with a magnesium fluoride moderator is applied to convert this flux into a beam of epithermal neutrons with characteristics suitable for clinical testing of BNCT [10].

The device is capable of producing a beam of thermal neutrons with a plexiglas moderator. This beam is employed to irradiate cell cultures and laboratory animals for the boron neutron capture therapy (BNCT) development purposes [11, 12]. It is also used to measure hazardous impurities in boron carbide ceramics and 316L-IG austenitic stainless steel considered for ITER [13].

A beam of monoenergetic neutrons with energies from 10 to 100 keV is produced by kinematic collimation using several-micron-thick lithium foil targets. This beam is suitable for calibrating a dark matter detector [14] and is to be used for boron imaging by prompt gamma-ray spectroscopy.

Fast neutron flux is obtained via the ^{7}Li(*d, n*)-reaction [8]. It is employed to study the activation of B_4C ceramics and SS 316L ITER-grade steel by fast neutrons [15]. It is also intended for the radiation tests of fibers used in the laser calorimeter calibration system of the CMS electromagnetic detector developed for the High-Luminosity Large Hadron Collider at CERN.

A 478 keV-photon flux is produced by the ^{7}Li(*p, p'* γ)^{7}Li-reaction (inelastic proton scattering by a lithium atomic nucleus) at a proton beam energy below 1.882 MeV, the threshold value for the ^{7}Li(*p, n*)^{7}Be-reaction. This beam is used for *in situ* measuring of the lithium layer thickness [16] and for determining the doses of high-LET radiation [17].

To sum it up, the device is applicable to a wide range of research tasks, including the characterization of neutron detectors designed for fusion studies, in-depth investigation of the promising ^{11}B(*p*, α)αα neutronless fusion reaction, etc.

CONCLUSION

The accelerator-based neutron source can produce high neutron fluxes in different energy ranges, from thermal to fast, that can be useful in various fields of research, including thermonuclear fusion. The research team has already been involved in neutron activation experiments conducted under the ITER project.

The study was supported by a grant (project № 19-72-30005) from the Russian Science Foundation.

REFERENCES

1. **Neutron** Capture Therapy. Principles and Applications. Eds. W. Sauerwein, A. Wittig, R. Moss, Y. Nakagawa. — New York: Springer, 2012; doi: 10.1007/978-3-642-31334-9.
2. **Dymova M., Taskaev S., Richter V., Kuligina E.** Boron neutron capture therapy: current status and future perspectives. — Cancer Communications, 2020, vol. 40, p. 406—421; doi: 10.1002/cac2.12089.
3. **Bayanov B., Belov V., Bender E., Bokhovko M., Dimov G., Kononov V., Kononov O., Kuksanov N., Palchikov V., Pivovarov V., Salimov R., Silvestrov G., Skrinsky A., Taskaev S.** Accelerator based neutron source for the neutron-capture and fast neutron therapy at hospital. — Nucl. Instrum. and Methods A, 1998, vol. 413, p. 397—426; doi: 10.1016/S0168 9002(98)00425-2.
4. **Bayanov B., Belov V., Kindyuk V., Oparin E., Taskaev S.** Lithium neutron producing target for BINP accelerator-based neutron source. — Applied Radiation and Isotopes, 2004, vol. 61, p. 817—821; doi: 10.1016/j.apradiso.2004.05.032.
5. **Taskaev S.** Accelerator based epithermal neutron source. — Phys. Part. Nuclei, 2015, vol. 46, p. 956—990; doi: 10.1134/S1063779615060064.
6. **Badrutdinov A., Bykov T., Gromilov S., Higashi Y., Kasatov D., Kolesnikov I., Koshkarev A., Makarov A., Miyazawa T., Shchudlo I., Sokolova E., Sugawara H., Taskaev S.** *In situ* observations of blistering of a metal irradiated with 2-MeV protons. — Metals, 2017, vol. 7, 558; doi: 10.3390/met7120558.
7. **Lee C.L., Zhou X.-L.** Thick target neutron yields for the ^{7}Li(*p*, *n*)^{7}Be reaction near threshold. — Nucl. Instrum. and Methods in Phys. Res. Sect. B, 1999, vol. 152, p. 1—11; doi: 10.1016/S0168-583X(99)00026-9.
8. **Kasatov D., Koshkarev A., Makarov A., Ostreinov G., Taskaev S., Shchudlo I.** Fast-neutron source based on a vacuum-insulated tandem accelerator and a lithium target. — Instruments and Experimental Techniques, 2020, vol. 63, p. 611—615; doi: 10.1134/S0020441220050152.
9. **Bykov T., Kasatov D., Kolesnikov Ia., Koshkarev A., Makarov A., Shchudlo I., Sokolova E., Taskaev S.** Measurement of the ^{7}Li(*p*, *p*' γ)^{7} Li reaction cross-section and 478 keV photon yield from a thick lithium target at proton energies from 0.7 to 1.85 MeV. — Applied Radiation and Isotopes, 2021, vol. 175, 109821; doi: 10.1016/j.apradiso.2021.109821.
10. **Zaidi L., Belgaid M., Taskaev S., Khelifi R.** Beam shaping assembly design of ^{7}Li(*p*, *n*)^{7}Be neutron source for boron neutron capture therapy of deep-seated tumor. — Applied Radiation and Isotopes, 2018, vol. 139, p. 316—324; doi: 10.1016/j.apradiso.2018.05.029.
11. **Sato E., Zaboronok A., Yamamoto T., Nakai K., Taskaev S., Volkova O., Mechetina L., Taranin A., Kanygin V., Isobe T., Mathis B., Matsumura A.** Radiobiological response of U251MG, CHO-K1 and V79 cell lines to accelerator-based boron neutron capture therapy. — J. Radiat. Res., 2018, vol. 59, p. 101—107; doi: 10.1093/jrr/rrx071.
12. **Zavjalov E., Zaboronok A., Kanygin V., Kasatova A., Kichigin A., Mukhamadiyarov R., Razumov I., Sycheva T., Mathis B., Maezono S., Matsumura A., Taskaev S.** Accelerator-based boron neutron capture therapy for malignant glioma: a pilot neutron irradiation study using boron phenylalanine, sodium borocaptate and liposomal borocaptate with a heterotopic U87 glioblastoma model in SCID mice. — Intern. J. Radiat. Biology, 2020, vol. 96, p. 868—878; doi: 10.1080/09553002.2020.1761039.
13. **Shoshin A., Burdakov A., Ivantsivskiy M., Polosatkin S., Klimenko M., Semenov A., Taskaev S., Kasatov D., Shchudlo I., Makarov A., Davydov N.** Qualification of boron carbide ceramics for use in ITER ports. — IEEE Trans. on Plasma Science, 2020, vol. 48, p. 1474—1478; doi: 10.1109/TPS.2019.2937605.
14. **Makarov A., Taskaev S.** Beam of monoenergetic neutrons for the calibration of a dark-matter detector. — JETP Letters, 2013, vol. 97, p. 667—669; doi: 10.1134/S0021364013120072.
15. **Shoshin A., Burdakov A., Ivantsivskiy M., Polosatkin S., Klimenko M., Semenov A., Sulyaev Yu., Zaitsev E., Polozova P., Taskaev S., Kasatov D., Shchudlo I., Bikchurina M.** Test results of boron carbide ceramics for ITER port protection. — Fusion Engineering and Design, 2021, vol. 169, 112426; doi: 10.1016/j.fusengdes.2021.112426.
16. **Kasatov D., Kolesnikov Ia., Koshkarev A., Makarov A., Sokolova E., Shchudlo I., Taskaev S.** Method for *in situ* measuring the thickness of a lithium layer. — JINST, 2020, vol. 5, P10006; doi: 10.1088/1748-0221/15/10/P10006.
17. **Dymova M., Dmitrieva M., Kuligina E., Richter V., Savinov S., Shchudlo I., Sycheva T., Taskaeva I., Taskaev S.** Method of measuring high-LET particles dose. — Radiation Research, 2021, vol. 196; doi: 10.1667/RADE-21-00015.1.

Budker Institute of Nuclear Physics, 11 Lavrentiev ave., 630090, Novosibirsk, Russia; Novosibirsk State University, 1 Pirogov str., 630090, Novosibirsk, Russia

T.A. Bykov, graduate student; timaisabrony@gmail.com
A.A. Ivanov, PhD, Prof., Head of Laboratory; Budker Institute of Nuclear Physics, A.A.Ivanov@inp.nsk.su
D.A. Kasatov, PhD, researcher; kasatovd@gmail.com
Ia.A. Kolesnikov, graduate student; katyono@mail.ru
A.M. Koshkarev, engineer; kent_brockman4@mail.ru
G.M. Ostreinov, junior researcher; wtfsnoo@gmail.com
A.N. Makarov, PhD, senior researcher; alexxmak314@gmail.com
I.M. Shchudlo, researcher; cshudlo.i.m@gmail.com
E.O. Sokolova, graduate student; buiya@bk.ru
S.Yu. Taskaev, PhD, chief researcher; taskaev@inp.nsk.su

Статья поступила в редакцию 15 января 2021 г.
После доработки 16 марта 2021 г.
Принята к публикации 25 марта 2021 г.
Вопросы атомной науки и техники.
Сер. Термоядерный синтез, 2021, т. 44, вып. 2, с. 145—147.

UDC 544.022.341, 544.022.382

DIFFUSION CHARACTERISTICS OF RADIATION DEFECTS IN IRON: MOLECULAR DYNAMICS DATA

A.B. Sivak, D.N. Demidov, P.A. Sivak

NRC «Kurchatov Institute», Moscow, Russia

Temperature dependences of the diffusion characteristics of radiation defects, namely, clusters of up to five self-interstitial atoms (SIAs), were studied by the molecular dynamics method for bcc Fe at temperatures in the range of 300—1200 K. The above-mentioned diffusion characteristics included the diffusion coefficient, the tracer correlation factor, the mean distance traveled between changes in the migration direction, the frequency of migration direction changes, etc. The activation energy values for diffusion and changes in the migration direction were determined for the defects of interest for different temperature ranges. The temperature and size dependences of the SIA cluster diffusion mechanism (1D vs 3D) and their potential implications for the microstructure of materials exposed to irradiation are discussed.

Key words: iron, molecular dynamics, interatomic interaction potentials, radiation defects, diffusion mechanisms, diffusivities.

DOI: 10.21517/0202-3822-2021-44-2-148-157

ДИФФУЗИОННЫЕ ХАРАКТЕРИСТИКИ РАДИАЦИОННЫХ ДЕФЕКТОВ В ЖЕЛЕЗЕ: МОЛЕКУЛЯРНО-ДИНАМИЧЕСКИЕ ДАННЫЕ

А.Б. Сивак, Д.Н. Демидов, П.А. Сивак

НИЦ «Курчатовский институт», Москва, Россия

Методом молекулярной динамики исследованы температурные зависимости диффузионных характеристик радиационных дефектов — кластеров собственных межузельных атомов (СМА), содержащих до пяти СМА — в температурном диапазоне 300—1200 К в ОЦК Fe. Упомянутые диффузионные характеристики включали в себя коэффициент диффузии, корреляционный множитель меченых атомов, среднюю длину диффузионного пробега до смены направления диффузии, частоту смен направлений диффузии, др. Определены значения энергии активации диффузии и энергии активации смен направлений диффузии для рассмотренных типов дефектов для разных температурных диапазонов. Обсуждаются зависимости механизма диффузии кластеров СМА (1D vs 3D) от температуры и размера кластеров и их возможные следствия для эволюции микроструктуры материала под облучением.

Ключевые слова: железо, молекулярная динамика, потенциалы межатомных взаимодействий, радиационные дефекты, механизмы диффузии, коэффициенты диффузии.

INTRODUCTION

The diffusion of radiation defects to sinks (dislocations, grain boundaries, sub-boundaries, interfaces, etc.) and their subsequent absorption affect the microstructure evolution of fusion/fission reactor structural materials with resultant changes in their physical and mechanical properties (radiation creep and embrittlement, and void swelling) [1]. The physical modelling of changes in material properties induced by irradiation or mechanical/thermal loads requires the characteristics of radiation defects, to be used as inputs for such models.

Damaging neutron irradiation causes atomic collision cascades, which generate not only self-point defects (SPDs) but their clusters as well [2]. A molecular dynamics (MD) study of primary radiation damage in iron [3, 4] has shown that the higher the cascade damage energy, the greater is the tendency for self-interstitial atoms (SIAs) to form clusters: the fraction of single SIAs decreases from 70 to 40% with increase in the damage energy from 1 to 50 keV. In a given range of damage energies, 30% to 40% of surviving SIAs are grouped in clusters of two to five.

Because the properties of SIAs and their small clusters are difficult to assess experimentally due to small spatial sizes (~nm), computer simulation is actively used, which allowed to determine the diffusion characteristics of single SIAs and clusters of up to 91 SIAs in Fe [5—18]. The results of computer simulations are highly sensitive to the selection of applicable interatomic interaction potential. Elastic moduli determined experimentally for Fe and V were very much at variance with values calculated based on the density functional theory (DFT) [19]. Therefore, the applicability of DFT to the calculation of SPDs is questionable, as is the use of potentials with parameters fitted to DFT data. In this context, data from many publications cited above require validation and refinement using a reliable interatomic interaction potential, consistent with experimental data. It was shown in [19] that the interatomic interaction potential R01 [20—23], developed for the bcc metal Fe, agreed well with the experimentally measured crystal bulk properties (elastic constants at 0 K and the temperature dependence of the lattice parameter), the properties of SIAs and vacancies, as well as threshold displacement energies, and was therefore recommended for use in MD simulations of atomic collision cascades and SPDs. Using R01, the crystallographic, energetic, and diffusion properties of SIAs [8, 12, 13] and di-interstitials [9, 17, 18] were determined and atomic collision cascades were simulated [3, 4].

This paper describes the results of the study of the diffusion characteristics of clusters of three to five SIAs in bcc Fe at temperatures in the range of 300—1200 K, performed by MD using the R01 potential. The temperature and size dependences of the SIA cluster diffusion mechanism (1D vs 3D) and their potential implications for the microstructure of materials exposed to irradiation are discussed.

SIMULATION TECHNIQUE

Cluster size q is the number of SIAs in a cluster. An SIA cluster of size q is denoted as q-SIA. To study the diffusion of SIA clusters with q = 3—5, MD simulations were carried out using cubic model crystallites with periodic boundary conditions. Those crystallites represented a microcanonical ensemble. The lattice constant, a, was chosen to ensure that pressure P in the crystallite bulk was zero (accurate to 0.1 eV/nm^3) at given temperature T. The equations of motion were integrated by the Verlet algorithm [24]. The integration time step was selected to ensure that the average of atomic displacements per iteration was ~0.005a. The positions of clustered SIAs were determined from the numbers of atoms in Wigner—Seitz cells (WSCs). The position of the WSC closest to the cluster mass centre was taken as the position of the SIA cluster. The model crystallite size was chosen so that the boundary condition effect on the calculation results was insignificant. Crystallites with a side length of 13a (the total number of atoms was 4394 + 3 and 4394 + 4, respectively) were used to simulate the diffusion of 3-SIA and 4-SIA clusters. For 5-SIA clusters, the side length was 15a (6750 + 5).

The most stable SIA cluster configurations were chosen as initial configurations. Table 1 shows their formation and binding energies (E^F and E^B, respectively) for clusters of two to five SIAs (calculated in [9]), as well as their schematic spatial configurations (viewed from different perspectives). All SIA clusters with $q > 2$ are sets of crowdions or dumbbells split in the ⟨111⟩ direction (henceforth, the split direction will be referred to as cluster orientation). SIAs occupy the most compact set of adjacent close-packed directions projected onto the plane normal to the splitting direction (see Table 1).

T a b l e 1. **Crystallographic configurations of simulated SIA clusters in Fe, their formation energies E^F and binding energies E^B**

Cluster type	Crystallographic configuration	Formation energy and binding energy, eV
2-SIA	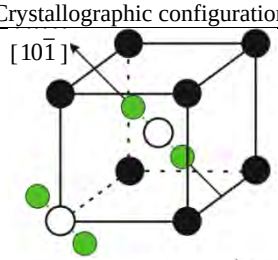	E^F = 7.884 E^B = 0.884
3-SIA	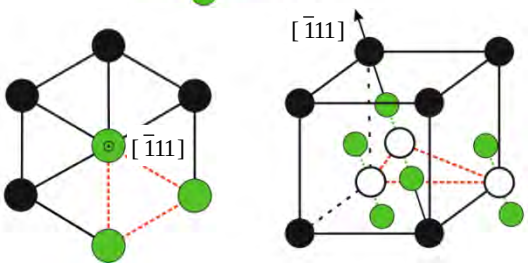	E^F = 11.04 E^B = 1.230
4-SIA	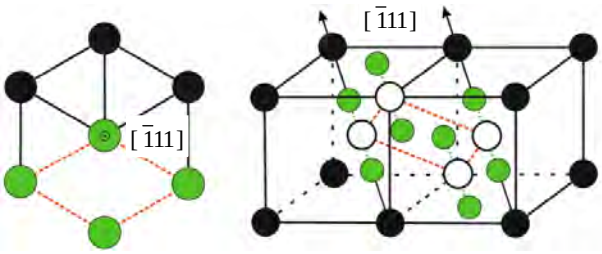	E^F = 13.37 E^B = 2.050
5-SIA	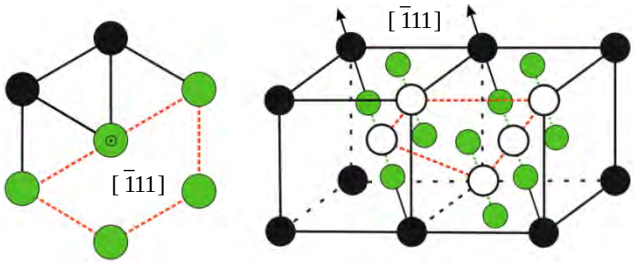	E^F = 15.95 E^B = 1.810

For each given cluster size and temperature, one hundred diffusion trajectories were obtained. Table 2 lists the total physical simulation time and the number of cluster jumps summed over all trajectories for clusters and temperatures of interest. To calculate the diffusivity D^{d} of an SIA cluster, each simulated diffusion trajectory was split into several isochronous segments of duration τ. The choice of the τ value is a trade-off between the need to have a large enough number of segments (to minimize random errors) and a large enough number of defect jumps at each of those segments to account for any significant spatial correlation associated with SIA cluster diffusion (to minimize systematic errors). The empirical dependence $\tau[\text{ps}] = 0.66\exp(-\beta\cdot 0.078\ \text{eV})$ with $\beta = (k_B T)^{-1}$ obtained in [18] for 2-SIAs, was used in this study to select τ for a given *T*. Our analyses proved that it is applicable to clusters of three to five SIAs. For all isochronous segments of all trajectories, values $r^2/6\tau$ were calculated, where *r* is the displacement of the SIA cluster during time τ for one segment. The value D^{d} was determined as the average of these values, and the D^{d} inaccuracy was estimated as the standard error for the specified set.

T a b l e 2. **Physical simulation time t_s and the number of jumps j_s for the discussed types of clusters in Fe (integral over all trajectories)**

T, K	3-SIA		4-SIA		5-SIA	
	t_s, μs	j_s	t_s, μs	j_s	t_s, μs	j_s
300	61.5	$2.87\cdot10^{7}$	122	$2.43\cdot10^{8}$	70.9	$1.89\cdot10^{8}$
400	34.7	$1.80\cdot10^{7}$	65.7	$1.50\cdot10^{8}$	47.1	$1.42\cdot10^{8}$
500	21.1	$1.20\cdot10^{7}$	33.1	$8.38\cdot10^{7}$	27.2	$9.07\cdot10^{7}$
700	15.0	$9.47\cdot10^{6}$	17.1	$4.72\cdot10^{7}$	18.7	$6.76\cdot10^{7}$
800	8.81	$5.97\cdot10^{6}$	8.84	$2.62\cdot10^{7}$	12.3	$4.76\cdot10^{7}$
900	5.23	$3.80\cdot10^{6}$	—	—	5.94	$2.44\cdot10^{7}$
1000	2.63	$2.00\cdot10^{6}$	1.05	$3.91\cdot10^{6}$	3.24	$1.40\cdot10^{7}$
1100	1.34	$1.08\cdot10^{6}$	—	—	—	—
1200	0.556	$4.73\cdot10^{5}$	0.126	$4.87\cdot10^{5}$	1.22	$5.52\cdot10^{6}$

Tracer diffusivity D^{tr} (self-diffusivity per one SIA) was calculated by Einstein-Smoluchowski relation [25] using the initial and end positions of each atom in crystallite models (100 program runs). For each dataset, self-diffusivity intermediate values were calculated. The final D^{tr} value was obtained by their averaging. The D^{tr} inaccuracy was estimated as the standard error over the specified set of 100 intermediate values.

Tracer correlation factor f^{tr} was determined as the ratio of D^{tr} to D^{d}. Because f^{tr} is affected by the cluster diffusion mechanism, it can be used to indicate changes in the mechanism of SIA clusters diffusion. E.g., in the case of a one-dimensional (1D) diffusion of a crowdion, $f^{tr} = 0$ [26], whereas in the case of a 3D diffusion of ⟨110⟩ dumbbells under Johnson's mechanism, $f^{tr} = 0.4151 \pm 0.0001$ [18]. Usually, cluster diffusion is promoted by a mixed mechanism: clusters make a number of jumps in one of the ⟨111⟩ directions, followed by a change in the migration direction, resulting from the cluster reorientation.

Other metrics that allow the contributions of the 1D/3D diffusion mechanisms to be assessed are the mean distance traveled between changes in the migration direction [27, 28], and the frequency of migration direction changes (l_{ch} and ν^{R}, respectively). To determine ν^{R} and l_{ch}, a special algorithm analyzing MD defect trajectories was developed. In this study, l_{ch} is expressed as $l_{ch} = (6D^{d}\langle\Delta t_{1D}\rangle)^{1/2}$, where $\langle\Delta t_{1D}\rangle$ is the average time between two successive reorientations.

The instants of time, at which the cluster reorientations occurred were determined using the following algorithm:

— (1) construct four cylinders of radius ρ with axes oriented along four close-packed directions ⟨111⟩ and passing through the initial position of the SIA cluster on the diffusion trajectory;

— (2) determine four instants of time, at which the trajectory leaves each cylinder;

— (3) the latest of the four instants of time, identified in step 2, is taken as the instant, at which the cluster is reoriented;

— (4) construct cylinders of radius ρ with axes oriented along ⟨111⟩ and passing through the cluster's new position at the instant the last cluster reorientation is detected;

— (5) repeat steps 2—4 until the last cluster reorientation on the diffusion trajectory is detected.

Upon the completion of this algorithm, the durations Δt_{1D} between successive moments of cluster reorientations are determined and averaged to obtain the desired $\langle \Delta t_{1D} \rangle$ value. Inaccuracy is determined as the standard error for the entire set of Δt_{1D} values.

Radius ρ was an algorithm parameter obtained using an iterative selection method, in which an initially large value (e.g., 5*a*) was successively decreased by *a*/2 until it stopped to produce any noticeable effect on the total number of detected 1D segments and the final values of l_{ch} and $\langle \Delta t_{1D} \rangle$. The obtained values of ρ are 1.5*a* for 1-, 2-SIA and 2*a* for 3-, 4-, 5-SIA.

Frequency ν^R was determined as the reciprocal of $\langle \Delta t_{1D} \rangle$. Since the time intervals between two successive reorientations have a Poisson distribution, the relative error $\delta\nu_R$ for the frequency of reorientations ν^R can be determined as $N_R^{-1/2}$, where N_R is the total number of reorientations detected at a given temperature. The $\delta\nu_R$ values at different temperatures vary from 1% to 50%. The least accurate ν^R values were obtained at temperatures below 500 K since reorientations were rare and their total number for the entire simulation period was usually ~10 (for all 100 diffusion trajectories at a given *T*).

RESULTS AND DISCUSSION

Figs. 1, 2 show typical MD trajectories of single and clustered SIAs at temperatures of 300, 700 and 1200 K, as well as the physical simulation time for each illustrated trajectory τ_m. Data for single SIAs and 2-SIA clusters were obtained in [8, 12, 13] and [17, 18], respectively. The diffusion of single SIAs and 2-SIA clusters has a much higher degree of three-dimensionality compared with larger clusters.

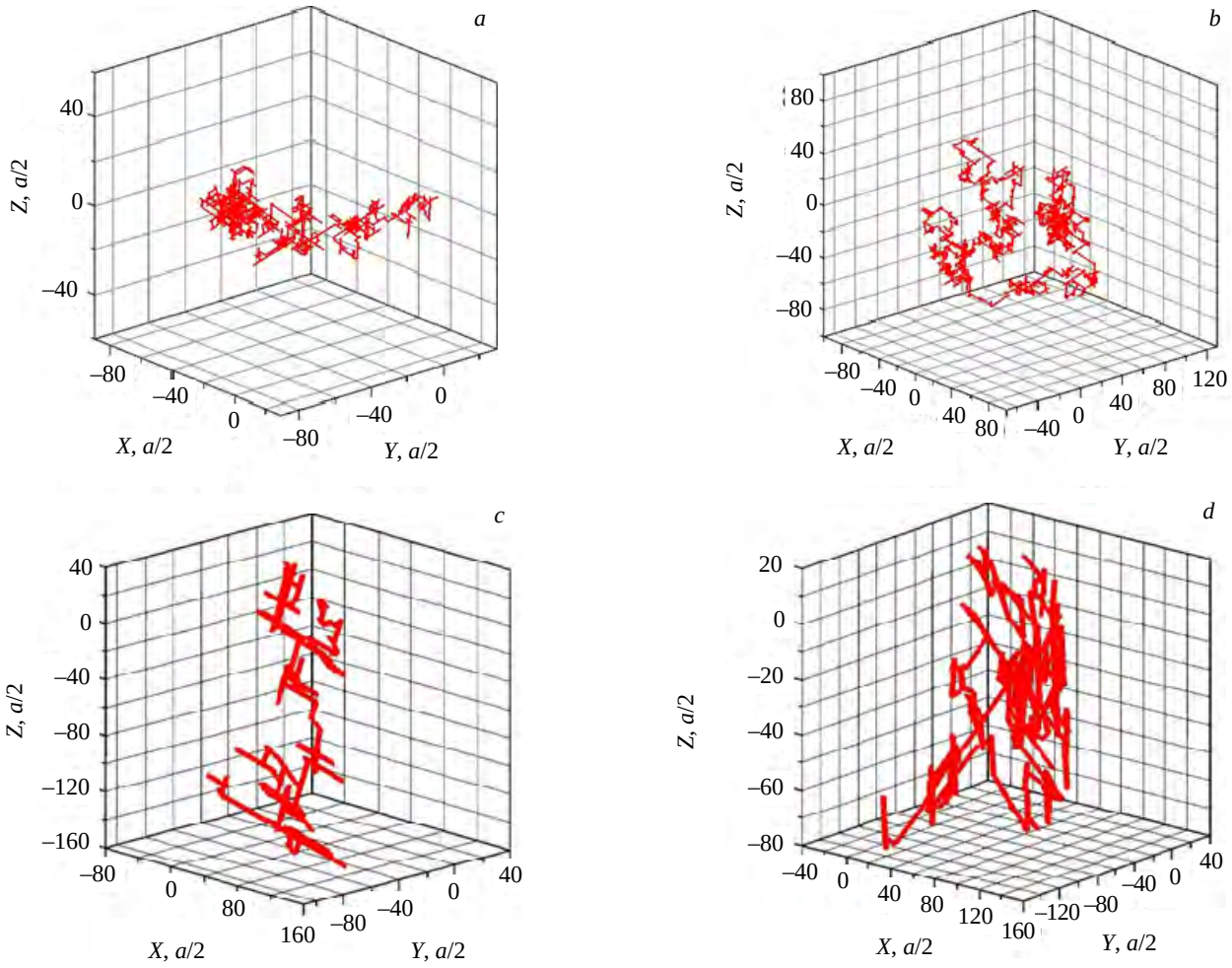

Fig. 1. MD trajectories of single SIAs (*a*, *b*) and 2-SIA (*c*, *d*) clusters at 300 K (*a*, *c*) and 700 K (*b*, *d*), τ_m: 65.4 (*a*), 2.97 (*b*), 7.74 (*c*), 4.12 ns (*d*)

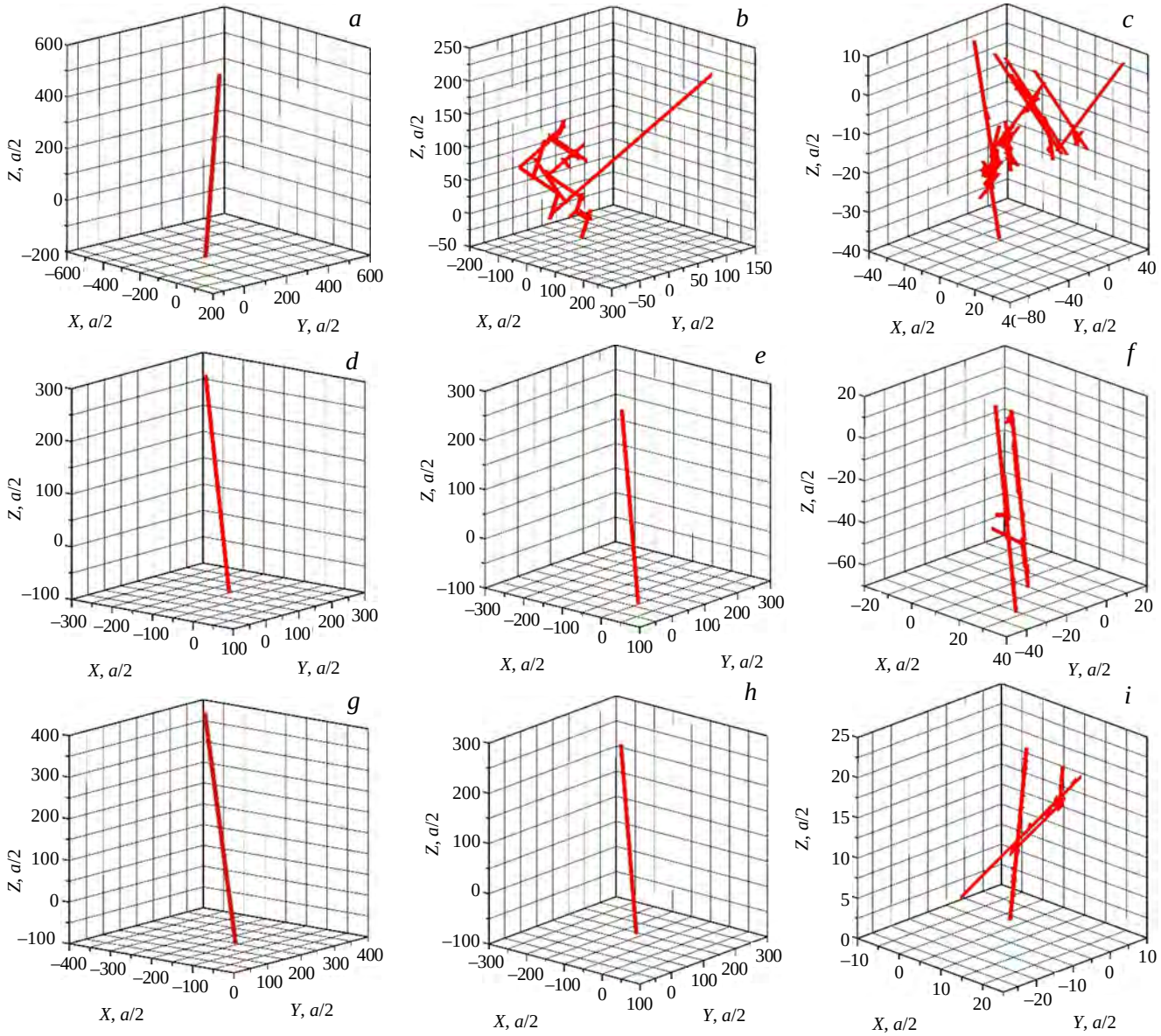

Fig. 2. MD trajectories of q-SIAs, q = 3 (*a*, *b*, *c*), 4 (*d*, *e*, *f*), 5 (*g*, *h*, *i*) at 300 (*a*, *d*, *g*), 700 (*b*, *e*, *h*), 1200 K (*c*, *f*, *i*), τ_m = 25.6 (*a*), 9.52 (*b*), 5.21 (*c*), 160 (*d*), 17.1 (*e*), 0.422 (*f*), 11.0 (*g*), 12.4 (*h*), 0.297 ns (*i*)

Fig. 3 shows the calculated temperature dependences of diffusivity D^d and tracer correlation factor f^{tr} for q-SIAs (q = 1—5).

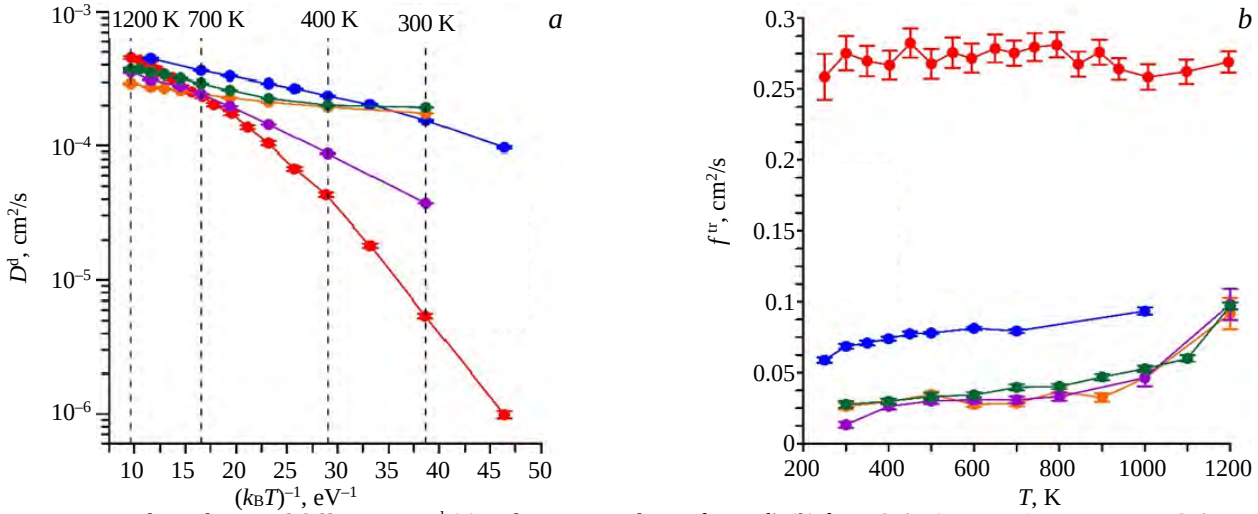

Fig 3. Temperature dependences of diffusivities D^d (*a*) and tracer correlation factor f^{tr} (*b*) for q-SIAs (q = 1—5) in Fe: ● — 1-SIA, ● — 2-SIA, ● — 3-SIA, ● — 4-SIA, ● — 5-SIA

Values D^d for the discussed defects differ slightly at high temperatures, with the largest difference (30%) observed between 2-SIA and 5-SIA clusters at 1000 K. This difference is much more significant at low temperatures (e.g., the diffusivities of single SIAs and those of 3-SIA clusters differ by a factor of 36 at 300 K). 3-SIA clusters show the greatest diffusivity among all defect types under review at $T < 350$ K. The temperature dependences of D^d are not linear in Arrhenius coordinates (Fig. 3, *a*). Therefore, an accurate description of MD data can be obtained by Arrhenius dependences only for particular temperature ranges.

Table 3 lists the fitting parameters of such dependences (preexponential factor D_0 and diffusion activation energy E^{AD}) with indication of temperature ranges, for which those parameters have been obtained. In the case of 3- and 5-SIA clusters, D^d is weakly dependent on T at $T \leq 400$ K ($E^{AD} \leq 0.01$ eV). The low E^{AD} value for 3-SIA clusters (0.004 eV) is consistent with the result of direct molecular statics calculations [9] of the energy barrier for cluster migration, which is less than 10^{-4} eV. At $T \geq 700$ K, the E^{AD} value for the clusters under review is 2—4 times lower than that for a single SIA (see Table 3).

T a b l e 3. **Arrhenius approximation parameters for $D^d(T)$ for q-SIA (q = 1—5) in Fe**

q	Low temperature approximation			High temperature approximation		
	D_0, cm^2/s	E^{AD}, eV	T range, K	D_0, cm^2/s	E^{AD}, eV	T range, K
1	$2.59 \cdot 10^{-2}$	0.219	250—350	$1.25 \cdot 10^{-3}$	0.101	600—1200
2	$1.33 \cdot 10^{-3}$	0.056	250—350	$6.43 \cdot 10^{-4}$	0.034	400—800
3	$2.25 \cdot 10^{-4}$	0.004	300—400	$5.38 \cdot 10^{-4}$	0.036	700—1200
4	$1.03 \cdot 10^{-3}$	0.086	300—700	$5.72 \cdot 10^{-4}$	0.051	700—1200
5	$2.82 \cdot 10^{-4}$	0.013	300—500	$3.70 \cdot 10^{-4}$	0.025	600—1200

The E^{AD} values obtained in this study are very much at variance with data reported in [6], where $E^{AD} = 0.024 \pm 0.004$ eV regardless of cluster size. The potential used in [6] was developed by Osetsky et al. [29]. The most stable SIA configuration allowing for that potential is ⟨111⟩ dumbbell, which does not agree with experimental data [30].

As one can see from Fig. 3, *b*, the one-dimensionality of the SIA clusters' diffusion becomes much more pronounced as the cluster size, q, increases from 1 to 3 (f^{tr} decreases from ~0.28 to 0.03—0.08 depending on the temperature), while the f^{tr} value becomes almost independent of q at $q \geq 3$. The f^{tr} value does not go to zero even where the clusters' diffusion is almost completely one-dimentional (as in the case of a 5-SIA cluster at 300 K). The reason for $f^{tr} \neq 0$ is that atoms forming a SIA cluster may move from their original positions in the lattice to neighboring close-packed rows. Therefore, even if the cluster's mass centre moves one-dimensionally all the time, the cluster is unable to completely «cover up the footprints», the result being the non-zero D^{tr} and f^{tr}. The inability of f^{tr} to take the zero value is almost entirely determined by such changes of atomic positions within a q-SIA cluster, where $q \geq 3$. Incidentally, f^{tr} does not characterize the diffusion mechanism of such clusters. In this context, the f^{tr} value is useless for the identification of the cluster diffusion mechanism, and other characteristics are called for.

Fig. 4 shows the temperature dependences of the frequency of changes in the migration direction and the average distance traveled between migration direction changes for q-SIAs (q = 1—5) in Fe. The inaccuracy of

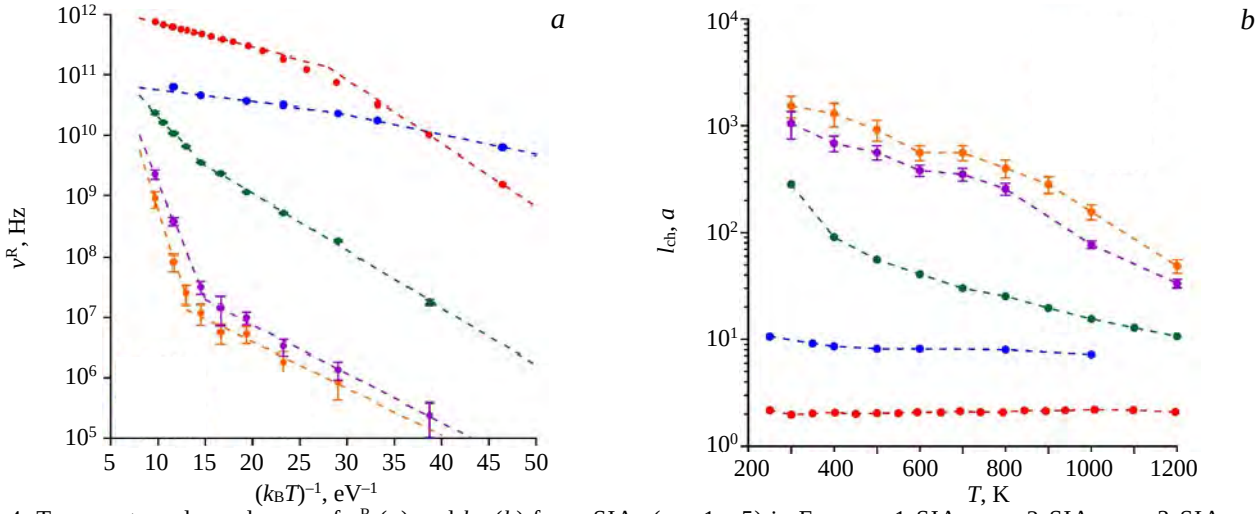

Fig. 4. Temperature dependences of ν^R (*a*) and l_{ch} (*b*) for q-SIAs (q = 1—5) in Fe: ● — 1-SIA, ● — 2-SIA, ● — 3-SIA, ● — 4-SIA, ● — 5-SIA

v^R and l_{ch} is not indicated in the plots, if smaller than the size of the points. Both v^R and l_{ch}, in contrast to f^{tr}, are much dependent on q across the whole range of q values under review.

The temperature dependences of v^R are not linear in Arrhenius coordinates (Fig. 4, *a*); therefore, an accurate description of the MD data can only be obtained by Arrhenius dependences for particular temperature ranges. Table 4 lists the fitting parameters of such dependences (preexponential factor v_0 and reorientation activation energy E^R) with indication of temperature ranges, for which those parameters have been obtained. At low temperatures, the E^R values for q-SIA clusters with $q \geq 3$ are close to each other and equal ~0.2 eV. At high temperatures, E^R becomes 2—6 times higher (the higher q, the higher the difference) suggesting the roles of different mechanisms in cluster reorientations at low and high temperatures.

T a b l e 4. **Arrhenius approximation parameters for $v^R(T)$ for q-SIAs (q = 1—5) in Fe**

q	Low temperature approximation			High temperature approximation		
	ν_0, Hz	E^R, eV	T range, K	ν_0, Hz	E^R, eV	T range, K
1	$1.16\cdot10^{14}$	0.242	250—300	$1.81\cdot10^{12}$	0.093	600—1200
2	$2.16\cdot10^{11}$	0.076	250—400	$8.67\cdot10^{10}$	0.045	400—800
3	$8.38\cdot10^{10}$	0.217	300—800	$1.01\cdot10^{12}$	0.390	800—1200
4	$3.11\cdot10^{8}$	0.186	300—700	$1.20\cdot10^{13}$	0.888	800—1200
5	$1.35\cdot10^{8}$	0.177	300—800	$4.50\cdot10^{13}$	1.125	900—1200

The l_{ch} value for single SIAs becomes temperature independent in the temperature range of 250—1200 K. Its average value (2.1*a*) is consistent with the temperature independent f^{tr} for the corresponding temperature range (see Fig. 3, *b*). For 2-SIA clusters, l_{ch} decreases from 10.6*a* to 7.2*a* with temperature rising from 250 K to 1000 K, respectively, which is also consistent with the f^{tr} increase. For clusters with $q \geq 3$, l_{ch} decreases dozens of times with temperature rising from 300 K to 1200 K (from 283*a* to 10.7*a*, from 1051*a* to 33.5*a*, from 1535*a* to 48.7*a* for clusters with q = 3, 4, 5, respectively).

The sink strengths of various microstructure elements are sensitive to the dimensionality of radiation defects' diffusion (sink strengths for 1D and 3D diffusion types may differ by several orders of magnitude) [27]. For example, sink strength k^2 of spherical absorbers with radius R and number density N (the number of absorbers per unit volume) is

$$k^2_{3D} \approx 4\pi RN \quad \text{for a 3D diffusion [31, 32],} \tag{1}$$

and is

$$k^2_{1D} = 6(\pi R^2 N)^2 \text{for a 1D diffusion [33].} \tag{2}$$

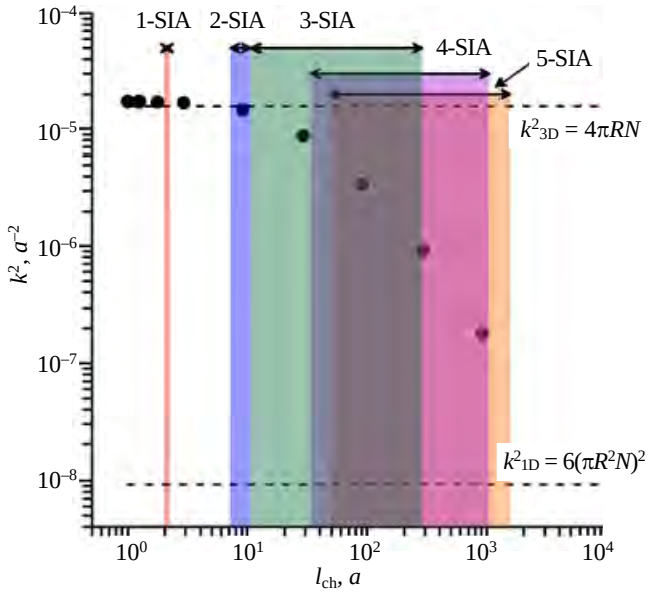

Fig. 5. Dependence of the sink strength of spherical absorbers with radius $R = 10a$ and number density $N = (200a)^{-3}$ on the average distance traveled between migration direction changes, l_{ch}. The color fields indicate the ranges of values l_{ch} values for q-SIAs (q = 1—5) in Fe. The dashed lines indicate theoretical sink strengths for 1D and 3D diffusion mechanisms calculated by Eqs. (1) and (2)

As an illustration, if $R = 10a$ and $N = (200a)^{-3}$, $k^2_{3D} / k^2_{1D} \approx 1700$.

The sink strength for a mixed 1D/3D defect diffusion can be calculated using the object kinetic Monte Carlo method (OKMC) [27, 28]. Such calculations have been carried out in this study for spherical absorbers with $R = 10a$ and $N = (200a)^{-3}$ to estimate sink strength k^2 dependence on l_{ch} by a technique similar to the techniques proposed in [27, 28], but different in the following aspects: 1) migration directions may change at each time step of the algorithm in accordance with a given probability for such an event (not every n jumps, where n is a parameter, as in [27, 28]); 2) the absorbers were not randomly located in the computational cell as in [27, 28] but formed a simple orthorhombic lattice with parameters 125*a*, 256*a*, 250*a*. Fig. 5 shows the resulting dependence.

k^{-1} is the radiation defects' diffusion length (the average distance that the defects can travel from their origination sites to the sinks where they are absorbed

or annihilated). Let us denote the diffusion length for the case of fully 3D- and 1D-migrating defects as k_{3D}^{-1} and k_{1D}^{-1}, respectively. For the considered spatial configuration of absorbers, Eqs. (1) and (2) give $k_{3D}^{-1} = 252a$ and $k_{1D}^{-1} = 10\,396a$, respectively. As one can see from Fig. 5, $k^2 \approx k_{3D}^2$ at $l_{ch} \ll k_{3D}^{-1}$. Similarly, $k^2 \approx k_{1D}^{-1}$ at $l_{ch} \gg k_{1D}^{-1}$. The OKMC values of k^2 deviate from k_{3D}^2 by not more than 10% at $l_{ch} \le 10a$. Such a criterion can be used to assess the need to account for the contribution of the 1D diffusion mechanism to the diffusion when constructing OKMC models of SIA clusters diffusion. For example, for the discussed configuration of absorbers, one can conclude, using this criterion, that the effect of the 1D diffusion mechanism on the sink strength must be considered for SIA clusters with $q \ge 3$. For single SIAs and 2-SIA clusters, the effect of the 1D mechanism is too small to modify k^2 in any noticeable way.

In iron, the cluster distributions of SIAs generated in atomic collision cascades depend on the cascades' damage energy [3, 4]. Correspondingly, neutron damage irradiations with different neutron energy spectra generate different cluster distributions of SIAs. As the sink strengths of various microstructure elements for radiation defects are sensitive to radiation defects diffusion mechanism, the difference of the fluxes of radiation defects of different signs (vacancies, SIAs) to the microstructure elements is determined not only by the generation rate for radiation defects (dpa) but also by the cluster distribution of SIAs specific for the given neutron spectrum.

CONCLUSIONS

MD simulation of diffusion trajectories of the SIA clusters (clusters of three, four and five SIAs) has been performed for a temperature range of 300—1200 K in bcc Fe. Temperature dependences of diffusion characteristics (diffusivity D^d, tracers correlation factor f^{tr}, frequency of migration direction changes ν^R, average distance traveled between migration direction changes l_{ch}) for single SIAs and SIA clusters containing up to 5 SIAs have been obtained based on MD data from this study and previous research. Their diffusion activation energies E^{AD} and reorientation activation energies E^R have been also determined.

At $T \ge 700$ K, D^d for single SIAs and SIA clusters differs by 30% at most. The E^{AD} values for all types of SIA clusters (0.025—0.051 eV) are 2—4 times lower than those for single SIAs (0.101 eV). At room temperature, the difference of D^d values for different defect types can exceed an order of magnitude. At $T \le 400$ K, D^d weakly depends on T for 3-SIA and 5-SIA clusters ($E^{AD} \le 0.01$ eV). The E^{AD} values for SIA clusters vary from 0.004 eV for 3-SIA clusters to 0.09 eV for 4-SIA clusters, which is significantly lower than the value for single SIAs (0.24 eV).

Single SIAs show a predominantly 3D diffusion at temperatures 250—1200 K, with $l_{ch} \approx 2.1a$. For 2-SIA clusters, the effect of mixed 1D/3D diffusion is most pronounced, with l_{ch} varying from $7.2a$ to $10.6a$ at temperatures 250—1000 K. The 1D diffusion mechanism prevails for 3-, 4-, 5-SIA clusters: l_{ch} varies from $283a$ to $10.7a$ for 3-SIA clusters, from $1051a$ to $33.5a$ for 4-SIA clusters, and from $1535a$ to $48.7a$ for 5-SIA clusters when T rises from 300 K to 1200 K. The E^R values are temperature sensitive: $E^R \approx 0.2$ eV for clusters of three to five SIAs at $T < 700$—800 K; $E^R \approx 0.4$ eV for 3-SIA clusters, $E^R \approx 0.9$ eV for 4-SIA, $E^R \approx 1.13$ for 5-SIA clusters at $T > 800$ K.

The dependence of diffusion mechanism of SIA clusters on the number of their constituent SIAs together with the dependence of the cluster distributions of SIAs on the atomic collision cascades damage energy and the sensitivity of the sink strengths of microstructure elements to the radiation defects diffusion mechanism cause the evolution of the radiation microstructure under irradiation in different neutron spectra to be different at the same damaging doses (dpa) which must be taken into account when analyzing and interpreting the results of radiation tests of materials of nuclear fission and fusion energy.

The study was supported by NRC «Kurchatov Institute» (grant № 1934a from 28.09.2020) and carried out using computing resources of the Federal collective usage center Complex for Simulation and Data Processing for Mega-science Facilities at NRC «Kurchatov Institute», http://ckp.nrcki.ru/.

REFERENCES

1. **Indenbom V.L., Lothe J. (Eds.)** Elastic Strain Fields and Dislocation Mobility. — Netherlands: North-Holland, 1992.
2. **Stoller R.E., Zarkadoula E.** 1.20 — Primary Radiation Damage Formation in Solids. — Comprehensive Nuclear Materials (Second Edition), Elsevier, 2020, vol. 1, p. 620—662, https://doi.org/10.1016/B978-0-12-803581-8.00661-5.
3. **Sivak A.B., Demidov D.N., Zolnikov K.P., Korchuganov A.V., Sivak P.A., Romanov V.A., Chernov V.M.** The primary radiation damage in bcc metals Fe and V: analysis of molecular dynamic data. — VANT. Ser. Materialovedenie i Novye Materialy, 2019, vol. 4(100), p. 25—57 (in Russian); https://www.elibrary.ru/item.asp?id=44630371.
4. **Shpanskiy Yu.S., the DEMO-FNS project team.** Progress in the design of the DEMO-FNS hybrid facility. — Nuclear Fusion, 2019, vol. 59, 076014, p. 1—8; https://doi.org/10.1088/1741-4326/ab14a8.
5. **Gao F., Bacon D.J., Osetsky Yu.N., Flewitt P.E.J., Lewis T.A.** Properties and evolution of sessile interstitial clusters produced by displacement cascades in α-iron. — J. Nucl. Mater., 2000, vol. 276, p. 213—220, https://doi.org/10.1016/S0022-3115(99)00180-4.
6. **Osetsky Yu.N., Bacon D.J., Serra A., Singh B.N., Golubov S.I.** One-dimensional atomic transport by clusters of self-interstitial atoms in iron and copper. — Philos. Mag., 2003, vol. 83, p. 61—91, https://doi.org/10.1080/0141861021000016793.
7. **Gao F., Heinisch H., Kurtz R.J., Osetsky Yu.N.** Migration and directional change of interstitial clusters in α-Fe: searching for transition states by the dimer method. — Philos. Mag., 2005, vol. 85, p. 619—627, https://doi.org/10.1080/02678370412331320062.
8. **Romanov V.A., Sivak A.B., Chernov V.M.** Crystallographic, energetic and kinetic properties of self-point defects and their clusters in bcc-iron. 5. Self-interstitial atoms. — VANT. Ser. Materialovedenie i Novye Materialy, 2006, vol. 1(66), p. 202—222 (in Russian), https://www.elibrary.ru/item.asp?id=22614324.
9. **Romanov V.A., Sivak A.B., Chernov V.M.** Crystallographic, energetic and kinetic properties of self-point defects and their clusters in bcc-iron. 6. Clusters of self-interstitial atoms. — VANT. Ser. Materialovedenie i novye materialy, 2006, vol. 1(66), p. 223—232 (in Russian), https://www.elibrary.ru/item.asp?id=22614325.
10. **Terentyev D.A., Klaver T.P.C., Olsson P., Marinica M.-C., Willaime F., Domain C., Malerba L.** Self-trapped interstitial-type defects in iron. — Phys. Rev. Letters, 2007, vol. 100, 145503, p. 1—7, https://doi.org/10.1103/PhysRevLett.100.145503.
11. **Terentyev D.A., Malerba L., Hou M.** Dimensionality of interstitial cluster motion in bcc-Fe. — Phys. Rev., 2007, vol. 75, 104108, p. 1—13, https://doi.org/10.1103/PhysRevB.75.104108.
12. **Sivak A.B., Romanov V.A., Chernov V.M.** Diffusion characteristics of self-point defects in bcc iron. — Perspektivnye Materialy, 2009, № 6, p. 5—11 (in Russian), https://elibrary.ru/item.asp?id=12975968.
13. **Sivak A.B., Romanov V.A., Chernov V.M.** Diffusion of self-point defects in body-centered cubic iron crystal containing dislocations. — Crystal. Rep., 2010, vol. 55, p. 97—108, https://doi.org/10.1134/S1063774510010153.
14. **Anento N., Serra A., Osetsky Yu.N.** Atomistic study of multimechanism diffusion by self-interstitial defects in α-Fe. — Modelling Simul. Mater. Sci. Eng., 2010, vol. 18, 025008, p. 1—18, https://doi.org/10.1088/0965-0393/18/2/025008.
15. **Malerba L., Ackland G.J., Becquart C.S., Bonny G., Domain C., Dudarev S., Fu C.-C., Hepburn D., Marinica M.C., Olsson P., Pasianot R.C., Raulot J.M., Soisson F., Terentyev D., Vincent E., Willaime F.** Ab initio calculations and interatomic potentials for iron and iron alloys: Achievements within the Perfect Project. — J. Nucl. Mater., 2010, vol. 406, p. 7—18, https://doi.org/10.1016/j.jnucmat.2010.05.016.
16. **Ryabov V.A., Pechenkin V.A., Molodtsov V.L., Terentyev D.** Contribution of di-SIA to mass transport in Fe—Cr alloys. — J. Nucl. Mater., 2016, vol. 472, p. 43—46, https://doi.org/10.1016/j.jnucmat.2016.01.025.
17. **Demidov D.N., Sivak A.B., Sivak P.A.** Thermal dissociation of di-interstitials in bcc Fe and V: a molecular dynamics study. — PAS&T. Ser. Thermonuclear Fusion, 2019, vol. 42, p. 99—107 (in Russian), https://doi.org/10.21517/0202-3822-2019-42-2-99-107.
18. **Demidov D.N., Sivak A.B., Sivak P.A.** Crystallographic, energetic and diffusion characteristics of di-interstitials in bcc metals Fe and V. — PAS&T. Ser. Thermonuclear Fusion, 2019, vol. 42, p. 85—96 (in Russian), https://doi.org/10.21517/0202-3822-2019-42-3-85-96.
19. **Sivak A.B., Romanov V.A., Demidov D.N., Sivak P.A., Chernov V.M.** Interatomic interaction potentials for simulation of atomic collision cascades and self-point defects in bcc Fe and V metals. — VANT. Ser. Materialovedenie i Novye Materialy, 2019, vol. 4(100), p. 5—24 (in Russian), https://www.elibrary.ru/item.asp?id=44630370.
20. **Sivak A.B., Romanov V.A., Chernov V.M.** Influence of stress fields of dislocations on formation and spatial stability of point defects (elastic dipoles) in anisotropic bcc crystals of vanadium and iron. — VANT. Ser. Materialovedenie i Novye Materialy, 2002, vol. 1(59), p. 29—40 (in Russian).
21. **Sivak A.B., Romanov V.A., Chernov V.M.** Influence of stress fields of dislocations on formation and spatial stability of point defects (elastic dipoles) in V and Fe crystals. — J. Nucl. Mater., 2003, vol. 323, p. 380—387, https://doi.org/10.1016/j.jnucmat.2003.08.014.
22. **Romanov V.A., Sivak A.B., Chernov V.M.** Crystallographic, energetic and kinetic properties of self-point defects and their clusters in bcc-iron. 1. Semi-empirical model of bcc iron and interatomic interaction potential. — VANT. Ser. Materialovedenie i Novye Materialy, 2006, vol. 1(66), p. 129—150 (in Russian), https://www.elibrary.ru/item.asp?id=22614316.
23. **Romanov V.A., Sivak A.B., Chernov V.M.** Crystallographic, energetic and kinetic properties of self-point defects and their clusters in bcc-iron. 2. Basic relations for calculations of defect characteristics and testing results for applied model. — VANT. Ser. Materialovedenie i Novye Materialy, 2006, vol. 1(66), p. 151—171 (in Russian), https://www.elibrary.ru/item.asp?id=22614317.
24. **Verlet L.** Computer «experiments» on classical fluids. I. Thermodynamical properties of Lennard-Jones molecules. — Phys. Rev., 1967, vol. 159, p. 98—103, https://doi.org/10.1103/PhysRev.159.98.
25. **Allnatt A.R., Lidiard A.B.** Atomic Transport in Solids. — Cambridge University Press, 1993.
26. **Manning J.R.** Diffusion Kinetics for Atoms in Crystals. — Toronto, Canada: D. Van Nostrand Company, 1968.

27. **Heinisch H.L., Singh B.N., Golubov S.I.** A kinetic Monte Carlo study of mixed 1D/3D defect migration. — J. Comput. Aided Mater. Des., 1999, vol. 6, p. 277—282, https://doi.org/10.1023/A:1008777901639.
28. **Malerba L., Becquart C.S., Domain C.** Object kinetic Monte Carlo study of sink strengths. — J. Nucl. Mater., 2007, vol. 360, p. 159—169, https://doi.org/10.1016/j.jnucmat.2006.10.002.
29. **Osetsky Yu.N., Mikhin A.G., Serra A.** Study of copper precipitates in α-iron by computer simulation. I. Interatomic potentials and properties of Fe and Cu. — J. Nucl. Mater., 1994, vol. 212—215, p. 236—240, https://doi.org/10.1080/01418619508239930.
30. **Schultz F.** Atomic defects in metals Fe. — In: Ullmaier H. (ed.), Atomic Defects in Metals. Landolt-Börnstein — Group III Condensed Matter. Berlin: Springer-Verlag, 1991, vol. 25, p. 125—134, https://doi.org/10.1007/10011948_46.
31. **Wiedersich H.** On the theory of void formation during irradiation. — Radiat. Eff., 1972, vol. 12, p. 111—125, https://doi.org/10.1080/00337577208231128.
32. **Brailsford A.D., Matthews J.R., Bullough R.** The effect of recombination on sink strengths in the rate theory of void-swelling. — J. Nucl. Mater., 1979, vol. 79, p. 1—13, https://doi.org/10.1016/0022-3115(79)90428-8.
33. **Barashev A.V., Golubov S.I., Trinkaus H.** Reaction kinetics of glissile interstitial clusters in a crystal containing voids and dislocations. — Philos. Mag. A, 2001, vol. 81, p. 2515—2532, https://doi.org/10.1080/01418610108217161.

AUTHORS

Alexander Borisovich Sivak, PhD., head of laboratory; NRC «Kurchatov Institute», 1, Academika Kurchatova sq., Moscow, 123182, Russia, Sivak_AB@nrcki.ru

Dmitry Nikolaevich Demidov, PhD. student, research engineer; NRC «Kurchatov Institute», 1, Academika Kurchatova sq., Moscow, 123182, Russia, Demidov_DN@nrcki.ru

Polina Alexandrovna Sivak, engineer; NRC «Kurchatov Institute», 1, Academika Kurchatova sq., Moscow, 123182, Russia, Sivak_PA@nrcki.ru

Статья поступила в редакцию 15 января 2021 г.
После доработки 16 марта 2021 г.
Принята к публикации 25 марта 2021 г.
Вопросы атомной науки и техники.
Сер. Термоядерный синтез, 2021, т. 44, вып. 2, с. 148—157.

Кроме 20 докладов, представленных на 4-й Международной конференции по подкритическим гибридным системам синтеза-деления, одобренных рецензентами и публикуемых в настоящем выпуске, редколлегия журнала получила восемь кратких сообщений о докладах, также сделанных на конференции. Далее публикуются эти сообщения.

In addition to the 20 reports presented at the 4th International Conference on Fusion-Fission Subcritical Hybrid Systems, approved by reviewers and published in our journal above, the editorial board of the journal received eight brief messages on the reports also made at the conference. These brief messages are published below.

UDC 621.039.674.3

NRNU MEPHI ACTIVITY TOWARDS FUSION-FISSION HYBRID SYSTEMS

(*short message*)

Yu.M. Gasparyan[1], D.M. Bachurina[1], L.B. Begrambekov[1], S.A. Krat[1], V.A. Kurnaev[1], A.M. Litnovsky[1, 2], O.V. Ogorodnikova[1], A.A. Pisarev[1], O.N. Sevryukov[1], A.N. Suchkov[1]

[1]National Research Nuclear University MEPhI (Moscow Engineering Physics Institute), Kashirskoe sh. 31, Moscow, 115409 Moscow, Russia
[2]Forschungszentrum Jülich GmbH, Institut für Energie und Klimaforschung, Julich, 52425, Germany

The development of fusion-fission hybrid systems is a very complex and ambitious task. MEPhI is a key Russian University for students training in many areas related to this topic. The University is actively involved in research and development activities. MEPhI has a unique complex of plasma and ion beam facilities allowing for irradiation of candidate plasma-facing materials using hydrogen, deuterium and helium in a wide range of parameters thus advancing fundamental investigations of plasma-wall interaction [1]. These facilities allow studies of plasma-induced surface modification, erosion and various aspects of hydrogen isotopes retention, including co-deposition and influence of radiation damage. Most of research are currently performed with tungsten and advanced W alloys (in cooperation with Research Center Jülich, Helmholtz Society, Germany [2]), steels and aluminum acting as a proxy of beryllium. Addressing a concept of a renewable surface of plasma-facing components, experiments and theoretical studies of resistance of liquid lithium [3] and B_4C coatings [4] are carried out. With such a fundamental knowledge, new methods of edge plasma and surface diagnostics, tritium and dust removal are developed for ITER and other tokamaks. To join dissimilar materials in fusion devices, various methods of brazing using rapidly solidified amorphous alloys are developed for an application in ITER [5] and DEMO [6]. Recently, a small spherical tokamak MEPHIST [7] has been built for student training and as a testbed for new methods of plasma and surface diagnostics and various engineering solutions. Research related to analysis of non-conventional nuclear fuels and involvement of fusion reactors in nuclear power production is described separately in [8].

Key words: MEPhI, nuclear fusion, plasma wall interaction, tokamak, brazing.

DOI: 10.21517/0202-3822-2021-44-2-158-159

ДЕЯТЕЛЬНОСТЬ НИЯУ МИФИ ПО СОЗДАНИЮ ГИБРИДНЫХ СИСТЕМ СИНТЕЗА-ДЕЛЕНИЯ

(*краткое сообщение*)

Ю.М. Гаспарян[1], Д.М. Бачурина[1], Л.Б. Беграмбеков[1], С.А. Крат[1], В.А. Курнаев[1], А.М. Литновский[1, 2], О.В. Огородникова[1], А.А. Писарев[1], О.Н. Севрюков[1], А.Н. Сучков[1]

[1]Национальный исследовательский ядерный университет МИФИ (Московский инженерно-физический институт), Каширское шоссе 31, 115409 Москва, Россия
[2]Исследовательский центр Jülich GmbH, Институт энергетических и климатических исследований, Юлих, 52425, Германия

Разработка гибридных систем, основанных на синтезе и делении ядер, — это очень сложная и амбициозная задача. МИФИ является ключевым российским университетом для подготовки студентов по многим аспектам, связанным с этой тематикой, а также активно участвует в НИОКР. В частности, МИФИ располагает уникальным комплексом плазменных и ионно-лучевых установок для HD- и He-плазменного облучения материалов в широком диапазоне параметров и фундаментальных исследований взаимодействия плазмы со стенкой [1]. Проводятся исследования плазменно-индуцированной модифи-

кации поверхности, эрозии и различных аспектов удержания изотопов водорода, включая захват в переосаждённых слоях и влияние радиационного повреждения материалов. Большинство исследований в настоящее время проводится с вольфрамом и новыми перспективными сплавами на его основе (в сотрудничестве с Гельмгольцевским научным центром в Юлихе, Германия [2]), сталями и алюминием в качестве аналога бериллия. В поддержку концепции возобновляемой поверхности обращённых к плазме элементов проводятся эксперименты и теоретические работы по стойкости жидколитиевых [3] и B_4C-слоёв [4]. На основе знаний о происходящих элементарных процессах в МИФИ проводится разработка для ИТЭР и других токамаков новых методов диагностики пристеночной плазмы и поверхности, удаления трития и пыли. Для соединения материалов с сильно отличающимися свойствами разрабатываются различные методы пайки с использованием быстрозакалённых аморфных сплавов, что может быть использовано при изготовлении обращённых к плазме элементов для ИТЭР [5] и ДЕМО [6]. Недавно в МИФИ был построен небольшой сферический токамак «МИФИСТ» [7] для обучения студентов и отработки новых методов диагностики плазмы и поверхности стенок, а также различных инженерных решений. Еще одно направление деятельности связано с анализом нетрадиционного ядерного топлива и вовлечением термоядерных реакторов в ядерные энергетические системы и подробнее описано в [8].

Ключевые слова: МИФИ, термоядерный синтез, взаимодействие плазмы с поверхностью, токамак, пайка.

СПИСОК ЛИТЕРАТУРЫ

1. **Kurnaev V. et al.** — Physics Procedia, 2015, vol. 71, p. 2—8.
2. **Litnovsky A. et al.** — Fusion Engineering and Design, 2020, vol. 159, p. 111742.
3. **Marenkov E.D. et al.** — Nuclear Fusion, 2021, vol. 61, 034001.
4. **Buzhinskij O.I. et al.** — ВАНТ. Сер. Термоядерный синтез, 2015, т. 38, вып. 2.
5. **Gervash A. et al.** — Fusion Eng. Des., 2019, vol. 146, p. 2292—2296.
6. **Bachurina D. et al.** — Fusion Engineering and Design, 2021, vol. 162, 112099
7. **Kurnaev V. et al.** — Physics of Atomic Nuclei, 2019, vol. 82(10), p. 1329—1331.
8. **Kulikov E. et al.** — ВАНТ. Термоядерный синтез, 2021, т. 44, вып. 2, с. 21.

YMGasparyan@mephi.ru

UDC 621.039.61:533.952

PILOT FFHR BASED ON A RFP AS A FUSION CORE

(*short message*)

R. Piovan[1], P. Agostinetti[1], C. Bustreo[1], F. Bruno[2], R. Cavazzana[1], A. Cemmi[3, 4], N. Cherubini[3], M. Ciotti[3], D.F. Escande[1], E. Gaio[1], R. Iacovacci[2], G. Lombardi[2], G. Lomonaco[5, 6], F. Lunardon[1], G.A. Marzo[3], A. Maistrello[1], E. Mancini[2], A. Mariani[2], G. Mingrone[2], M. Osipenko[6], F. Panza[3, 6], M.E. Puiatti[1], G. Ricco[6, 7], M. Ripani[6, 7], M. Valisa[1], T. Vignaroli[2], G. Zollino[1], M. Zuin [1]

[1]*Consorzio RFX (CNR, ENEA, INFN, Università di Padova, Acciaierie Venete S.p.A.), Corso Stati Uniti 4, I-35127 Padova, Italy.*
[2]*Sogin — Società Gestione Impianti Nucleari, Roma, Italy*
[3]*ENEA, — Dipartimento Fusione e Tecnologie per la Sicurezza Nucleare, Frascati, Italy*
[4]*Istituto Nazionale di Fisica Nucleare — Sezione di Roma Tre, Roma, Italy*
[5]*GeNERG, DIME/TEC — Università di Genova, Genova, Italy*
[6]*Istituto Nazionale di Fisica Nucleare — Sezione di Genova, Genova, Italy*
[7]*Centro Fermi — Museo Storico Della Fisica e Centro Studi e Ricerche Enrico Fermi, Roma, Italy*

Studies are in progress in order to revisit the status and the potentiality of the Reversed Field Pinch (RFP) as a fusion core in FFHR, taking into account: (i) the recent progress in RFP physics brought by the results of RFX-mod (R = 2, a = 0.46, I_p = 2MA), mainly about MHD modes control, (ii) the expected performance improvements resulting from the ongoing upgrade of the machine. To cover the gap between the existing experiments and the hybrid reactor, according to the strategy emerged in FUNFI3, an intermediate step with a FFHR pilot experiment in which a RFP is the neutron fusion source is proposed. Three different categories of issues are considered which require the assessment of:

— the RFP physics and the scaling laws at increased level of current and machine size;

— the technologies allowing increased RFP performances and continuous operation;

— a test bench for a hybrid blanket, combining Tritium production and fission reactions.

In order to optimize the pilot experiment approach in terms of cost reduction, best use of the step-by-step acquired knowledge and clear milestones towards the realization of a low power FFHR, a staged approach with increased complexity and investment is introduced [1]. In the proposed pilot FFHR the aim is the production of D—T-fusion power with a RFP configuration ($P \approx 30$ MW, $Q \approx 0.4$, continuous pulsed operation) and testing the blanket with limited fission fuel. The overall strategy of this approach and the details for each stage of the plant requirements, the tackled issues and the expected results in order to pass to the next phase will be presented in the talk.

Key words: pilot FFHR, RFP, RFX-mod.

DOI: 10.21517/0202-3822-2021-44-2-159-160

ПИЛОТНЫЙ ГИБРИДНЫЙ РЕАКТОР СИНТЕЗА-ДЕЛЕНИЯ НА ОСНОВЕ ПИНЧА С ОБРАЩЁННЫМ ПОЛЕМ В КАЧЕСТВЕ ТЕРМОЯДЕРНОГО ИСТОЧНИКА

(*краткое сообщение*)

Р. Пиован[1], Р. Агостинели[1], С. Бюст[1], Ф. Бруно[2], Р. Савасса[1], А. Джеми[3,4], Н. Херувимов[3], М. Чиотти[3], Д.Ф. Есканде[1], Е. Гай[1], Р. Иаковасси[2], Г. Ломбарди[2], Г. Lоманако[5,6], Ф. Лунардон[1], Г.А. Марзо[3], А. Мастрелло[1], Е. Мансини[2], Г. Мингроне[2], М. Осипенко[6], Ф. Панза[3,6], М.Е. Пиатти[1], Г. Рикко[6,7], М. Рипани[6,7], М. Валиса[1], Т. Виньяроли[2], Г. Золино[1], М. Зейн[1]

[1]*Консорцио RFX (CNR, ENEA, INFN, университет Падуи, сталелитейные заводы Venete S. p.A.), курс США 4, I-35127, Италия*
[2]*Согин — Компания по управлению ядерными установками, Рим, Италия*
[3]*ENEA — Отдел ядерного синтеза и технологий безопасности, Фраскати, Италия*
[4]*Национальный Институт ядерной физики — раздел три, Рим, Италия*
[5]*GeNERG, DIME/TEC — Университет Генуи, Генуя, Италия*
[6]*Национальный институт ядерной физики, Генуя, Италия*
[7]*Центр Ферми — Исторический музей физики и Центр Исследований и исследований Энрико Ферми, Рим, Италия*

В настоящее время ведутся исследования с целью пересмотра статуса и потенциала пинча с обращённым полем (RFP) в качестве термоядерного источника в гибридном реакторе синтеза-деления (FFHR) с учётом следующих факторов: (i) недавний прогресс в физике RFP, вызванный результатами на установке RFX-mod ($R = 2$, $a = 0{,}46$, $I_p = 2$ МА), главным образом в области управления МГД-режимами, (ii) ожидаемые улучшения результатов после окончания модернизации этой установки. Чтобы устранить разрыв между существующими экспериментами и гибридным реактором, в соответствии со стратегией, разработанной в ходе FUNFI3, предлагается промежуточный этап с пилотным экспериментом FFHR, в котором RFP будет являться источником термоядерных нейтронов. Рассматриваются три различные категории вопросов, требующих оценки:

— физика RFP и законы масштабирования при повышенном уровне тока и размере установки;

— технологии, позволяющие повысить производительность RFP и обеспечить непрерывную работу;

— испытательный стенд для гибридного бланкета, сочетающего производство трития и реакции деления.

Для оптимизации подхода пилотного эксперимента с точки зрения снижения затрат, наилучшего использования поэтапно приобретённых знаний и чётких вех на пути к реализации маломощного FFHR вводится поэтапный подход с постепенным увеличением сложности и инвестиций [1]. В предлагаемом пилотном FFHR с конфигурацией RFP целью является получение термоядерной мощности в D—T-реакции ($P \approx 30$ МВт, $Q \approx 0{,}4$, непрерывная импульсная работа) и испытание бланкета с ограниченным делением топлива. Представлены общая стратегия этого подхода и описание требований к каждому этапу, решаемые вопросы и ожидаемые результаты для перехода к следующему этапу.

Ключевые слова: пилотный FFHR, RFP, RFX-mod.

СПИСОК ЛИТЕРАТУРЫ

1. **Piovan R. et al.** Status and Perspectives of a Reversed Field Pinch as a Pilot Neutron Source. — IEEE Trans. on Plasma Science, 2020, vol. 48, Issue 6; DOI: 10.1109/TPS.2019.2957888.

roberto.piovan@igi.cnr.it

UDC 621.039.634:669.884

COMPARISON OF LITHIUM DIVERTOR OPTIONS FOR DEMO-FNS TOKAMAK

(*short message*)

V.G. Skokov[1], V.Yu. Sergeev[1], E.A. Anufriev[1], B.V. Kuteev[2]

[1]Peter the Great St. Petersburg Polytechnic University, 29, Politechnicheskaya str. St. Petersburg 195251, Russia
[2]NRC «Kurchatov Institute», 1, Academika Kurchatova sq., Moscow, 123182, Russia

The issues of heat loads into the tokamak divertor still remain unresolved engineering and physical problems of a thermonuclear reactor development. Several approaches are being discussed and studied to reduce the heat flux onto divertor plates below 10 MW/m^2. Among them, the attractive approaches proposed by Y. Nagayama [1] and R. Goldston [2] are based on a liquid lithium evaporation in a limited amount of divertor boxes. They are relatively simple in practical applications and allow one to achieve necessary steady-state regimes both for heat fluxes and for plasma effluxes from a plasma column to the divertor region. In order to choose one of them for prospective tokamaks the comparative analysis was conducted and presented in this report. The design of the divertor zone for the DEMO-FNS tokamak is proposed. The superconductive tokamak DEMO-FNS [3] that is currently being developed in Russia will operate in the regime of fusion neutron source (fusion power during a steady-state regime up to 40 MW, neutron production rate above $1\cdot10^{19}$ s^{-1}). It was shown that the system with «cold» box walls (about 200 ºC) which can condense Li (like in [1]) looks more suitable compared with «hot» (up to 800 ºC) box wall system [2]. Both approaches fit the criterion for heat loads onto the divertor walls. Both approaches also fit the criterion for the lithium flow into the main plasma, but the cold wall approach is on the verge of being applicable because of the lithium flow value into SOL. The «cold» box walls design is preferable due to an engineering simplicity of realization as well. It was demonstrated that lithium efflux into the main plasma is suppressed mainly due to the ionization process within SOL which exponentially depends on its width. It is necessary to perform detailed 2D-modeling of SOL and divertor construction with lithium for DEMO-FNS plasma parameters determination in divertor and SOL. Engineering and technological study of such design is also required. Acknowledgments. This work was supported by the Ministry of science and higher education of Russian Federation in the framework of the state contract in the field of science under project No. 0784-2020-0020 using the Federal Joint Research Center Material science and characterization in advanced technology» (project RFMEFI62119X0021), including the unique scientific facility «Spherical tokamak Globus-M».

Key words: divertor, lithium, heat loads, DEMO-FNS.

DOI: 10.21517/0202-3822-2021-44-2-161-162

СРАВНЕНИЕ ВАРИАНТОВ ЛИТИЕВОГО ДИВЕРТОРА ДЛЯ ТОКАМАКА ДЕМО-ТИН

(*краткое сообщение*)

В.Г. Скоков[1], В.Ю. Сергеев[1], Е.А. Ануфриев[1], Б.В. Кутеев[2]

[1]Санкт-Петербургский политехнический университет Петра Великого, 195251 Санкт-Петербург, ул. Политехническая, д. 29, Россия
[2]НИЦ «Курчатовский институт», 123182 Москва, пл. Академика Курчатова, д. 1, Россия

Вопросы тепловых нагрузок на дивертор токамака продолжают оставаться нерешённой инженерно-физической проблемой в ходе разработки термоядерного реактора. Было предложено несколько подходов к снижению теплового потока на пластины дивертора до значений ниже 10 МВт/м^2. В их число входят привлекательные подходы, предложенные Ю. Нагаямой [1] и Р. Голдстоном [2], которые основаны на испарении жидкого лития в ограниченном количестве диверторных секций. Они относительно просты в практическом применении и позволяют достичь необходимых стационарных режимов как для тепловых потоков, так и для потоков плазмы из плазменного шнура в область дивертора. С целью выбора одного из них для перспективных токамаков был проведён сравнительный анализ. Предложена конструкция диверторной зоны для токамака ДЕМО-ТИН. Разрабатываемый в настоящее время в России

сверхпроводящий токамак ДЕМО-ТИН [3] будет работать в режиме термоядерного источника нейтронов (мощность термоядерного синтеза в стационарном режиме до 40 МВт, скорость выработки нейтронов свыше $1 \cdot 10^{19}$ $с^{-1}$). Было показано, что система с «холодными» стенками секции (около 200 ºС), способная конденсировать Li (как в [1]), выглядит более подходящей по сравнению с системой с «горячими» (до 800 ºС) стенками секций [2]. Оба подхода соответствуют критерию тепловых нагрузок на стенки дивертора. Критерию по потоку лития в основную плазму также удовлетворяют оба подхода, но подход с конденсирующими стенками находится на грани применимости по потоку лития в SOL. Конструкция «холодных» стенок секций предпочтительна также из-за инженерной простоты реализации. Показано, что выход лития в основную плазму подавляется, в основном, за счёт процесса ионизации внутри SOL, экспоненциально зависящего от его ширины. Для определения параметров плазмы ДЕМО-ТИН в диверторе и SOL необходимо выполнить детальное 2D-моделирование конструкции SOL и литиевого дивертора. Требуется также инженерно-технологическая проработка такой конструкции.

Настоящая работа поддержана Министерством науки и высшего образования Российской Федерации в рамках государственного задания в сфере науки по проекту № 0784-2020-0020 с использованием Федерального центра коллективного пользования «Материаловедение и диагностика в передовых технологиях» (проект RFMEFI62119X0021), включающего уникальную научную установку «Сферический токамак Глобус-М».

Ключевые слова: дивертор, литий, тепловые нагрузки, ДЕМО-ТИН.

СПИСОК ЛИТЕРАТУРЫ

1. **Nagayama Y.** — Fusion Eng. Des., 2009, vol. 84, p. 1380.
2. **Goldston R.J. et al.** — Phys. Scr., 2016, vol. 167, p. 014017.
3. **Shpanskiy Yu.S. et al.** — Nucl. Fusion, 2019, vol. 59, p. 076014.

V.Skokov@spbstu.ru

UDC 621.039.619

DESIGN AND RESEARCH PROGRAM OF THE ALIANCE-T EXPERIMENT

(*short message*)

D. Yakovlev[1], T. Akhmetov[1], P. Bagryansky[1], Z. Chen[2], A. Ivanov[1], I. Kotelnikov[1], E. Kuzmin[1], V. Prikhodko[1], I. Shikhovtsev[1], Q. Zeng[2]

[1]Budker Institute of Nuclear Physics of Siberian Branch Russian Academy of Sciences, Novosibirsk, 630090, Russia
[2]Institute of Nuclear Energy Safety Technology, Hefei Institutes of Physical Science, Chinese Academy of Sciences, Hefei, Anhui, 230031, China

ALIANCE-T is a pilot experiment aiming to test the core principles of operation of the ALIANCE [1] volumetric fusion neutron source and to study specific plasma physics problems related to continuously operating gas dynamic mirror traps [2]. Research program of ALIANCE-T focuses on achievement of continuous discharge in axisymmetric magnetic field with high mirror ratio (~100) with parameters of plasma suitable for neutral beam injection. The research program includes experimental evaluation of several possible plasma generation techniques, studies of plasma stability against magneto hydrodynamic (MHD) perturbations, testing of stabilization methods most suitable for a continuous discharge, studies on interaction between neutral gas and plasma and its influence on the overall energy confinement time. As a technology demonstration experiment, ALIANCE-T will feature several technical solutions envisioned for ALIANCE-1 [1] and succeeding machines such as modular magnet system with compact superconducting magnetic mirror solenoids, electrode-based plasma stabilization and limiting technologies suitable for a continuous discharge, continuous gas feed for plasma density control and cycling of neutral gas through pumping and gas feed systems. Successful completion of the experimental program is expected to provide well-defined solutions for the ALIANCE-1 experiment with

neutral beam injection. The report presents general structure and parameters of the machine's subsystems, including the description of plasma source and its expected performance.

Key words: gas dynamic trap, fusion neutron source, superconducting magnets, plasma source.

DOI: 10.21517/0202-3822-2021-44-2-162-163

ПРОЕКТ И ИССЛЕДОВАТЕЛЬСКАЯ ПРОГРАММА ЭКСПЕРИМЕНТА ALIANCE-T

(*краткое сообщение*)

Д. Яковлев[1], Т. Ахметов[1], П. Багрянский[1], Ц. Цзэн[2], А. Иванов[1], И. Котельников[1], Е. Кузьмин[1], В. Приходько[1], И. Шиховцев[1], Ч. Чэнь[2]

[1]Институт ядерной физики им. Г.А. Будкера Сибирского отделения Российской академии наук, Новосибирск, 630090, Россия
[2]Институт технологии безопасности ядерной энергии, Хэфэйские институты физических наук, Китайская академия наук, Хэфэй, Аньхой, 230031, Китай

ALIANCE-T — пилотный эксперимент, направленный на проверку основных принципов работы объёмного термоядерного источника нейтронов ALIANCE [1] и изучение вопросов удержания плазмы в газодинамических пробочных ловушках, работающих в непрерывном режиме [2]. Исследовательская программа ALIANCE-T направлена на достижение непрерывного разряда в осесимметричном магнитном поле с высоким пробочным отношением (~100) и параметрами плазмы, пригодными для инжекции нейтрального пучка. Программа исследований включает экспериментальную проверку нескольких возможных методов генерации плазмы, исследования устойчивости плазмы по отношению к магнитогидродинамическим (МГД) возмущениям, тестирование методов стабилизации, наиболее подходящих для непрерывного разряда, а также исследования взаимодействия нейтрального газа с плазмой и его влияния на общее время удержания энергии. В качестве эксперимента для демонстрации технологий ALIANCE-T представит несколько технических решений, которые предлагается применить в ALIANCE-1 [1] и последующих установках, таких как модульная магнитная система с компактными сверхпроводящими соленоидами магнитных пробок, технологии стабилизации и контроля границы плазмы при помощи электродов, пригодные для непрерывного разряда, непрерывная подача газа для поддержания плотности плазмы, а также замыкание газового цикла через системы откачки и подачи газа. Ожидается, что успешное выполнение экспериментальной программы позволит выработать готовые решения для эксперимента ALIANCE-1 с инжекцией нейтрального пучка. В отчёте представлены общая структура и параметры подсистем экспериментальной установки, включая описание источника плазмы и его ожидаемых характеристик.

Ключевые слова: газодинамическая ловушка, источник термоядерных нейтронов, сверхпроводящие магниты, источник плазмы.

СПИСОК ЛИТЕРАТУРЫ

1. **Bagryansky P.A. et al.** — Nucl. Fusion, 2020, vol. 60, p. 036005.
2. **Ivanov A.A., Prikhodko V.V.** — Plasma Phys. Control. Fusion, 2013, vol. 55 p. 063001.

D.V.Yakovlev@inp.nsk.su

UDC 621.039.672

DEVELOPMENT AND APPLICATIONS OF HINEG HIGH INTENSITY NEUTRON SOURCES

(*short message*)

Yican Wu

Institute of Nuclear Energy Safety Technology, FDS Team, Chinese Academy of Sciences, Hefei, Anhui, 230031, China

Neutron sources are the important experimental platforms for the R&D of advanced nuclear energy and nuclear technology application. The High Intensity Neutron Generator (HINEG) has been developed in China with different missions including neutronics design validation, material & components irradiation test, nuclear waste

burning and nuclear technology application. HINEG-I has achieved the fusion neutrons with the yield of $6.4 \cdot 10^{12}$ n/s at maximum, and has been coupled with the Lead-based Zero Power Critical/Subcritical Reactor named CLEAR-0. Such a facility is actually an accelerator-driven Fusion-Fission Hybrid System. Series of typical experiments have been carried out on HINEG-I, including neutronics and code validation, core physics study of advanced reactors, neutron radiography, neutron detector calibration, neutron biological effects, neutron radiation hardening, and so on. HINEG-II is an accelerator-based neutron source with the yield of 10^{14}—10^{15} n/s. It aims to apply to multi-purposes, e.g. neutron capture therapy, isotope production, etc. The design and R&D for key technologies of HINEG-II are performed on-going. HINEG-III is initially conceived as a GDT-based or accelerator-based neutron source with the intensity of 10^{17}—10^{18} n/s. The objectives of HINEG-III are to conduct test of nuclear materials, components test and reliability data collection of nuclear components, nuclear waste burning test, etc. This contribution presents an overview of the series recent activities.

Key words: neutron source, HINEG, high intensity.

DOI: 10.21517/0202-3822-2021-44-2-163-164

РАЗРАБОТКА И ПРИМЕНЕНИЕ ВЫСОКОИНТЕНСИВНЫХ НЕЙТРОННЫХ ИСТОЧНИКОВ HINEG

(*краткое сообщение*)

Й. Ву

Институт технологии безопасности ядерной энергии, Команда FDS, Китайская академия наук, Хэфэй, Аньхой, 230031, Китай

Источники нейтронов являются важными экспериментальными установками для исследований и разработок в области передовой ядерной энергетики и применения ядерных технологий. Высокоинтенсивный нейтронный генератор (HINEG) был разработан в Китае с различными задачами, включая проверку нейтронно-физических расчётов, испытание под облучением материалов и компонентов, сжигание ядерных отходов и применение ядерных технологий. На HINEG-I достигнут максимальный выход термоядерных нейтронов $6{,}4 \cdot 10^{12}$ н/с. Этот нейтронный источник был соединён со свинцовым критическим/подкритическим реактором нулевой мощности CLEAR-0. Полученная установка является гибридной системой синтеза-деления на основе ускорителя. На HINEG-I была проведена серия типичных экспериментов, включая проверку нейтроники и валидацию нейтронного кода, изучение нейтронной физики активной зоны перспективных реакторов, нейтронную радиографию, калибровку нейтронных детекторов, нейтронные биологические эффекты, нейтронное радиационное упрочнение и т.д. HINEG-II — источник нейтронов на основе ускорителя с выходом 10^{14}—10^{15} н./с. Он предназначен для применения в различных целях, например, в нейтронно-захватной терапии, производстве изотопов и т.д. Проектирование и НИОКР по ключевым технологиям HINEG-II ведутся в постоянном режиме. HINEG-III изначально задумывался как источник нейтронов на основе ГДЛ или ускорителя с интенсивностью 10^{17}—10^{18} н./с. Целями HINEG-III являются проведение испытаний ядерных материалов, испытание компонентов и сбор данных о надёжности ядерных компонентов, испытание на сжигание ядерных отходов и т.д. Доклад представляет собой обзор серии недавних работ.

Ключевые слова: источник нейтронов, HINEG, высокая интенсивность.

yican.wu@fds.org.cn

UDC 621.039.624

SHIELDING DESIGN AND NEUTRONICS CALCULATION OF THE GDL BASED FUSION NEUTRON SOURCE ALIANCE

(*short message*)

W. Yang[1, 2], Q. Zeng[1], Ch. Chen[1], Zhibin Chen[1], Jun Song[1], Zhen Wang[1], Jie Yu[1], Dmitry Yakovlev[3], Vadim Prikhodko[3, 4]

[1]Institute of Nuclear Energy Safety Technology, Hefei Institutes of Physical Science, Chinese Academy of Sciences, Hefei, Anhui, 230031, China

[2]University of Science and Technology of China, Hefei, Anhui, 230027, China

[3]Budker Institute of Nuclear Physics of Siberian Branch Russian Academy of Sciences, Novosibirsk, 630090, Russia

[4]Novosibirsk State University, Novosibirsk, 630090, Russia

The Axisymmetric Linear Advanced Neutron source (ALIANCE) is a GDT based fusion neutron source, aiming to produce 10^{18} of D—T-neutrons per second and to provide a large testing volume required for fusion materials and components testing. A similar neutron source could also be valuable in the long run for medical isotopes production and as a driver of sub-critical fission reactor. This presentation presents the high flux neutron shielding design and extensive neutronics calculations of GDT based fusion neutron source ALIANCE. Neutron distribution of ALIANCE is strongly inhomogeneous along the axis: significant portion of the neutron flux is generated near the two mirrors, while the rest of it is spread over the remaining central volume of plasma. The shielding design includes 40 cm stainless steel as the main shielding layer and an additional tungsten shielding layer at mirror plugs to protect superconducting coils from neutron damage and reduce nuclear heating. The simulations have been carried out by using Monte-Carlo transport code Super MC with nuclear data library FENDL 3.1. Results show that the nuclear heating on the mirror coils can be reduced by more than two thirds with additional tungsten shield, and fast neutron fluence by 30%. The highest nuclear heating and the highest fast neutron fluence zones are located at the mirror coils, and the values are about 300 W/m^3 and 9×10^{18} n/cm^2 respectively, which meets the threshold of ITER superconducting coils. The specific activities of shielding layers are on the order of 10^{12} Bq/kg. Ten years after shutdown, specific activities of structural materials will decrease by more than 98% to meet the safety requirements. The modeling and calculations reported in this paper will be beneficial for the pre-conceptual engineering design of ALIANCE.

Key words: gas dynamic trap, fusion neutron source, shielding optimization, specific activity.

DOI: 10.21517/0202-3822-2021-44-2-164-166

РАСЧЁТЫ И ПРОЕКТ НЕЙТРОННОЙ ЗАЩИТЫ ИСТОЧНИКА ТЕРМОЯДЕРНЫХ НЕЙТРОНОВ ALIANCE НА ОСНОВЕ ГАЗОДИНАМИЧЕСКОЙ ЛОВУШКИ

(*краткое сообщение*)

В. Ян[1, 2], Ц. Цзэн[1], Ч. Чэнь[1], Чж. Чэнь[1], Ц. Сон[1], Чж. Ван[1], Ц. Юй[1], Д. Яковлев[3], В. Приходько[3, 4]

[1]*Институт технологии безопасности ядерной энергии, Хэфэйские институты физических наук, Китайская академия наук, Хэфэй, Аньхой, 230031, Китай*

[2]*Научно-технический университет Китая, Хэфэй, Аньхой, 230027, Китай*

[3]*Институт ядерной физики им. Г.А. Будкера Сибирского отделения Российской академии наук, Новосибирск, 630090, Россия*

[4]*Новосибирский государственный университет, Новосибирск, 630090, Россия*

Осесимметричный линейный усовершенствованный источник нейтронов (ALIANCE) — это проект источника термоядерных нейтронов на основе газодинамической ловушки, производящего 10^{18} нейтронов в секунду в реакции DT и обладающего тестовой зоной большого объёма, необходимой для испытаний термоядерных материалов и компонентов. Подобный источник нейтронов также может быть полезен в долгосрочной перспективе для производства медицинских изотопов и в качестве «драйвера» подкритического реактора деления. В докладе представлены конструкция системы защиты от потока нейтронов высокой интенсивности и подробные результаты нейтронных расчётов источника ALIANCE на основе газодинамической ловушки. Распределение потока нейтронов в ALIANCE сильно неоднородно вдоль оси установки: значительная часть полного потока нейтронов генерируется вблизи магнитных пробок, а оставшаяся его часть распределена по центральному объёму плазмы. Нейтронная защита включает в себя слой нержавеющей стали толщиной 40 см в качестве основного экранирующего слоя и дополнительный вольфрамовый экранирующий слой в области магнитных пробок для защиты сверхпроводящих катушек от повреждения нейтронами и уменьшения ядерного нагрева. Моделирование проводилось с использованием транспортного кода Монте-Карло Super MC с библиотекой ядерных данных FENDL 3.1. Результаты показывают, что ядерный нагрев магнитных пробок может быть уменьшен более чем на две трети при помощи дополнительного вольфрамового экрана, а флюенс быстрых нейтронов на 30%. Наибольший ядерный нагрев и зоны с наибольшим флюенсом быстрых нейтронов находятся в магнитных пробках, и их значения составляют около 300 Вт/м^3 и 9×10^{18} н./см^2 соответственно, что соответствует порогу облучения сверхпроводящих катушек ИТЭР. Удельная активность слоёв нейтронной защиты составляет порядка 10^{12} Бк/кг. Через десять лет после прекращения работы установки удельная активность конструкционных материалов снизится более чем на 98%, что позволит удовлетворить тре-

бованиям безопасности. Моделирование и расчёты, представленные в этой статье, могут быть использованы для подготовки концептуального и инженерного проекта установки ALIANCE.

Ключевые слова: газодинамическая ловушка, источник термоядерных нейтронов, оптимизация нейтронной защиты, удельная активность.

v.v.prikhodko@inp.nsk.su

UDC 621.039.624

SIMULATION OF PLASMA PARAMETERS FOR ALIANCE PROJECT

(*short message*)

V.V. Prikhodko[1, 2], Z. Chen[3], I.A. Kotelnikov[1, 2], D.V. Yakovlev[1], J. Yu[3], Q. Zeng[3]

[1]Budker Institute of Nuclear Physics of Siberian Branch Russian Academy of Sciences, Novosibirsk, Russia
[2]Novosibirsk State University, Novosibirsk, Russia
[3]Institute of Nuclear Energy Safety Technology Chinese Academy of Sciences, Hefei, China

An international project named ALIANCE was jointly started by INEST CAS and BINP SB RAS [1]. The project assumes design of three mirror devices with increasing power. Results of plasma parameters simulation by DOL code [2] will be discussed in this talk. The first is a prototype of continuously operating beam-driven device. It will have low power of injected beams and deep gas-dynamic regime of confinement. The second is an intermediate step. Beam power will be increased by an order of magnitude reaching the transition between gas-dynamic and kinetic confinement regimes. And the third is a full-scale neutron source. The key parameters of these configuration are presented in Table.

Results of plasma simulations for ALIANCE project

Parameters	ALIANCE-I	ALIANCE-II	ALIANCE-III
Isotope mix	100% D	100% D	50% D + 50% T
Mirror-to-mirror length, m	4.4	7.7	20
Plasma radius at the central plane, m	0.3	0.3	0.3
Magnetic field in plugs/centre, T	12/0.2	13/0.3	25/0.8
Power of injected beams, MW	0.1	4	50
Ion/electron temperatures, keV	0.04/0.03	0.5/0.4	1.2/2.6
Neutron yield rate, 1/s	$4\cdot10^{9}$	$5\cdot10^{13}$	$1\cdot10^{18}$

Key words: fusion neutron source, gas-dynamic trap.

DOI: 10.21517/0202-3822-2021-44-2-166-167

МОДЕЛИРОВАНИЕ ПАРАМЕТРОВ ПЛАЗМЫ ДЛЯ ПРОЕКТА ALIANCE

(*короткое сообщение*)

В.В. Приходько[1, 2], Ч. Чэнь[3], И.А. Котельников[1, 2], Д.В. Яковлев[1], Ц. Юй[3], Ц. Цзэн[3]

[1]Институт ядерной физики им. Г.А. Будкера Сибирского отделения Российской академии наук, Новосибирск, Россия
[2]Новосибирский государственный университет, Новосибирск, Россия
[3]Институт технологии ядерной энергетической безопасности, Китайская академия наук, Хэфэй, Китай

Международный проект «ALIANCE» был начат совместно INEST CAS и ИЯФ СО РАН [1]. Проект предполагает разработку трёх открытых ловушек с увеличивающейся мощностью нагрева. Результаты моделирования параметров плазмы с помощью кода DOL [2] представлены в настоящем докладе. Первая — это прототип непрерывно работающей ловушки с нагревом атомарными пучками. Мощность инжектируемых пучков будет невысокой, а режим удержания глубоко газодинамическим. Вторая — это ловушка с промежуточными параметрами. Мощность пучка будет увеличена на порядок, а режим удержания достигнет переходной области между газодинамическим и кинетическим. И третья — это полномасштабный источник нейтронов. Основные параметры этих конфигураций представлены в таблице.

Результаты моделирования плазмы для проекта ALIANCE

Параметр	АЛЬЯНС-I	АЛЬЯНС-II	АЛЬЯНС-III
Смесь изотопов	100% D	100% D	50% D + 50% T
Длина от зеркала до зеркала, м	4.4	7.7	20
Радиус плазмы в центральной плоскости, м	0.3	0.3	0.3
Магнитное поле в штекерах/центре, Т	12/0.2	13/0.3	25/0.8
Мощность инжектируемых пучков, МВт	0.1	4	50
Температура ионов/электронов, кэВ	0.04/0.03	0.5/0.4	1.2/2.6
Скорость выхода нейтронов, 1/с ·	$4\cdot10^{9}$	$5\cdot10^{13}$	$1\cdot10^{18}$

Ключевые слова: источник термоядерных нейтронов, газодинамическая ловушка.

СПИСОК ЛИТЕРАТУРЫ

1. **Bagryansky P.A. et al.** — Nucl. Fusion, 2020, v. 60, p. 036005.
2. **Юров Д.В. и др.** — Физика плазмы, 2016, т. 42, с. 217.

v.v.prikhodko@inp.nsk.su

UDC 621.039.553

RADIATION DEFECT FORMATION IN BCC METALS IRRADIATED WITH HIGH ENERGY PROTONS, SELF-IONS AND NEUTRONS WITH DIFFERENT SPECTRA

(*short message*)

O.V. Ogorodnikova[1], M. Majerle[2], J. Čížek[3], S. Simakov[4], V.V. Gann[5], P. Hruška[3], J. Kameník[2], J. Pospíšil[6], M. Štefánik[2], M. Vinš[7], J. Štursa[2]

[1]National Research Nuclear University MEPHI (Moscow Engineering Physics Institute), Kashirskoe sh. 31, Moscow, Russia
[2]Nuclear Physics Institute of the CAS, Řež 130, 250 68 Řež, Czech Republic
[3]Charles University, Department of Low-temperature physics, V Holešovičkách 2, 180 00, Prague, Czech Republic
[4]Institute for Neutron Physics and Reactor Technology, Karlsruhe Institute of Technology, Hermann-von-Helmholtz-Platz 1, 76344 Eggenstein-Leopoldshafen, Germany
[5]National Science Centre «Kharkov Institute of Physics and Technology», Kharkov, Ukraine
[6]Charles University, Faculty of Mathematics and Physics, Department of Condensed Matter Physics, Ke Karlovu 5, 121 16 Prague 2, Czech Republic
[7]Research Centre Řež, Řež 130, 250 68 Řež, Czech Republic

Currently, tungsten and tungsten coatings are the reference materials of the ITER divertor and DEMO reactors and the possibility of using low-activated ferrite-martensitic, RAFM, steels not only as structural materials, but also as the material of the first wall of the fusion reactor is considered. Also, these steels, together with a new generation of RAFM steels with oxide dispersion strengthened by adding Y_2O_3 nanoparticles, the so-called ODS steels, are considered as promising materials for fast neutron fuel cladding. Neutron damage results in degradation of properties and activation of materials, and therefore affects performance and safety aspects. As a power fusion neutron source does not exist yet, to simulate fusion neutron-induced damage in materials, fission neutrons and charged particles are widely used. In this work, the size and density of radiation-induced defects in bcc metals (W, Mo and Fe) produced by high-energy self-ions, protons and neutrons with different spectrum have been compared by well-established method of positron-annihilation lifetime-spectroscopy (PALS). We found a formation of the larger size of the defects with lower density in the case of irradiation with high-energy neutrons from the *p* (35 MeV) — Be source compared to fission neutron- and proton- irradiations. New experimental data together with data available from the literature are compared with the dpa theory, including molecular dynamic simulations. Second, He/dpa ratios in different neutron facilities have been compared. We show that He/dpa ratios in the facilities with the hard energy spectra (fusion like) *p* (35 MeV) — Be source and DEMO are one-two orders larger than in the fission ones LVR-15, HFIR and BOR60. Methods to obtain the best approach to model fusion neutron damage and to overcome the gap between theory prediction of primary defect formation and long-term damage are discussed taking into account the uncertainties.

Key words: radiation-induced defects, bcc metals, high-energy neutrons and protons.

DOI: 10.21517/0202-3822-2021-44-2-167-168

ОБРАЗОВАНИЕ РАДИАЦИОННЫХ ДЕФЕКТОВ В ОЦК-МЕТАЛЛАХ, ОБЛУЧЁННЫХ ВЫСОКОЭНЕРГЕТИЧЕСКИМИ ПРОТОНАМИ, СОБСТВЕННЫМИ ИОНАМИ И НЕЙТРОНАМИ С РАЗЛИЧНЫМИ СПЕКТРАМИ

(*краткое сообщение*)

О.В. Огородникова[1], М. Майерле[2], Я. Чижек[3], С. Симаков[4], В.В. Ганн[5], П. Грушка[3], Я. Каменик[2], Я. Поспишил[6], М. Штефаник[2], М. Винш[7], Я. Штурса[2]

[1]*Национальный исследовательский ядерный университет «МИФИ» (Московский инженерно-физический институт), Каширское ш. 31, Москва, Россия*

[2]*Ядерный физический институт КАС, Ржеж 130, 250 68 Ржеж, Чешская Республика*

[3]*Университет Шарлеса, кафедра физики низких температур, В Голешовичкач 2, 180 00, Прага, Чешская Республика*

[4]*Институт нейтронной физики и реакторной технологии, Технологический институт Карлсруэ, Герман-фон-Гельмгольц-Плац 1, 76344 Эггенштейн-Леопольдсхафен, Германия*

[5]*Национальный научный центр «Харьковский физико-технический институт», Харьков, Украина*

[6]*Университет Шарлеса, математико-физический факультет, Кафедра физики конденсированных сред, Ke Karlovu 5, 121 16 Прага 2, Чешская Республика*

[7]*Исследовательский центр Ржеж, 130, 250 68 Ржеж, Чешская Республика*

В настоящее время вольфрам и вольфрамовые покрытия являются эталонными материалами диверторных и демонстрационных реакторов ИТЭР и рассматривается возможность использования низкоактивированных феррит-мартенситных, РАФМ-сталей не только в качестве конструкционных материалов, но и в качестве материала первой стенки термоядерного реактора. Кроме того, эти стали вместе с новым поколением РАФМ-сталей с оксидной дисперсией, упрочнённых добавлением наночастиц Y_2O_3, так называемых СОД-сталей, рассматриваются как перспективные материалы для оболочек твэлов на быстрых нейтронах. Нейтронное повреждение приводит к ухудшению свойств и активации материалов, а следовательно, влияет на эксплуатационные характеристики и безопасность. Поскольку источника термоядерных нейтронов ещё не существует, для моделирования термоядерных нейтронных повреждений в материалах широко используются нейтроны деления и заряженные частицы. В данной работе проведено сравнение размеров и плотности радиационно-индуцированных дефектов в ОЦК-металлах (W, Mo и Fe), полученных высокоэнергетическими собственными ионами, протонами и нейтронами с различным спектром, с помощью хорошо зарекомендовавшего себя метода позитронно-аннигиляционной прижизненной спектроскопии (PALS). Обнаружено образование большего размера дефектов с меньшей плотностью при облучении высокоэнергетическими нейтронами от источника *p* (35 МэВ) — Be по сравнению с нейтронами деления и протонным облучением. Во-первых, новые экспериментальные данные вместе с данными, имеющимися в литературе, сравниваются с теорией сна, включая молекулярно-динамическое моделирование. Во-вторых, было проведено сравнение соотношений He/dpa в различных нейтронных установках. Показано, что соотношения He/dpa для исследуемых материалов в установках с термоядерными энергетическими спектрами, полученными из *p* (35 МэВ) — Be-источника и для реактора DEMO на один-два порядка больше, чем для нейтронов деления в реакторах LVR-15, HFIR и BOR60. Обсуждаются методы получения наилучшего подхода к моделированию термоядерных нейтронных повреждений и преодоления разрыва между теоретическим прогнозированием первичного дефектообразования и долговременным повреждением с учётом неопределённостей.

Ключевые слова: радиационно-индуцированные дефекты, ОЦК-металлы, высокоэнергетические нейтроны и протоны.

olga@plasma.mephi.ru

ПАМЯТИ ЮРИЯ ГРИГОРЬЕВИЧА КАЛИНИНА
05.11.1940—05.03.2021

Ушёл из жизни блестящий учёный, прекрасный добрый человек Юрий Григорьевич Калинин — доктор физико-математических наук, начальник Отдела источников излучения ККЯТЭТ НИЦ «Курчатовский институт». Детство и школьные годы Юрия Григорьевича прошли в Киеве. Во время учёбы в Московском физико-техническом институте, как и многие студенты, на волне романтики активно участвовал в новом движении КВН, ездил в геологические экспедиции в Якутию в качестве радиста. Первый экзамен теоретического минимума по физике сдал лично Льву Давидовичу Ландау. Свою научную работу начал в секторе Е.К. Завойского Института атомной энергии им. И.В. Курчатова. Его кандидатская диссертация была одной из первых, связанных с открытием турбулентного нагрева в плазме. Бóльшая часть его научных работ посвящена мощным импульсным генераторам релятивистских электронных пучков и инерциальному подходу к управляемому термоядерному синтезу. Красной линией через его исследования проходит использование эффекта Штарка для выявления особенностей в поведении импульсной плазмы. Под его руководством и с его активным участием были проведены пионерские работы на установках НПР-2, «Мираж», «Ангара-1», модуль «Ангары-5», РС-20, «Кальмар», в которых были опробованы новые экспериментальные схемы: многократно увеличенный энерговклад в мишень за счёт магнитного стоппинга сильноточных электронных пучков и острая фокусировка пучков; схема «лайнер—мишень», позволяющая трансформировать энергию сжимающейся цилиндрической оболочки в поток тепла на мишень и укоротить время энерговклада; двухоболочечные лайнеры, стабилизирующие процесс сжатия вещества проходящим по нему током. Была продемонстрирована возможность пропускания мегаамперных токов по линиям с магнитной самоизоляцией в миниатюрных миллиметровых масштабах.

В возглавляемом им отделе на уникальной по энергетике установке «Стенд-300» проводились многочисленные совместные эксперименты с коллегами из Франции, Чехии и Китая.

Ю.Г. Калинин — один из ведущих российских специалистов в области физики плазмы и термоядерного синтеза, автор более чем 200 оригинальных научных работ и монографий. В последнее время он вёл несколько важнейших проектов в фундаментальной и прикладной научной тематике, в том числе связанных с поддержанием обороноспособности нашей Родины.

Ю.Г. Калинин был членом диагностической комиссии Министерства среднего машиностроения, заместителем председателя диссертационного совета по физике плазмы, экспертом нескольких научных фондов и председателем экспертного совета по физике плазмы Российского фонда фундаментальных исследований.

Юрий Григорьевич воспитал целую плеяду молодых исследователей, занимаясь со студентами, дипломниками и аспирантами МГУ, МФТИ, МИФИ, МЭИ и других столичных вузов. Для многих он был не просто научным руководителем и начальником, но и наставником, учителем и другом.

Нам будет очень не хватать Юрия Григорьевича…

Коллеги

ПАМЯТИ ГЕОРГИЯ ИВАНОВИЧА ДОЛГАЧЁВА

16.03.1938—21.02.2021

После тяжёлой продолжительной болезни от нас ушёл замечательный экспериментатор доктор физико-математических наук Георгий Иванович Долгачёв.

Георгий Иванович после срочной службы в Советской Армии окончил Московский физико-технический институт и пришёл в Институт атомной энергии им. И.В. Курчатова в сектор Е.К. Завойского, где начал работу по тематике управляемого термоядерного синтеза и высокотемпературной плазмы. В работе его отличали принципиальность и прямота, стремление докопаться до самой сути явления. Он является соавтором нескольких десятков изобретений и более чем 150 научных трудов. Главным достижением его научного творчества было создание нового класса мощных электромагнитных генераторов наносекундного диапазона длительности, основанного на разработанных им плазменных размыкателях тока. В последние годы он активно помогал молодым коллегам в постановке и интерпретации экспериментов, проводившихся на сильноточном генераторе РС-20, делясь огромным опытом и знаниями.

Георгий Иванович очень любил природу, на протяжении всей своей жизни постоянно ходил в походы. Сам конструировал и строил яхты для водных путешествий. Осенью по первому снегу непременно уезжал на несколько дней с друзьями на сбор клюквы в Тверскую область. Он увлекался плаванием в ледяной воде, лыжами, для которых, будучи верен себе, придумал новый вид креплений — прообраз тех, что в настоящее время используются повсеместно.

Когда Георгий Иванович защищал свою докторскую диссертацию, совершенно справедливо прозвучали слова оппонента: «Курчатовский институт должен гордиться тем, что в нём работают и творят такие замечательные специалисты, как Георгий Иванович Долгачёв». Память об этом прекрасном человеке, о его целеустремлённости, дружелюбии и жизнерадостности будет жить и воодушевлять всех, кто был с ним рядом.

Коллеги

ПАМЯТИ ВЛАДИМИРА ВАСИЛЬЕВИЧА АРСЕНИНА

10.09.1938—23.03.2021

Пандемия унесла жизнь Владимира Васильевича Арсенина, главного научного сотрудника Курчатовского комплекса ядерных транспортных энергетических технологий (ККЯТЭТ) НИЦ «Курчатовский институт», доктора физико-математических наук, выдающегося исследователя в области физики плазмы.

Владимир Васильевич Арсенин родился в 1938 г. Его мать была учителем, отец — известный математик, работал в коллективе, руководимом выдающимся математиком А.Н. Тихоновым. После окончания школы Владимир Васильевич поступил в МИФИ. Его научная судьба складывалась удачно. На старших курсах ему посчастливилось попасть в группу, находящуюся под опекой замечательного педагога В.И. Когана. В 1961 г. он стал руководителем Владимира Васильевича в аспирантуре МИФИ. В 1965 г. В.В. Арсенин защитил кандидатскую диссертацию, в которой разработана теория колебаний и устойчивости сильно неоднородной плазмы. За годы учебы сложились контакты Владимира Васильевича с сотрудниками отдела ОГРА ИАЭ им. И.В. Курчатова, руководимого И.Н. Головиным. Этот коллектив исследовал перспективы открытых магнитных ловушек как термоядерного реактора. Серьёзным препятствием для этого являлась желобковая неустойчивость плазмы. Один из методов её стабилизации связан с использованием так называемых обратных связей. Этот метод был предложен ранее в абстрактной форме. В.В. Арсенин и В.А. Чуянов нашли простую схему, которая позволила реализовать идею обратных связей в существовавших открытых ловушках. Эти пионерские работы инициировали исследования, в которых метод обратных связей использовался и для стабилизации других неустойчивостей. Данный метод вошёл в «золотой фонд» физики плазмы. За работы по этой тематике В.В. Арсенину и В.А. Чуянову в 1972 г. была присуждена престижная премия Ленинского комсомола. В том же году Владимир Васильевич защитил докторскую диссертацию.

Большинство работ Владимира Васильевича посвящено вопросам равновесия и устойчивости плазмы в открытых ловушках. Когда такие ловушки прекратили своё существование в Курчатовском институте, Владимир Васильевич остался верен термоядерному направлению, переключившись на токамаки. Работы Владимира Васильевича отличались ясностью и математической строгостью. Его авторство бы-

ло гарантией высокого качества работ, поэтому они, как правило, принимались для публикации без серьёзных замечаний.

В.В. Арсенин был научным руководителем или научным консультантом пяти соискателей, защитивших кандидатские диссертации. Он был лауреатом институтского конкурса научных работ им. И.В. Курчатова. Владимир Васильевич имел почётное звание «Ветеран труда» и нагрудный знак «Ветеран атомной энергетики и промышленности».

Продуманность, стремление «докопаться до истины», которые определяли научную деятельность Владимира Васильевича, проявились и в отношениях с коллегами. Вместе с доброжелательностью и нежеланием концентрироваться на отрицательных моментах человеческих отношений, неизбежных в любых коллективах, эти качества заработали высокую репутацию Владимиру Васильевичу. Благодаря ей Владимир Васильевич являлся членом множества комиссий, в том числе и разбиравших этические вопросы.

Владимир Васильевич многие годы был членом редколлегии журнала «Физика плазмы» и одновременно её научным редактором. Его суждения о работах в силу продуманности и взвешенности имели большой вес при оценке обсуждаемых статей. В качестве научного редактора Владимир Васильевич проявлял присущие ему добросовестность и аккуратность. Он не только старался привести редактируемую работу в соответствие с принятыми стандартами, но и вникал в её суть. Некоторые из принятых к публикации работ отклонялись в процессе редактирования.

Интересы Владимира Васильевича не ограничивались физикой. Он был опытным туристом, получил звание «Мастер спорта СССР» по спортивному туризму (1977 г.). К своим увлечениям он относился так же основательно, как и к профессиональной деятельности. Особенно детально им были изучены туристические маршруты Западного Кавказа. Об этом он написал книгу «Горные путешествия по Западному Кавказу». Интересовала Владимира Васильевича также история. Он держал в памяти огромное число фактов из истории России и Европы. Были любопытны подмеченные им аналогии давно прошедших событий с современностью.

Нас постигла тяжёлая утрата — ушёл из жизни замечательный учёный и человек.

Коллеги

ПАМЯТИ АЛЕКСАНДРА ИВАНОВИЧА РЯЗАНОВА
12.03.1948—23.03.2021

Трудовой коллектив НИЦ «Курчатовский институт» понёс тяжёлую утрату. 23 марта 2021 г. скоропостижно скончался в результате болезни руководитель Отделения физики твёрдого тела и радиационного материаловедения Курчатовского ядерно-физического комплекса, доктор физико-математических наук, профессор Александр Иванович Рязанов.

Александр Иванович Рязанов родился 12 марта 1948 г. После окончания в 1972 г. Московского инженерно-физического института по специальности «Теоретическая ядерная физика» он был распределён на работу в ИАЭ им. И.В. Курчатова, с которым неразрывно связана вся его дальнейшая трудовая биография. Александр Иванович начал работу инженером-исследователем в Отделе радиационного материаловедения, которым руководил П.А. Платонов. Становление Александра Ивановича как учёного прошло под большим влиянием Л.А. Максимова, под его руководством он в 1979 г. защитил кандидатскую диссертацию. В 1979 г. Александр Иванович перешёл в Отдел инженерно-физических исследований под руководством В.В. Орлова в Отделении физики плазмы под руководством Б.Б. Кадомцева для решения материаловедческих проблем термоядерного реактора. Позднее по приглашению С.Т. Беляева он перешёл в Отделение общей и ядерной физики в Курчатовском институте и возглавил группу радиационных исследований материалов, которая выросла впоследствии в лабораторию, а затем и в Отдел радиационных исследований материалов. Бессменным руководителем этого подразделения Александр Иванович оставался на протяжении всей своей жизни.

В период с 1973 по 1982 г. А.И. Рязанов являлся победителем в конкурсах молодых научных сотрудников в Курчатовском институте. В 1998 г. Александр Иванович Рязанов защитил докторскую диссертацию, а в 2000 г. ему было присвоено учёное звание профессора.

А.И. Рязанов являлся ведущим специалистом в России по радиационной физике твёрдого тела, а также по теоретическим и экспериментальным исследованиям в области радиационного материаловедения для развития атомной энергетики и создания термоядерной энергетики. Он разработал новые теоретические модели радиационного распухания и радиационной ползучести в облучаемых материалах

атомных реакторов. А.И. Рязанов был научным руководителем ряда проектов Госкорпорации «Росатом». Им опубликовано свыше 150 научных статей в ведущих отечественных и зарубежных научных журналах, он участвовал в многочисленных российских и международных конференциях. А.И. Рязанов активно сотрудничал с коллективами зарубежных учёных из Западной Европы, США и Японии.

Для развития работ в области будущей термоядерной энергетики А.И. Рязанов проводил большой цикл экспериментальных и теоретических работ по исследованию радиационной стойкости новых материалов для будущих термоядерных реакторов с использованием облучения быстрыми частицами на циклотроне в НИЦ «Курчатовский институт» и взаимодействия плазмы с облучёнными и необлучёнными материалами.

В период с 2008 г. по настоящее время А.И. Рязанов руководил работами по разработке теоретических моделей и созданию расчётно-теоретической методики оценки радиационной стойкости электронной компонентной базы при воздействии ионизирующих излучений в НИЦ «Курчатовский институт» и ФГУП «РФЯЦ — ВНИИЭФ».

Александр Иванович руководил многими студентами и аспирантами, из которых около десяти человек стали кандидатами наук и один доктором наук. За успешную научную деятельность и подготовку в НИЦ «Курчатовский институт» кандидатов наук А.И. Рязанову решением Высшей аттестационной комиссии России в 2000 г. присуждено учёное звание профессора по специальности «Физика твёрдого тела».

В период с 2009 по 2015 г. А.И. Рязанов возглавлял работы по исследованию радиационной стойкости материалов коллиматоров и сверхпроводящих материалов для магнитов Большого адронного коллайдера (БАК) в ЦЕРНе. А.И. Рязановым разработана теоретическая модель и создана программа для численных расчётов образования и распространения ударных волн в материалах коллиматоров БАК.

Коллеги, друзья и ученики знали Александра Ивановича как большого учёного, настоящего энтузиаста своего дела, открытого и отзывчивого человека. Его всегда отличали высокий профессионализм, жизнелюбие и оптимизм, искренний и глубокий интерес к научным задачам, открытию нового и неизведанного.

Александр Иванович награждён памятной медалью «В память 850-летия Москвы», юбилейной медалью «70 лет атомной отрасли России», нагрудным знаком «Ветеран атомной энергетики и промышленности», был лауреатом институтской премии им. И.В. Курчатова.

Ушёл из жизни крупный учёный, талантливый физик, преданный науке. Светлая память об Александре Ивановиче навсегда сохранится в наших сердцах.

Коллеги

ПАМЯТИ АЛЕКСАНДРА АЛЕКСЕЕВИЧА СКОВОРОДЫ
01.11.1949—07.03.2021

7 марта 2021 г. ушёл из жизни главный научный сотрудник Отдела теории плазмы ККТЭиПТ НИЦ «Курчатовский институт» доктор физ.-мат. наук Александр Алексеевич Сковорода.

Во время учёбы в аспирантуре МГУ им. М.В. Ломоносова Александр Алексеевич впервые опробовал метод измерения электронной температуры по форме линии циклотронного поглощения при прохождении электромагнитной волны через минимум магнитного поля.

В 1977 г. А.А. Сковорода поступил на работу в ИАЭ им. И.В. Курчатова, в отдел ОГРА, руководимый И.Н. Головиным. Продолжая аспирантскую тематику, А.А. Сковорода провёл измерения электронной температуры «горячей» плазмы, удерживаемой в открытой ловушке. В экспериментах по ЭЦР-нагреву плазмы в этой системе был обнаружен преимущественный выход электронов через одну из пробок ловушки — по ходу электромагнитного луча. Он осознал, что этот эффект обязан явлению, которое можно использовать для поддержания тока в замкнутых системах, что привело к предложению об ЭЦР-методе поддержания тока в режиме авторезонанса. Для оценки эффективности предлагаемого метода требовалось создать соответствующий численный код. Александр Алексеевич организовал группу, которая решила эту задачу. Был разработан код OGRAY, успешно используемый для теоретического обеспечения экспериментов, проводимых на токамаке Т-10 и планируемых на Т-15МД и ИТЭР.

При участии Александра Алексеевича был создан и успешно опробован плазменный нейтрализатор — мультикасповая ловушка для низкотемпературной плазмы. По-видимому, именно такой способ превращения ускоренных отрицательных ионов водорода в пучки быстрых атомов будет использован в инжекторах Демонстрационного термоядерного реактора (ДЕМО).

Результаты многолетних исследований равновесия плазмы в магнитных ловушках А.А. Сковорода обобщил в монографии «Магнитные ловушки» (Физматлит, 2009). Продолжая эти исследования, он пришёл к необходимости анализа общегеометрических свойств магнитных полей. А.А. Сковорода также внёс вклад в актуальную проблему взаимодействия плазмы со стенкой. Им совместно с учениками были проведены уникальные экспериментальные исследования проницаемости поликристаллических мембран при плазменном облучении, обнаружены и объяснены эффекты сверхпроницаемости ниобиевых фольг.

Большой научный авторитет, завоёванный благодаря широте познаний и самостоятельности мышления, способствовал тому, что А.А. Сковорода активно работал в ряде экспертных советов и конкурсных комиссий.

Александра Алексеевича отличали широкий научный и культурный кругозор, доброжелательность и чувство юмора, которые делали беседы с ним одновременно приятными и полезными для всех, кому посчастливилось с ним общаться.

Светлая память об Александре Алексеевиче навсегда сохранится в наших сердцах.

Коллеги

ПАМЯТИ АНДРЕЯ АЛЕКСЕЕВИЧА БОРИСОВА
09.11.1955—22.05.2021

На 66-м году жизни скоропостижно скончался наш коллега, старший научный сотрудник Отдела ИТЭР НИЦ «Курчатовский институт» Андрей Алексеевич Борисов.

Андрей Алексеевич в 1979 г. закончил МИФИ по специальности «физико-энергетические установки» и был принят на работу в ИАЭ им. И.В. Курчатова (ныне НИЦ «Курчатовский институт»), в Лабораторию нейтронно-физических исследований профессора Г.Е. Шаталова Отделения физики плазмы (ОФП) на должность инженера.

Будучи инициативным, квалифицированным специалистом, он быстро прошёл путь от инженера до старшего научного сотрудника и в 1985 г. закончил заочную аспирантуру Курчатовского института по специальности «теоретическая и математическая физика».

В область научных интересов А.А. Борисова входила оптимизация нейтронно-физических свойств бланкетов для первого отечественного гибридного Опытного термоядерного реактора токамака ОТР и демонстрационного энергетического квазистационарного реактора-токамака ДЕМО-С, а также термоядерных реакторов на основе открытой ловушки (ТРОЛ) и Z-пинча. Для ДЕМО-С он выполнял расчёты скорости выгорания лития в процессе работы реактора в бридинговых элементах разных типов, проводил анализ параметров реактора с гелиевым и литиевым теплоносителями.

Андрей Алексеевич участвовал в создании программ обработки библиотек ядерных данных и программ подготовки групповых констант для кодов переноса излучения, различных интерфейсных программ и программ обработки результатов. Он также занимался анализом возможности и эффективности трансмутации актинидов в окисном и нитридном топливе в бланкете термоядерного реактора.

А.А. Борисов сумел разработать инженерные модели испытательных модулей бланкетов высокой геометрической сложности и различных российских диагностических систем, входящих в состав международного проекта первого термоядерного реактора ИТЭР. Используя эти модели, он выполнил методом Монте-Карло скрупулёзный трёхмерный анализ нейтронных полей, мгновенного и остаточного гамма-излучения, ожидаемого после остановки реактора в местах размещения анализатора атомов, диагностики томсоновского рассеяния в диверторе, системы спектроскопии водородных линий и примесей, дивертoрного монитора нейтронного потока, обосновал эффективность конструкции радиационной защиты портов и диагностических систем. Вместе с коллегами он разработал и предложил для реализации методику калибровки нейтронных мониторов мгновенной термоядерной мощности ИТЭР.

Андрей Алексеевич определил нейтронно-физические и активационные характеристики различных компонентов и материалов диагностических систем, оценил их радиационную стойкость, предложил и выполнил оптимизацию элементов радиационной защиты, положенных в основу проекта российского диагностического модуля, получившего признание Международной организации и принятого для установки в ИТЭР.

В последнее время в связи с возобновлением работ в поддержку стратегии развития ядерных энергетических систем с реакторами синтеза и деления А.А. Борисов подготовил геометрические модели гибридного ТЯР малой и большой мощности как базовых инструментов для системного анализа их нейтронно-физических характеристик и выполнил тестовые расчёты реактора с торием для наработки U-233 как топлива реакторов деления.

Андрей Алексеевич Борисов пользовался заслуженным авторитетом в коллективе Отдела инженерно-физических исследований и Отдела термоядерных реакторов. Участвовал в международном сотрудничестве со специалистами ГДР и ЧССР. Выдвигался на Доску почёта отдела и Отделения физики плазмы Курчатовского института. Принимал активное участие в общественной жизни коллектива. В течение ряда лет являлся председателем профбюро отдела, членом бюро футбольной секции с/к «Малахит». Свой опыт и знания передавал молодым коллегам в НИЦ «Курчатовский институт» и в российском ИТЭР-Центре, участвующем в проведении нейтронно-физических расчётов для проекта ИТЭР. Он автор и соавтор более 30 научных работ.

Андрей Алексеевич был не только замечательным специалистом и коллегой, но и отличным и заботливым семьянином, вырастил троих детей и заботливо помогал воспитывать пятерых внуков. Очень гордился своей большой семьёй. Светлая память об Андрее Алексеевиче навсегда останется в наших сердцах.

Коллеги

СОДЕРЖАНИЕ

CONTENTS

Вопросы атомной науки и техники
С е р и я: Термоядерный синтез
Том 44, выпуск 2

Ответственные за выпуск Б.Н. Колбасов, Е.А. Филимонова
Редактор Н.В. Бокша. Верстальщик И.Н. Альбицкая-Коростелева. Корректор Н.В. Бокша.
Программист-переводчик И.В. Скорюпина. IT-инженер Е.Н. Николаев.
Редактор английского текста Е.Б. Григорьева.

Подписано в печать 12.06.21. Формат 60×90/8
Печать цифровая. Усл. печ. л. 17. Уч.-изд. л. 18. Тираж 156. Индекс 3648. 20 статей, 8 сообщений. Заказ 16
Адрес редакции: Россия, 123182, Москва, пл. Академика Курчатова, 1
Отпечатано в Национальном исследовательском центре «Курчатовский институт»

123182, Москва, пл. Академика Курчатова, 1